CHARACTERIZATION AND DISTRIBUTION OF LUNAR MARE BASALT TYPES USING REMOTE SENSING TECHNIQUES

by

CARLĒ PIETERS

B.A., Antioch College
(1966)

B.S., Massachusetts Institute of Technology
(1971)

S.M., Massachusetts Institute of Technology
(1972)

SUBMITTED IN PARTIAL FULFILLMENT
OF THE REQUIREMENTS FOR THE
DEGREE OF

DOCTOR OF PHILOSOPHY

at the

MASSACHUSETTS INSTITUTE OF TECHNOLOGY

MAY, 1977

Signature of Author **Signature redacted**
Department of Earth and Planetary
Sciences, May 6, 1977

Certified by **Signature redacted**
Thesis Supervisor: Dr. Thomas B. McCord

Accepted by **Signature redacted**
Chairman, Department Committee

CHARACTERIZATION AND DISTRIBUTION OF LUNAR MARE BASALT TYPES USING REMOTE SENSING TECHNIQUES

by

Carle Pieters

ABSTRACT

Although their composition is narrowly defined, basalts are igneous rocks emplaced on a planet's surface as melts generally derived through partial melting of the planet's interior. Variations in the age, volume and chemistry of basalts from different provinces provide clues to the composition and structure of the interior. The types of basalt that can be identified on the surface of the moon have been studied using spectral reflectance measurements. Reflectance spectra (.3 to 1.1 μm) have been obtained using earth based telescopes for a wide variety of lunar mare surfaces and craters and have been classified according to their spectral features. Geochemical interpretations are provided from a background of laboratory reflectance measurements of lunar, terrestrial and meteoritic samples. Some of the principal results of this study are: a) There are major (regionally extensive) basaltic units on the moon not returned by Apollo or Luna missions to date. About 2/3 of the lunar maria are not represented in the lunar sample collection. b) Particular extensive units unsampled include: i. medium to high-Ti basalts near Flamsteed in southern Procellarum and in western Imbrium, ii. medium high-Ti basalts of Humorum and SE Procellarum and iii. low-Ti basalts of NE Imbrium and Frigoris. c) The existence of late stage high-titanium basalts is confirmed although these young basalts are distinctly different in mafic composition from the early high-titanium basalts. d) All mare surfaces contain abundant lateral variations of compositionally heterogeneous basalts. e) Some maria are vertically inhomogeneous with subsurface basalts being distinctly different in composition (eg. low-Ti surface, high-Ti subsurface). f) Some basalt types are spectrally gradational suggesting minor variations in geochemistry. Three regional series can be identified. g) The data suggest that most ($\gtrsim$ 80%) of the lunar surface is composed of a finite number of discrete describable compositional units. h) Mineral components of unsampled units can be defined if spectra are obtained with sufficient spectral coverage (.3 to 2.5 μm) and spatial resolution ($\sim$ .5 km).

Thesis Supervisor: Dr. Thomas B. McCord
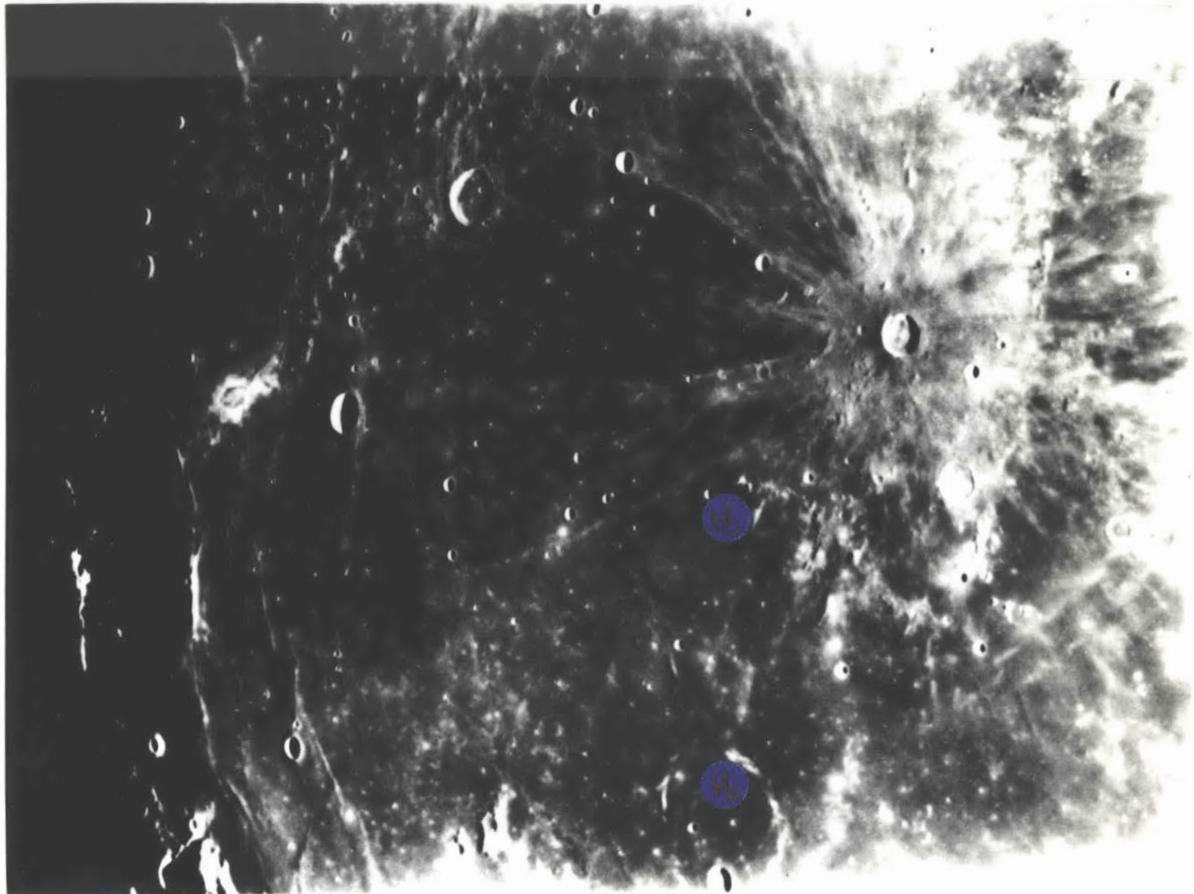Title: Associate Professor of Planetary Physics
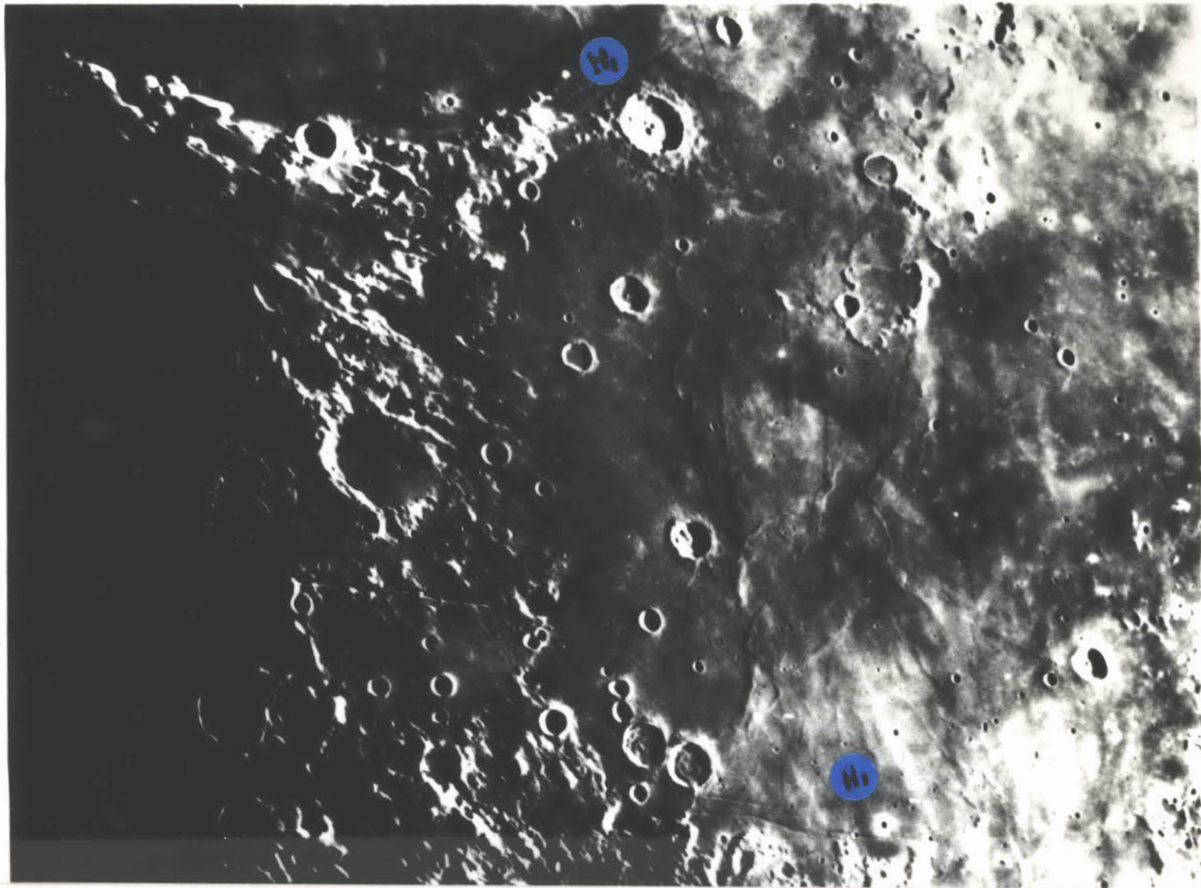
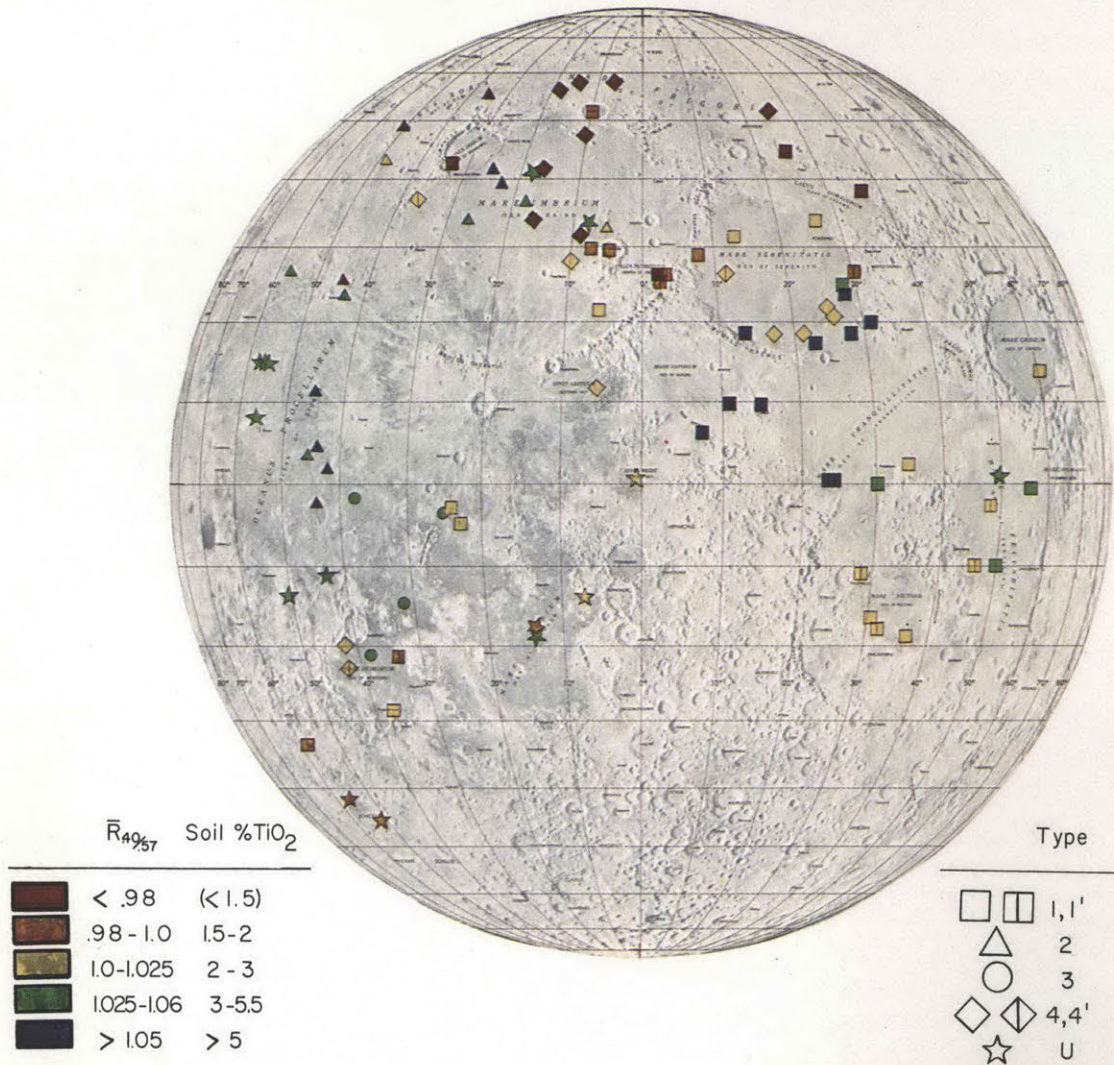# CHARACTERIZATION AND DISTRIBUTION OF LUNAR MARE BASALT TYPES USING REMOTE SENSING TECHNIQUES

Carle Pieters
May 1977

Department of Earth and Planetary Sciences
Massachusetts Institute of Technology

MARE BASALT CLASSIFICATION

$\bar{R}_{.40/.57}$ Soil $\%TiO_2$

	$\bar{R}_{.40/.57}$	Soil $\%TiO_2$
■	< .98	(< 1.5)
■	.98 – 1.0	1.5 – 2
■	1.0 – 1.025	2 – 3
■	1.025 – 1.06	3 – 5.5
■	> 1.05	> 5

Type

□ ▯ 1,1'
△ 2
○ 3
◇ ◈ 4,4'
☆ U

Classification of nearside lunar basalt types using telescopic reflectance spectra from .3 to 1.1 μm of small (5–20 km diameter) mare areas (Pieters and McCord, Vol. 3). The shape of the oversized symbols indicates a distinction of basalt types based on near-infrared features of the soil spectra. The color of the symbol indicates the percent TiO_2 of surface soil as derived from continuum slope of the spectrum: R .40/.57 = reflectance at .40 μm relative to a standard area in Mare Serenitatis (MS-2) and scaled to unity at .57 μm. The data indicate that there exists a variety of basalt types unsampled by the landing missions.

ACKNOWLEDGEMENTS

A PhD thesis represents the formal part of a transition in a person's life from clever student to professional. The process that leads to a PhD degree is different for each student. When I obtained by first undergraduate degree eleven years ago, it never occurred to me that a doctor's degree in science was a realistic goal in my life. The process that led to this thesis perhaps first started with a vague dissatisfaction with my previous position as a high school teacher and a non-directed but avid interest in astronomy and planetary science. During the last seven and a half years at MIT (three of which were as a junior staff scientist), the foundation for a strong and confident scientific career was gradually developed. A few key people provided the essential personal and academic support so important in this process. I will always be deeply and warmly grateful to Drs. Tom McCord, John Adams, Jim Head, Tom McGetchin, and Roger Burns. Without their help and encouragement it is unlikely I would ever have developed scientific enthusiasm nor faith in my own contributions. The continuous manner in which Dr. Tom McCord was able to integrate the difficult roles of teacher, advisor, friend and colleague is specially appreciated.

5

The roots of the thesis content presented here are
difficult to define and are imbedded in almost all the work
I have been involved with at MIT in association with Tom
McCord and John Adams. However, three people have gener-
ously acted as principal advisors throughout the period
of thesis preparation and contributed significantly to the
content and structure of the project: Drs. Tom McCord,
Jim Hays, and Roger Burns.

Much of the telescopic data used in this thesis was
obtained while I was a guest observer at the following ob-
servatories: (1) Mount Wilson Observatory (24-inch tele-
scope) which is operated by the Department of Geological
Sciences, California Institute of Technology, Pasadena;
(2) Cerro-Tololo Inter-American Observatory, which is op-
erated by the Association of Universities for Research in
Astronomy, Inc., under contract with the National Science
Foundation; and (3) Mauna Kea Observatory, Institute for
Astronomy, University of Hawaii. The research was supported
by NASA grants NSG-7048 and NGL-22-009-790 (Tom McCord,
principal investigator).

TABLE OF CONTENTS

Characterization and Distribution of Lunar Mare Basalt Types
Using Remote Sensing Techniques

EXTENDED OUTLINE

I. Basalt Types: An Overview
   A. Basalts as a planetary phenomenon
      1. Brief description of known and implied basalts
         a. Earth
         b. The Moon
         c. Mars
         d. Meteorites and asteroids
         e. Mercury
         f. Venus
      2. Limits of planetary chemical composition set by Solar System models
      3. Formation of basaltic liquids--possible heat sources
         a. Accretional energy
         b. Radioactive isotopes
         c. Solar wind electrical heating
         d. Other heat sources
      4. Formation of basaltic liquids--partial melting
         a. Major elements
         b. Minor and trace elements
         c. Isotopes
      5. Crystallization of basaltic liquids
         a. Geochemical changes
            i. Differentiation/crystal fractionation
            ii. Assimilation
         b. Petrological results of cooling conditions
            i. Crystal grain size
            ii. Vesicles
            iii. Mineralogy
      6. Surface alteration of basalts
         a. Mechanical alteration
         b. Chemical alteration
         c. Current surface environment of the terrestrial planets
   B. Terrestrial basalt types
      1. Geochemical variations
         a. Relation of basalts to other igneous rocks
         b. Magma types
      2. Basalt types associated with specific environments
         a. Ocean ridge and floor basalts
         b. Ocean islands
            i. Tholeiite series
            ii. Alkali basalt series
            iii. Tholeiite--alkali basalt associations
              Galapagos
              Hawaii
              Canary islands
         c. Subduction zone

        d. Continental basalts
           i.   Tholeiitic flood basalts
           ii. Alkali basalt regions (rift zones?)
     3. Terrestrial volcanism in time
  C. Lunar basalt types
     1. Major element geochemistry of lunar mare basalt
        types
        a. High-Ti
        b. Low-Ti
        c. Other (feldspathic, VLT, Luna 24) basalts
     2. Role of basalts in current understanding of the
        moon
        a. Comparison with terrestrial basalts
        b. Chronology
        c. Two stage melting hypothesis
        d. Mare basalt source regions
     3. Unanswered questions
II. Remote Sensing of the Moon
  A. General: Current techniques of remote sensing
  B. Outline of previous work in spectral reflectance
     1. Laboratory reflectance measurements: General
     2. Telescopic reflectance measurements: General
     3. Telescopic spectral images
     4. Laboratory reflectance measurements: Applied
     5. Telescopic reflectance measurements: Applied
     6. Spectral reflectance: Application with other
        forms of remote sensing
  C. Principles of spectral reflectance
     1. Optical properties of minerals
        a. Crystal field transitions of transition
           metal ions
        b. Charge transfer transitions
     2. Reflectance of minerals and rocks
        a. Physical components of reflection
        b. Mean optical path length (MOPL)
        c. Spectral features of minerals
           i. Pyroxenes
           ii. Olivine
           iii. Feldspars
           iv. Glass
        d. Spectral components of a whole rock spectrum
  D. Spectral reflectance of lunar material
     1. Soils
        a. Agglutinates
           i. Fe-Ti rich glass
           ii. Fe^0
           iii. Ilmenite and opaques
           iv. Mineral components
        b. Soil spectra
           i. Strong absorptions
           ii. Subtle absorptions

PREFACE

The content of this thesis can be considered in three parts: a background section (I) that discusses what basalts are and why they are interesting, a section (II) that provides detailed background of spectral reflectance remote sensing techniques, and three sections (III, IV, and V) that discuss the application of spectral reflectance techniques to understanding the geochemistry of the lunar maria. The length of each section is not necessarily proportional to its contribution to the scientific output of this thesis, but is determined more by an attempt for completeness.

Section I is a brief description of basalts in the solar system and could easily be skipped by geochemists and petrologists familiar with terrestrial and lunar basalts. It is clear this section is too short for the detailed discussion that the topic merits. On the other hand, I realize the length of this background material is perhaps out of proportion with its direct relevance to the content of the thesis. I hope that sufficient detail has been presented so that readers unfamiliar with basalts are able to understand what they are and why they are interesting.

Section II provides detailed information concerning spectral reflectance studies of lunar material. Although much of this material has appeared in the literature during the last ten years, some of the basic concepts presented have not been discussed fully or are currently being prepared for publica-

tion by the ∿5 people involved in the field. Emphasis is placed in this section on establishing a basis for interpretation of remotely-obtained spectral reflectance data.

Sections III, IV, and V contain most of the scientific contributions of this thesis. This material is largely in the form of self-contained manuscripts that were prepared as the thesis progressed. The content concerns the classification of remotely-obtained lunar reflectance spectra and the applications of spectral reflectance data to the characterization and distribution of lunar mare basalt types. The material presented in Section I and II provides the detailed background on the nature of basalts and spectral reflectance techniques that cannot be included in a (page-limited) published manuscript. The major conclusions that can be drawn from the currently available spectral reflectance data are summarized in Section V.

I. BASALT TYPES: AN OVERVIEW

I. BASALT TYPES: AN OVERVIEW

The formal definition of a basalt concerns its chemistry, mineralogy, and mode of emplacement. Basaltic composition is generally 45-52% SiO_2, $MgO + FeO + Fe_2O_3 > 15\%$, and $CaO/Al_2O_3 > .60$. The mineralogy of common basalts is dominated by calcic plagioclase ($An_{>50}$), augite, ±Ca-poor pyroxenes, ±olivine, and a minor amount of opaques. Basalts are extrusive igneous rocks, i.e., melts which have cooled in a low pressure environment on the surface.

Basalts are suspected to have erupted on the earth's surface for at least the last 2.7 billion years. They were emplaced on the moon's surface between about 3.9 and 3.0 billion years ago (AE) and account for 17% of the moon's surface area. From photogeologic studies, basalts are expected to also have occurred in particular regions on Mars and Mercury. Laboratory studies of basalt samples from the earth and moon show they have crystallized from a melt derived from sub-crustal material and as such provide an opportunity to study the composition of the interior. The composition and age of basalts put limits on the thermal evolution of the planet. The basaltic achondrite class of meteorites fits the above chemical definition, and texturally are often considered igneous. Since there are asteroids

that have similar geochemical properties, asteroids are often considered to be the parent bodies for the achondrites.

More loosely, basalts are considered the major igneous rock types derived more or less directly by partial melting of a mantle source. As such, basalts provide important geochemical constraints on mantle composition. (The relation of basalts to the mantle at times involves a circular definition.) It is this more general description of basalts that makes them interesting as a planetary phenomenon. However, since the nature of the mantle, or source region of 'basalts', is not likely to be the same for all terrestrial[1] planets, the prevalent igneous rock type derived by partial melting of the interior may not necessarily be a basalt. For example, the lunar high-titanium 'basalts' commonly contain <40% SiO_2, primarily because of their high TiO_2 content. The likely igneous rock type derived from the mantle of Mars would be extremely ultramafic (McGetchin and Smyth, 1977) and well beyond the range of terrestrial[1] basalts.

It is tempting to postulate a common period of 'basaltic' volcanism for all solid surface planets. Volcanism

---

[1]The adjective 'terrestrial' usually means pertaining to earth. However, in planetary science, it is often used to describe a whole class of solid surface objects. The 'terrestrial' planets include Mercury, Venus, Earth, Mars, and often the moon and asteroids.

is certainly a common occurrence on the terrestrial planets, but each planet (and the asteroids) has evolved in a unique manner. It is hoped that a detailed study of the basalts on each planet will help define some of the general principles of planetary evolution.

I. BASALT TYPES: AN OVERVIEW

A. Basalts as a planetary phenomenon

1. Brief description of known and implied basalts

a. Earth

There are about 800 known active volcanoes on the surface of the earth today (Verhoogen et al., 1970, p. 262) and an undetermined number of dormant or extinct volcanoes. The composition, mineralogy and mode of occurrence of material from these sources are a function of the specific environment and planetary processes associated with the region (see Section I-B). It is clear that the earth is a dynamic planet and has been for most likely all its 4.5 AE history. The current surface of the planet is constantly undergoing severe alteration and rejuvenation from both tectonic and meterological processes. The effects of plate tectonics which dominate the geology of the earth may be unique in the solar system. Nevertheless, there does exist stable regions in the continental plates that still contain a record of early volcanic rocks (see Section IB-3), implying that some form of basaltic volcanism occurred early in the earth's history, perhaps before 3.0 AE.

Of recent terrestrial basalts, the largest surface area and perhaps the largest volume of basalts occur

on the ocean floor and are generated by the midocean spread-
ing centers. Additional forms of volcanism occur near the
region of a subduction zone as oceanic and continental lith-
ospheric plates collide: (1) the island arc volcanics
which include a variety of basalts and more silicious ma-
terial, and (2) the continental volcanics which are gener-
ally more silica-rich (e.g., andesite). Major volumes of
basalts can also occur within a lithospheric plate such
as is observed with the Hawaiian series of shield volcanoes
and the extensive continental flood basalts (e.g., Columbia
River, Deccan). Alkali-rich basalts occur both on ocean
islands and also well within a continental plate. Addition-
al continental volcanics associated with rift zones are
often extremely complex and may include such 'exotic' com-
positions as carbonatites as well as more familiar compo-
sitions such as basalt-rhyolite associations. In short,
terrestrial volcanism is not only currently active in a
sometimes perplexing variety of forms, but it also has
a complex history as a planetary phenomenon, much of which
has been erased.

     b.   The Moon

       There are two major geochemical families of
material on the lunar surface: the mare basalts and the
feldspathic highland crust. The composition, mineralogy

and texture of returned mare rocks are clearly basaltic (Section I-C). Although a component of highland material (perhaps 20%, Taylor, 1975, p. 255) can be considered basaltic in composition, many highland rocks with igenous textures are considered to be the result of impact melts (Irving, 1975) and the highlands in general are not basaltic.

Mare basalts account for about 17% of the lunar surface area and less than 1% of the total volume for an estimated 60 km thick lunar crust. [This and much of the details that follow can be found in a review by Head (1976)]. Basaltic volcanism occurred on the front side of the moon filling the lowlands and forming the maria from about 3.8 to 2.5 AE (estimate). Some form of volcanism may also have occurred in the highlands prior to the filling of the lowlands by mare basalts. Lunar mare lavas were very fluid and voluminous and formed extensive flows. The lunar crust formed early in the evolution of the planet (<4.1 AE). The mare basalts were derived from partial melts of sub-crustal materials and were later emplaced in the low-lying regions of the fractured surface. The total volume of basalt is estimated to be about 10×10^6 km^3. The process of filling the maria took place over about 1.3 billion years and produced complex deposits of smooth plains. About 2.5 billion years ago, lunar volcanism ended. The

evolution of the atmosphereless surface was then essentially

frozen with only meteoroid bombardment to alter its form.

Unlike the earth, the moon provides an opportunity to study

early stages of the evolution of a planet.

c.   <u>Mars</u>

The largest known volcano in the solar system

is the Martian Olympus Mons [500 km diameter, 23 km high,

2.12×10^6 km^3 volume (Blasius and Cutts, 1976)]. From,

Mariner imagery many such volcanoes (but smaller) can be

identified (Carr, 1973) with a variety of ages. Although

much of the highly cratered surface of Mars could have

an age comparable to the lunar highland crust, the Thar-

sis volcanoes could be younger than 750 m.y. old (Soderblom

et al., 1974). Some of the volcanic plains (similar to

the lunar maria) could be as old as 2.4 AE. The composi-

tion of Martian soil as determined by the x-ray florescence

experiments of Viking could be consistent with many mineral

assemblages which range from ultramafic igneous rock to

an iron-rich extensively weathered product (Toulmin et al.,

1976; Baird et al., 1976). Earth-based spectral studies

of the Martian dark regions are consistent with oxidized

basalt (Adams and McCord, 1969); laboratory and theoreti-

cal studies show photostimulated oxidation is the likely

chemical alteration process (Huguenin, 1974). Although

Martian volcanism probably extended over a period longer

than that demonstrated by the moon, Mars is clearly not

as active as the earth today and may even have been dormant

for the last billion years. The martian surface has under-

gone extensive mechanical and chemical weathering causing

some of the record to be blurred.

d. Meteorites and asteroids

Prior to the Apollo missions, the only samples

of extraterrestrial material available were fragments of

unknown origin that fall to earth as meteorites. (See Was-

son, 1974, for a detailed discussion.) Most (>70%) of these

falls are ordinary chondrites, or chondrule-bearing sili-

cate assemblages with textures that indicate they have not

experienced a severe heating process. About 8% of the

meteorite falls are classified as differentiated silicate-

rich achondrites, or mineral assemblages (without chondrules)

that possess mineralogical and textural properties which

imply crystallization from a melt and perhaps fractional

crystallization in a gravity field (Duke and Silver, 1967).

The composition of the achondritic eucrites (monomict pig-

eonite breccias), which constitute <3% of falls, is essen-

tially basaltic. The extrusive origin of some such eucrites

is demonstrated by the existence of vesicles presumably

formed by the expansion of gas evolved from a magma as the

result of   pressure drop during extrusion onto a parent

body surface.

The return of lunar samples allowed geochemical stu-
dies that effectively eliminated the moon as a possible
source for the meteorites. Comets, belt asteroids (main
body of asteroids in orbit 2.2 - 3.2 AU from the sun), and
the Apollo asteroids (earth-orbit crossing) are the remain-
ing possible meteorite sources. Spectrophotometry of over
100 asteroids (e.g., McCord and Chapman, 1975a, b; Chapman
et al., 1975) and the mineralogical interpretation of the
spectra (McCord and Gaffey, 1974; Gaffey and McCord, 1976)
indicate that most asteroids can be understood in terms
of mineral assembalges common to meteorite samples. The
earth, however, receives a biased distribution of samples.
Basaltic achondrite-like material is extremely uncommon
among the asteroids with the main belt being dominated by
material much like the relatively 'primitive' carbonaceous
chondrites. The asteroid 4 Vesta is the singular example
(McCord et al., 1970) of possible basaltic material; the
spectrum of this asteroid indicates a surface with a pig-
eonite basalt assemblage much like the eucrites. Somehow
it seems a small body with a radius 245-300 km having a
density around 3.0 g cm^{-3} (4 Vesta) was able to develop
a basaltic surface, while in the same part of the solar

system a larger object with a radius 465-590 km having

a density around 2.1 g cm^{-3} (1 Ceres) remains undifferen-

tiated (Matson et al., 1976).

e.   <u>Mercury</u>

Although Mercury was strongly suspected to

have a lunar-like surface, little was known about the plan-

et's surface until the Mariner mission in 1974. Earthbased

spectrophotometric measurements of the whole planet (McCord

and Adams, 1972) indicated that the composition of the sur-

face was comparable to the lunar highlands--being rich in

the dark impact generated silicate glasses. Polarization

measurements indicated that the surface microstructure

was also lunar-like (Dollfus and Auriere, 1974). Meticu-

lous low resolution visual observations implied there were

at least albedo differences across the surface (Dollfus,

1961). There is, however, no direct evidence for basalts

from the astronomical data.

The Mariner images showed the surface morpho-

logy of Mercury to be remarkably similar to the moon (Mur-

ray et al., 1974, 1975). Much of the surface is heavily

cratered but there exist many level and less cratered sur-

faces (plains) including the floors and surrounding terrain

of many craters and basins. The smooth plains are somewhat

darker than the heavily cratered terrain, but the albedo

contrast is less than that observed for the moon. Although

no direct evidence for volcanism such as cones or domes

is observed, the volume and areal extent of the Mercurian

plains material suggest a volcanic origin. If the lunar

analogy holds for Mercurian early differentiation, the plains

material could be basaltic.

      f. Venus

      The size and density of the planet Venus is

not much different from that of the earth, but little is

known about the surface of the planet due to the extensive

and opaque atmosphere ($\sim$100 bars). Images of the surface

were obtained in 1975 by the Soviet spacecrafts Venera 9

and 10 and described by Florensky et al. (1977). The sur-

face contains both fine material and rocks. Some rocks

are flat and show evidence of layering. One region contains

sharp-edged "slabs" of rock whereas the other region shows

rocks with smooth edges. Earth-based radar measurements

(e.g., Goldstein et al., 1976) reveal major surface features

reminiscent of the large basins on the moon and Mars. There

is currently no evidence for or against the existence of

volcanic material on the surface of Venus.

2.   Limits of planetary chemical composition set by

Solar System models

Since basalts are the products of crystallization from a magma, they are at least second generation material and are directly related to the original composition of the premelt material. Although some basaltic material has probably passed through more than one sequence of melting and differentiation, it is worthwhile to consider the possible initial starting material for the terrestrial planets. Models of condensation from a primitive solar nebula (PSN) describe simple condensation sequences that can account for most of the observed bulk densities of the planets and can also provide an estimate of their   intial bulk chemistry (Lewis, 1974a, b; Barshay and Lewis, 1976).

The condensation models assume a PSN composition (Cameron, 1973) and a reasonable description of the pressure and temperature with radial distance along the PSN disk. In order to examine the predictive ability of a given model, the elemental composition of the PSN is assumed uniform throughout. This second assumption, although not purely accurate, is necessary; unconstrained deviations from simplicity can result in an infinite variety of predictions. The principles of chemical thermodynamics are applied to the assumed PSN and the primordial composition of material is predicted in the region where each planet formed. Both

equilibrium and disequilibrium models have been examined.
The results of such models indicate that, with respect
to major element composition and bulk density of the result-
ing planet, the terrestrial planets and asteroids are likely
to have condensed under equilibrium or near equilibrium
conditions and that the assumptions of the PSN model were
thus not likely to be grossly different from reality.

Compositions of various solar system objects pre-
dicted by the equilibrium condensation model are summarized
in Figure IA1,2 (from Lewis, 1974b). Mercury is predicted
to contain a major amount of refractory metals and minerals
with an iron-nickel alloy core and a limited amount of
$MgSiO_3$ enstatite. Venus contains the same components
as Mercury but with major amounts of enstatite and perhaps
some alkali aluminosilicates. Venus is expected to have
little if any sulfur or water. The Earth, by this model,
contains a small amount of water and iron occurs as Fe metal,
FeO, and FeS. Mars, on the other hand, contains little
or no unoxidized iron and more water than the earth.

A few serious discrepancies exist, however, between
predictions and observations. For example, the models do
not allow the earth (density = 5.5 g cm^{-3}) and the moon
(density = 3.3 g cm^{-3}) to form in the same region of the

MERCURY

MANTLE RICH IN PYROXENE WITH <.01% FERROUS OXIDE

VENUS

MANTLE OF ENSTATITE AND .5% FERROUS OXIDE

EARTH

MANTLE OF OLIVINE, PYROXENE, ~10% FERROUS OXIDE, ~.05% WATER

MARS

MANTLE OF OLIVINE ~50% FERROUS OXIDE AND .3% WATER

IO

GANYMEDE

CALLISTO

TITAN

	SOLUTION OF $NH_3 \cdot H_2O$ HYDRATE
	WATER ICE
	$CH_4 \cdot 7H_2O$ ICE
	REFRACTORY OXIDES OR CRUST

	FERROMAGNESIAN SILICATES
	"WET" SERPENTINE MANTLE
	CORE OF TROILITE
	CORE OF IRON-NICKEL ALLOY

CROSS SECTION OF OBJECTS IN THE SOLAR SYSTEM as predicted by the equilibrium-condensation model agrees with what is known about the earth and other planets. Io, Ganymede and Callisto are three of the four largest moons of Jupiter. Titan is the largest moon of Saturn. "Wet" mantle of serpentine contains much water bound into the rock. The boundary between the inner mantle and the outer mantle of the earth is not shown because it is a change in the mineral structure and not a difference in chemical composition.

Figure IA 1.   (from Lewis, 1974b)
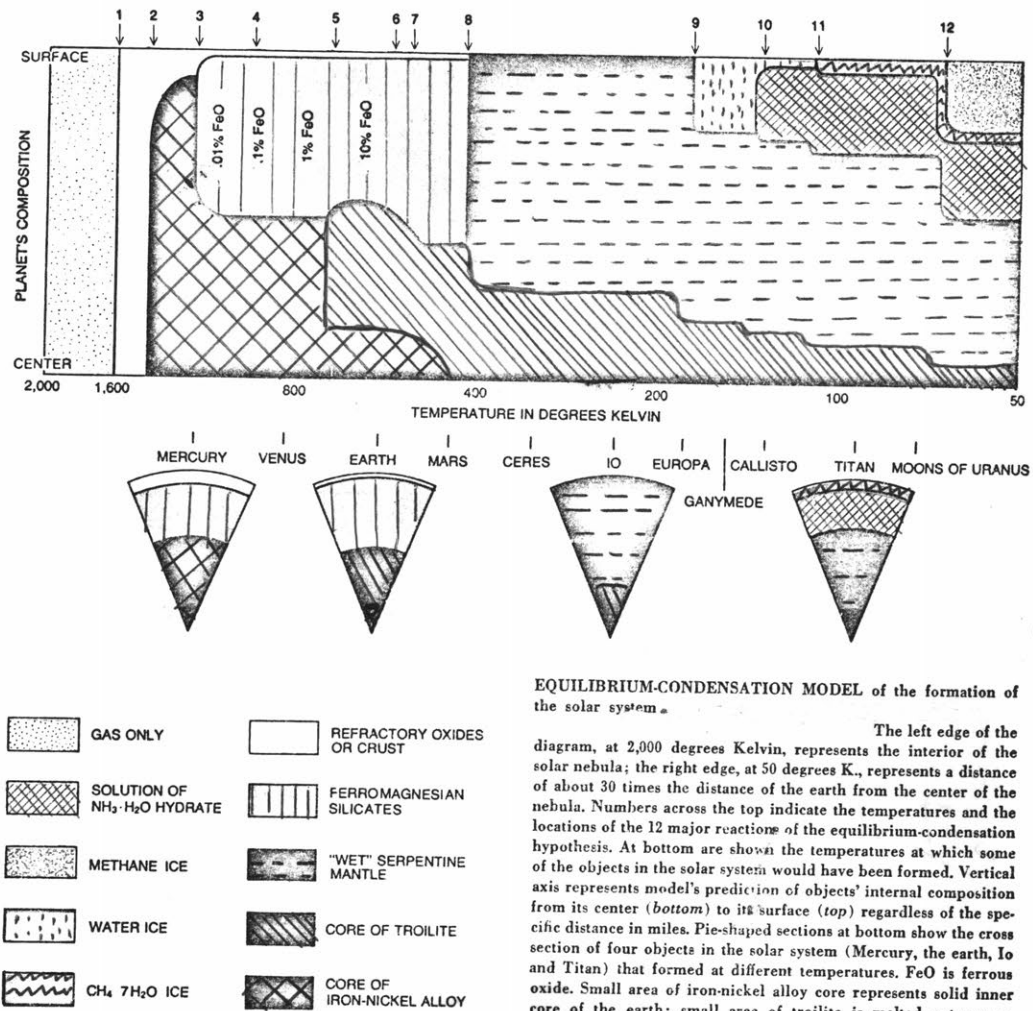
EQUILIBRIUM-CONDENSATION MODEL of the formation of the solar system.

The left edge of the diagram, at 2,000 degrees Kelvin, represents the interior of the solar nebula; the right edge, at 50 degrees K., represents a distance of about 30 times the distance of the earth from the center of the nebula. Numbers across the top indicate the temperatures and the locations of the 12 major reactions of the equilibrium-condensation hypothesis. At bottom are shown the temperatures at which some of the objects in the solar system would have been formed. Vertical axis represents model's prediction of objects' internal composition from its center (*bottom*) to its surface (*top*) regardless of the specific distance in miles. Pie-shaped sections at bottom show the cross section of four objects in the solar system (Mercury, the earth, Io and Titan) that formed at different temperatures. FeO is ferrous oxide. Small area of iron-nickel alloy core represents solid inner core of the earth; small area of troilite is melted outer core.

Figure IA 2.   (from Lewis, 1974b)

solar system without some secondary processes affecting

the moon. Secondly, the nebular adiabat, along which con-

densation is presumed to have occurred, does not cross

the graphite stability field, but carbonaceous chondrites

(and probably some asteroids) are known to contain signi-

ficant graphite. It is suggested by Barshay and Lewis (1976)

that the carbon found in meteorites may be a remnant of

interstellar dust and is an exception to the equilibrium

condensation models.

Furthermore, there is an indication from the study

of oxygen isotopic composition (e.g., Clayton et al., 1976)

that inhomogeneities existed in the solar nebula prior to

condensation. This evidence indicates that the earth, the

moon, and the parent bodies of differentiated stony and

stony-iron meteorites must have been derived from the same

batch of solar nebular material. Five other groups of solar

system material can be identified on the basis of oxygen

isotopic composition, none of which can be derived from

another by direct chemical fractionation processes. One

of these groups, the ordinary chondrites which constitute

the majority of meteorite falls on earth, cannot have been

derived from the same homogeneous region of the solar nebula

as the earth. The difference may imply that the earth

had a higher mean condensation temperature.

3.   Formation of Basaltic Liquids--Possible Heat Sources

Basaltic rocks by definition are igneous and crystallized from a melt. On the earth, basaltic magmas are thought to be derived by partial melting of a mafic or ultramafic mantle (See IB). The lunar mare basalts are also thought to be derived by partial melting of the interior (see IC). A number of possible heat sources for producing these melts are outlined below. A recent review of possible terrestrial melting processes is provided by Yoder, Chapter 4 (1976). The relative importance of each heat source is perhaps different for each planetary object.

a.   Accretional Energy

The earliest history of a solar system has not been observed astronomically and is, therefore, derived from a mixture of fact and conjecture. At some time greater than 4.6 billion years ago (limiting age of meteorites; Wasson, 1974) solid particles condensed from a cooling solar nebula. These small grains began to agglomerate into larger objects. At some point the neo-planet became sufficiently large to allow gravitational accretion of enough mass to form a planet. For a given homogeneous mass M with a radius R, the accretional energy released is:

$$E = \frac{3}{5} \frac{GM^2}{R}$$

For a uniform earth, the gravitational energy per unit
mass would be about 4×10^{11} ergs/g--enough to vaporize
the earth twiceover (Verhoogen et al., 1970, p. 600-601).

The key to how much of this accretional energy
affects the original thermal state of the new planet is
the degree to which the heat generated can be radiated
away into space (see Mizutani et al., 1972). The amount
of heat generated per unit time is a function of the rate
of accretion. Accretional energy is expected to play a
significant role in the initial temperature profile for
a planet. Most models for the early history of the moon
(e.g., Wood et al., 1970) require an original magma ocean
hundreds of kilometers deep (see IC2). Accretional energy
is usually cited as the probable heat source (e.g., Hubbard
and Minear, 1975) with accretion time being less than 1000
years.

b. <u>Radioactive Isotopes</u>

Kinetic energy of the α-particles and γ radia-
tion emitted from radio nuclides is absorbed by surround-
ing atoms and converted to thermal energy. The heat pro-
ducted during any given period is a function of the type
and amount of radioactive isotopes. Using the estimated
abundances of heat-producing elements on earth, the radio-
genic heat production can be calculated as a function of

time as shown in Figure IA3 (from Mason).   In the earth,

the melting temperature of iron was reached after about 600

million years at a few hundred kilometers depth.   Thermal

evolution models of the moon (e.g., Toksöz and Solomon,

1973), Mars (Johnson et al., 1974), and Mercury (Solomon,

1976) require estimates of these long-lived radio nuclides

(U^{238}, U^{235}, Th^{232}, and K^{40}).   Estimates are derived from

solar abundances information as well as measured amounts

in terrestrial, lunar, and meteoritic samples.   The lunar

basalts are generally believed to be results of partial

melting of the interior caused by radiogenic heating about

4.0 to 3.0 AE ago (e.g., Taylor, 1975).

It is unlikely, however, for small planetary

objects such as the asteroids to contain sufficient long-

lived heat producing elements to allow post-accretional

melting.   Since the radiometric ages of most achondrites

are close to 4.5 AE, an alternative heat source is required

to account for the early melting of achondrite parent bodies.

Short-lived radio nuclides such as ^{26}Al ($\tau_{1/2}$ = .72 x 10^6 yr.)

have been suggested as a possible short term heat source

in the early solar system (Reeves and Audouze, 1969).

Although at first no evidence of ^{26}Al could be established

in meteorites, the recent discovery of a ^{26}Mg excess in

an Allende chondrule suggests the early existence of

now extinct ^{26}Al (Lee et al., 1976).
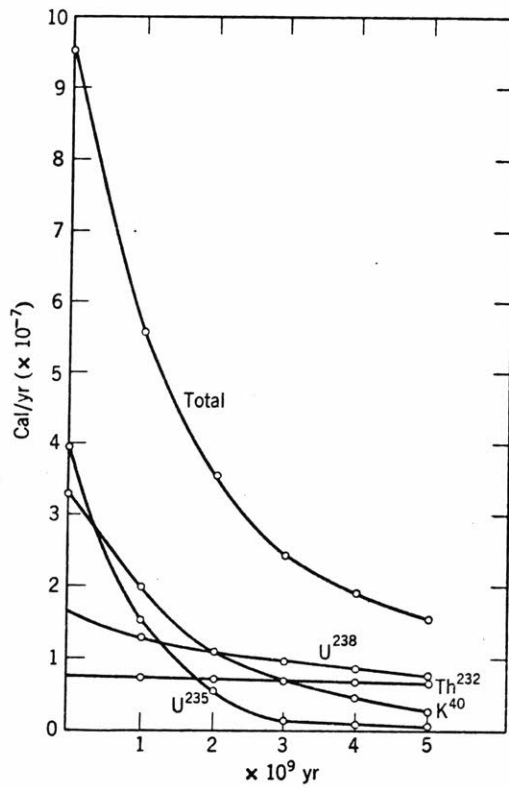
Radiogenic heat formed in the Earth
by U, Th and ^{40}K separately and together plotted
against time. (After Vinogradov) 1961

Figure IA 3.

c.   Solar Wind Electrical Heating

Early solar wind heating of small objects assumes that young solar-type stars rapidly loose mass (~ .1 original mass) and maintain an enhanced magnetic field (~10 x present) during a T-Tauri phase of stellar evolution. As a planetoid moves through this early plasma, conditions can be favorable (e.g., no atmosphere) to allow an exchange of charge between the plasma and planet. These electric currents cause ohmic heating of the interior of the planetoid. This concept first proposed by Sonnet et al. (1969) has recently been reevaluated in light of additional information about asteroids and meteorites (Briggs, 1976). Briggs pointed out that the differences in low temperature electrical conductivity of different types of carbonaceous chondrites would cause dramatic differences in solar wind heated asteroids of such material. For objects less than 500 km in diameter, C1 and C2-type bodies would survive a T-Tauri phase of the sun intact, whereas the cores of C3 and C4-type bodies would be either metamorphosed or melted.

d.   Other Heat Sources

Core formation. For most of the major terrestrial planets including the earth, a combination of the above heat sources caused (early?) extensive fractionation of the planetary material. The separation of the denser

material into a core releases additional gravitational energy
(on the earth estimated to be 10^{38} ergs [Verhoogen et
al., 1970, p. 640]). Core formation is a major event in
the thermal evolution of a planet (a summary for most ter-
restrial planets is given in Soloman and Chaiken, 1976).

Impact melting. After crustal formation (on
the moon at ∿4.2 AE) the surfaces of planetary objects con-
tinue to be bombarded by various objects. The heat gener-
ated by a high velocity impact onto a surface is generally
sufficient not only to vaporize the projectile, but to
crush and melt the host material to some degree. Glasses
found in the lunar soils and breccias have clearly had such
an origin. No major bodies of impact melt, however, have
been identified although a few of the returned lunar sam-
ples are hypothesized to be crystallized from an im-
pact melt (e.g., Irving, 1975).

Tidal friction. When two bodies interact (with-
out colliding) the gravitational deformation is dissipated
as heat. The regular interactions of the earth and moon
is estimated to account for 10% of the earths' heat flow
(Verhoogen et al., 1970, p. 640). Tidal dissipation in
regions of high density contrast has been proposed as a
possible heat source for some lunar magmas derived along
the margins of basins when the moon was closer to the earth
3.0 AE ago (Wones and Shaw, 1975).

4.   Formation of Basaltic Liquids--Partial Melting

If the other terrestrial planets are like the

earth and moon, then basaltic (or planetary) volcanism,

if it exists, is probably the result of partial melting

of mantle material. Experimental data for terrestrial ma-

terial will be used here to show the type of systematics

that can occur in a crystal-liquid environment. A limited

amount of experimental data also exists for lunar material

and has been reviewed by Kesson and Lindsley (1976) (see

Section IC). The formation of mafic melts from the mantle

of Mars has also been considered (McGetchin and Smyth,

1977).

There is much confusion concerning the terms "prim-

itive, primary and parental" as applied to igneous material

(e.g., see Carmichael et al., 1974, p. 44-46). To avoid

confusion in later sections, these terms will be used

throughout the discussion presented here with the following

meanings. Primitive refers to early solar system material,

generally which has not undergone a thermal reworking.

Presumably carbonaceous chondrites represent primitive ma-

terial; the achondrites are less primitive being perhaps

only one step removed from primitive material. Primary

melts are those that have not been compositionally altered

in any way since their derivation. It may be unlikely that

an ideal primary liquid ever reaches the surface of a pla-
net. Parental melts may or may not be observed. Parental
magmas are those which have generated an observed material
through some fractionation or assimilation process.

During melting, the composition of a liquid pro-
duced is generally different from the composition of the
remaining minerals. The behavior of major and minor ele-
ments are not the same: the major element composition of
a partial melt is controlled largely by the residual min-
eral assemblages, whereas the trace element abundances
are more sensitive to the degree of melting.

a. Major elements

The earth's upper mantle is often considered
to be composed of some form of peridotite (olivine with
orthopyroxene, clinopyroxene, ± spinel, ± garnet). A sim-
plified system containing olivine (Fo), clinopyroxene (Di),
and garnet (Py) at 40 k bars pressure (Figure IA-4) was
discussed by Yoder (1976, chapter 6) to illustrate the prin-
ciples that apply to partial melting. When the temperature
of a mineral assemblage with composition X (60% Fo) reaches
1670°C, melting begins at the eutetic composition E. As
more heat is added to the system, the degree of partial
melting increases but the composition of the melt remains
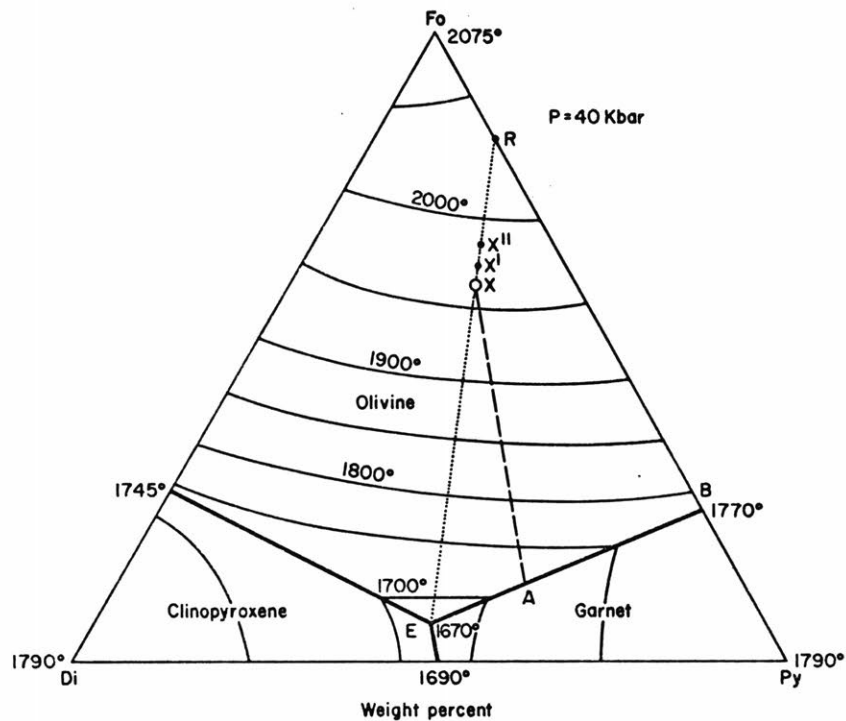
The forsterite(Fo)–diopside(Di)–pyrope(Py) system at $P = 40$ kbar (after Davis and Schairer, 1965, p. 124, Figure 35). E is the piercing-point composition. The temperature of the beginning of melting is assumed to be sufficiently close to 1670°C that the behavior is eutecticlike. X is a bulk composition considered analogous to a peridotite, and X' and X'' are successive residual compositions resulting from the fractional melting of X. B is the composition of liquid produced from the fractional melting of R. The dotted line is a construction line to illustrate the lever rule, and the dashed line is the locus of compositions of liquids produced by melting of X at temperatures indicated by the isotherms. (With permission of the Carnegie Institution of Washington.)

Figure IA 4.   (from Yoder, 1976)

at E; the composition of the residual is driven toward R until the Di component is exhausted. If the melt remains in contact with the residual as more heat is added, the melt composition trends toward A and then to X (equilibrium or "batch" melting). If the melt is removed as it is produced (fractional melting), no melt will be produced as the temperature is raised from 1670 to 1770°C and a melt of composition B will occur when 1770°C is reached.

For a given source region, a large amount of liquid of a single composition can be produced; the major element composition changes as a function of how and when the liquid is removed from the residuum. Melting curves for real systems are perhaps more complicated than that represented in Figure IA-4, and depend on the starting mineral assemblage. Melting curves for two natural peridotites shown in Figure IA-5 (from Mysen and Halloway, 1977) illustrate the same principle, however: liquids of roughly the same major element composition can be produced from a given source region with distinct changes of composition as different mineral phases participate in the melting event.

The experimental data (e.g., Yoder and Tilley, 1962; Green, 1971; Mysen and Boettcher, 1975 a,b) show that the melt composition is also dependent on the temperature, pressure, f_{H_2}, and H_2O and CO_2 content of the source region.
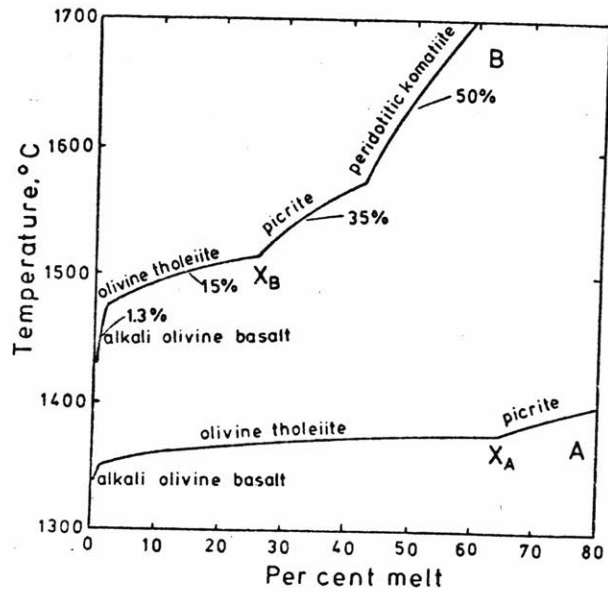
Melting curves of two natural peridotites at 20 kbar under volatile-absent conditions. *A*, sample 66SAL-1; *B*, sample 1611. Percentages on curve *B* denote conditions selected for the present experiments. Rock names are based on normative compositions of partial melts. X_A and X_B, see text.

Figure IA 5.   (from Mysen and Halloway, 1977)

In short, "...it appears that we can produce almost any

liquid composition from andesite to olivine nephelinite

by partial melting of mantle peridotite provided we select

the appropriate starting material composition, temperature,

pressure, f_{H_2}, f_{H_2O}, and f_{CO_2}." (Mysen and Boettcher, 1975b,

p. 588).

b. Minor and trace elements

Only the rare earth elements (REE) and Rb

and Sr concentrations in basaltic liquids will be discussed

here as examples. Gast (1968) pointed out that although

major element composition varies only a few percent for

various basalts, the abundance of trace elements can vary

as much as two orders of magnitudes. His models of REE

partitioning between liquid and solids indicate that REE

chemistry and major element chemistry of liquids produced

by partial melting are in many cases effectively "decoupled".

Some trace elements are strongly concentrated in the first

melt. For example, Rb, and to a lesser extent K, are both

greatly enriched in the liquid for small degrees of partial

melt (Figure IA-6, after Gast, 1968). Actual partition

coefficients for trace elements are difficult to predict;

they are dependent on the minerals present in the source

region, the size and charge of the ion, the degree of par-

tial melting, and to some extent the temperature and pres-

Fractionation of Rb and K during ideal fractional melting of lhe₁zolite (diopside 10, enstatite 20, olivine 65, spinel 5%). Ratios for 3% equilibrium partial melting are given by circled points X (Rb), Y (K). (After Gast, 1968, p. 1073.)
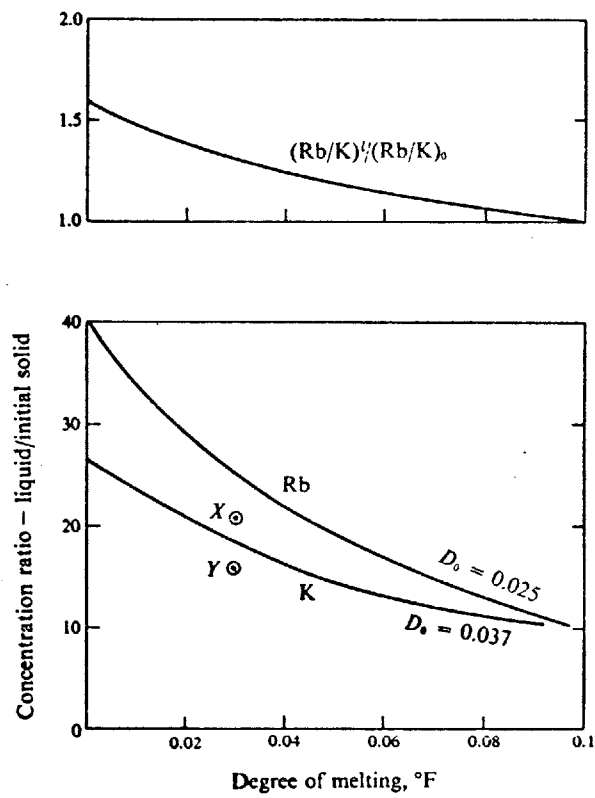
Figure IA 6.   (after Gast, 1968)

sure of the melting conditions. Shown in Figure IA-7 (com-
piled by Yoder, 1976) are representative partition coeffi-
cients for the rare earth elements between common crystals
and melt liquid. Olivine in the source region would strong-
ly affect the degree of enrichment of REE in a liquid,
whereas garnet strongly affects the relative REE pattern.
The REE patterns of various partial melts from peridotite
B in Figure IA-5 were examined by Mysen and Halloway (1977)
and are shown in Figure IA-8. The degree of enrichment
and the REE patterns are very dependent on the degree of
partial melting.

c.   Isotopes

Although there is no evidence for isotopic
fractionation during partial melting, special mention is
due radiogenic isotope systematics such as Rb-Sr (see Faure
and Powell, 1972). ^{87}Rb is radioactive with a half life
of about 4.7×10^{10} years and decays to the stable isotope
^{87}Sr. During partial melting both Rb and Sr are concentrated
in the liquid (Rb generally more than Sr). During crystal-
lization Rb is incorporated preferentially into K-bearing
minerals and Sr into Ca-bearing minerals. The ratio of
the two stable isotopes of strontium, $^{87}Sr/^{86}Sr$, regularly
increases in time from some initial value (I) at a rate
determined by the amount of ^{87}Rb present. The Rb-Sr iso-
tope systematics can thus be used to date the crystallization
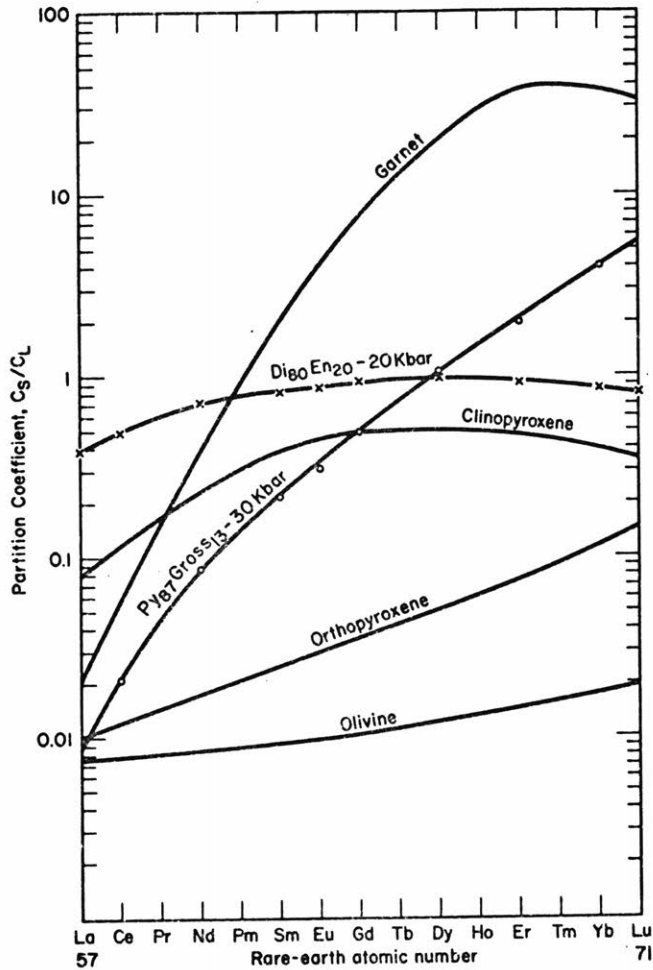
Representative partition coefficients for the rare-earth elements between natural crystals (olivine, orthopyroxene, clinopyroxene, and garnet) and deduced liquid compiled by Helmke and Haskin (1973, p. 1520, Figure 3), between synthetic clinopyroxene ($Di_{80}En_{20}$) and glass at 20 kbar (Masuda and Kushiro, 1970, p. 44, Table 2), and between synthetic garnet ($Py_{87}Gross_{13}$) and glass at 30 kbar (Shimizu and Kushiro, 1975, p. 413, Table 1). C_S = concentration of rare-earth element in the residual crystal; C_L = concentration of rare-earth element in coexisting liquid.

Figure IA 7.   (Yoder, 1976)
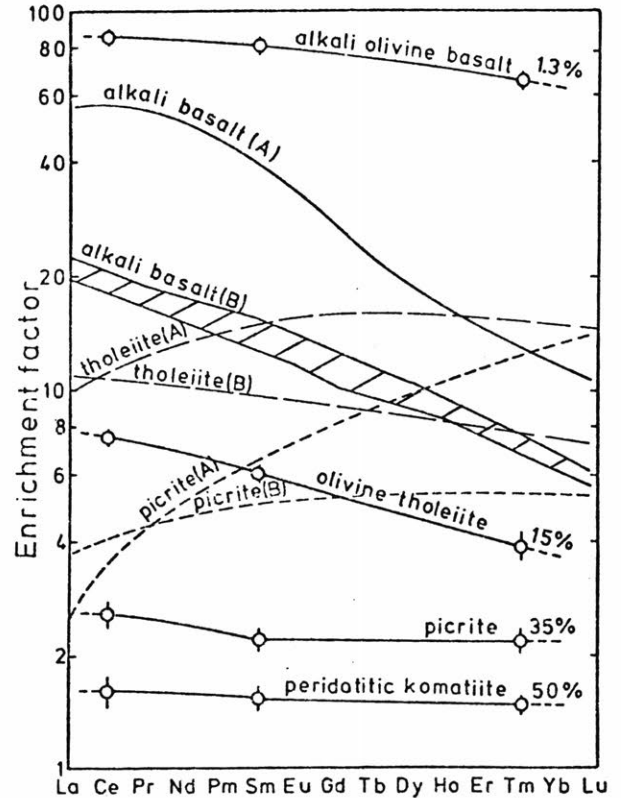
Experimentally determined REE fractionation patterns of experimentally produced partial melts. Alkali basalt (A), Hawaiian alkali basalt.   Alkali basalt (B), range of REE contents of alkali basalts from the Lesser Antilles.   Tholeiite (A), oceanic tholeiite from the Nazca plate.   Tholeiite (B), abyssal tholeiite, Baffin Bay.   Picrite (A), picrite basalt, Azores.   Picrite (B), picrite, Baffin Bay.

Four patterns for partial melts of sample B (in Fig. IA-5) are indicated.
Figure IA 8.   (Mysen and Halloway)

age for a given melt (Papanastassiou and Wasserburg, 1969).

Furthermore, the initial strontium isotope ratio I describes

the character of the source region at the time of separa-

tion of the melt. One of the most primitive values of I

(.69898) is that measured for the basaltic achondrites (age

$\sim$ 4.5 AE)(Papanastassiou and Wasserburg, 1971). Initial

strontium ratios of basalts are generally compared to this

value when the history of the source region is investiga-

ted.

5. Crystallization of Basaltic Liquids

If a basaltic liquid is allowed to cool in a closed
system under equilibrium conditions, the crystallization
sequence and resulting mineralogy can be well defined as
a function of chemistry and pressure from observational,
theoretical, and experimental data (e.g., Bowen, 1928; Yoder
and Tilley, 1962; Green and Ringwood, 1967). Such an equi-
librium situation rarely occurs in nature, however, and
most igneous materials undergo some form of geochemical
alteration where either (1) the final bulk chemistry is
not the same as for the original magma and/or (2) the final
mineralogy is different from the predicted for equilibrium
situations.

a. Geochemical Changes

i. DIFFERENTIATION/CRYSTAL FRACTIONATION.
As a basaltic body of magma cools, the first crystals to
form are the high temperature minerals, such as Mg-rich
olivine (fosterite, Mg_2SiO_4) or calcium-rich plagioclase.
The liquidus minerals are, of course, dependent on the com-
position and pressure of the melt and can be determined
experimentally for a given melt composition. Once crystal-
lization has commenced, the bulk composition of the crystals
is different from the composition of the liquid (except
for unique liquids of eutectic composition). Any process

that separates the crystals from the melt before the cool-

ing sequence is complete is termed "fractional crystalli-

zation" (e.g., Carmichael et al., 1974, p. 62-65). If

early-formed crystals are more dense than the residual

liquid, gravitational settling will occur, thus effectively

removing these minerals from the melt and changing the bulk

compositon of the system.   For basaltic liquids,

the removal of olivine or any other early phase to a cumu-

late layer below is a major process of chemical differentiation.

ii. ASSIMILATION. Either during transit from

the source or while being emplaced, a magma may react with

the surrounding host rock. The process by which components

of the host rock are incorporated into the melt is called

"assimilation" and produces a change in magma composition

difficult to detect and evaluate. Low-temperature minerals

may be melted and become part of the magma, thus altering

the bulk chemistry of the magma. On the other hand, ionic

exchange may occur between crystalline host phases and a

saturated magma and may only affect the trace element con-

centrations.

b. Petrological results of cooling conditions

From the time a magma leaves the source region,

it begins to cool. The texture and to some degree the min-

eralogy of the solidified rock is a function of the cooling

conditions.

      i.   CRYSTAL GRAIN SIZE.   In general, only a few crystal nuclei are formed in slowly cooled liquids but the rate of crystal growth is rapid.   This results in relatively few large crystals.   For rapidly cooled liquids, there are many nuclei with slow growth rates resulting in abundant very small crystals.   During the cooling sequence, conditions are not often constant.   For example, slow cooling rates could exist during a long rise to the surface or while remaining in a magma reservoir allowing some early crystals to nucleate and grow.   When the magma is extruded onto the surface, however, it is cooled more rapidly and the resulting texture is "porphyritic" with the large crystals, or phenocrysts, enclosed by a fine-grained groundmass. Similar textures can also be produced by entirely different conditions.   A loss of volatiles, for example, can have a considerable effect in raising the crystallization temperatures of silicate phases and may produce a texture comparable to rapid cooling.

      ii.   VESICLES.   If a magma is generated under pressure (at depth) and contains H_2O, CO_2, or any gas phase, spherical or tabular cavities are formed as the gas is released at lower pressure when the magma is extruded onto

the surface.   If cooling is rapid, the gas is trapped dur-
ing solidification of the rock.   These frozen cavities
are called vesicles and are characteristic of many volcanic
surfaces.

iii.   MINERALOGY.   Since cooling rate essen-
tially controls whether or not equilibrium conditions are
maintained, it has a major effect on the resulting miner-
alogy.   The extreme example is a quenched liquid that is
primarily glass.   Intermediate are the rapidly-cooled ba-
salts that contain substantial glass in the groundmass
along with the fine-grained crystals.   Non-equilibrium
cooling is commonly indicated by compositional zoning of
crystals in which the core is a high temperature phase
and the rim is a lower temperature phase (e.g., a decrease
in calcium from core to rim of a plagioclase crystal).
Composition trends on crystal zoning can often be complex
since the composition of the liquid can change locally
in a non-uniform manner as other minerals begin to crystal-
lize (e.g., see Hollister et al., 1971).

6. Surface alteration of basalts

Few basaltic surfaces are composed of unaltered material, a fact which is of interest to geochemists who study either samples or remote sensing data. As will be discussed in Sections II through V, the geochemical information that can be derived using remote sensing techniques is restricted to planetary surface material. It is thus imperative that the possible and probable effects of the environment to alter the surface mineralogy and/or geochemistry be reasonably understood. A clear description of surface alteration effects is currently perhaps the most difficult step in interpreting remotely sensed data. A rather detailed discussion of lunar soil properties is provided in Section IID. Terrestrial surfaces are perhaps an order of magnitude more complex than lunar. (Unfortunately, inadequate attention has been given to the systematics of surface alteration to be immediately useful in remote sensing exploration of terrestrial resources.) Outlined below are some of the types of environmental alteration that can and do occur on planetary surfaces. The distinction between mechanical and chemical alteration is for discussion purposes only; in reality, the two are intimately related.

a. Mechanical aleration

A variety of processes break an original solid surface into blocks or finer particles. During the first billion years of planetary evolution, it is unlikely that any of the terrestrial objects escaped high velocity impacts by other (smaller) solid objects. The observable crust

of the moon, Mercury, Mars, and possibly Venus and the Earth
have been permanently scarred by these early impacts. Crus-
tal material was also somewhat redistributed by these events.
Meteorite bombardment continues to the present day in di-
minishing amounts. For atmosphereless bodies, the surface
has been crushed and broken to some depth which varies ac-
cording to the scale of the definition. For example, the
lunar "mega-regolith" (a result of the last major crustal
impacts about 4 AE) probably extends to a depth of about
25 km. The mare regolith (a result of cumulative random
bombardment since $\sim$3.5 AE) is typically $\sim$5 m.   A mature
lunar soil, on the other hand, has a mean particle size
of about 100μm and is dominantly the result of cumulative
micrometeoroid bombardment during the last few 100 million
years.

For planets with atmospheres, a variety of
erosional and depositional processes occur depending on
the type of weather inherent on the planet. Conditions
on earth are perhaps the most severe in that water (rain,
oceans, ice) erosion has redistributed material for much
of the planet's history. It is suggested from photogeologic
evidence that episodic fluid erosion has also been signi-
ficant on Mars. Aeolian (wind carried particles) erosion
and deposition are familiar in arid regions on earth and
are perhaps the dominant form of current mechanical surface

alteration on Mars.

b. Chemical alteration

Some form of geochemical alteration is asso-
ciated with each of the mechanical alteration processes
mentioned above. During an impact event, surface materials
are mixed both vertically and laterally. A portion of the
surface is melted and often mixed with the crushed but
still crystalline host rock. If these impact derived ma-
terials accumulate over long periods of time, the total
mineralogy of the surface can be drastically changed (see
Section IID1). Contamination of the surface by the impact-
ing object is very small, but often detectable (e.g., Anders
et al., 1973).

Atmosphereless bodies have been exposed to
a history of solar wind particle bombardment. An exten-
sive literature exists concerning solar and galatic parti-
cle composition and track studies for the lunar soils and
the regolith history that can be derived from such studies
(e.g., Price et al., 1975). Although it has not been con-
clusively demonstrated, there is evidence that solar wind
emplanted H and C contribute significantly to the reduction
of iron (to Fe^0) during melting by micrometeorite impact
of lunar soils (e.g., Housley et al., 1973).

For the earth and Mars, the dominant chemical

alteration is oxidation of surface material. A number
of oxidation processes are possible but do not provide unique
products; i.e., the same result can be achieved by a var-
iety of means. Hydrothermal alteration of terrestrial ba-
salts can occur prior to or after eruption. Oxidation ef-
fects on Mars, which may mimic terrestrial processes, are
more likely due to a process by which surface material
is stimulated by high energy UV radiation and oxidized by
interaction with atmospheric O_2 (e.g., Huguenin, 1973a,
b, 1974). Huguenin (1974) estimated a 30m thick layer of clay
minerals could be developed in 10^9 years in the Martian
environment. Meteorological and biological oxidation ef-
fects are quickly (within 100 years) noticeable on earth
for fresh volcanic material, except in extreme high or
arid regions.

    c. <u>Current surface environment of the terrestrial
planets</u>

      i. MERCURY. Atmosphereless. Meteorite bom-
bardment extensive and continuing to present. Development
of regolith and soil likely. Possibly strong interaction
with solar wind although existing magnetic field should
deflect a significant portion of particles. Strong ther-
mal surface environment (-180 to +350°C).

ii.   VENUS.   Dense opaque atmosphere ($\sim 10^2$ bars).   Currently unaffected by small meteorites.   Possible wind erosion.   Possible corrosive atmospheric environment.   HOT (480°C).

iii.   EARTH.   Atmosphere (1 bar) opaque to UV radiation.   Surface unaffected by micrometeorites.   Extensive fluid and wind erosion and deposition.   Multitude of oxidation processes.   3/4 surface covered with fluid water.   Extensive biological environment.

iv.   MOON.   Atmosphereless.   Meteorite bombardment extensive and continuing to present.   Well-developed regolith with accumulation of glass-rich soil.   Surface material often saturated with solar wind particles (H, C, N).

v.   MARS.   Thin $\sim$ transparent atmosphere ($\sim .01$ bar).   Surface unaffected by micrometeorites.   Wind erosion and deposition significant.   (Possible fluid erosion in past.)   Oxidized surface (photostimulated).   Developed soil.

vi.   ASTEROIDS.   Atmosphereless.   Periodic impact events.   Accumulation of mature soil improbable due to weak gravity.   Relatively 'fresh' dusty broken surface probable.

I.   BASALT TYPES: AN OVERVIEW

B.   Terrestrial basalt types

There is no universally accepted classification of terrestrial rock types.   One of the problems of classification is the fact that there is a gradation from one rock type into another and boundaries are somewhat indistinct. For igneous rocks there has developed a nonstructured list of terms that are widely used to describe the interrelated mineralogy and chemistry of common rock types (see Carmichael et al., 1974, Chapter 2).

Basalts are volcanic igneous rocks; they have cooled in a low pressure environment (on the surface).   Their texture is thus relatively fine grained, generally $\lesssim 1$ mm. The mineralogy of basalts is dominated by plagioclase and pyroxene and usually includes olivine or quartz and a minor amount of opaques.   The plagioclase is calcium rich $(An_{>50})$; there can be one or two types of pyroxene, augite $\pm$ Ca-poor pyroxene.   Phenocrysts of olivine, pyroxene or feldspar are often present.

The chemistry of basaltic rocks is basic: 45-53% SiO_2. Iron and magnesium content is generally high (MgO + FeO + $Fe_2O_3 \geq .15$%).   Calcium and aluminum are major elements with CaO/Al_2O_3 generally greater than .60.   Potassium, sodium and titanium are present in various proportions; these

three elements are often used to distinguish different ba-
salt types.

Because the earth is tectonically active and many (if
not all) of the surface materials are recycled a number
of times, it has been difficult to develop a classification
scheme for igneous rocks that relates directly to their
origin. All igneous rocks are solidified melts that were
derived from some pre-existing material. The chemistry
of basalts suggests they are a class of igneous rocks which
are probably related directly to melts from the earth's
mantle. Although other types of igneous rocks are related
to or associated with basalts, they will only be discussed
briefly where appropriate and not in detail here.

1. Geochemical Variations

There are three chemical and mineralogical descrip-
tions of a rock that represent its geochemistry and allow
basalts to be classified. (1) Bulk chemical analyses are
derived from whole rock analyses and are expressed in weight
percent of the major oxides. All rock geochemistry is
thus expressed in the same units. (2) Modal mineralogical
analyses, on the other hand, is concerned with the mineralogy
of a rock; each mineral is identified petrographically,
counted, and expressed as a statistical percentage. For-
tunately, the number of minerals that comprise the bulk

of igneous rocks is relatively small.   (3) A third repre-

sentation of geochemistry is the normative composition,

a recalculation of bulk chemistry into about 10 "ideal min-

eral" components rather than the chemical oxide analyses.

Since a wide range of mineralogy can result as a magma cools

(see Section IA-5) most comparative discussions of basalt

geochemistry are concerned with chemical oxide compositions

or norms (the "mineralogical" equivalent). For ease of

comparison, the chemistry rather than mineralogy of basal-

tic materials will be emphasized in this section. Detailed

petrological studies of the mineralogy are used to under-

stand the history (fractionation, cooling conditions, mode

of emplacement, etc.) of a particular sample.

   a.   Relation of basalts to other igneous rocks

        Chemical analyses and norms for representative

igneous rocks (from Verhoogen et al., 1970) are listed

in Table IB1.   Approximate mineralogical compositions for

common igneous rock types is illustrated in Figure IB-1

(from Mason, 1966). Frequency distribution for SiO_2 in

cenozoic volcanic rocks compiled by Chayes (1975) is shown

in Figure IB-2. The variation of SiO_2 is clearly not reg-

ular: a maximum occurs near 49% including average basalts

but the distribution is strongly skewed towards higher sil-

ica content. Figure IB-3 is a variation diagram for the

Chemical analyses and norms of some representative igneous rocks (expressed as weight percentages)

No.:	1	2	3	4	5	6
SiO_2	42.86	48.04	50.02	60.31	66.57	72.80
TiO_2	2.94	1.83	2.23	1.02	0.60	0.46
Al_2O_3	11.46	12.04	15.05	17.53	15.14	13.12
Fe_2O_3	3.34	2.35	3.77	3.30	1.15	1.32
FeO	9.03	8.80	7.37	3.85	1.90	1.62
MnO	0.13	0.17	0.17	0.16	0.06	0.04
MgO	13.61	14.41	7.01	2.59	0.56	0.60
CaO	11.24	8.76	10.17	5.97	1.50	2.20
Na_2O	3.02	1.60	2.05	3.20	4.18	3.63
K_2O	0.93	0.30	0.33	1.20	5.02	3.71
H_2O	0.56	1.63	1.65	0.90	3.01	0.24
P_2O_5	0.52	0.12	0.27	0.14	0.19	0.04
Others	CO_2. 0.30				BaO 0.25	BaO 0.06
Total	99.94	100.05	100.09	100.17	100.13	99.84
Q			6.30	19.50	16.9	32.34
Or	5.56	1.67	1.67	7.12	29.5	21.68
Ab	5.76	13.62	17.29	27.04	35.6	30.39
An	15.29	24.74	31.14	28.72	7.0	8.62
Ne	10.51					
Di	29.43	14.20	13.84	0.86		1.83
Hy		27.47	17.72	9.01	3.0	1.79
Ol	20.79	9.51				
Mt	4.87	3.25	5.57	4.78	1.6	1.86
Il	5.62	3.50	4.26	1.93	1.2	0.91
Ap	1.34	0.34	0.67	0.34	0.3	
Total	99.17	98.30	98.46	99.30	95.1	99.42

Explanation of column headings:

1. Highly undersaturated lava of nephelinite family, Honolulu Series, Oahu, Hawaii (H. Winchell, *Geol. Soc. Am. Bull.* vol. 58, p. 30, no. 13, 1947).

2. Somewhat undersaturated olivine basalt, Haleakala volcano, Maui, Hawaii (G. A. MacDonald and T. Katsura, *J. Petrol.* vol. 5, p. 122, no. C-122, 1964).

3. Oversaturated basalt (tholeiite) Waianae volcano, Oahu, Hawaii (MacDonald and Katsura, *ibid.*, no. C-27, 1964).

4. Pyroxene andesite, northeastern Japan (Y. Kawano, K. Yagi, and K. Aoki, *Sci. Rept. Tohoku University*, ser. 3, vol. no. 1, p. 32, no. 70, 1961).

5. Trachyte, Main Range, Queensland, Australia (N. C. Stevens, *Proc. Royal Soc. Queensland*, vol. 87, no. 4, p. 46, no. 1965).

6. Hornblende-biotite granodiorite (granite) Mt. Hale, Southern California, Batholith (E. S. Larsen, *Geol. Soc. Amer. Mel* 29, p. 91, 1948).

Table IB 1. (CTV)
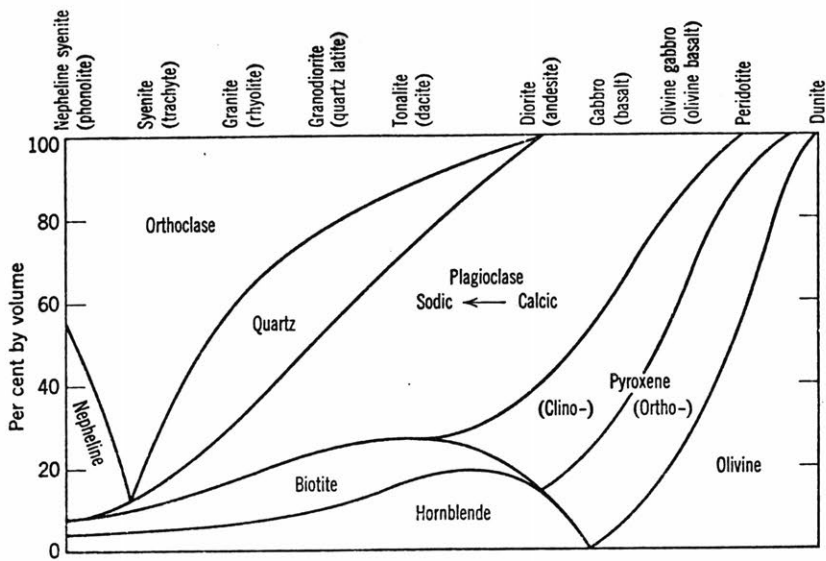
Approximate mineralogical composition of the commoner types of igneous rocks (effusive types in brackets).

Figure IB 1.
(Mason, 1966)
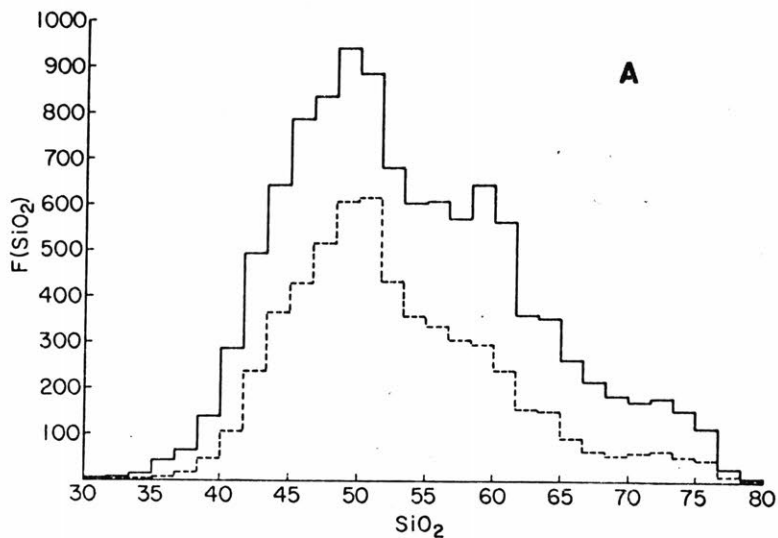
Distribution of SiO_2 in 10,870 analyses of Cenozoic volcanic rocks. (A) Solid line, all data; dashed line, 5697 analyses with $H_2O < 2$ and $Fe^{3+}/Fe^{2+} < 1$.

Figure IB 2.
(Chayes, 1975)
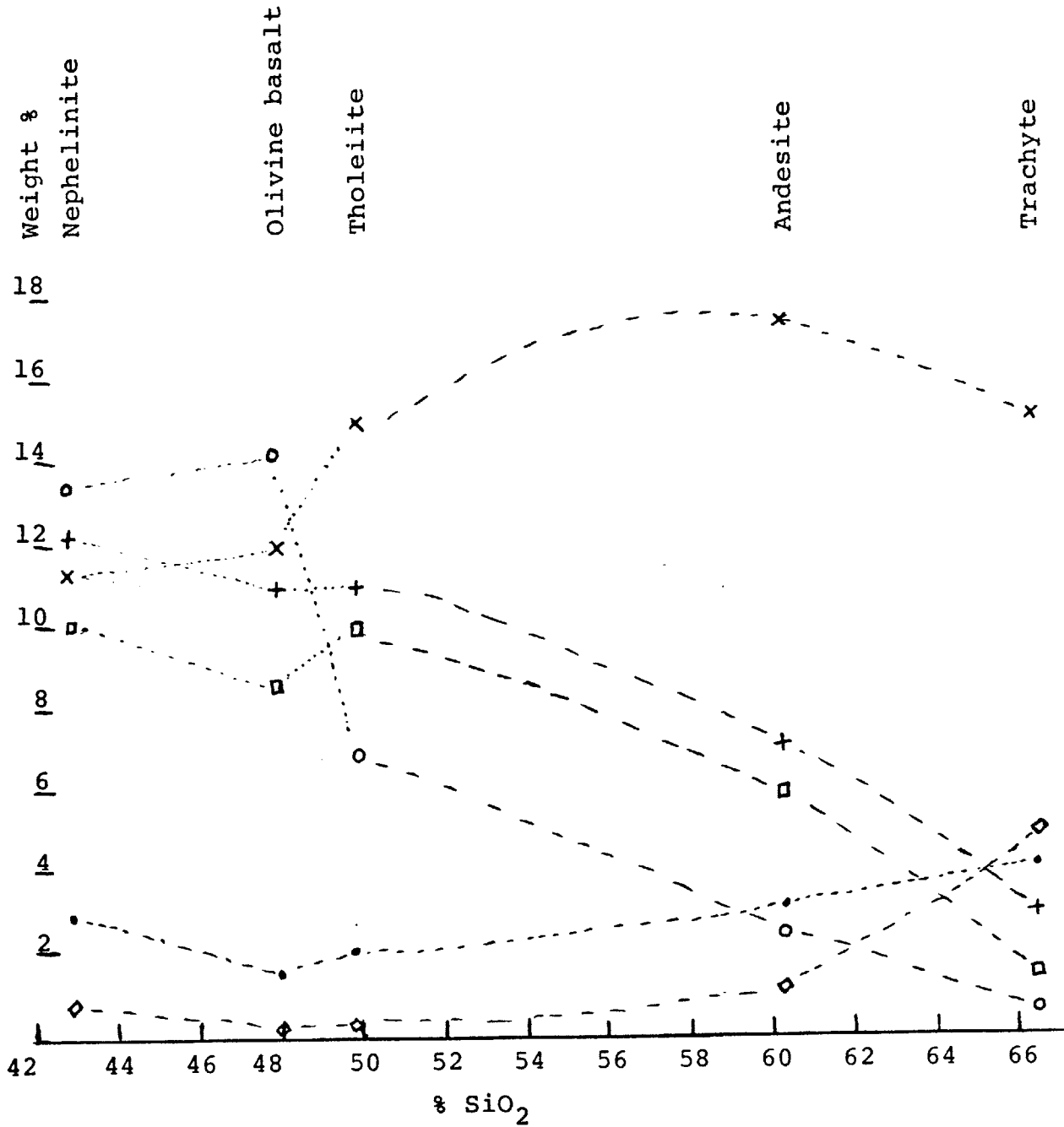
Figure IB-3   Variation diagram for representative igneous rocks

rocks of Table IB-1 illustrating the general geochemical relationship between the different rock types. As silica increases, iron, magnesium, and calcium decrease. Although SiO_2 content generally identifies basalts from other igneous rocks, it is not a parameter that readily distinguishes among the variety of basalt compositions. (Most terrestrial basalts, nevertheless, can be grouped into only a few magma types (see below), although the distinguishing boundaries become very diffuse upon closer inspection.)

The derivation of more silicic igneous rocks from basaltic magmas through fractional crystallization (e.g., removal of Mg, Fe-rich olivine, Fe-rich opaques, or Ca-rich plagioclase) is a fairly well accepted concept, although perhaps not universally applicable. Such a trend is generally compatible with the variation diagram of Figure IB-3. The sequence of mineral-liquid reactions that occur during crystallization was described by Bowen (1928) and forms the basis for many suggested series of differentiated rocks. Such a sequence suggests the relation of basalts to other more acidic igneous rocks is one of primary to secondary, or more extensively processed, material.

b. Magma types

In the early part of the century, Bowen (1928)

recognized and convincingly established the parental role

of basaltic magma. The Scottish island of Mull became a

case area where two main basaltic magma types were recognized.

Kennedy (1933) then described what appeared to be two world-

wide basaltic magma types: (1) olivine-basalt containing

(in addition to plagioclase) olivine, augite and alkali

feldspar, nepheline or zeolites; and (2) tholeiite basalt

containing pigeonite, augite and siliceous material. Oli-

vine basalt would lead to trachytes with differentiation

and tholeiites would lead to rhyolites.

Experimental studies of natural and synthetic

rock systems led Yoder and Tilley (1962) to describe a gen-

eralized simple basalt system that can be expressed in

terms of normative components (Figures IB-4a,b from Yoder

and Tilley). They further defined the chemistry of tholeiites

(normative hypersthene, with modal augite or subcalcic

augite, plagioclase, iron oxides, ± olivine, ± quartz)

and alkali basalt (normative nepheline and olivine and modal

high-Ca augite, plagioclase, olivine, and generally Na_2O

+ K_2O > 3%). An important criterion in their classifica-

tion is the degree of silica saturation, indicated by whether

or not quartz is present in the norms. Widely used termin-

ology for three commonly observed basalt compositions has

IB 65

Schematic representation of the system Di-Fo-Ne-Qz showing the plane of silica saturation, Di-En-Ab, and the critical plane of silica undersaturation, Di-Fo-Ab. This iron-free simple basalt system includes the principal components of the major phases of basalt.

Figure IB 4.
(Yoder and Tilley 1962)

Alkali Basalt Group   Olivine Tholeiite Group   Tholeiite Group

Exploded view of generalized simple basalt system illustrated in upper right inset. Entered are names of rocks whose major normative phases are contained in the tetrahedra. Names underlined are within tetrahedra. Names in faces are written parallel to base. Lherzolite is in Ol-Cpx-Opx face. An additional inset, Ol-Cpx-An, gives alternative nomenclature when plagioclase is rich in An.

emerged: (1) <u>tholeiite</u>--oversaturated with normative quartz and hypersthene; (2) <u>olivine tholeiite</u>--somewhat undersaturated, with normative hypersthene and olivine; and (3) <u>alkali basalt</u>--undersaturated with normative olivine and nepheline. Yoder and Tilley emphasized that there is a continuum between all basalt types even though at low pressures there is a thermal divide which roughly corresponds to the 'critical plane of silica undersaturation' (Fo-Ab-Di in Figure IB-4b). This equilibrium thermal divide, however, changes with pressure and the two basalt types may be related at depths with the alkali basalt type magma having a deeper source.

As pointed out by Carmichael et al. (1974) such simplified terminology is a geochemical convenience and does not necessarily imply the same origin for two rocks with similar gross chemistry. Not only do some basaltic materials seem out of place in such a universal classification, but the unique distinguishing characteristics of each basaltic province in reality defines an infinite number of basalt types.

If and how one variety of basaltic material is related to another is the subject of many professional papers, each with a (slightly) different emphasis. Yoder

(1976) has written a book to expand on the concept of how common pressure-temperature-dependent phase relations control the restriction of magma types. MacDonald (1968) summarized a variety of data linking the Hawaiian alkalic rocks with the main olivine tholeiites and concludes that crystal fractionation plays the major role. Engel et al. (1965) come to a similar conclusion. A grand scheme for the derivation of all basalt types was ambitiously described by Green (1971) involving different degrees of melting at different depths with and without water and with later fractionation (Figure 1B-5a,b from Green, 1971). Allowing variations through contamination and hybrid theories (e.g., Eichelberger, 1974; Moorbath and Welke, 1968) it is truely amazing that some real similarity does indeed exist allowing a gross classification of basalt magma types.

2. Basalt Types Associated with Specific Environments

Great volumes of magma are being extruded along the ocean rift zones as two lithosphere plates are separating. Such extrusion of volcanic material results from perhaps the most simple terrestrial plumbing system between source (presumably the mantle) and vent. The avenues that all other terrestrial basalt magmas take to reach the surface and the processes that occur along the way are less clearly understood but are certainly dependent on the geo-

IB 68
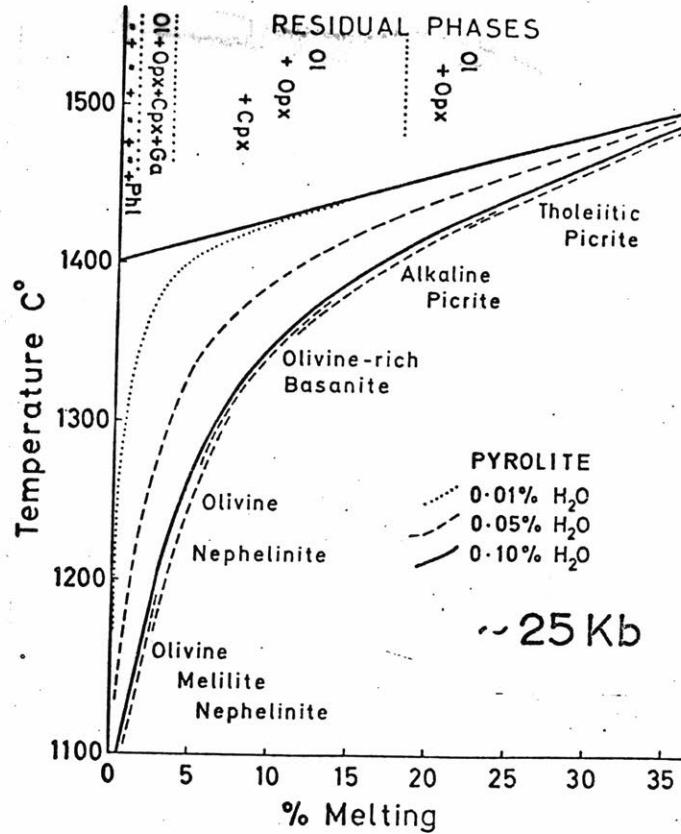
Partial melting of a "pyrolite" model of the upper mantle.
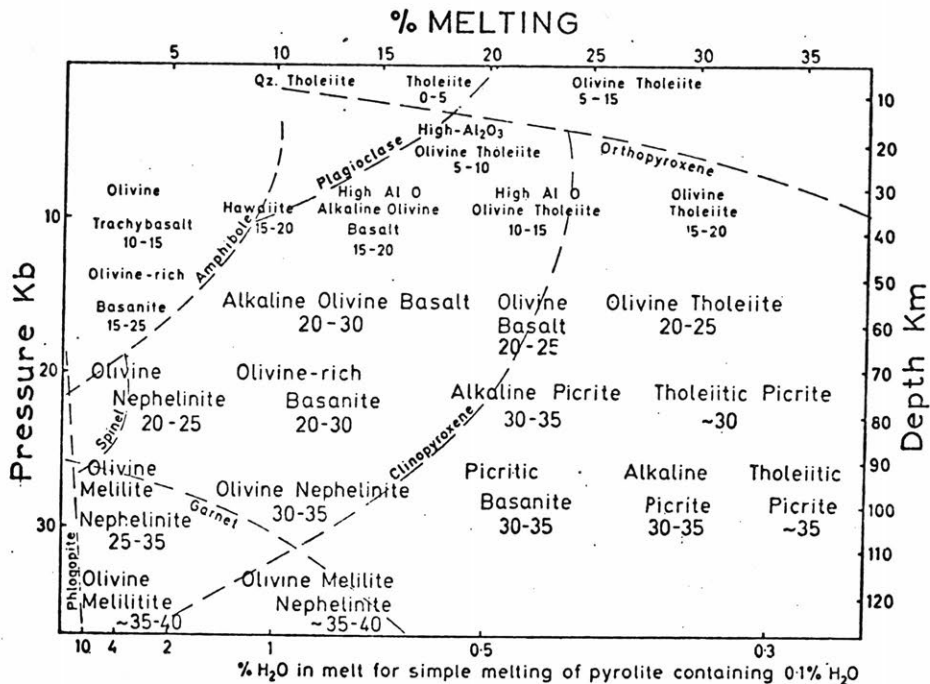
Figure IB 5. (from Green, 1971)

logical setting. The major basalt types and associations
that occur in particular terrestrial environments (summa-
rized in Figure IB-6, from McGetchin, 1975) are discussed
briefly below. Except as otherwise noted, the tables of
chemical composition and regional summaries are from Car-
michael et al. (1974), referred to a CTV.

  a. Ocean ridge and floor basalts

    Geochemical data accumulating over the last
few decades indicates that the rock type covering most of
the earth's surface (the ocean floor) is a young basalt
of distinctive and roughly universal composition: olivine
tholeiite (Engel et al., 1965; Kay et al., 1970). This
basaltic crust is formed at the spreading centers (ridges).

    The geochemistry of representative oceanic
tholeiites is presented in Tables IB-2a,b. In general,
these basalts are characterized by normative olivine, low
Fe_2O_3/FeO, low potassium, high K/Rb (700-1000), and very
low Sr^{87}/Sr^{86} (.7023-.70245, Tatsumoto et al., 1965; Hart,
1971). Oceanic tholeiites show a relative depletion of
large ion lithophile elements. The rare earth element pat-
tern is roughly chondritic but with the light rare earths
depleted--a pattern perhaps unique to the ocean ridge ba-
salts (Figure IB-7, from Gast, 1972). Al_2O_3 is variable

Tectonic Setting
of the
World's Volcanoes

3. Island Arc Subduction Zone

1. Mid-Ocean Ridge

2. Seamount Chain

4. Subduction of Ocean Crust Under Continental Margin

6. Continental Rift Zones

7. Mid-Continent Volcanism on Stable Platforms

5. Subduction of Continental Crust Under Continent

MID OCEAN VOLCANISM

SUBDUCTION ZONES

CONTINENTAL VOLCANISM
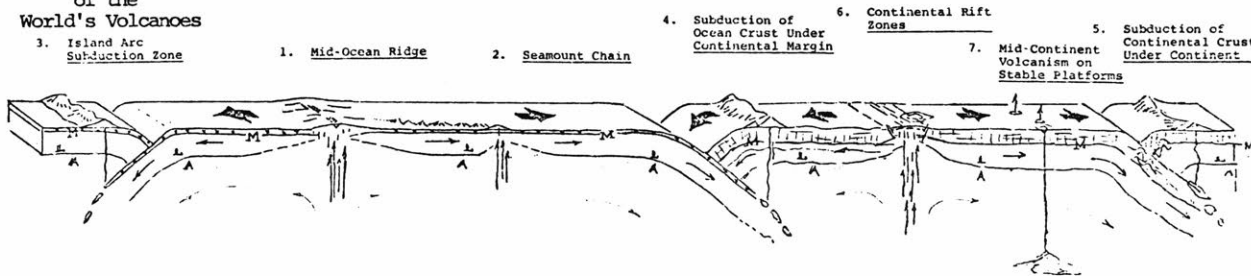
	Setting	Dominant Processes	Igneous Processes and Melting Mechanisms	Rock Types Produced	Structure and Style of Volcanism	Location and Example Volcano
1.	Mid-Ocean Ridge	Creation of oceanic crust-lithosphere; separation of oceanic lithosphere	Partial melting of the upper mantle upon adiabatic decompression in rising convection cell	Principally primitive oceanic basalts; locally andesitic types. Tholeiitic types	Effusive submarine flood basalts; rare supraoceanic volcanic shields with andesitic edifaces	Iceland - Hekla; Galapagos - Fernandino
2.	Seamount Chain	Local melting in mantle; redeposition due to transport of melt on surface	Partial melting of upper mantle due to transport over hot spot (plum) or due to decompression accompanying tensional rifts	Predominantly primitive oceanic basalts; minor alkalic basalts	Large shield volcanoes produced from effusive tholeiitic basalt flows capped with alkali basalt, largely pyroclastic	Hawaii - Kilauea Mauna Loa
3.	Island Arc	Destruction of oceanic crust by partial melting	Partial melting of downgoing slab; locally differentiation and contamination occur	Dominantly andesite; subordinate high Al-basalt	Andesite stratovolcanoes; long repose times and episodic violent explosive activity	Japan - Asama; W. Aleutians
4.	Continental Margin - Oceanic crust under continental crust	Destruction of oceanic crust by partial melting	Partial melting of downgoing slab; locally differentiation and contamination occur	Dominantly andesite; subordinate high Al-basalt (less basalt than #3, above)	Andesite stratovolcanoes; long repose times and episodic violent explosive activity	California - Shasta; Guatemala - Pacaya; Chile - Puyehue; Ecuador - Cotopaxi; E. Aleutians - St. Augustine
5.	Continental collision; continental crust under continental crust	Deformation and partial melting of continental crust	Partial melting downgoing slab; locally differentiation and contamination occur	Dominantly andesite; subordinate high Al-basalt (less basalt than #3, above)	Andesite stratovolcanoes; long repose times and episodic violent explosive activity	Italy - Etna Stromboli
6.	Continental rift zones	Separation of crust-lithosphere; and volcanism	Same as #1 but with partial melting of lower crust to produce acidic volcanics in addition	Bimodal suite of volcanic rocks. Basaltic suite like #1; rhyolitic suite produced by partial melting of crust	Effusive flood basalts; explosive rhyolitic ash and caldera complexes	New Mex. - Jemez; E. Africa - Erta ale
7.	Stable platform volcanism	Penetration of stable platforms by exotic volcanic types	Volatile-rich volcanism from within or below lithosphere; varying degree of partial melting	Generally exotic types - kimberlite carbonatite, alkalic basalts, lamprophyres. Deep seated source within the mantle; xenoliths common	Diatremes common explosive gas-charged eruptions. Breccia dikes and pipes common	Utah - Moses Rock; So. Africa - Kimberley Mine

Basalt   Oceanic crust   Continental Crust   Andesite
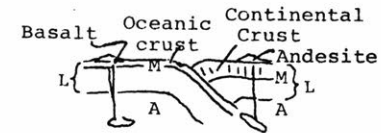
M = Mohorovicic discontinuity (Crust-mantle boundary)

L = Lithosphere (rigid plate)

A = Asthenosphere (plastic interior)

Tectonic setting of the world's volcanoes.

Figure IB 6.   (from McGetchin, 1975)

Chemical compositions (oxides, wt %) and CIPW norms of rocks from mid-Atlantic ridge

	1	2	3	4	5	6	7	8	9	10
SiO_2	49.20	49.02	49.27	47.94	49.00	47.50	49.70	48.65	43.15	48.56
TiO_2	2.03	1.46	1.26	0.75	1.46	1.83	1.49	1.44	2.70	0.24
Al_2O_3	16.09	18.04	15.91	17.45	15.50	16.00	14.85	15.99	13.46	18.69
Fe_2O_3	2.72	1.58	2.76	1.21			2.16	2.18	4.52	2.27
FeO	7.77	6.22	7.60	8.47	9.77	12.20	8.27	6.19	8.22	4.30
MnO	0.18	0.13	0.13	0.13	—	—	0.18	0.15	0.11	0.11
MgO	6.44	7.85	8.49	10.19	8.00	5.37	8.56	9.66	10.80	9.26
CaO	10.46	11.51	11.26	11.26	10.80	11.40	11.17	11.52	9.80	12.67
Na_2O	3.01	2.92	2.58	2.37	2.90	2.57	2.69	2.71	3.47	1.88
K_2O	0.14	0.08	0.19	0.09	0.21	0.49	0.15	0.57	1.63	0.07
P_2O_5	0.23	0.12	0.13	0.08	—	—	0.13	0.21	0.75	0.02
H_2O^+	0.70	0.64	0.35	0.23			0.61	0.75	1.21	1.72
H_2O^-	0.95	0.57	0.51	0.15	1.19	3.28	0.16	0.30	0.15	0.17
Total	99.92	100.14	100.44	100.32	98.83	100.64	100.12	100.32	99.97	99.96
Q	0.3									
or	0.8	0.5	1.1	0.6	1.27	2.96	1.11	3.34	9.63	0.56
ab	25.7	24.4	21.8	20.0	25.03	22.25	23.06	23.06	9.67	15.72
an	29.8	36.3	31.2	36.7	29.23	31.38	27.52	29.75	16.34	42.46
ne									10.67	
di	17.4	16.6	19.2	15.2	16.19	15.42	21.81	21.10	22.23	15.96
hy	16.2	7.7	13.6	4.5	9.14	6.63	13.19	1.26		14.07
ol		9.0	5.9	19.7	10.08	9.48	6.33	14.45	16.76	4.95
mt	4.0	2.3	4.0	1.8	2.22	2.22	3.25	3.25	6.55	3.25
il	3.8	2.7	2.4	1.4	2.83	3.56	2.89	2.74	5.13	0.46
ap	0.5	0.3	0.3	0.2	0.33	0.34	0.34	0.48	1.64	0.05
Total	98.5	99.8	99.5	100.1	96.32	94.24	99.50	99.43	98.62	97.48

Explanation of column headings

1 Oceanic tholeiite, depth 2910 m; 20°40′S, 13°16′W (Engel and Engel, 1964a, D2–1)
2 Oceanic tholeiite (diabase), depth 2388 m; 9°39′N, 40°27′W (Engel and Engel, 1964a, D5–5)
3 Oceanic tholeiite, depth 3566 m, rift floor; 28°53′N, 43°20′W (G. D. Nicholls, 1965, table 1, analysis 1)
4 High-alumina basalt, some locality as 3 (G. D. Nicholls, 1965, table 2, analysis 2)
5 Oceanic tholeiite, depth 4200 m, rift floor; 30°08′N, 43°37′W (Kay et al., 1970, analysis A150–21–1C)
6 Basalt, depth 3700 m; 31°49′N, 42°25′W (Kay et al., 1970, analysis GE160)
7 Basalt, depth 3700 m; 31°49′N, 42°25′W (Muir and Tilley, 1966, p. 195, analysis 3)
8 Basalt, depth 3600 m, rift floor; 45°44′N, 27°44′W (Muir and Tilley, 1964b, table 1, analysis 5)
9 Alkali olivine basalt, depth between 2000 and 3000 m; a few kilometers northeast of St. Paul's Rocks; 1°1′N, 29°21′W (Melson et al., 1967)
10 Laminated gabbro, depth 4000 to 5000 m, Romanche trench; 0°14′N, 17°7′W (Melson and Thompson, 1970)

Table   IB 2a.   (CTV)

Chemical compositions (oxides, wt %), CIPW norms,* and atomic abundances and abundance ratios of trace elements and isotopes of ocean-floor lavas, rises of East Pacific Ocean

	1	2	3	4	5	6		1a	3a	4a
SiO_2	49.80	49.13	48.30	59.00	49.90	50.10	Ba	25	19.4	54.8
TiO_2	2.02	1.23	2.19	1.75	1.08	2.18	Ce		16.5	75
Al_2O_3	14.88	14.97	· 14.30	12.60	17.30	13.80	Cs		0.074	0.082
Fe_2O_3	1.55	3.28	11.70	12.00	7.60	12.30	Co	35		
FeO	10.24	5.72					Cr	160		
MnO	0.21	0.16					Ni	58	58	10
MgO	6.74	7.68	6.70	1.70	7.08	6.11	Pb	0.49		
CaO	10.72	12.68	10.10	5.60	12.78	10.90	Rb	1.06	5	7.25
Na_2O	2.91	2.37	2.75	4.25	2.45	2.83	Sr	110 (86)	107	105
K_2O	0.24	0.16	0.18	0.65	0.18	0.16	Th	0.21		
P_2O_5	0.28	0.15					U	0.09		
H_2O^+	·0.54	1.06	1.29	1.78	0.80		V	400		
H_2O^-	0.06	1.25					Zr	150		
							K/Rb	1890	310	770
Total	100.19	99.84	97.51	99.33	99.17	98.38	Cs/Rb		0.014	0.011
							Th/U	2.3		
Q		0.79		13.66		0.04	Sr^{87}/Sr^{86}	0.7025		
or	1.1	0.89	1.10	3.92	1.08	0.96	Pb^{206}/Pb^{204}	18.24		
ab	24.6	20.01	24.08	36.70	20.99	24.25	Pb^{207}/Pb^{204}	15.53		
an	26.7	29.75	27.06	13.66	36.12	24.79	Pb^{208}/Pb^{204}	38.03		
di	22.0	25.73	19.59	11.84	21.90	23.96	U^{238}/Pb^{204}	6.4		
hy	13.7	12.79	17.73	14.27	13.16	19.27				
ol	5.7		3.54		2.12					
mt	2.3	4.76	2.25	2.22	2.20	2.20				
il	3.7	2.36	4.30	3.39	2.08	4.19				
ap	0.6	0.35	0.34	0.33	0.33	0.33				
Total	100.4	97.43	99.99	99.99	99.98	99.99				

* For analyses 3–6, norms are calculated (Kay et al., 1970) assuming a low state of oxidation of Fe (Fe_2O_3 = 1.50 percent) and reasonable values of MnO (0.18 percent) and P_2O_5 (0.15 percent).

Explanation of column headings

1 Glassy basalt, East Pacific rise, depth 2300 m; 12°52′S, 110°57′W (Engel et al., 1965, table 1, analysis PVD-3)

1a Trace-element and isotopic data for analysis 1 (Engel et al., 1965; Tatsumoto et al., 1965; Tatsumoto, 1966)

2 Basalt, Mohole drill core, depth 3746 m; off Guadalupe Island (East Pacific rise), 28°59′N, 117°30′W (Engel and Engel, 1961, p. 1799, analysis 1)

3, 3a Basalt, East Pacific rise, depth 3120 m; 7°08′N, 103°15′W (Kay et al., 1970, p. 1593, analysis V2023)

4, 4a "Andesite" glass, East Pacific rise, depth 3182 m; 5°31′S, 106°46′W (Kay et al., 1970, p. 1593, analysis V2140)

5 Basalt, Gordo rise, depth 2500 m; 41°15′N, 127°28′W (Kay et al., 1970, p. 1592, analysis 13E)

6 Basalt, Juan de Fuca rise, depth 2502 m; 44°36′N, 130°19′W (Kay et al., 1970, p. 1591, analysis 2C)

Figure IB 2b.   (CTV)

and sometimes high.

In spite of their general primary nature, most dredged basalts nevertheless show small compositional variations that are ascribed to shallow differentiation or fractionation in the ascending magma (Kay et al., 1970; Frey et al., 1974; Mazzullo and Bence, 1976). Removal of plagioclase and olivine at shallow depth from a mantle derived liquid would account for most of the observed major and minor element trends. For example, TiO_2 is concentrated in the more fractionated magmas (Figure IB-8, from Mazzullo and Bence).

Samples obtained from the fracture zones and aseismic ridges associated with the mid-Atlantic rift valley are more fractionated types of basaltic rocks than those from the rift itself (Hekinian and Thompson, 1976). The transform fault rocks are depleted in olivine and have a higher range of TiO_2 content. Variation diagrams for basalts from the mid-ocean ridge, fracture zones, and aseismic ridges are shown in Figure IB-9 (from Hekinian and Thompson). Some recovered rocks are gabbroic and may be part of an instrusive layer (Miyashiro et al., 1970).

The basalt cores obtained from the Atlantic floor away from the rift axis show no obvious systematic compositional differences as a function of distance from
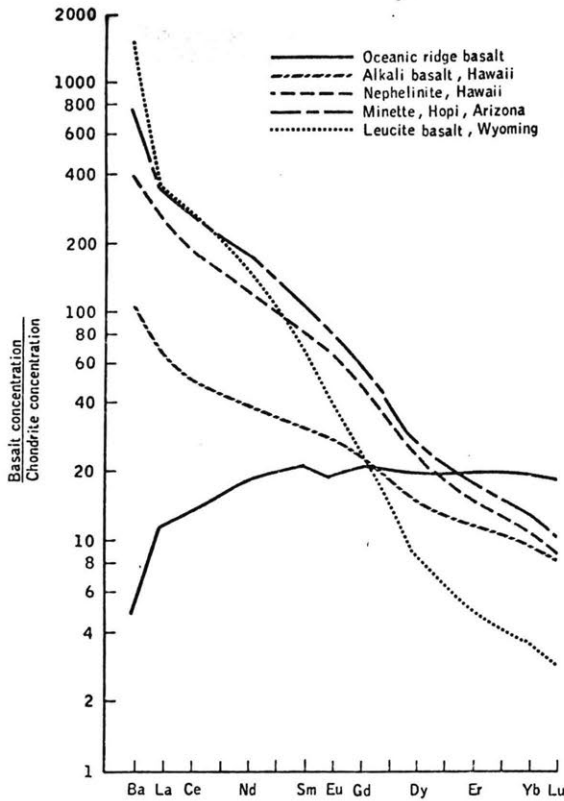
Chondrite normalized terrestrial LIL abundance patterns. Data are from Kay (1970),
Kay *et al.* (1970), and unpublished data. Uranium data on oceanic basalts
were furnished by Tatsumoto (personal communication).
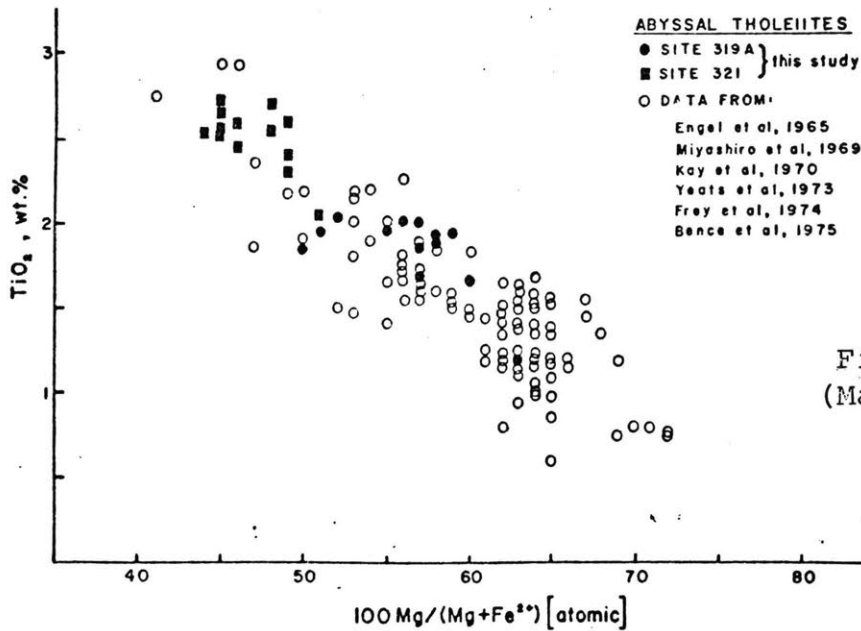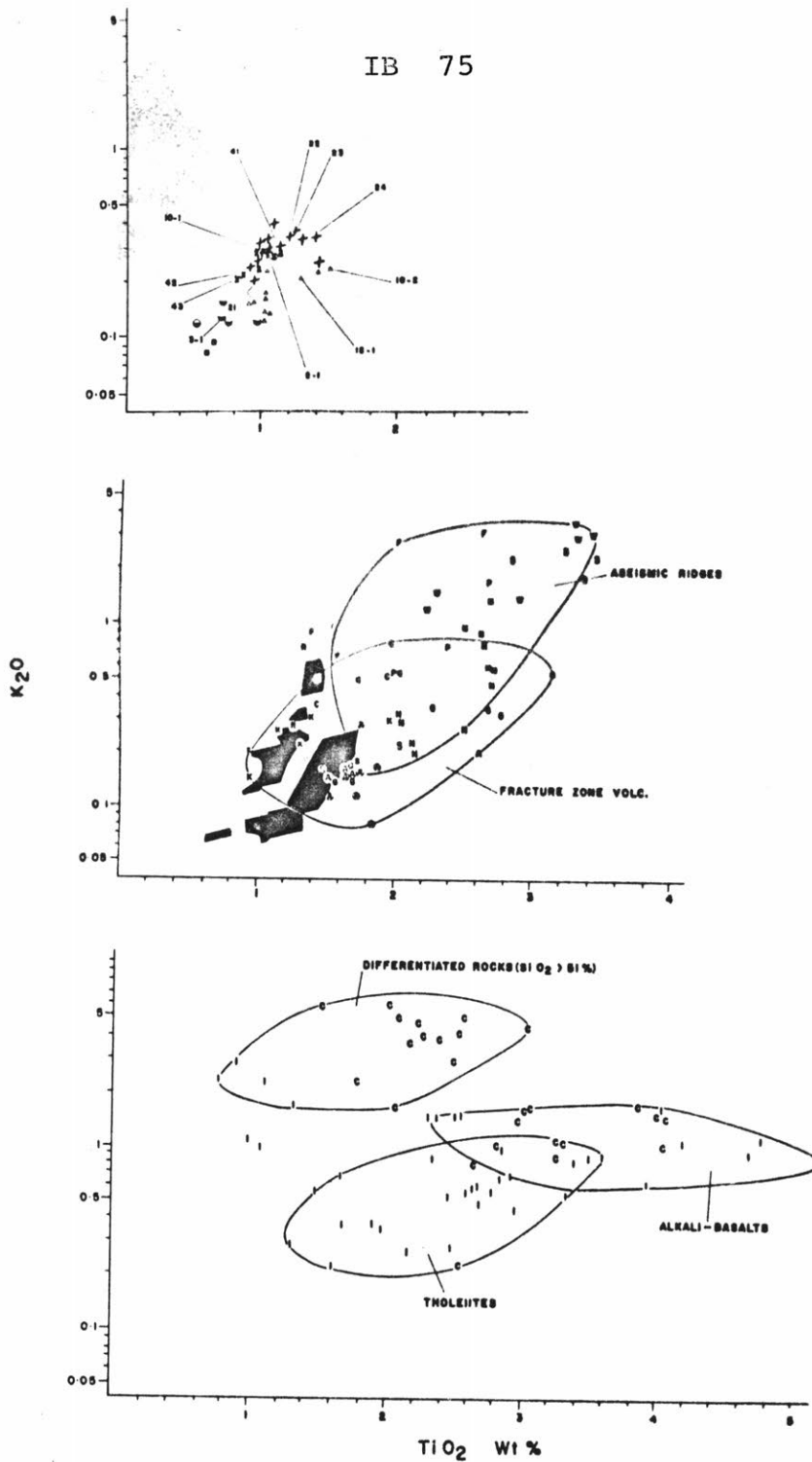
Figure IB 7.
(Gast, 1972)

Figure IB 8.
(Mazzullo and
Bence)

TiO_2 versus $Mg/(Mg + Fe^{2+})$ diagram, showing whole rock chemical data from leg 34 basalts **and**
additional data from other abyssal tholeiites. All data are plotted assuming $Fe^{3+}/(Fe^{3+} + Fe^{2+}) = 0.1$ (atomic).

K$_2$O-TiO$_2$ Variation diagram of basaltic and other differentiated rocks from various oceanic provinces. The top diagram represents the various types of basaltic rocks encountered near 36° 50′ N. The middle diagram shows the field of M.A.R. Rift Valley rocks (black area) compared to transform faults and aseismic ridge rocks. S, F, W and N indicate the volcanics from the Cocos, the Iceland-Faeroes, the Walvis and the Ninetyeast Ridge respectively. The bottom diagram shows the volcanics from Iceland (I) and those from the Azores (C). The alkali-basalts data are from Esenwein (1929), Sigvaldason (1969) and Thorarinson et al. (1973). The andesitic rocks are from Carmichael (1964) and from Girod (1972). The tholeiites are from Carmichael (1964) and from Sigvaldason (1969)

Figure IB 9.   (Hekinian and Thompson, 1976)

the ridge (Frey et al., 1974). No oceanic rock has been recovered older than Triassic and there is no indication that the source region for North Atlantic ridge basalts has evolved since the late Mesozoic. Because the Atlantic Ocean basement appears to be roughly spatially and temporally homogeneous and composed of large ion lithophile element depleted tholeiites, Frey et al. support the suggestion by Kay et al. that the source rock for this material (the upper mantle) is a (extensive) residue from an earlier melting event.

Although an increasing number of exceptions will be found (e.g., Bryan et al., 1976), it is clear from the data in hand that the major rock type that forms the oceanic crust is tholeiitic basalt depleted in large ion lithophile elements. The source of these basalts (the upper mantle) and the geological processes of formation, fractionation, and extrusion have produced on a global scale immense volumes of magma with roughly the same composition. Our understanding of these young oceanic basalts is closely associated with plate tectonics. It is unclear, however, whether any comparable terrestrial basaltic volcanism occurred prior to the breakup of the continents during the Triassic period.

b. <u>Ocean Islands</u>

The volcanic islands and seamounts that occur
in the ocean environment show a much more complicated var-
iation of chemistry than the great volumes of ocean floor
basalt. Almost all islands show a variety of igneous rock
types, the sequence of which can generally be interpreted
as differentiation series. Although a few trends are sim-
ilar in widely separated islands, it is clear that there
are significant differences in either the source composi-
tion, the melting conditions, or the sequence of processes
(including fractionation) that occur prior to extrusion.
For the discussion below, the volcanic island provinces
have been grouped according to whether the series of observed
rocks seem to follow a sequence with (i) tholeiite--rhyolite,
(ii) alkali basalt--trachyte--phonolite, or (iii) both.

i. THOLEIITE SERIES. Islands that occur on
or near a current oceanic ridge invariably consist to some
degree of tholeiitic basalt although the chemistry of such
basalts is not identical to the ocean ridge basalts. Po-
tassium is generally slightly higher for non-ridge tholeiites.
The rare earth element patterns of island basalts usually
show no depletion in LIL elements.

Iceland, centered on the Atlantic rift,
consists predominantly of oversaturated (olivine-free)

tholeiites (Carmichael, 1964). About 10% of the total
accumulation of volcanics is rhyolite and andesite. A low
pressure fractionation scheme is proposed from a parental
olivine tholeiite.

Olivine tholeiites also predominate on
Ascension Island (on the mid-Atlantic ridge) as well as
on a number of Pacific islands such as Guadalupe, Clarion,
and a few of the Samoan islands. Minor amounts of silicic
trachyte and andesite occur as associated volcanics for
these islands.

ii. ALKALI BASALT SERIES. Most of the non-
ridge oceanic islands and seamounts contain basalts enriched
in alkalies and undersaturated in silica. These alkali
basalts show a rare earth pattern regularly enriched in
the light rare earths (Figure IB-7). The associated rocks
(differentiates) are highly alkaline trachytes, phonolites,
or peralkaline rhyolites. A potassium variation diagram
(Figure IB-10 from Engel et al., 1965) shows a fairly sharp
distinction between the chemistry for these oceanic island
basalts and those from the ocean ridges.

Various rock series can be found on a num-
ber of ocean islands with alkali basalt magma generally
the hypothesized parent. One extreme, represented by the
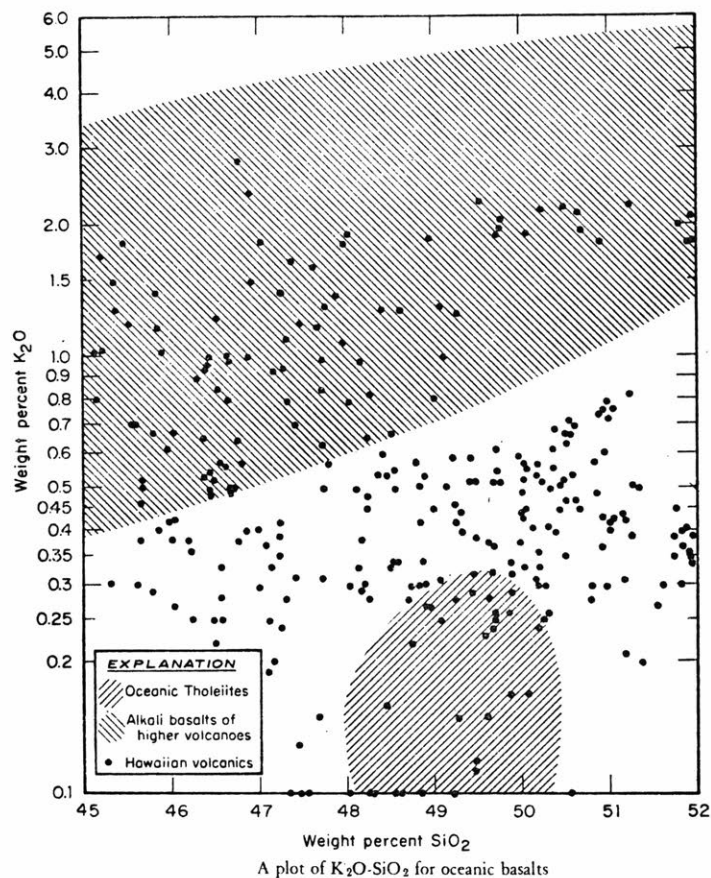islands of Trinidad and Fernando de Noronha, far off the

A plot of K_2O-SiO_2 for oceanic basalts

Figure IB 10. (Engel et al, 1965)

Chemical compositions (oxides, wt %) of volcanic rocks from Trinidade and Fernando de Noronha

	1	2	3	4	5	6	7	8	9
SiO_2	39.00	40.08	44.80	51.16	38.42	42.68	44.23	54.82	60.81
TiO_2	3.60	2.30	1.60	0.49	4.01	2.00	4.33	0.50	0.65
Al_2O_3	11.86	15.67	17.76	21.53	13.55	16.65	10.12	22.46	18.88
Fe_2O_3	6.20	6.75	5.55	2.64	3.32	5.08	3.50	1.84	2.57
FeO	9.55	5.17	3.81	1.86	9.40	8.11	6.58	0.72	0.00
MnO	0.19	0.15	0.20	0.07	0.21	0.20	0.18	0.12	—
MgO	12.31	4.49	3.47	0.68	12.54	5.57	11.70	0.07	0.61
CaO	10.40	10.60	7.80	1.92	11.75	11.00	11.45	1.42	1.70
Na_2O	3.68	6.49	6.87	10.53	3.72	5.04	3.20	10.22	6.20
K_2O	1.80	1.35	3.87	5.69	0.86	1.69	1.12	5.93	5.80
P_2O_5	0.55	1.40	0.88	0.05	1.01	0.67	0.78	0.12	
H_2O^+	0.50	3.40	1.10	1.72	1.15	0.52	2.04	0.82	
H_2O^-	0.30	2.20	2.30	0.45	n.d.	0.78	0.50	0.02	2.22
Cl				0.34				0.28	
SO_3				1.14			0.31*	0.98	
Total	99.94	100.05	100.01	100.27	99.94	99.99	100.04	100.32	99.44

* CO_2.

Explanation of column headings

1 Nephelinite (ankaratrite), Trinidade (Almeida, 1961, p. 168, table 19, no. 6)
2 Nephelinite, Trinidade (Almeida, 1961, p. 122, table 9, no. 1; p. 168, table 19, no. 10)
3 Sanidine nephelinite (grazinite), Trinidade (Almeida, 1961, p. 137, table 13, no. 1; p. 168, table 19, no. 17)
4 Phonolite (tinguaite), Trinidade (Almeida, 1961, p. 108, table 6, no. 3; p. 168, table 19, no. 24)
5 Nephelinite (ankaratrite), Fernando de Noronha (Almeida, 1955, p. 154, no. 30)
6 Alkali basalt, Fernando de Noronha (Almeida, 1955, p. 150, no. 18)
7 Nepheline basanite, Fernando de Noronha (W. C. Smith and Burri, 1933, p. 430; Almeida, 1955, p. 150, no. 19)
8 Sodalite phonolite, Fernando de Noronha (W. C. Smith and Burri, 1933, p. 412; Almeida, 1955, p. 145, no. 3)
9 Trachyte, Fernando de Noronha (Almeida, 1955, p. 147, no. 10)

Table IB 3. (CTV)

coast of Brazil, is a nepheline--phonolite series. All
of the rocks are exceptionally high in alkali and low in
silica and contain high normative nepheline (Table IB-3).
Another extreme is represented in the rocks of Tristan de
Cunha (Table IB-4) where alkali basalts exist in only minor
amounts relative to the (differentiated) trachybasalts
and trachytes that are greatly enriched in potassium (and
thus, Rb, Ba, Sr, Th and U).

More typical (?) of the oceanic alkaline
basalt series are the rocks of St. Helena (Baker, 1969)
an island about 800 km east of the mid-Atlantic ridge.
Alkali basalts make up ~70% of exposed rock generally fol-
lowed by mugearites, trachytes, and phonolites (Table IB-5).
Chemical variation diagrams (Figure IB-11a,b,c,) are con-
sistent with a fractional crystallization model (early →
late: olivine, chrome spinel, pyroxene, plagioclase, al-
kali feldspar) of parental alkali olivine basalt liquid
(or + ab + ne = 35).

iii. THOLEIITE--ALKALI BASALT ASSOCIATIONS.
Although tholeiites and alkali basalts appear to be distinct
and separate parental material in a wide variety of oceanic
environments, there are also significant oceanic provinces
where they are not only both present, but perhaps related.

Galapagos. The currently active Galapagos

Chemical compositions (oxides, wt %), CIPW norms, and atomic abundances (ppm) of trace elements in volcanic rocks of Tristan da Cunha (P. E. Baker et al., 1964) and Gough Island (Le Maitre, 1962, table 10)

	1	2	3	4	5	6	7
SiO$_2$	42.43	46.01	54.95	58.0	47.73	48.79	54.41
TiO$_2$	4.11	2.19	1.58	1.2	3.30	3.18	1.67
Al$_2$O$_3$	14.15	16.84	19.63	19.5	15.53	17.39	17.37
Fe$_2$O$_3$	5.84	7.61	1.62	1.7	2.02	2.48	4.02
FeO	8.48	5.37	3.31	2.2	8.95	7.39	3.29
MnO	0.17	0.18	0.18	0.1	0.14	0.10	0.12
MgO	6.71	4.75	1.42	1.0	8.37	4.00	2.27
CaO	11.91	9.36	5.73	3.3	8.71	8.97	4.36
Na$_2$O	2.77	3.74	5.89	6.5	2.89	3.28	4.94
K$_2$O	2.04	2.72	4.95	5.3	1.70	2.28	4.69
P$_2$O$_5$	0.58	1.18	0.43	0.2	0.29	0.26	0.46
H$_2$O$^+$	0.34	0.01	0.00	0.2	0.18	0.98	0.86
H$_2$O$^-$	0.44	0.08	0.01	0.1	0.06	0.76	1.50
Total	99.97	100.04	100.05*	99.3	99.87	99.86	100.09†
or	12.06	16.08	29.27	31.33	10.01	13.34	27.80
ab	6.95	21.63	29.99	40.12	24.10	27.77	39.30
an	20.16	21.13	13.57	8.38	24.46	26.13	11.40
ne	8.93	5.43	9.66	8.06			1.42
di	28.01	13.73	9.60	5.36	13.69	13.57	5.19
hy					0.86		
ol	5.48	4.03	0.94	0.55	16.57	6.99	2.40
mt	8.47	11.03	2.34	2.46	3.02	3.71	5.80
il	7.81	4.16	3.00	2.28	6.23	6.08	3.19
ap	1.37	2.78	1.01	0.47	0.67	0.67	1.34
Total	99.24	100.00	99.38	99.01	99.61	98.26	97.84

	1a	2a	3a	4a	5a	6a	7a
Ba	750	950	1200	1000	800	700	1400
Co	40	20			22	100	5
Cr	65	18			220	100	
Li	4	4	10	15	16	5	7
Ni	50				100	30	2
Pb	10	18	14	28			
Rb	110	110	230	350	100	40	100
Sr	1000	1100	1300	650	650	1000	850
V	400	200	95	50	140	250	80
Zr	200	300	350	350	125	220	450

* Including Cl = 0.27, F = 0.08.
† Including F = 0.13.

Explanation of column headings

Numbers in parentheses refer to specimen numbers in sources cited.

1, 1a   Alkali basalt (6), Tristan da Cunha
2, 2a   Trachybasalt (369), Tristan da Cunha
3, 3a   Trachyandesite (657), Tristan da Cunha
4, 4a   Trachyte (560), Tristan da Cunha
5, 5a   Olivine basalt (G111), Gough Island
6, 6a   Trachybasalt (G22), Gough Island
7, 7a   Trachyandesite (G86), Gough Island

Table IB 4.   (CTV)

Chemical composition (oxides, wt %), CIPW norms, and atomic abundances (ppm) of trace elements of volcanic rocks of St. Helena (I. Baker, 1969, table 2) and Mauritius (Shand, 1933)

	1	2	3	4	5	6		1a	2a	3a	4a
SiO_2	45.50	54.88	59.64	59.92	46.90	60.69	Ba	290	790	1100	1100
TiO_2	3.44	1.11	0.42	0.06	3.31	0.15	Cr	36			
Al_2O_3	15.71	17.41	17.67	19.86	15.05	19.74	Rb	40	50	90	220
Fe_2O_3	3.61	2.44	2.59	1.69	1.11	1.92	Sr	510	545	280	85
FeO	8.64	6.79	3.92	1.70	10.46	2.33	Zr	195	490	645	1085
MnO	0.22	0.23	0.22	0.18	0.16	0.17					
MgO	5.37	1.88	0.50	0.05	8.41	0.01	Rb/Sr	0.08			
CaO	9.43	3.48	2.09	1.07	10.92	1.02	K/Rb	300	400	350	180
Na_2O	3.47	6.04	7.62	8.94	3.13	7.95					
K_2O	1.38	2.89	4.02	4.93	0.27	5.50					
P_2O_5	0.29	0.41	0.29	0.17	Tr.	Tr.					
H_2O^+	0.60	0.77	0.08	0.07	0.27	0.58					
H_2O^-	2.49	1.53	1.04	1.29	0.23	0.28					
Total	100.15	99.86	100.10	99.93	100.22	100.34					
or	8.16	17.08	23.76	29.14	1.67	32.80					
ab	24.79	51.07	53.68	46.68	23.35	47.16					
an	23.22	11.86	2.14		26.13	1.67					
ne	2.48	0.02	5.85	15.18	2.27	10.79					
ac				0.83							
di	15.97	0.32	6.65	4.29	21.84	2.97					
ol	9.60	10.15	1.96	0.03	16.74	1.81					
mt	5.23	3.54	3.76	2.04	1.62	2.55					
il	6.53	2.11	0.80	0.11	6.23	0.30					
ap	1.42	1.82	0.19	0.17	—	—					
Total	97.40	97.97	98.79	98.47	99.85	100.05					

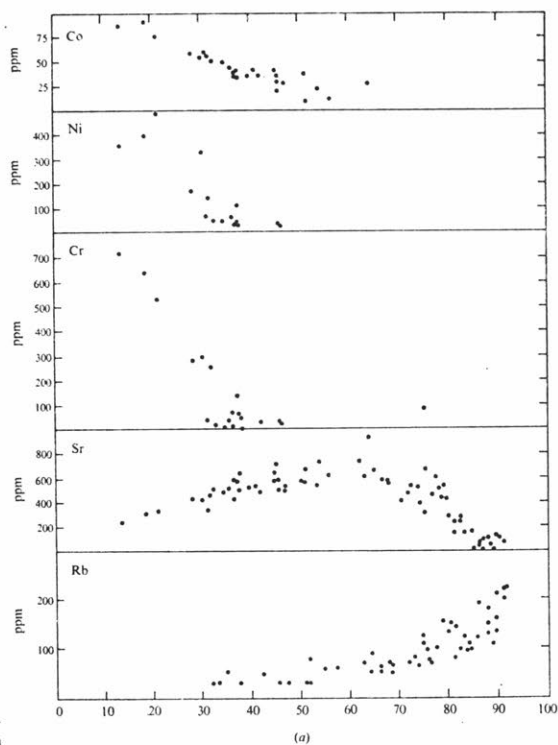*Explanation of column headings*

1, 1a   Basalt, St. Helena (803)
2, 2a   Mugearite (trachyandesite), St. Helena (822)
3, 3a   Trachyte, St. Helena (763)
4, 4a   Phonolite, St. Helena (11)
     5   Olivine basalt, Mauritius (A, p. 5)
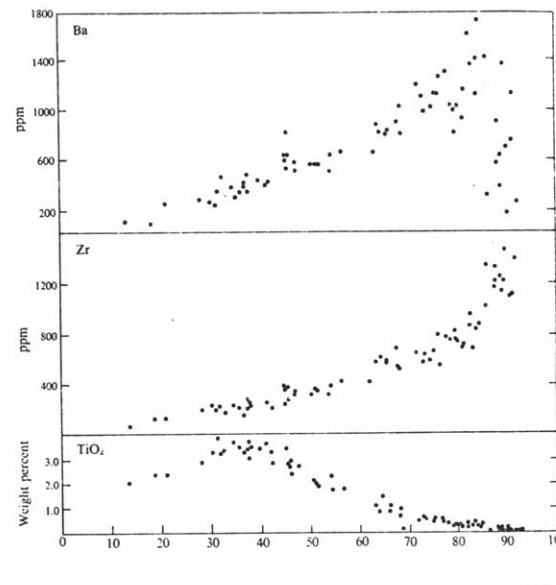   6   Phonolitic trachyte, Mauritius (A, p. 8)

Table IB 5. (CTV)
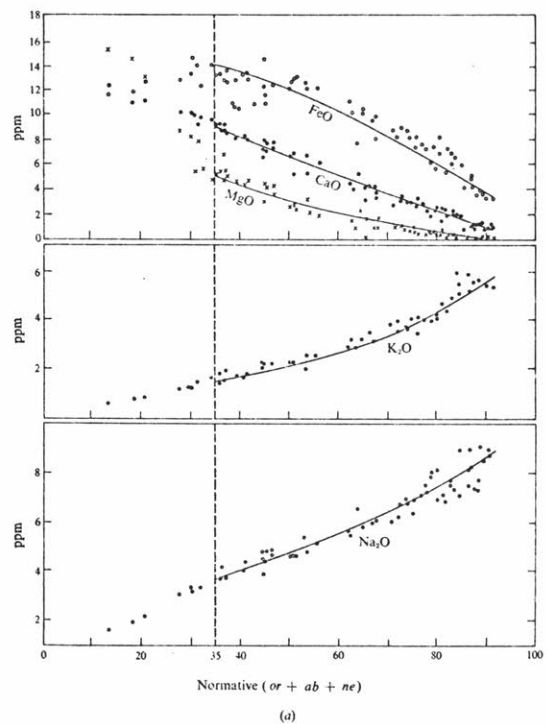
Chemical variation in lavas of St. Helena (data from I. Baker, 1969). Total iron plotted as FeO.

Trace- and minor-element variation in lavas of St. Helena. (Data from I. Baker, 1969.) Abundances (ppm) plotted against normative (or + ab + ne). (a) Co, Ni, Cr, Sr, Rb.

Figure IB 11.   (CTV)

islands are located on a platform (1.5 km below sea level)
east of the East Pacific Rise. The islands are composed
predominantly of basalts (Table IB-6) that range from slightly
saturated tholeiites to alkali basalts (McBirney and Williams,
1969) but that are spatially separated. Alkali basalts
make up the central and eastern islands whereas tholeiitic
lavas and their derivitive trachytes made up the western
islands.

Hawaii. The Hawaiian Islands are a series
of volcanoes extending into the Emperor Seamounts that
form a line along the central floor of the Pacific plate,
increasing in age towards the west (Figure 1B-12; from
Dalrymple et al., 1973). Due to the great diversity of
rock types found on the islands and the constant level
of recent activity, Hawaii has become a testing ground for
many studies of terrestrial basalts. The age of the ocean
floor in this part of the Pacific is about 100 million years
(Larson and Chase, 1972). Most investigators agree that
the origin of the Hawaiian chain is due to the relative
motion of the Pacific plate and some melting zone within
the mantle, which has been active for at least 50 m.y. (for
a review of proposed hypothesis concerning this melting
zone, see Dalrymple et al., 1973). From estimates of ex-
trusion rates, Mauna Loa could have grown to its present

Chemical compositions (oxides, wt %), CIPW norms, and atomic abundances of trace elements; volcanic rocks of western Galápagos

	1	2	3	4	5		2a	4a
SiO_2	47.01	48.45	48.54	55.34	66.87	Ba	76	285
TiO_2	3.20	3.39	4.20	1.93	0.66		(65)	(280)
Al_2O_3	15.57	13.75	14.49	14.02	12.55	Co	55	54
Fe_2O_3	2.32	4.72	4.67	3.31	1.84	Cr	47	17
FeO	11.57	8.60	9.16	8.73	2.53		(142)	
MnO	0.20	0.20	0.16	0.17	0.09	Mn	1440	1600
MgO	5.25	6.05	4.58	2.71	0.60	Ni	70	14
CaO	9.77	10.71	8.29	6.54	1.10	Sr	235	250
Na_2O	3.00	2.79	3.58	4.54	5.32		(323)	(266)
K_2O	0.31	0.50	0.84	1.33	3.08	V	310	98
P_2O_5	0.32	0.36	0.47	0.65	0.05	Zr	(255)	(538)
H_2O^+	1.40	0.36	0.68	0.64	4.66			
H_2O^-	0.24	0.02	0.16	0.18	0.33			
Total	100.16	99.90	99.82	100.09	99.68			
Q	—	2.21	2.04	5.95	20.82			
or	1.83	2.95	4.96	7.86	18.20			
ab	25.39	23.61	30.29	38.42	45.02			
an	28.10	23.52	20.99	13.95	1.27			
di	15.17	22.00	13.86	11.97	3.24			
hy	11.92	11.12	11.00	11.16	2.15			
ol	5.93	—	—	—	—			
mt	3.36	6.84	6.77	4.80	2.67			
il	6.08	6.44	7.98	3.67	1.23			
ap	0.76	0.75	1.11	1.54	0.12			
Total	98.54	99.44	99.00	99.32	94.72			

Explanation of column headings

1   Basalt, Albemarle Island (McBirney and Williams, 1969, p. 124, table 3, no. 8)

2   Tholeiitic basalt, Albemarle Island (McBirney and Williams, 1969, p. 121, table 2, no. 63)

3   Ferrobasalt, Jervis Island (McBirney and Williams, 1969, p. 147, table 10, no. 65)

4   Icelandite, Duncan Island (McBirney and Williams, 1969, p. 146, table 10, no. 71).

5   Siliceous trachyte pumice, Alcado volcano, Albemarle Island (McBirney and Williams, 1969, p. 146, table 10, no. 130)

2a, 4a   Trace-element abundances, same rocks as analyses 2 and 4. Determinations by emission spectrography. Values in parentheses determined by neutron activation (Cr) or x-ray fluorescence (Ba, Sr, Zr).

Table IB 6.   (CTV)
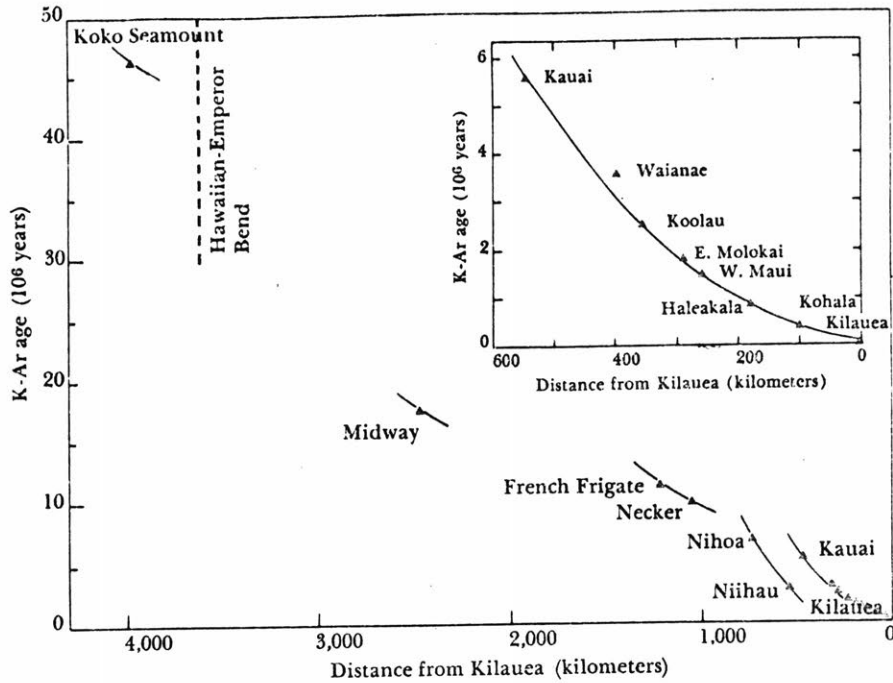
Potassium-argon age of tholeiitic volcanism on the Hawaiian-Emperor chain as a function of distance from Kilauea. Inset shows the detailed relations for the principal Hawaiian islands. Lines connect ages of shield volcanoes that lie on common or adjacent loci. Although the ages of the volcanoes increase more or less systematically to the northwest along the chain, the age-distance relations are not linear. (Data from McDougall 1964; Dalrymple 1971; Doell and Dalrymple 1973; McDougall and Swanson 1972; Clague and Dalrymple 1973; and unpublished data of the U.S. Geological Survey.)

Figure IB 12.   (Dalrymple et al., 1973)

size (about 9 km above the ocean floor) in 1.5 million years

(MacDonald and Abbot, 1970) and the smaller Kilauea could

have required less than .4 my (Swanson, 1972).

The lavas forming the islands

follow a well-defined sequence: the major mass of each

volcano is made up to tholeiites, followed by and interbedded

with small amounts ($\sim$1%) of alkalic lavas (Table IB-7 from

MacDonald, 1968). After a period of volcanic quiescence,

nephelinic magmas are erupted. No sharp chemical boundary

exists between these three major rock suites as is demon-

strated by the alkali variation diagram of Figure IB-13

(from MacDonald, 1968) and the potassium variation diagram

in Engel et al. (Figure IB-10). When fewer data were avail-

able, the vague distinction between alkali and tholeiitic

basalts was originally believed to be a sharp chemical

boundary (Tilley, 1950).

Short-term fractionation trends within

a given suite of rocks is rarely disputed for Hawaiian lavas.

Although the dominant material that makes up the volcanoes

is a slightly saturated tholeiite, it is largely agreed (e.g.,

O'Hara, 1965; MacDonald, 1968; Carmichael et al., 1974)

that the primary magma type was olivine tholeiite with much

of the olivine lost either during the assent from the source

($\sim$60km) or during fractionation in a near surface magma

AVERAGE COMPOSITIONS OF HAWAIIAN LAVAS

Type of rock	Tholeiitic suite		Alkalic suite							Nephelinic suite					
	Oceanite	Tholeiite and olivine tholeiite	Ankaramite	Alkalic olivine basalt	Feldspar-phyric basalt	Hawaiite	Mugearite	Benmoreite	Soda trachyte	Alkalic olivine basalt (basanitoid)	Basanite	Mimosite	Nephelinite	Ankaratrite	Melilite nephelinite
Number of analyses	14	200	9	35	6	62	23	5	5	11	11	4	10	1	7
SiO_2	46.4	49.4	44.1	45.4	46.6	47.9	51.6	57.1	61.7	44.8	44.1	41.3	39.7	39.4	36.6
Al_2O_3	8.5	13.9	12.1	14.7	16.8	15.9	16.9	17.6	18.0	12.7	12.7	10.4	11.4	10.2	10.8
Fe_2O_3	2.5	3.0	3.2	4.1	4.5	4.9	4.2	4.8	3.3	3.2	3.6	5.6	5.3	6.5	5.7
FeO	9.8	8.5	9.6	9.2	8.1	7.6	6.1	3.0	1.5	9.4	9.1	8.3	8.2	7.0	8.9
MgO	20.8	8.4	13.0	7.8	5.8	4.8	3.3	1.6	0.4	11.4	11.2	13.8	12.1	14.1	12.6
CaO	7.4	10.3	11.5	10.5	9.3	8.0	6.1	3.5	1.2	11.4	10.6	12.1	12.8	12.3	13.6
Na_2O	1.6	2.2	1.9	3.0	3.2	4.2	5.4	5.9	7.4	2.7	3.6	2.8	3.8	2.7	4.1
K_2O	0.3	0.4	0.7	1.0	0.8	1.5	2.1	2.8	4.2	0.9	1.0	0.9	1.2	1.2	1.0
TiO_2	2.0	2.5	2.7	3.0	3.3	3.4	2.4	1.2	0.5	2.3	2.6	2.7	2.8	3.3	2.8
P_2O_5	0.2	0.3	0.3	0.4	0.4	0.7	1.1	0.7	0.2	0.5	0.5	0.7	0.9	0.8	1.1
MnO	0.2	0.2	0.2	0.2	0.2	0.2	0.2	0.2	0.2	0.2	0.2	0.2	0.2	0.1	0.1
$FeO:Fe_2O_3$	4.0	2.8	3.0	2.2	1.8	1.6	1.4	0.6	0.4	2.9	2.5	1.5	1.5	1.1	1.6

TABLE 8. (CONTINUED)

NORMS (CIPW)

|		Oceanite	Tholeiite	Ankaramite	Alkalic ol. basalt	Feldspar-phyric	Hawaiite	Mugearite	Benmoreite	Soda trachyte	Alkalic ol. basalt	Basanite	Mimosite	Nephelinite	Ankaratrite	Melilite neph.
Q		....	2.2	....	....	....	....	....	....	....	....	....	....	....	....	....
or		1.7	2.2	3.9	6.1	5.0	8.9	12.2	16.7	25.0	5.6	6.1	5.6	....	....	....
ab		13.1	18.3	11.5	20.4	27.2	35.1	45.6	49.8	62.4	12.1	11.0	2.6	....	....	....
an		15.6	27.0	22.5	23.6	28.9	20.0	15.8	12.8	3.3	19.7	15.6	13.1	10.6	12.2	8.1
ne		....	....	2.6	2.6	....	0.3	....	....	....	6.0	10.5	11.4	17.3	12.2	18.7
lc		....	....	....	....	....	....	....	....	....	....	....	....	5.7	5.7	4.8
di	wo	8.5	9.3	13.6	10.8	6.0	6.3	2.9	....	0.7	13.9	13.9	17.6	17.5	18.1	11.4
di	en	6.1	6.0	9.4	6.9	4.0	4.2	2.5	....	0.6	9.2	9.5	13.4	13.0	15.0	8.3
di	fs	1.6	2.6	3.0	3.2	1.6	1.6	....	....	....	3.7	3.3	2.4	2.8	0.8	2.0
hy	en	12.7	14.9	....	....	4.4	....	2.7	4.0	0.4	....	....	....	....	....	....
hy	fs	3.2	6.6	....	....	1.8	....	....	....	....	....	....	....	....	....	....
ol	fo	23.2	....	16.2	8.8	4.3	5.5	2.1	....	....	13.5	13.0	14.8	12.0	14.3	16.2
ol	fa	6.3	....	6.0	4.4	2.1	1.2	....	....	....	5.8	4.9	3.2	2.9	1.0	4.0
cs		....	....	....	....	....	....	....	....	....	....	....	....	1.7	....	7.6
mt		3.5	4.4	4.6	6.0	6.5	7.2	1.9	7.0	4.2	4.6	5.3	8.1	7.7	9.5	5.5
il		3.8	4.7	5.2	5.8	6.2	6.5	4.6	2.3	0.9	4.4	5.0	5.6	5.3	6.2	5.3
ap		0.3	0.7	0.7	1.0	1.0	1.7	2.7	1.7	0.3	1.3	1.3	1.7	2.0	2.0	2.7
c		....	....	....	....	....	....	....	0.2	....	....	....	....	....	....	....

Table IB 7. (Macdonald, 1968)
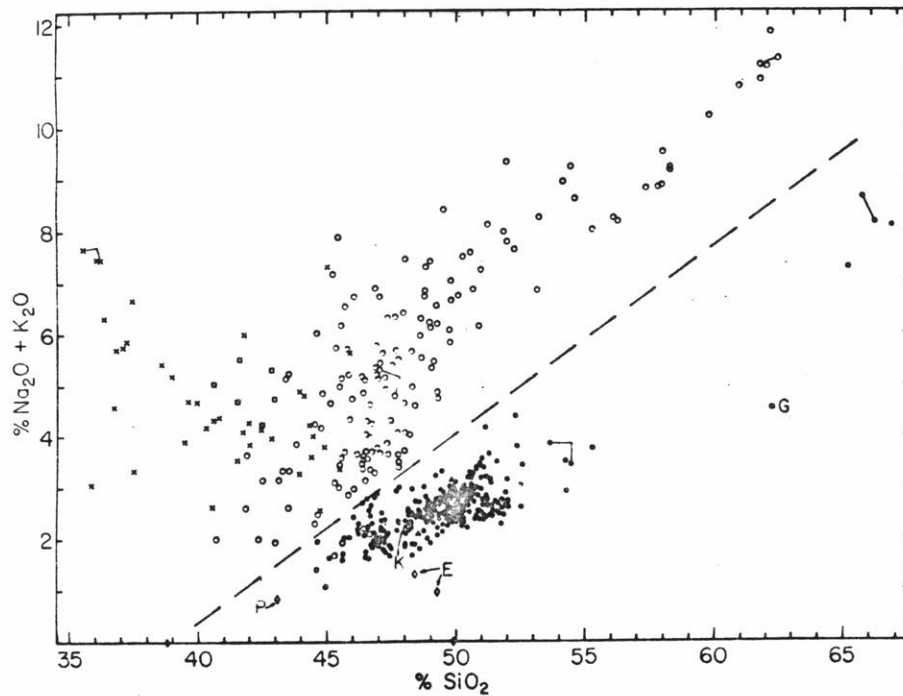
Alkali:silica diagram of Hawaiian rocks. Solid circles, tholeiitic rocks; open circles, rocks of the alkalic suite; crosses, posterosional rocks of the nephelinic suite; G, granophyre associated with the Palolo quartz diabase; open triangles, low-K tholeiites of the deep Pacific basin (Engel and others, 1965); K, weighted average of first phase of 1959 eruption of Kilauea (Murata and Richter, 1966); P, pyrolite (Green and Ringwood, 1963); E, "eclogite" inclusions from Salt Lake tuff (Yoder and Tilley, 1962, p. 482; Macdonald and Katsura, 1964, p. 123). The pairs of points connected by lines represent analyses of the same rock powder by two different laboratories.

Figure IB 13.   (Macdonald, 1968)

chamber. Magma chambers are known to exist for the two
most recently active volcanoes: for Kilauea it is estimated
to be 3-5 km below the current summit, whereas for Mauna
Loa the chamber is deeper--10-15 km (e.g., Wright and Fiske,
1971; Lipman, 1977). There is no obvious link in the plumb-
ing of these two neighboring volcanoes. The chemistry of
a series of summit and flank eruptions for Kilauea was stu-
died by Wright and Fiske (1971) and showed clear olivine
fractionation control which presumably occurred largely
in the magma chamber (Figure IB-14 from Wright and Fiske).
Rift lavas show distinct fractionation from parental summit
material.

There is less agreement as to the relation
between the various rock suites. The regularity of the
tholeiite--alkali basalt--nepheline basalt sequence, the
gradational geochemistry of these basalt types and their
similarity in Sr^{87}/Sr^{86} (Table IB-8) indicate that they
are related in some way. The processes involved in their
petrogenesis must be repeatable. Green and Ringwood (1967)
and Green (1971) have stressed results from experimental
studies that the composition of a partial melt is greatly
controlled by conditions of pressure, temperature, and water
content in the source region. Their 'pyrolite' models of
the upper mantle (peridotite composition) can produce mag-
mas of tholeiitic or alkaline composition by changing the
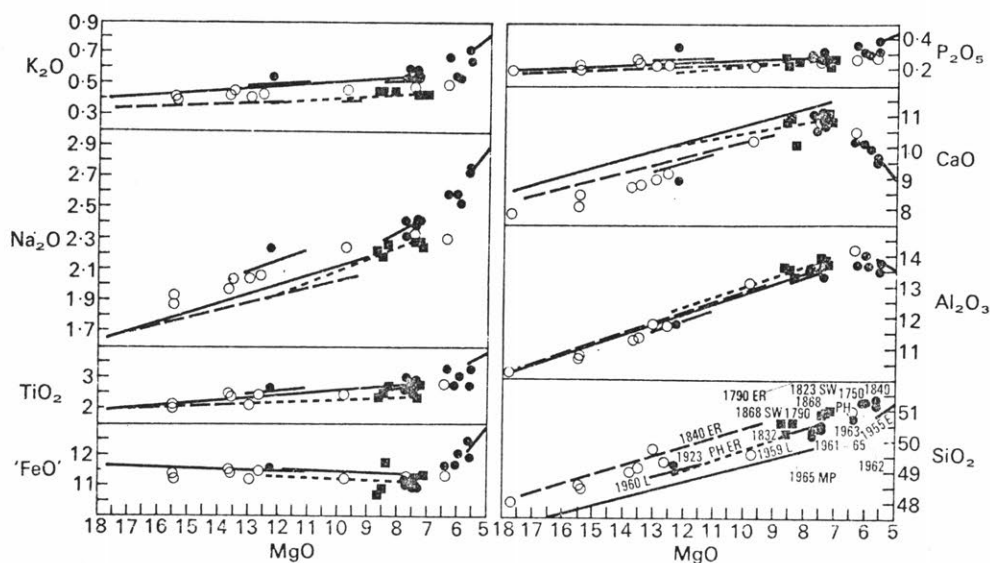
MgO variation diagrams: differentiated lavas of the east rift zone and selected undifferentiated lavas of historic age. Average control lines (essentially straight olivine control) have been computed for the several eruptions labeled on the SiO₂-MgO plot: Ancient Makaopuhi lava lake = PH ER (analyses from Moore & Evans, 1967, and additional unpublished analyses); 1840 undifferentiated lavas = 1840 ER; later lavas of the 1960 eruption = 1960 L (analyses from Murata & Richter, 1966a); March, 1965, eruption in Makaopuhi crater = 1965 MP (analyses from Wright *et al.*, 1968, and additional unpublished analyses of Makaopuhi lava lake). A control line for the early 1955 lavas = 1955 E, obviously not olivine control, is also plotted. A control line for undifferentiated lava from Kilauea summit, the latter part of the 1959 eruption in Kilauea Iki crater = 1959 L is given for reference.

All other eruptions are identified as follows on the SiO₂-MgO plot: Filled squares = undifferentiated historic lavas, Kilauea summit, south-west and east rift zones. Filled circles = differentiated lavas of historic age, east rift zone. Open circles = differentiated lavas of prehistoric age, east rift zone. All lavas represented by open circles are submarine except that labeled PH.

Figure IB 14.   (Wright and Fiske, 1971)

Isotopic compositions of Sr* and Pb in oceanic volcanic series

PROVINCE	ROCKS		Sr^{87}/Sr^{86}	Pb^{206}/Pb^{204}
Réunion	Basalts (5)		0.7040–0.7046	
(McDougall and	Mugearites (3)		0.7042–0.7044	
Compston, 1965)	Syenite (1)		0.7046	
Easter Island	Basalts (2)		0.7030, 0.7036	19.280, 19.301
(Hedge and Peterman, 1970;	Icelandite (1)		0.7030	19.253
Tatsumoto, 1966a)	Rhyolite obsidian (1)			19.308
Hawaiian Islands	Hawaii	Kilauea tholeiites (3)	0.7039–0.7041	
(Hedge, 1966;		Hualalai, alkali basalt		17.92
Tatsumoto, 1966b		Hualalai, trachyte	0.7035	18.08
Hedge and Peterman, 1970)		Mauna Kea, picrite basalt	0.7034	18.48
		Mauna Kea, hawaiite	0.7033	18.47
	Oahu	Koolau basalts	0.7039	18.09
		Waianae basalts	0.7032	
		Honolulu series		
		(nephelinites)	0.7031	18.17, 18.24
Iceland	Pleistocene-Recent basalts (3)		0.7028–0.7033	
(Moorbath and	Recent obsidians (1)		0.7017	
Walker, 1965)	Tertiary basalts (6)		0.7021–0.7032	
	Tertiary rhyolites (3)		0.7014–0.7015	
	Late Tertiary granophyres (6)		0.7010–0.7033	
Guadalupe Island	Alkali basalts (4)		0.7033–0.7036	20.172–20.436
(Tatsumoto, 1966a;				
Peterman and Hedge, 1971)				
St. Helena	Alkali basalts (2)		0.7031, 0.7032	
(Hedge, 1966)	Phonolites (2)		0.7047, 0.7054	
Tutuila, Samoa	Basalt		0.7057	
(Hedge, 1966)	Trachytes (2)		0.7062, 0.7066	
Upolu and Savaii, Samoa	Potassic alkali basalts (10)		0.7051–0.7066	
(Hedge et al., 1972)				
Gough Island	Basalt		0.7045	18.36
(Gast et al., 1964)	Trachyandesite, trachybasalt		0.7050, 0.7043	18.37, 18.43
	Trachytes (2)		0.7094, 0.7050	18.63, 18.73
Ascension Island	Basalts (2)		0.7025	18.43, 19.55
(Gast et al., 1964)	Trachyandesite		0.7025	
	Trachytes (2)		0.7045, 0.7073	19.72
	Obsidian			19.50

* All values normalized to $Sr^{86}/Sr^{88} = 0.1194$, $Sr^{87}/Sr^{86} = 0.7080$, for standard E. and A. $SrCO_3$.

Table IB 8.   (CTV)

the degree and/or depth of partial melting (see Figures
IB-5). These systematics, along with Yoder and Tilley's
(1962) low pressure thermal barrier, have led most propo-
nents (e.g., MacDonald, 1968) of primary liquid differen-
tiation producing alkali basalts to hypothesize deep-seated
processes, perhaps involving remelting at depth. Others
(e.g., Verhoogen et al., 1970; Carmichael et al., 1972)
would prefer an independent origin (change of melting pa-
rameters) for each magma type. Currently neither alterna-
tive can be entirely ruled out.

Canary Islands. The seven Canary Islands
lie off the coast of Africa with the eastern two boarder-
ing on the continental coast. The islands are shield vol-
canoes formed largely of alkali olivine basalt (Table IB-9)
with the youngest to the west. The basalts seem to dif-
ferentiate with time towards phonolites by removal of oli-
vine, titanomagnitite, then plagioclase (Ridley, 1970).
The two eastern (older) islands present a more complicated
picture. They not only contain the typical alkali basalt
differentiation sequence, but also an old intrusion of
tholeiitic composition and a historic flow of olivine
tholeiite with normative hypersthene (analysis #6 in Table
IB-9). Not only does the tholeiite on these Canary islands

Chemical analyses (oxides, wt %) and CIPW norms of rocks from the Canary Islands

	1	2	3	4	5	6	7	8	9
SiO_2	42.50	43.20	46.10	45.86	47.80	49.30	52.55	59.20	64.20
TiO_2	2.20	3.93	2.38	2.95	2.22	2.06	1.23	0.73	0.35
Al_2O_3	13.50	16.30	14.24	15.81	13.19	13.43	19.32	20.10	16.29
Fe_2O_3	5.16	8.09	3.95	4.65	2.21	1.02	2.76	1.26	2.77
FeO	7.14	4.69	7.90	5.24	8.88	9.23	2.33	1.12	0.62
MnO	0.17	0.16	0.15	0.18	0.14	0.15	0.18	0.15	0.05
MgO	10.44	5.16	9.25	6.31	10.50	11.39	1.74	0.91	1.05
CaO	10.99	10.74	10.45	9.77	9.90	9.39	4.97	2.40	2.36
Na_2O	3.28	3.12	3.10	5.04	3.19	2.48	8.12	7.32	7.00
K_2O	1.20	1.64	0.63	3.11	0.93	0.74	4.88	5.00	4.40
P_2O_5	1.04	0.88	0.53	0.70	0.58	0.36	0.34	0.16	0.05
H_2O^+	2.67	2.03	1.12		0.24	0.17			
H_2O^-							}0.40	1.36	0.66
Rest			0.10*	0.37			1.18†	0.20*	
Total	100.29	99.94	99.90	99.99	99.78	99.72	100.00	99.91	99.80

* CO_2 † Cl = 0.24; SO_3 = 0.94.

Explanation of column headings

Analyses 1–6 are cited from Ibarrola (1969), analysis 7 from Hernández-Pacheco (1969), and analyses 8 and 9 from Muñoz (1969a). Tables and numbers given in parentheses refer to these works.

1 Olivine basalt (first episode), Lanzarote (table 1, no. 7)
2 Olivine basalt (first episode), Gomera (table 4, no. 8)
3 Olivine basalt (first episode), Fuerteventura (table 2, no. 12)
4 Average Quaternary basalt (tephrite), Gran Canaria (table M4, no. 2)
5 Olivine basalt, last Quaternary episode, Lanzarote (table 5, no. 27)
6 Olivine basalt, historic flow of 1730–1736 eruptions, Lanzarote (table 5, no. 30)
7 Tahitite, Gran Canaria (table 1, no. 4)
8 Nepheline syenite, central stock, Pájara, Fuerteventura (table 1, no. 3)
9 Syenite, La Peñitas ring dike, Pájara, Fuerteventura (table 1, no. 16)

Table IB 9. (CTV)

not conform to the compositional trend of the majority

of neighboring islands, but the relation of tholeiite to

alkali basalt is sequentially opposite that observed in

the well-documented Hawaiian sequence.

In summary, for the ocean environment, basalts

and their derivatives are young ($\stackrel{<}{\sim}$ 200 my) and uncontami-

nated by continental material. A variety of basalt compo-

sitions can be observed, perhaps the most primary occurring

at the spreading ocean ridges. All are presumed to be

derived from the upper mantle by one or more sequences of

partial melting. The oceanic upper mantle itself is roughly

homogeneous in major element geochemistry, but may be heter-

ogeneous either vertically or laterally in incompatible

elements.

     c. Subduction Zone

Most recent,   active volcanoes are located

along margins of lithospheric plates which are in motion

relative to each other a few centimeters a year. Three

quarters of the world's active surface volcanoes occur

along the pacific margin (CTV, p.528). The ocean floor

basalts are formed as two oceanic plates separate. When

two plates collide, one is generally forced to descend in-

to the mantle creating a subduction zone of intense earth-

quake activity (Figure IB-15 from Toksoz, 1972) and initiating a variety of volcanic materials. The rock type generally associated with subduction zone volcanics is andesite (the rock name being derived from the Andes of South America). Since it is the nature of this tectonic setting that the subducted (oceanic) plate encounters changing temperatures and pressure (and perhaps H_2O content) as it descends, the chemistry of igneous melts associated with this environment would be expected to be different from those associated with simple partial melting of the upper mantle that occurs in the ocean environment.

Although the subduction zone continental igneous rocks are predominantly andesite and related differentiates, basalts are also abundant in the island arc environment, especially in younger arcs (Baker, 1968). Again there is no uniform sequence for all environments but a few patterns can be recognized:

(1) Chemically, the circumoceanic basalts are different from ocean floor or ocean island basalts. No material associated with island arcs or continental margins contains the very low strontium ratio (<.703) of abyssal basalts (Table IB-10). For some provinces, the initial strontium isotopic ratios for a range of rock types are essentially uniform implying a genetic relationship. The moderately

Average initial strontium isotopic values (Sr^{87}/Sr^{86}) for selected rock types of active volcanic arcs and continental margins (all data adjusted to a value of 0.7080 for MIT $SrCO_3$)*

	BASALT (< 52% SiO_2)	BASALTIC ANDESITE (52–55% SiO_2)	ANDESITE (55–63% SiO_2)	DACITE (63–68% SiO_2)	RHYOLITE (> 68% SiO_2)
New Britain	0.7035	0.7036	0.7036	0.7036	0.7035
Tonga	—	0.7037	0.7042	0.7043	
Marianas	0.7042	—	0.7042	0.7038	—
Izu Islands	0.7036	—	0.7040	—	0.7034
Caribbean					
St. Kitts	0.7036	0.7040	0.7038	—	—
St. Vincent	0.7042	0.7040	0.7039	—	—
Carriacou	0.7052	—	0.7054	—	—
North Japan	0.7043	—	0.7041	—	—
California					
Mt. Shasta	—	0.7039	0.7030	0.7032	—
Mt. Lassen	0.7039	0.7032	0.7040	—	—
Medicine Lake	0.7034	0.7037	—	—	0.7040
Central America	0.7035	0.7042	0.7036	0.7036	0.7042
New Zealand					
Taupo	0.7042	—	0.7055	0.7051	0.7053
Average†	0.7040	0.7038	0.7040	0.7037	0.7038

* Data taken from Pushkar (1968), Peterman et al. (1970a, 1970b), Hedge (1966), Hedge and Knight (1969), Hedge and Lewis (1971), Ewart and Stipp (1968), Oversby and Ewart (1972), Ewart et al. (1973).
† Excludes New Zealand average andesite, dacite, and rhyolite.

Table IB 10. (CTV)

Cross-section of calculated stress model (upper) and the distribution of earthquakes (lower) in descending lithosphere under Japan. The units of stress are "bars" (very closely, atmospheric pressures). Inset diagram indicates the Young's modulus variation inside the slab due to temperature effects. Arrows point the direction of maximum principal stress. In the lower diagram earthquake foci are indicated by black dots. The shallow quakes are located along the boundary between the descending lithosphere and the stable lithosphere. Deep quakes are located along the interior of the slab where the slab is coolest and where calculated stresses are maximum. Low Q (high attenuation of seismic waves) and Low V (low velocity) indicate the asthenosphere.

Figure IB 15. (Toksoz, 1972)

low ratios for the entire series of rock types imply minor,

if any, crustal contamination.

(2)   Kuno (1967) noted that volcanoes extruding tholeiitic

basalts occurred closest to oceanic trenches (start of

the subduction zone) and that volcanoes with high-aluminum

basalts and alkali-olivine basalts occurred respectively

further inland (Figure IB-16 from Kuno, 1967). The corre-

lation of this pattern with deep foci earthquakes suggested

the generation of different basalts at successively greater

depths.

(3)   The association of magma generation with descending

lithospheric plates is further strengthened by the tendency

of K_2O content of lavas (andesite) to be correlated with

depth of the subduction zone as inferred from earthquake

foci (Figure IB17 from CTV, p. 562).

       d.   Continental basalts

A thorough discussion of continental volcanics

must include extreme compositions (e.g., carbonatites) and

modes of emplacement (e.g., kimberlites) and is well beyond

the scope of this summary. Two common types of continental

basaltic provinces will be mentioned here: the voluminous

tholeiitic flood basalts and the complex alkali basalt re-

gions. In both cases, plate tectonics have been implicated

in the ultimate origin of the basalts. However, only in
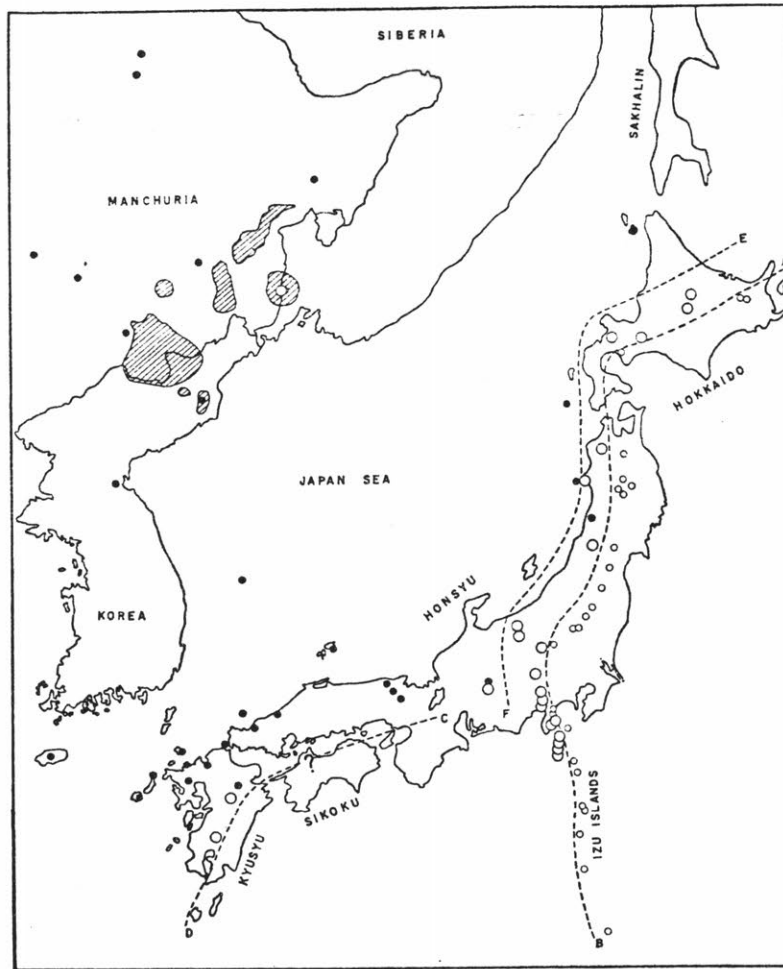
a
Distribution of tholeiite (o), high-alumina basalt (O) and alkali olivine basalt (⊙) among Quaternary volcanoes of Japan, Korea and Manchuria. The shaded areas in east Manchuria are Tertiary lava plateaus mostly of alkali olivine basalt.
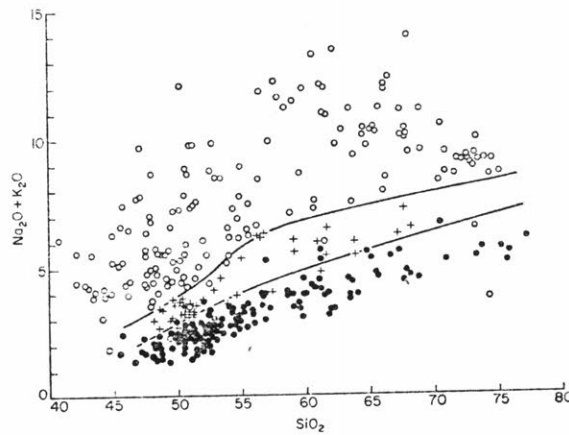
Figure IB 16.
(Kuno, 1967)

b
Alkali-silica relations of tholeiite series (⊙) (basalt, andesite, dacite and rhyolite; high-alumina basalt series (+) (basalt, andesite and dacite); alkali rock series (O) (basalt, mugearite, trachyandesite, trachyte and alkali rhyolite), occurring along a traverse zone from the Izu Islands, passing through central Honsyū, to the Japan Sea region including Korea and Manchuria.
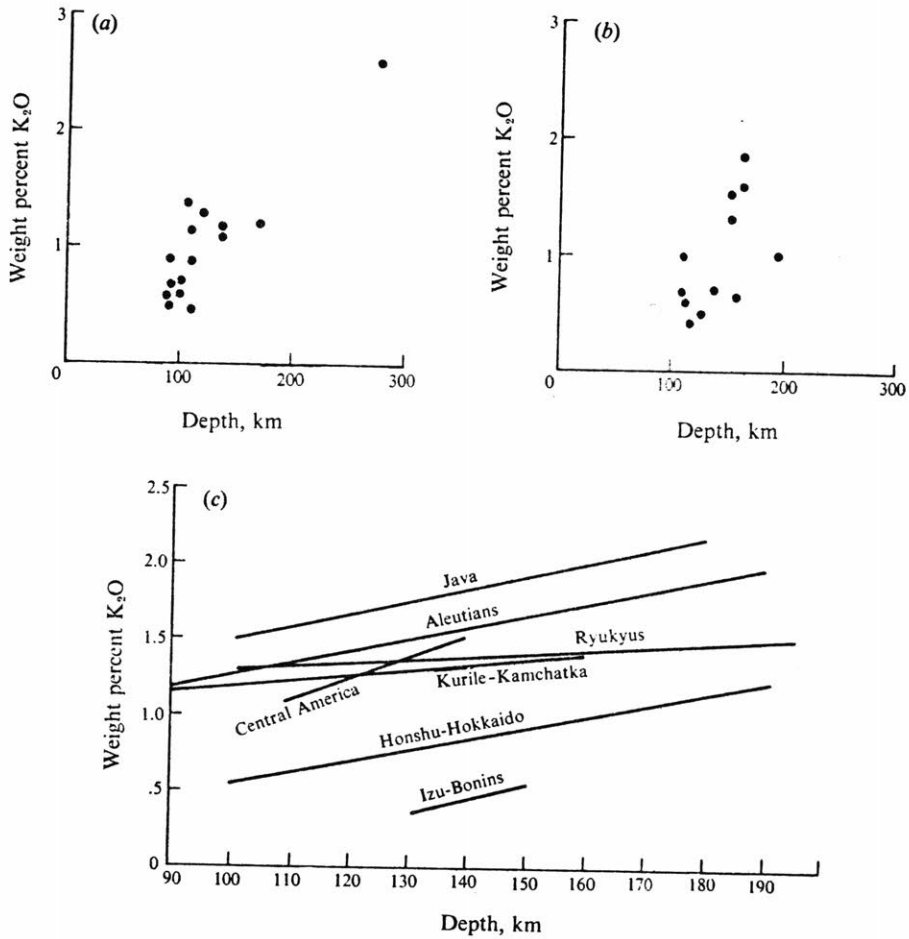
Plot of K_2O content (at 55 percent SiO_2) of lava series against depth in kilometers from the volcano to the inclined seismic zone beneath: (a) Kuriles-Kamchatka; (b) Honshu, Japan; (c) Circum-Pacific volcanic arcs. Length of lines represent range of data for each region, and their position is obtained by statistical regression of published analyses (after Dickinson, 1970 and Nielson and Stoiber, 1973).

Figure IB 17. (CTV)

the case of alkali basalt association with continental rift zones has it been substantiated. An example of each province will be discussed.

        i. THOLEIITIC FLOOD BASALTS. Although granitic rocks are the dominant continental plutonic rock type, the most voluminous continental lavas are basalts (CTV, p. 427). Immense outpouring over short time periods of essentially tholeiitic lava has occurred within the last 150 m.y. on a number of continental regions. These occur as a series of relatively thin flows that cover an area up to 10^6 km^2. The total volume of such regions of flood basalt can approach 10^6km^3, many times the volume of basalts that built the shield volcano Mauna Loa (see Table IIB-11, compiled from CTV, and Head,1975). These tholeiitic lavas are generally similar to the oceanic tholeiites but are more potassium-rich and show enrichment of light rare earth elements.

        A substantial amount of geochemical data has become available for the Columbia River basalt group (Figure IIB-18, from Verhoogen et al., 1970, p. 299). The geology and geochemistry of this area was extensively described by Waters (1961) and further major and minor element abundances were measured by McDougall (1976). The Columbia River basalts are oversaturated tholeiites; the independent

Table IB2-11 Estimated volume of tholeiitic flood basalts.

Location	Estimated volume $(x\ 10^6 km^3)$
Decca, India	.7
Columbia and Snake River	.3
Siberia	.25
Parana, Brazil	.20
(Mauna Loa	.05)
Bushveld (plutonic complex)	.10
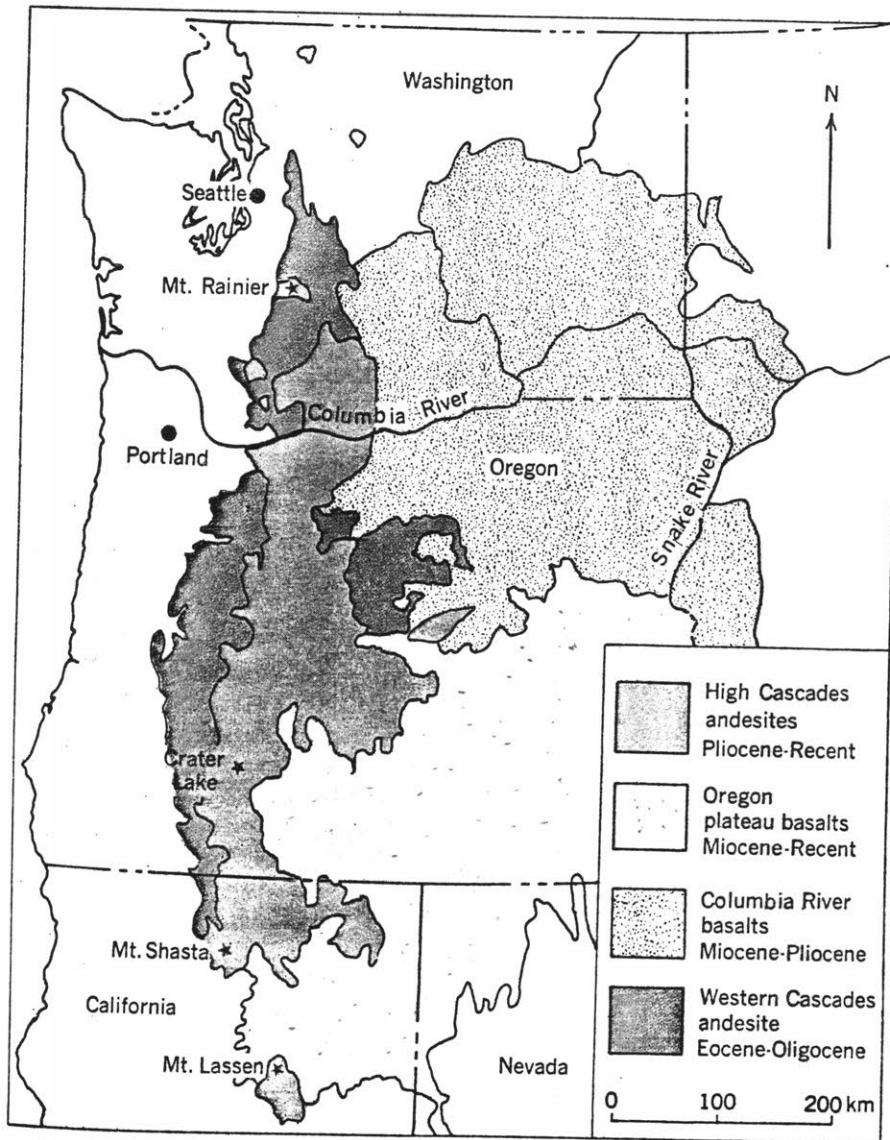
Figure IB 18. Columbia and Snake River Basalts
(Verhoogen et al., 1970)

Oregon plateau basalts to the south are much higher in

Al_2O_3 content. Four distinct basalt sequences of the Colum-

bia River group were described from these studies, all

tholeiites: Picture Gorge basalts and Lower, Middle, and

Upper Yakima basalts. The Lower and Middle Yakima basalts

can be easily distinguished by TiO_2 content (Siems et al.,

1974). Variation diagrams for major element chemistry for

these sequences are shown in Figure IB-19 (from McDougall,

1976). Waters showed that these basalts were erupted from

fissure systems into a broad basin.

The Sr isotopic studies of McDougall (Figure

IV-20) distinguished the Picture Gorge basalts from the

Yakima and indicated they were likely to have been derived

from upper mantle sources with little modification. The

Yakima basalts with higher initial Sr show a correlation

of increasing $^{87}Sr/^{86}Sr$ with decreasing age. This pattern

could either be the result of progressive crustal contam-

ination or derivation from inhomogeneous upper mantle source

materials. McDougall suggests the ultimate source of the

Yakima lavas was the upper mantle with partial melting caused

by tectonic events related to plate motions in the Pacific

NW during that time.

ii. ALKALI BASALT REGIONS (RIFT ZONES?).

Alkali basalts frequently dominate a small continental prov-

ince, but almost always with a very complex association

Legend: △ Picture Gorge Basalt ▲ Imnaha basalt □ Lower Yakima basalt, Imnaha Valley ● Lower Yakima basalt, Grande Ronde sequence ○ Lower Yakima basalt, Crescent Bar ◆ Middle Yakima basalt, Vantage area
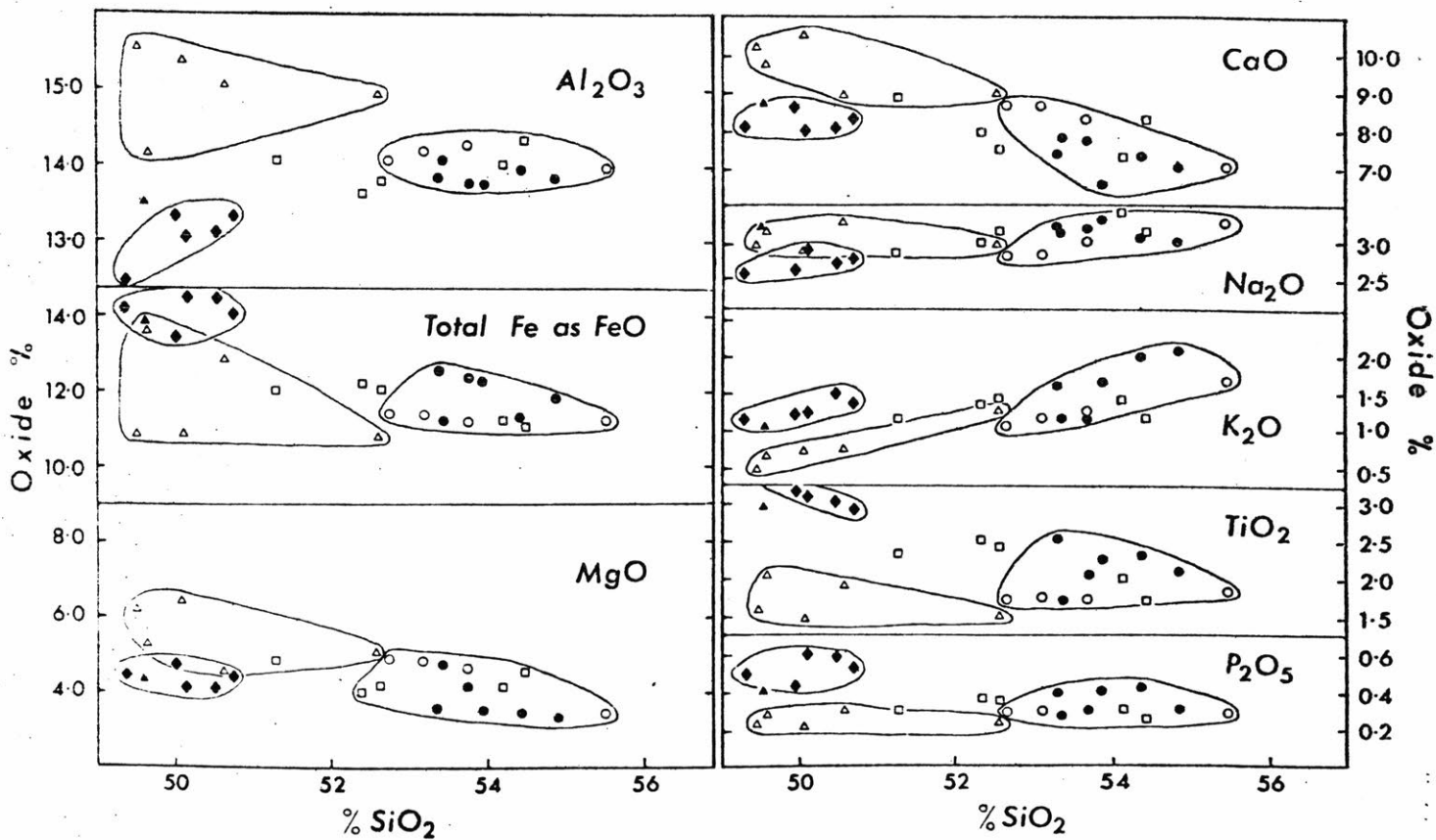
Oxide percentages of major elements plotted relative to SiO_2 for samples from sequences indicated. Fields drawn enclose data from Picture Gorge Basalt, lower Yakima basalt from Crescent Bar and Grande Ronde, and middle Yakima basalt.

Figure IB 19. (McDougall, 1976)

Plot of average initial Sr^{87}/Sr^{86} ratio relative to Rb/Sr ratio for each of main sequences of basalt sampled in Columbia River Group. Bars represent one standard deviation for each parameter in each case (not standard deviation of mean).

Figure IB 20.
(McDougal, 1976)
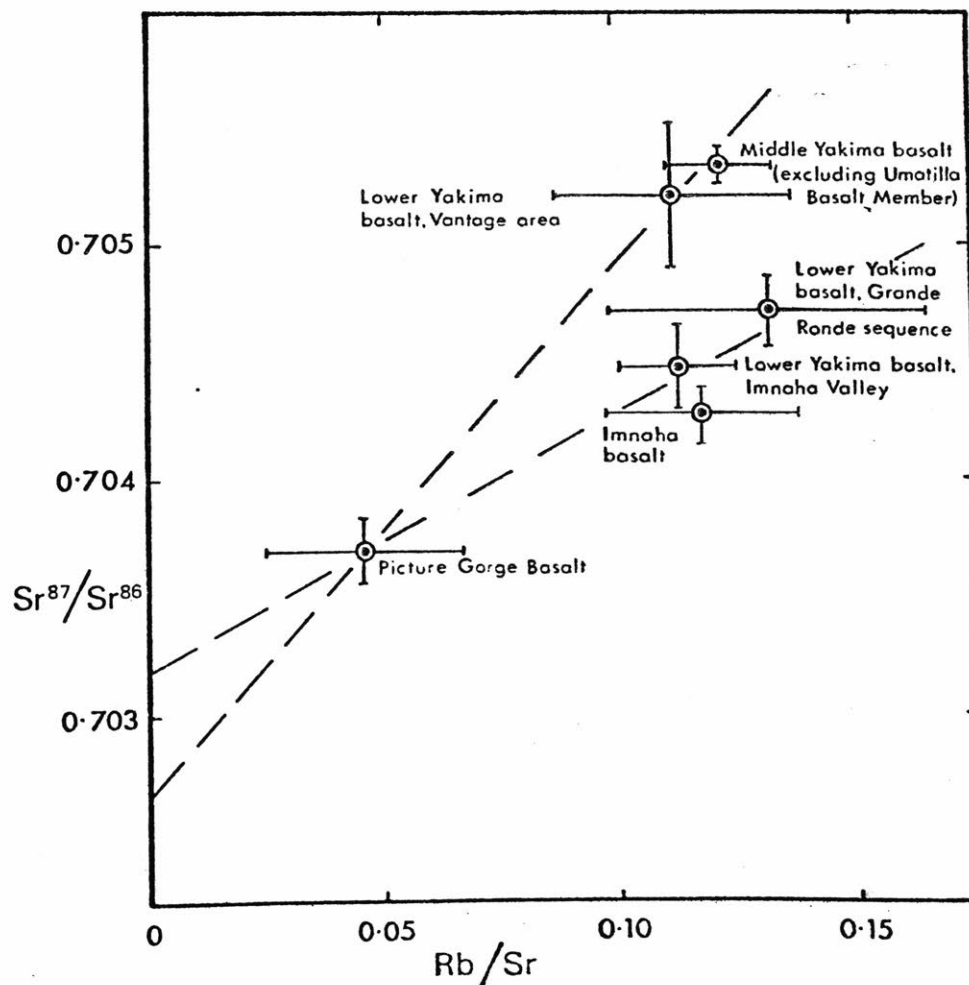
of other magma types. The range of rock types associated with continental alkali basalts is much greater than those associated with oceanic alkali basalts (CTV, p. 505-506). From high pressure experiments, alkali basalts are assumed to have a deep source (between 40-100 km) which is consistent with derivation from continental sub-crustal material. (Only rarely are tholeiitic basalts associated with continental alkali basalts and the question of fractionation relationships between the two basalt types, as is often suggested for oceanic basalts, does not generally occur.)

The tectonic setting for continental alkali basalts is perhaps simply a zone of crustal weakness. The classic example, in complexity, occurs in the East African rift zones. In this region (e.g., CTV, Chapter 10) are found alkali olivine-trachyte-phonolite series, nephelinites, and carbonatites in somewhat random temporal and spatial realtionship.

Another continental alkali basalt region, the northern and eastern San Francisco volcanic field in Arizona (Moore et al., 1976), consists of flows of predominantly alkali-olivine basalt, most of which occurred during the last 3 m.y. Associated with these basalts are high alumina basalt, basaltic andesite, andesite, dacite, rhyodacite, and rhyolite. Chemical variation diagrams

VOLCANIC ROCKS, SAN FRANCISCO VOLCANIC FIELD, ARIZONA
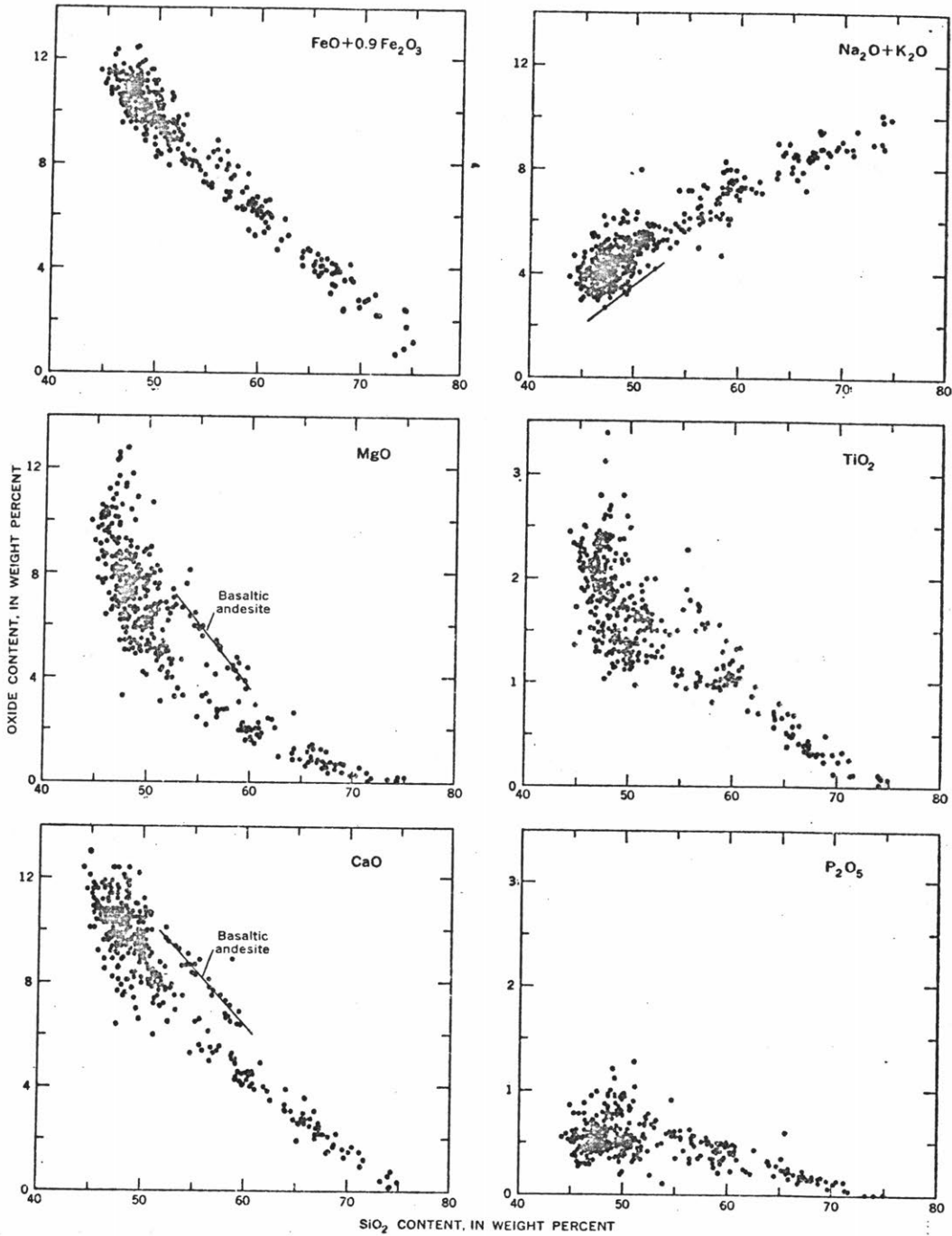
—Silica variation diagrams, San Francisco volcanic field. Line on plot of Na₂O + K₂O relative to SiO₂ separates alkali olivine basalts from tholeiitic basalts of Hawaii (MacDonald and Katsura, 1964).

Figure IB 21. (Moore et al, 1976)

(Figure IB-21) from Moore et al.) suggest these basalts
are consanguineous although no simple evolution pattern
is recognized. Strontium isotope values are low for all
members of this series (.7026 - .7050) implying derivation
from the mantle with little contamination of crustal mater-
ial. (It is perhaps noteworthy that contemporaneous with
some of the San Francisco volcanics 3 m.y. ago were the
basalts of the Taos plateau a few hundred kilometers to
the east. The Taos basalts are predominantly olivine
tholeiites with less extensive alkali basalts and associ-
ated rock types [Lipman, 1977].)

In summary, a variety of basalt types exist
on the current surface of the earth, most of which are ul-
timately related to mantle sources. Although chemical frac-
tionation processes and host material contamination often
clearly affect compositional trends, it also seems apparent
that the general geophysical environment (plate tectonics,
type and thickness of crustal material) plays a major role
in determining the basalt types erupted on the surface.
The source region of basalts for each of the provinces dis-
cussed above differ in probable temperature and pressure
(depth) environment.

A variety of questions, often with no obvious answers, exist for oceanic basalts as well as those found well within a thick continental plate. Are the volcanics derived from partial melting of crustal or mantle material? What degree of melting is involved? If the magma originated in the mantle, to what degree has it been contaminated by crustal material? How does the sub-continental mantle compare with the oceanic mantle? To what degree is it heterogeneous vertically or laterally? These question are difficult to answer not only because of the likely complexity of each volcanic event, but also because often not all the relevant information is available (e.g., major element chemistry, minor element chemistry, REE, absolute age, isotopic chemistry, areal and volume estimates, etc.).

Increasingly sophisticated thermal models, experimental petrology results, and isotopic analyses are becoming available and may eventually lead to answers for the above questions. For example, a recent discussion of Nd and Sr isotopic abundances for continental and oceanic rocks (DePaolo and Wasserberg, 1976) provided evidence to indicate that all types of continental igneous rocks (flood basalts to carbonatites) are derived from a mantle reservoir with chondritic REE patterns. Mid-ocean ridge basalts, on the other hand, are derived from a <u>different</u> (shallower?)

ancient reservoir and the source area for ocean island basalts
is intermediate between the two.

Probing the lateral and vertical compositional
variations of the earth's mantle seems within reach of plan-
etary scientists using a synthesis of current geophysics
(thermal models, plate tectonics, seismic internal struc-
ture patterns), experimental petrology (melting conditions
as a function of P, T, and composition), and basalt geochem-
istry (major and minor elements, and isotopic abundances).
Currently, the terrestrial data are incomplete and scattered
in a variety of forms. Such a synthesis is equally appli-
cable for probing the compositional structure of each of
the other terrestrial planets, but fewer of the variables
are defined.

3. Terrestrial Volcanism in Time

A characteristic feature of terrestrial basalts
in the preceding discussion is their youth; most basaltic
material that has been seriously studied is less than 200
million years old, or very recent in terms of geologic time.
Basaltic materials from other solar system objects are
much older: the basaltic achondrites are generally much
older than $\sim$3000 m.y.; the lunar basalts are between $\sim$3000
and 3900 m.y. old; and the surface age of the largest vol-
cano on Mars is estimated to be at least 1000 m.y. (Soderbloom,

1974). What, then, can be said about the early history
of terrestrial volcanism?

Only recently has data become available concerning
ancient terrestrial material. A variety of models concern-
ing the early history of the earth have been proposed, many
of which have been included in a recent anthology of papers
edited by B.F. Windley (1976a). The earth appears to be
tectonically unique in the solar system and has recycled
much of its surface material perhaps more than once. It
has not been defined to what extent the current patterns
of terrestrial volcanism, which are closely linked to plate
tectonics, were also active in earlier periods of earth
history. The Archean rock associations and geochemistry,
for example, seem to be similar to modern continental mar-
gins and island arcs (Windley, 1976b) implying possibly
similar tectonic processes. Burke et al. (1976) describe
the early Archean deformation of greenstone terrains as
"permobile" deformation, or without rigid behavior during
collision. The model preferred by Green (1975) to describe
the character of Archean greenstone belts includes a steeper
Archean geotherm, a thin lithosphere, and an athenosphere
with about 5% melting. His model does _not_ allow subduction
of basaltic oceanic crust, but instead postulates such a
crust is "scraped off" as the lithosphere is subducted and,

eventually, forms the greenstone belts. A thin Archean

lithosphere was also proposed previously by Hart et al.

(1970) on the basis of trace element abundances of Archean

greenstones. These trace element studies indicated that

the Archean upper mantle was not depleted in K, Rb, Cs,

Sr, and Ba, unlike the present upper mantle (source region

for ocean floor basalts). Glikson (1976), on the other

hand, points out that the coherent pattern in the orienta-

tion of Archean greenstone belts in Gondwanaland argues

against large scale plate dispersions prior to the breakup

of Gondwanaland 300 million years ago. He suggests some

of the earliest earth volcanics (up to 2.6 AE) may have

been "relic terrestrial maria" similar to those common to

the moon. An earlier model by Green (1972) suggested a

similar link between the Archean greenstone belts and lunar

maria.

Although data concerning the terrestrial Archean

rocks are incomplete and there seems to be no general con-

sensus on how to interpret these data, they do provide

a few extremely significant facts and implications:

(a) Ancient crustal material does exist on earth.

Table IIB-12 (from Jahn and Nyquist, 1976) summarizes the

Rb-Sr isochron ages for a variety of Archean rocks. Granitic

as well as mafic surface material was formed during the

Age and initial Sr^{87}/Sr^{86} data for terrestrial Archean rocks

Rock unit	t = age in b.y. ± 2	$I = (Sr^{87}/Sr^{86})_0$ ± 2	References	Comments
Minnesota, U.S.A.				
Ely Greenstone	$2 \cdot 69 \pm 0 \cdot 08$	$0 \cdot 70056 \pm 26$	Jahn and Murthy (1975)	I obtained from WR isochron
Newton Lake Fm	$2 \cdot 65 \pm 0 \cdot 11$	$0 \cdot 70086 \pm 24$	Jahn and Murthy (1975)	I obtained from WR isochron
Vermilion Granite	$2 \cdot 70 \pm 0 \cdot 05$	$0 \cdot 70041 \pm 29$	Jahn and Murthy (1975)	I obtained from WR isochron Basic data from Peterman et al. (1972) and Jahn and Murthy (1975)
	$2 \cdot 68 \pm 0 \cdot 10$	$0 \cdot 7006 \pm 12$	Peterman et al. (1972)	I obtained from WR isochron
Northern Light Gneiss	$2 \cdot 74 \pm 0 \cdot 10$	$0 \cdot 7007 \pm 4$	Hanson et al. (1971)	I obtained from WR isochron
Saganaga Tonalite	$2 \cdot 71 \pm 0 \cdot 56$	$0 \cdot 7010 \pm 6$	Hanson et al. (1971)	I obtained from WR isochron
Icarus Pluton	$2 \cdot 69 \pm 0 \cdot 48$	$0 \cdot 7100 \pm 14$	Hanson et al. (1971)	I obtained from WR isochron
Giants Range Granite	$2 \cdot 67 \pm 0 \cdot 07$	$0 \cdot 7003 \pm 19$	Prince and Hanson (1972)	I obtained from WR isochron
Morton-Montevideo Gneisses	$3 \cdot 80$	$0 \cdot 700$	Goldich and Hedge (1974)	Both t and I are best values from an eye-ball fit through six data points
Canada				
Pyroxenes, Superior Prov.	$2 \cdot 70$	$0 \cdot 7010$ to $0 \cdot 7014$	Hart and Brooks (1974)	Seven age-corrected I values for primary pyroxenes from two extrusive and three intrusive mafic units
Keewatin + Coutchiching	$2 \cdot 69 \pm 0 \cdot 08$	$0 \cdot 7003 \pm 13$	Hart and Davis (1969)	I obtained from WR isochron
Chibougamau Greenstone belt: Dore Lake Complex	$2 \cdot 72 \pm 0 \cdot 50$	$0 \cdot 7011 \pm 10$	Jones et al. (1974)	I obtained from WR isochron
Anorthosite-1		$0 \cdot 70068 \pm 6$	Jahn (unpublished)	Age-corrected I value; Sr composition measured at JSC; $t = 2 \cdot 70$ b.y.
Anorthosite-2		$0 \cdot 70150 \pm 7$	Jahn (unpublished)	Age-corrected I value; Sr composition measured at JSC; $t = 2 \cdot 70$ b.y.
Chibougamau Pluton	$2 \cdot 56 \pm 0 \cdot 16$	$0 \cdot 7007 \pm 4$	Jones et al. (1974)	I obtained from WR isochron
Meta-meladiorite		$0 \cdot 70133 \pm 6$	Jahn (unpublished)	Age-corrected I value; Sr composition measured at JSC; $t = 2 \cdot 6$ b.y.
Yellowknife: SE Granodiorite	$2 \cdot 64 \pm 0 \cdot 08$	$0 \cdot 7011 \pm 16$	Green and Baadsgaard (1971)	I obtained from WR isochron
Metavolcanics	$2 \cdot 63 \pm 0 \cdot 16$	$0 \cdot 7022 \pm 23$	Green et al. (1968)	I obtained from WR isochron
South Africa				
Onverwacht: Komati	$3 \cdot 50 \pm 0 \cdot 20$	$0 \cdot 70048 \pm 5$	Jahn and Shih (1974)	I obtained from mineral isochron
Anorthositic norite		$0 \cdot 70061 \pm 6$	Jahn and Shih (1974)	Age-corrected I value ($t = 3 \cdot 5$ b.y.)
Anorthosites and komatiites		$0 \cdot 7000$ to $0 \cdot 7006$	Allsopp et al. (1973)	Age-corrected I values assuming $t = 3 \cdot 2$ b.y.
Middle Marker Horizon	$3 \cdot 36 \pm 0 \cdot 07$	$0 \cdot 7015 \pm 18$	Hurley et al. (1972)	I obtained from WR isochron
Rhodesia:				
Bulawayan	$3 \cdot 0 - 3 \cdot 1$	$0 \cdot 70110 \pm 5$	Jahn (unpublished)	Age-corrected I value assuming $t = 3 \cdot 0$ b.y. Measured $= 0 \cdot 70122$
Bulawayan limestones		$0 \cdot 7014$ to $0 \cdot 7019$	Bell and Blenkinsop (1974)	Measured values; uncorrected
Great Dyke	$2 \cdot 53 \pm 0 \cdot 09$	$0 \cdot 7024 \pm 8$	Davies et al. (1970)	I obtained from WR isochron
West Greenland:				
Amitsoq Gneisses: Narssaq Area	$3 \cdot 75 \pm 0 \cdot 09$	$0 \cdot 7015 \pm 8$	Moorbath et al. (1972)	All I's obtained from WR isochrons;
Qilangarssuit	$3 \cdot 74 \pm 0 \cdot 10$	$0 \cdot 7009 \pm 11$	Moorbath et al. (1972)	Best age $= 3 \cdot 70 - 3 \cdot 75$ b.y.
Praestefjord	$3 \cdot 69 \pm 0 \cdot 23$	$0 \cdot 7001 \pm 17$	Moorbath et al. (1972)	Best $I = 0 \cdot 7010 - 0 \cdot 7015$
Isua Area	$3 \cdot 70 \pm 0 \cdot 14$	$0 \cdot 7011 \pm 20$	Moorbath et al. (1972)	

Note: All I values have been adjusted based on NBS-SRM987 Sr Standard $= 0 \cdot 71025$ or E & A Sr Standard $= 0 \cdot 7081$.

Table IB 12. (Jahn and Nyquist, 1976)

<u>first billion years</u> of earth history and still constitutes

a minor part of the earth's crust. Although the earth

is a dynamically active planet, it has failed to destroy

a few pieces of its earlier history--it only deformed them

badly.

(b) The moon, with its ancient surface, and perhaps

also Mars and Mercury, provide excellent laboratories for

examining the early history of the solar system. All the

terrestrial planets may very well have been affected by

the same processes in their early history. Further examin-

ation of the Moon, Mars, and Mercury in conjunction with

investigations concerning the terrestrial Archean environ-

ment should eventually allow a unified theory of early plan-

etary evolution to be developed.

I.   BASALT TYPES: AN OVERVIEW

C.   Lunar Basalt Types

Lunar samples have been returned from nine areas on
the front side of the moon by the Apollo and Luna landing
missions.   The locations of these areas are shown in Figure
IC-1 and the coordinates are given in Table 1C-1 (updated
from Taylor, 1975).   Six of these landing areas were in
mare regions.

Although it has only been eight years since the first
samples were returned, it is easy to forget some of the
major facts the samples provided immediately.   Lunar rocks
have their own distinct character--different from terres-
trial samples and different from meteorites.   The lunar
samples contain essentially no water (and no organic mat-
ter).   The lunar surface is differentiated.   The lunar mar-
ia are basaltic in composition and igneous in origin.   The
lunar rocks are old ($\gtrsim 3.0$ AE).

The returned lunar samples fall into two distinct fam-
ilies: the highland feldspathic rocks and the mare basalts.
The light-colored highland rocks comprise over 80% of the
lunar surface and have been intensely brecciated by repeated
impacts.   The highlands are the oldest lunar surface and
consist of a variety of recognizable, although often mixed,
rock types (summarized by Taylor, 1975, Chap. 5).   The high-
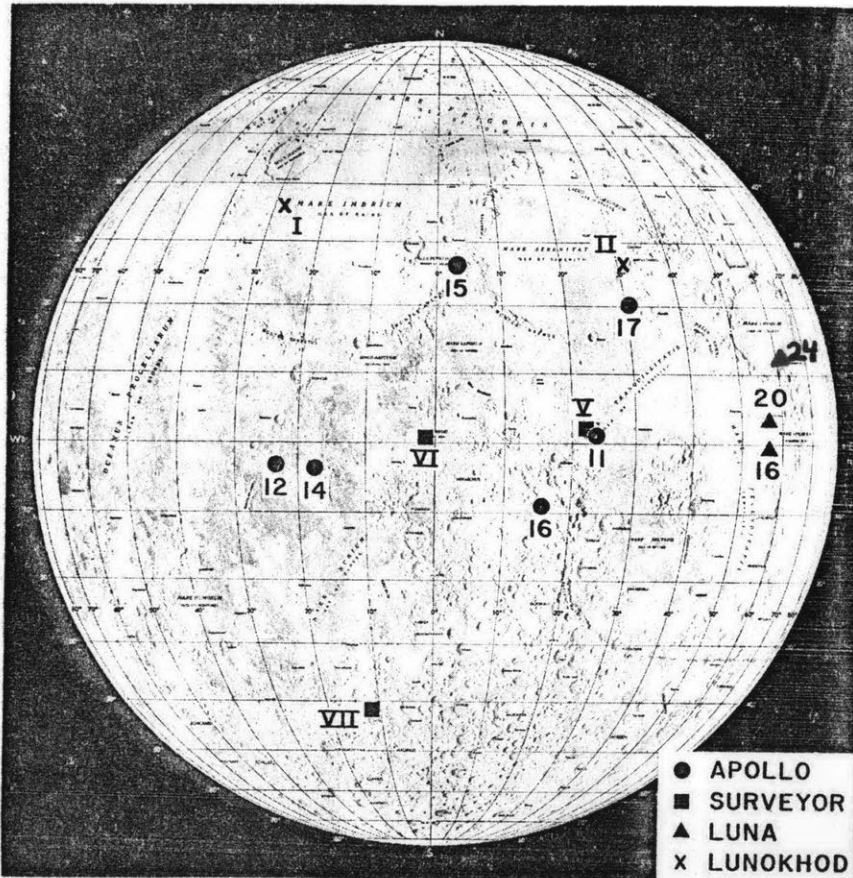
Figure IC1   Apollo, Luna, and Surveyor landing sites.

The Apollo Lunar Landings.

Mission	Landing site	Latitude	Longitude	EVA duration (hours)	Traverse distance (km)	Date
11	Mare Tranquillitatis	0°67'N	23°49'E	2.24	—	July 20, 1969
12	Oceanus Procellarum	3°12'S	23°23'W	7.59	1.35	Nov. 19, 1969
14	Fra Mauro	3°40'S	17°28'E	9.23	3.45	Jan. 31, 1971
15	Hadley-Apennines	26°06'N	3°39'E	18.33	27.9	July 30, 1971
16	Descartes	8°60'S	15°31'E	20.12	27	April 21, 1972
17	Taurus-Littrow	20°10'N	30°46'E	22	30	Dec. 11, 1972

Mission	Landing site	Latitude	Longitude	Date
Luna 16	Mare Fecunditatis	0°41'S	56°18'E	Sept., 1970
Luna 20	Apollonius highlands	3°32'N	56°33'E	Feb., 1972
Luna 24	Mare Crisium	12° 45'N	62° 12'E	Aug. 1976

(B) Russian Lunar Traverse Vehicles.

Vehicle	Landing site	Date	Traverse length
Lunokhod 1	Western Mare Imbrium	Nov., 1970	20 km
Lunokhod 2	Le Monnier Crater, Eastern Mare Serenitatis, 180 km north of Apollo 17 site	Jan., 1973	30 km

Table IC 1.   (Taylor 1975)

land crust contains abundant feldspar. Although some of

the highland rock types have basaltic compositions (e.g.,

Fra Mauro basalts), the average composition of the highlands

is too low in mafic elements (MgO + FeO < 16%) and too

high in Al_2O_3 (>20%) to be considered basaltic. The Fra

Mauro basalts, which may have been the products of early

near surface partial melting (e.g., Walker et al., 1973),

may make up 20% of the crust (Taylor, 1975, p. 252). The

impact history of the lunar highland crust, however, has

obscured any early magmatic history and the possibility

of lunar highland basalts will not be discussed here.

The dark mare basalts are perhaps less complicated.

They are igneous rocks that fill the crustal lowlands, but

are themselves old by terrestrial standards (3.8 - 3.0

AE). The lunar mare basalt types identified in the returned

samples are discussed in the following sections along with

the implications these basalts have for lunar evolution.

Remote sensing techniques (Sections II-V) are then used

to extend this information to unsampled areas in the attempt

to understand the global surface geochemistry of the moon.

1. Major Element Geochemistry of Lunar Mare Basalt

   Types

An immense literature on lunar samples studies exists,

largely in the 7 x 3 Proceedings Volumes, and cannot be

reviewed here in detail. Much of the discussion of lunar

basalt types that follows is derived from two excellent

recent reviews which include extensive references. Taylor

(1975) has summarized and synthesized in a readable book

much of the geological, geochemical and geophysical data

for the moon that has resulted from the Apollo missions.

The chemistry, mineralogy and petrology of lunar mare ba-

salts is extensively reviewed by Papike et al. (1976).

A variety of lunar basalt type classifications exist in

the literature. The classification by Papike et al., which

incorporates many of these previous classifications, is

based primarily on major element chemistry and is used

as the basis for the discussion presented here. A recent

pamphlet by McGee et al. (1977) provides a useful introduc-

tion to the petrology and geochemistry of representative

lunar igenous rocks.

One of the most useful chemical factors that distinguishes

various mare basalt types is TiO_2 content. Most of the

sampled lunar mare basalts can be placed into one of two

distinct chemical groups, high- and low-titanium basalts,

as shown in the variation diagram of Figure IC-2 (from Papike

et al., 1976; updated). To date no samples have been ob-

tained for intermediate titanium basalts. There is also

an apparent correlation between measured crystallization
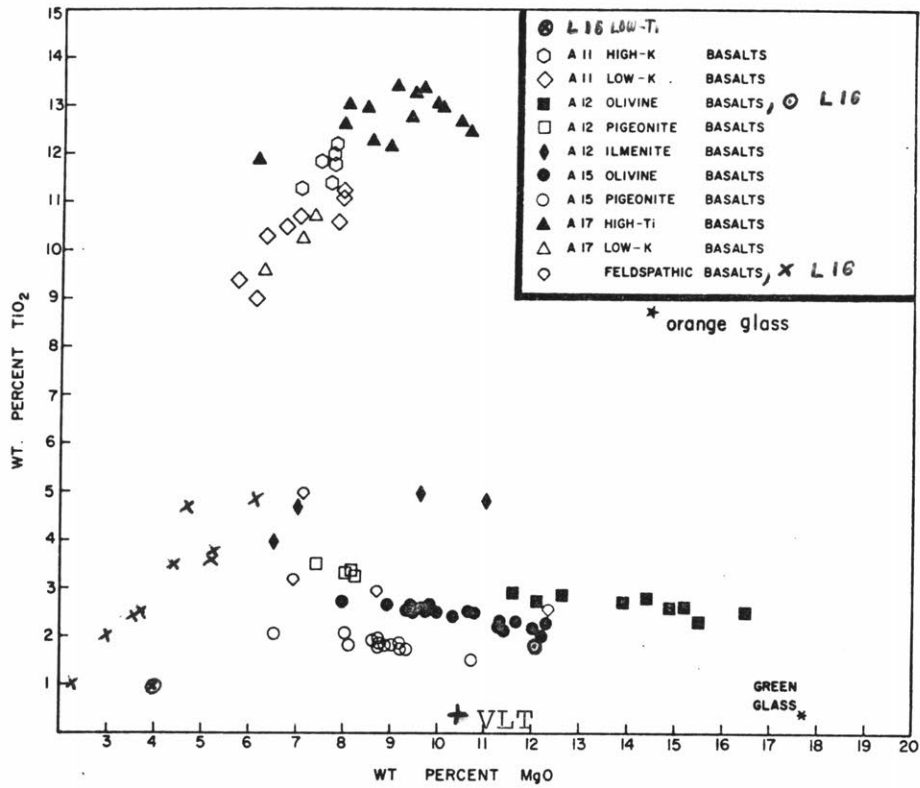
TiO₂ versus MgO (wt %) variation diagram for mare basalt major-element chemistry.

Figure IC 2. (update of Papike et al., 1976)

ages and TiO_2 content--the high-Ti basalts (Apollo 11, 17)
are older than the low-Ti basalts (Apollo 12, 15, Luna 16).
The bulk chemistry of these two major groups does not allow
a petrogenetic relation through fractional crystallization,
a distinction confirmed by melting experiments (Kesson,
1975; Walker et al., 1975).

The mare basalt samples can be further subdivided
into 10 distinct groups within which the major element
variations have likely been caused by near surface fraction-
ation. Major element chemistry for these basalt groups
are provided in Table IC-2 (from Papike et al., 1976).
The average modal mineralogy for nine of these groups is
presented in Table IC-3 and summarized in Figure IC-3 (from
Papike et al., 1976).

   a. High-Ti

      The high titanium basalts of Apollo 11 fall
into two groups which can be distinguished largely by K_2O
content. The low-K basalts (K_2O ~ .06-.09%) are somewhat
older than the high-K (K_2O ~ .30%). The petrological var-
iations observed in a variety of Apollo 11 low-K basalts
are consistent with these basalts representing the upper
portion of a single cooling unit. Initial $^{87}Sr/^{86}Sr$ data
for these two high-Ti groups indicate they cannot be derived
from the same source region (Papanastassiou and Wasserberg,
1971).

| | Apollo 11 | | | | | | Apollo 17 | | | | |
| | Low K | | | High K | | | | | | | |
	10003	10050	Avg (8)	10017	10057	Avg (6)	75055	70215	71055	74275	Avg (30)
SiO_2	39.76	40.62	40.67	40.64	39.79	40.37	41.27	37.79	38.14	38.43	38.84
TiO_2	10.50	9.61	10.18	11.78	11.44	11.77	10.17	12.97	13.41	12.66	12.35
Al_2O_3	10.43	10.87	10.40	7.98	10.84	8.84	9.75	8.85	8.62	8.51	8.84
FeO	19.80	16.51	18.68	19.65	19.35	19.28	18.24	19.66	19.20	18.25	18.94
MnO	0.30	0.26	0.27	0.24	0.20	0.24	0.29	0.27	0.26	0.25	0.27
MgO	6.69	7.82	6.92	7.68	7.65	7.56	6.84	8.44	9.04	10.26	8.52
CaO	11.13	12.65	11.70	10.65	10.08	10.59	12.30	10.74	10.77	10.38	10.80
Na_2O	0.40	0.35	0.41	0.51	0.54	0.52	0.44	0.36	0.31	0.37	0.32
K_2O	0.06	0.06	0.07	0.29	0.32	0.31	0.09	0.05	0.06	0.07	0.05
P_2O_5	0.12	0.07	0.09	0.16	0.17	0.17	0.07	0.09	0.08	0.07	0.06
S	0.18	0.11	0.16	0.22	0.22	0.22	0.19	0.18	0.17	0.14	0.17
Cr_2O_3	0.26	0.35	0.29	0.36	0.36	0.36	0.27	0.41	0.41	0.64	0.49
$\frac{Mg}{(Mg + Fe)}$	0.48	0.48		0.41	0.41		0.40	0.43	0.46	0.50	

Avg (8) indicates an average of eight samples. References and analyses used for averages are available on request.

| | Apollo 12 | | | | | | | | Aluminous Basalts | | |
| | Olivine | | | Pigeonite | | Ilmenite | | | | | |
	12009	12040	Avg (9)	12021	Avg (4)	12022	12064	Avg (4)	12038	14053	Luna 16
SiO_2	45.03	43.88	44.32	46.68	46.46	42.77	46.30	44.47	46.83	46.22	43.80
TiO_2	2.90	2.45	2.65	3.53	3.35	4.85	3.99	4.63	3.24	2.93	4.90
Al_2O_3	8.59	7.27	8.03	10.78	10.38	9.08	10.73	9.76	12.48	12.99	13.65
FeO	21.03	21.09	21.11	19.31	19.72	21.75	19.89	20.78	17.76	16.95	19.35
MnO	0.28	0.27	0.28	0.26	0.27	0.25	0.27	0.27	0.25	0.26	0.20
MgO	11.55	16.45	14.07	7.39	7.94	11.01	6.49	8.52	6.86	8.68	7.05
CaO	9.42	8.01	8.61	11.38	11.03	9.47	11.78	10.78	11.49	11.15	10.40
Na_2O	0.23	0.17	0.22	0.31	0.28	0.38	0.29	0.32	0.65	0.44	0.33
K_2O	0.06	0.05	0.06	0.07	0.07	0.07	0.07	0.07	0.07	0.10	0.15
P_2O_5	0.07	0.06	0.08	0.09	0.11	0.13	0.04	0.10	0.14	0.11	0.12
S	0.06	0.04	0.06	0.07	0.07	0.08	0.07	0.08	0.07	0.13	0.17
Cr_2O_3	0.55	0.63	0.63	0.40	0.47	0.56	0.37	0.42	0.31	0.40	0.28
$\frac{Mg}{(Mg + Fe)}$	0.49	0.58		0.41		0.47	0.38		0.41	0.48	0.39

| | Apollo 15 | | | | | | |
| | Olivine | | | | Pigeonite | | |
	15119	15555	15659	Avg (19)	15499	15076	Avg (13)
SiO_2	45.23	44.57	45.33	44.98	47.75	48.44	47.98
TiO_2	2.64	2.10	2.25	2.41	1.81	1.92	1.82
Al_2O_3	9.24	8.69	8.17	8.80	9.23	8.97	9.46
FeO	22.25	22.53	22.17	22.37	20.37	20.33	20.13
MnO	0.31	0.29	0.26	0.30	0.29	0.29	0.28
MgO	8.93	11.36	12.27	10.42	9.03	8.61	8.74
CaO	10.55	9.40	8.98	9.79	10.40	10.52	10.54
Na_2O	0.30	0.27	0.27	0.28	0.34	0.34	0.31
K_2O	0.05	0.04	0.06	0.05	0.06	0.07	0.06
P_2O_5	0.09	0.06	0.12	0.08	0.08	0.07	0.07
S	0.05	0.06	0.07	0.07	0.07	0.08	0.06
Cr_2O_3	0.47	0.61	0.50	0.57	0.52	0.31	0.47
$\frac{Mg}{(Mg + Fe)}$	0.42	0.47	0.50		0.44	0.43	

Table IC 2. Major element chemistry of lunar basalt types. (Papike et al., 1976)

Lunar basalt type   Textural Sequences

Group	Modal Mineralogy*				No. Averaged	Textural Sequence†
	cpx	ol	plag	opaq		
Apollo 11 low K	44–55 (49)	0–7 (2.2)	24–38 (31)	10–18 (14)	14	10020, 10045, 10062, 10003, 10050, (10044, 10058, 10047)
Apollo 17 low K	44–52 (48)		29–33 (31)	13–15 (14)	2	(75035, 75055)
Apollo 11 high K	47–59 (53)	0–1 (0.1)	15–27 (20)	15–26 (19)	9	10049, 10022, 10057, 10017, 10024, 10072
Apollo 17 very high Ti	42–51 (47)	1–10 (4.5)	14–29 (23)	18–30 (24)	5‡	74235, 70215, 74275, 71055, 75075, 70017, 70035
Apollo 12 ilmenite	55–61 (59)	0–20 (3.5)	12–33 (25)	7–11 (9)	6	12022, 12063, 12051, 12064
Apollo 12 olivine	32–64 (53)	36–11 (20)	5–27 (19)	3–14 (7)	14‡	12009, 12004, 12002, 12075, 12018, 12020, 12040, 12035
Apollo 12 pigeonite	62–71 (68)	0–4 (1.4)	17–31 (21)	5–12 (9)	7	12052, 12053, 12065, 12021
Apollo 15 olivine	61–64 (63)	5–9 (7)	22–27 (24)	4–6 (5.5)	3	15545, 15556, 15016, 15555
Apollo 15 pigeonite	46–70 (61)		24–48 (33)	3–4 (3.6)	3‡	15597, 15595, 15499, 15476, 15495, 15475, 15076, 15085, 15058, 15065

Values in parentheses are averages.
*Clinopyroxene is abbreviated cpx; olivine, ol; plagioclase, plag; and opaques, opaq.
†From fine at left to coarse at right.
‡Does not include vitrophyres.

MODAL MINERALOGY AND BULK COMPOSITION

Table IC 3. (Papike et al., 1976)
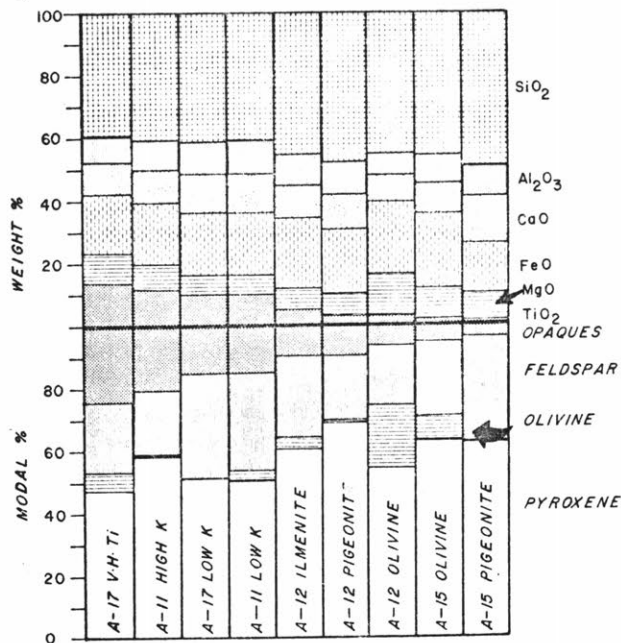
Diagram showing correlation between major-element chemistry and modal mineralogy for major mare basalt groups. Histogram is ordered left to right in terms of decreasing TiO_2 content. An obvious correlation between TiO_2 (wt %) and modal abundance of opaques is present.

Figure IC 3. (Papike et al., 1976)

There are also two major basalt types at <u>Apollo</u>
<u>17</u>. The minority <u>low-K</u> basalt samples are very similar
in composition and in age to the Apollo 11 low-K basalts.
The Apollo 17 <u>very high-Ti</u> samples are distinguished from
other high titanium basalts by their higher TiO_2, FeO,
and MgO content. The major element variations within the
very high-Ti suite of rocks can be interpreted in terms
of multiple crystal fractionation. Both Apollo 11 and
17 low-K basalt compositions could possibly have been pro-
duced by near surface fractionation from a magma similar
to that which formed the very high-Ti basalts.

   b. <u>Low-Ti</u>

      Three major groups of low titanium basalts
can be distinguished at the <u>Apollo 12 site</u>: olivine basalts,
pigeonite basalts, and ilmenite basalts. A few samples
of feldspathic basalts are also found. These three basalt
types can be distinguished in the chemical variation dia-
grams of Figure IC-4 (from Papike et al., 1976; Rhodes
et al., 1977). The major element variations for the Apollo
12 <u>olivine basalts</u> fall along olivine control lines indi-
cating the variations are due largely to the loss or gain
of olivine. The coarser-grained samples are interpreted
as olivine cumulates. The Apollo 12 <u>pigeonite basalts</u> con-
tain large zoned phenocrysts or pyroxene. They show lit-
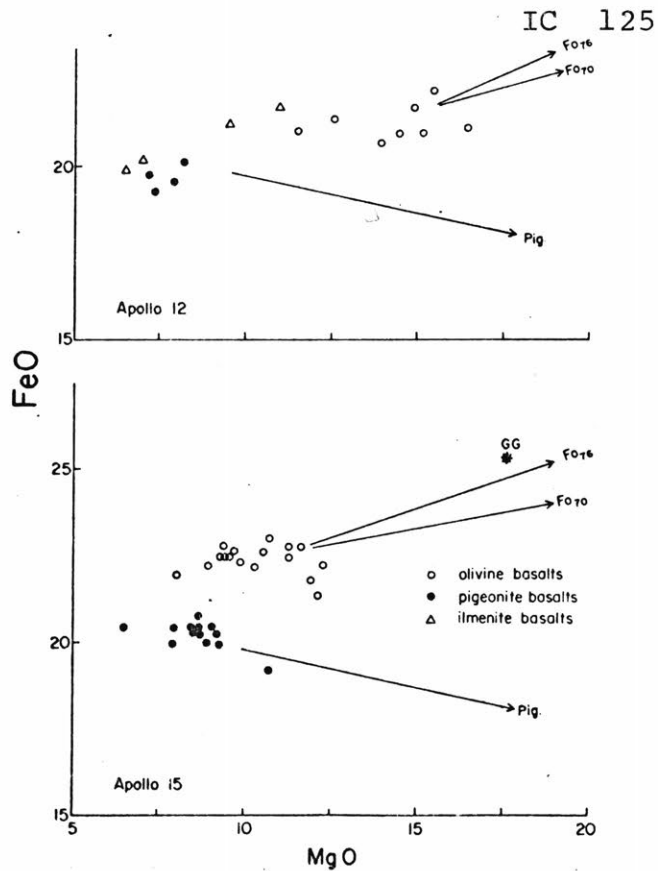
Fig. 4a. FeO versus MgO (wt %) variation diagrams for low-Ti mare basalts. Olivine and pigeonite control lines are indicated. G.G. refers to Apollo 15 emerald green glass.
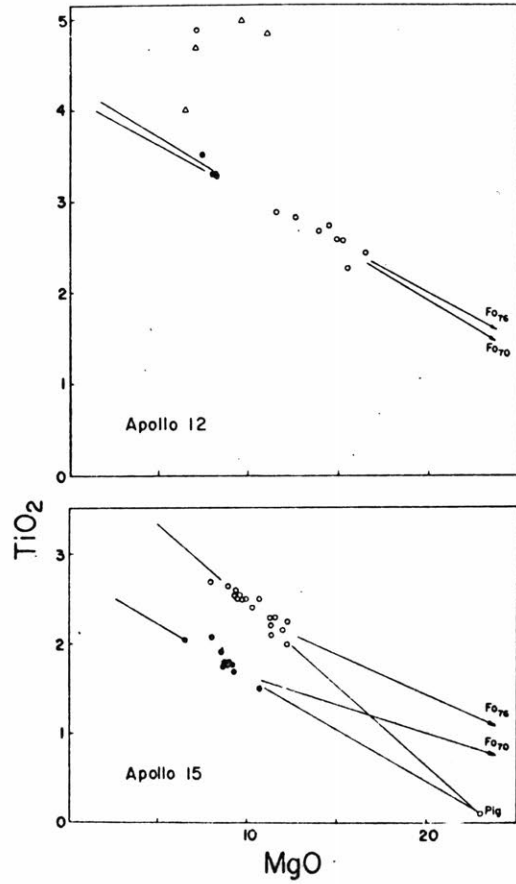
Fig. 4b. TiO₂ versus MgO (wt %) variation diagrams for low-Ti mare basalts. Olivine and pigeonite control lines are indicated.
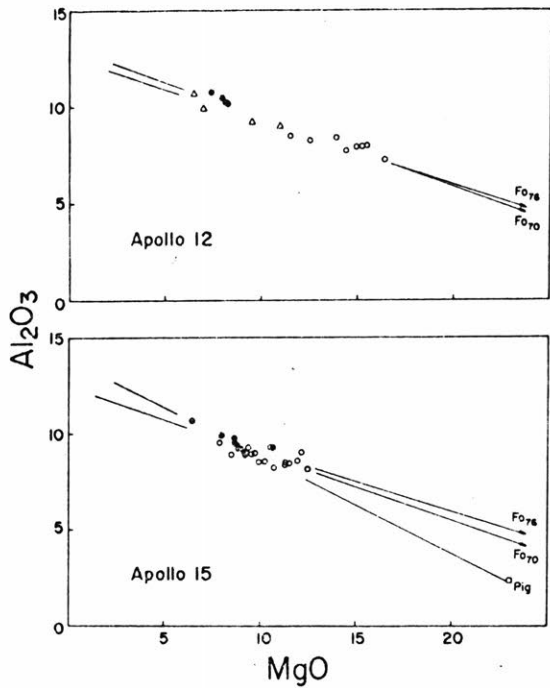
Fig. 4c. Al₂O₃ versus MgO (wt %) variation diagrams for low-Ti mare basalts. Olivine and pigeonite control lines are indicated.

Figure IC 4. (Papike et al.,1976)
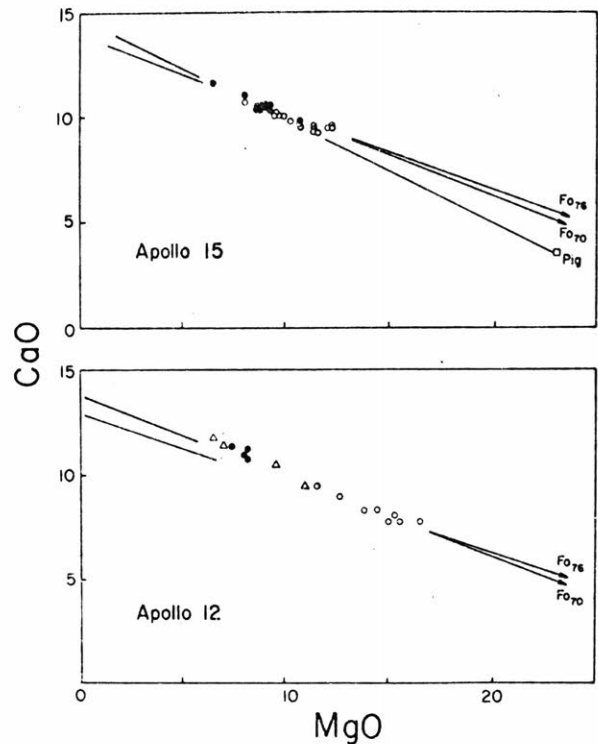
Fig. 4d. CaO versus MgO (wt %) variation diagrams for low-Ti mare basalts. Olivine and pigeonite control lines are indicated.
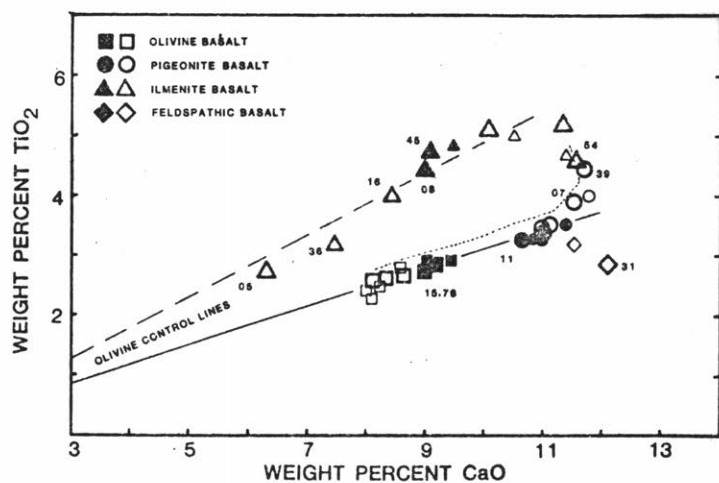
- TiO$_2$ vs CaO for Apollo12 mare basalts.

The liquid line of descent for 12002(12) is shown as a dotted line.

Figure IC 4e.   (Rhodes et al., 1977)

tle evidence of near surface fractionation although the relation of their major element chemistry to that of the olivine basalts (Figure IC-4) indicates they both could have been derived from similar parental magma. The Apollo 12 ilmenite basalts have recently been extensively studied (Rhodes et al., 1977, Nyquist et al., 1977). These results indicate that the major element compositional variations within the ilmenite basalt group can be attributable to near surface fractionation involving olivine + ilmenite (Figure IC-4e). The rare earth and isotopic data indicate the ilmenite basalt parental magma is probably derived from a distinctly different source region than that for the olivine-pigeonite basalts. Remote sensing data (see Section III) show two surface units in the Apollo 12 region with the landing site being within a few kilometers of a unit of slightly higher TiO_2 content.

The mare basalts of Apollo 15 include two basalt types similar to those at Apollo 12 but lower in TiO_2: olivine basalts and pigeonite basalts. The Apollo 15 olivine basalts are high in FeO (Figure 4a). The major element variations are consistent with a limited amount of olivine fractionation, and, together with textural evidence, indicate the samples are not olivine cumulates but are probably samples from the upper portion of cooling units.

The composition of the Apollo 15 <u>pigeonite basalts</u> do not
fall on the same olivine control lines as the olivine ba-
salts, although the two basalt types could be products
of fractionation of a single primary magma not sampled.
The major element variations of the pigeonite basalts are
consistent with a limited amount of pigeonite (and possi-
bly olivine and chrome spinel) fractionation.

    c. <u>Other (Feldspathic, VLT, Luna   24) basalts</u>

    It is possible, if not probable, that some of
the minor rock types found in the lunar samples are, in
fact, regionally important. Three general groups in par-
ticular may be significant: feldspathic basalts, very low
titanium (VLT) basalts, and the recently returned Luna 24
basalts.

    The <u>feldspathic</u> basalts (high aluminum) are
exemplified by a heterogeneous and perhaps unrelated num-
ber of samples found as minor components at several land-
ing sites (Hubbard et al., 1973; Ridley, 1975, Irving, 1975).
Their major element chemistry (Table IC-4, from Ridley,
1975) and petrographic relationships indicate they are in-
deed basaltic. Their high MgO + FeO content (Figure IC-5,
from Hubbard et al., 1973) and medium TiO_2 (Table IC-4)
distinguishes them from possible highland melt rocks. They
are distinguished from most other mare basalts by their

Major-element chemistry of aluminous mare basalts.

	1	2	3	4	5	6	7	8
SiO_2	45.9	45.2	46.3	46.82	45.50	43.80	40.2	43.7
TiO_2	7.3	2.57	2.79	2.33	4.04	4.90	7.2	3.3
Cr_2O_3	0.2	0.51	0.37	0.32		0.28		
Al_2O_3	14.4	11.1	13.7	13.81	13.95	13.65	13.2	13.2
MnO				0.26	0.26	0.20		
FeO	10.7	17.8	17.0	15.92	17.77	19.35	16.5	16.5
MgO	6.7	12.2	8.54	6.30	5.95	7.05	8.5	9.9
CaO	11.3	9.84	11.2	11.57	11.96	10.40	12.0	11.1
Na_2O	1.0	0.32	0.44	0.80	0.63	0.38	0.3	0.2
K_2O	0.1	0.08	0.11	0.25	0.21	0.15	0.10	0.16

(1) Average composition of basaltic clasts in 14063, broad beam analysis.
(2) XRF analysis of 14072, Hubbard et al. (1972).
(3) XRF analysis of 14053, Hubbard et al. (1972).
(4) Average 7 vitrophyric and variolitic clasts, 14321, Grieve et al. (1975).
(5) Basalt fragment in Luna 16 soil, Albee et al. (1972).
(6) Luna 16 basalt, Vinogradov et al. (1971).
(7), (8). Preferred glass compositions in Apollo 11, and 12 soils, respectively, Reid et al. (1972).

Table IC 4. (Ridley, 1975)
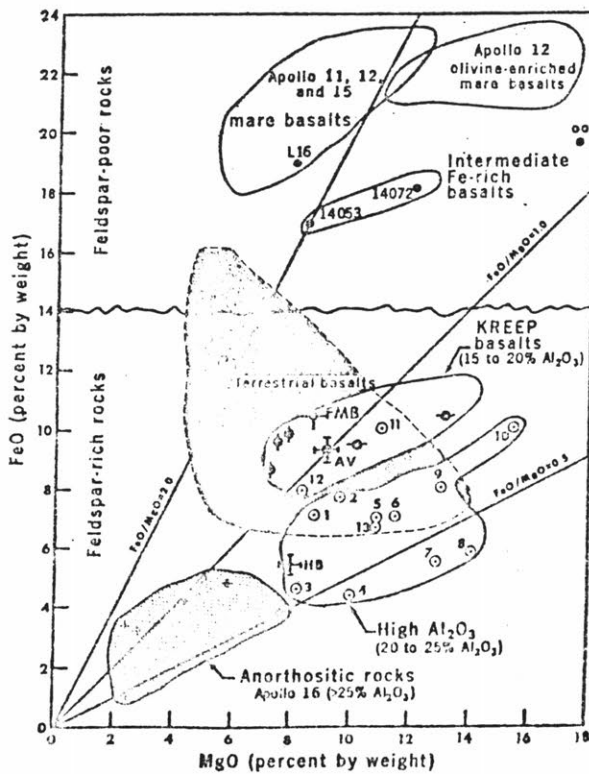
The FeO, MgO, and Al_2O_3 contents of different lunar rock types: +, rocks with more than 25 percent Al_2O_3; ⊙, rocks with 20 to 25 percent Al_2O_3; ◊, Apollo 15 KREEP basalts; ⊖, Apollo 16 KREEP basalts; AV, mean KREEP composition from broad-beam microprobe analyses of individual fragments; HB, "highland basalt" ; FMB, mean composition of Fra Mauro basalt glasses; GG, Apollo 15 green glass; L16, Luna 16 basalt. Points labeled 1, 2, 3, . . . correspond to samples 66095, 61156, 60335, 61016 (dark), 14073, 14083 (light), 15273,4,2, 62295, 22007, 15445,17, 22006, 14310, and 15273,4,3, respectively.

Figure IC 5. (Hubbard et al., 1973)

higher Al_2O_3 content, although they are frequently simply grouped with the low-Ti basalts. The few that have been dated demonstrate the heterogeniety of this 'group': 14053 is about 3.95 AE (Papanastassiou and Wasserberg, 1971; Turner et al., 1973) and predates most mare basalts, whereas a sample from Luna 16 (B-1) is about 3.45 AE (Papanastassiou and Wasserberg, 1972; Huenke et al., 1972).

Recently a comprehensive study of the mineralogy and petrology of 58 lithic fragments from the Luna 16 core has been made (Kurat et al., 1976). Three separate basalt types were identified in the samples. Fragments of the main type of Lunar 16 basalt show compositional variations (Figure IC-6, from Kurat et al.) indicative of near surface fractionation involving plagioclase, olivine, and ilmenite. These Luna 16 basalts are distinct among the returned samples and seem to form a class by themselves with low FeO and MgO, and high Al_2O_3, FeO/MgO, CaO and alkali content. Remote sensing data (Pieters and McCord, 1975) suggest the Luna 16 basalts are part of a family of basalts in the eastern maria.

A few fragments of a very low titanium basalt have been recently discovered in the Apollo 17 drill core (Vaniman and Papike, 1977). Preliminary major element chemistry of this basalt shown in Table IC-5 (Papike, per-
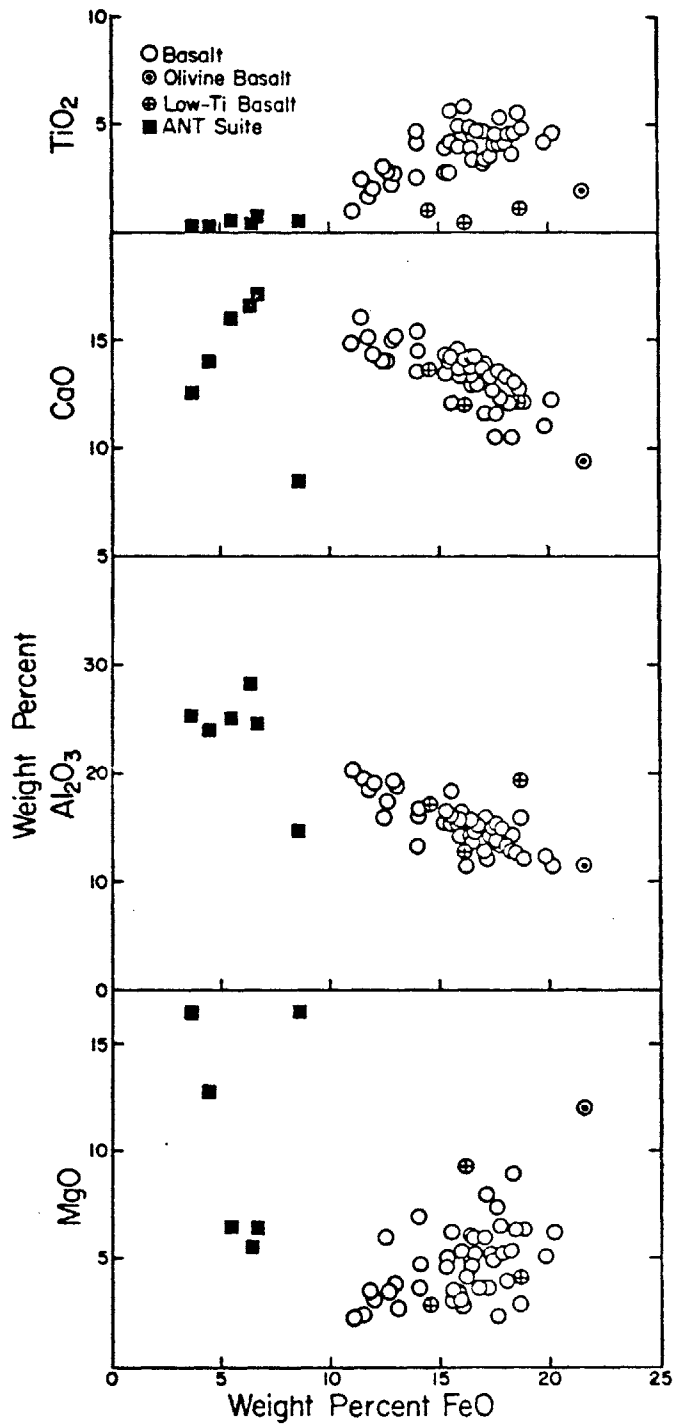
Bulk compositions of 58 igneous lithic fragments from Luna 16.

Figure IC 6. (Hurat et al., 1976)

March 12, 1977

PRELIMINARY Data on the

composition of Very Low Titanium

Mare Basalt (Apollo 17)

	phaneritic fragment[1] PTS 70008370 (1.75 mm fragment)	phaneritic fragment[1] PTS 70008356 (2.2 mm fragment)	vitrophyre[2] PTS 70007328
SiO_2	48.74	48.08	48.75
Al_2O_3	11.40	11.25	10.04
TiO_2	0.50	0.36	0.69
FeO	18.98	18.23	17.94
MnO	0.26	0.26	0.30
MgO	9.45	11.00	11.79
CaO	10.15	10.16	9.35
Na_2O	0.15	0.15	0.06
K_2O	0.04	0.01	0.02
Cr_2O_3	0.60	0.60	0.69
sum	100.27	100.10	99.63
Fe/ (Fe+Mg)	.53	.48	.46
CaO/Al_2O_3	.89	.90	.93

[1]recombination of microprobe mineral data using modal analyses obtained by counting 1000 points in each fragment. Averages of many probe analyses (e.g., 200 pyroxene spots in the fragment from PTS 70008356) were used to account for mineral zonation.

[2]recombination of microprobe mineral and glass analyses using modal data obtained by counting 1000 points in the vitrophyre.

[3]average of eight overlapping 50 micron spots within a single vitrophyre (about 85% glass, 15% small crystals up to 10 microns in diameter)

Table IC 5. (Papike, 1977, preliminary communication)

sonal communication) indicates they clearly are mare basalts

and not highland melt rocks. Their very low TiO_2 content

(which is comparable to the Apollo 15 green glass) distin-

guishes them from other mare basalts. The regional source

area of these basalts has not yet been identified.

On August 28, 1976, the Soviet Luna 24 automa-

tic probe obtained a core sample from SE Mare Crisium and

returned it to earth. Preliminary analyses of some of the

basalt fragments indicate a low titanium basalt ($\sim 1\%$ TiO_2)

with high aluminum content and low KREEP (Barsukov et al.,

1977). Although it is still uncertain which unit in Mare

Crisium was sampled (see Section IIIE-1), this low-Ti, high-

Al basalt may be unique among the samples.

2. Role of Basalts in Current Understanding of the

Moon

a. Comparison with terrestrial basalts

About 17% of the lunar surface is covered with

mare basalts (Head, 1975, 1976) compared to perhaps >75%

for the present terrestrial (e.g., oceanic) surface. The

distribution of mare basalts is shown in Figure IC-7 (from

Head, 1976). The style of volcanic eruption is dramatically

different for the two planets. Most of terrestrial volcanic

deposits are associated with recent plate tectonics, whereas

the moon has maintained a rigid lithosphere for at least

NEAR SIDE
N

60°
M. HUMBOLDTIANUM
30°
RURIS
M. FRIGORIS
S. RORIS
MORTIS
L. SOMNIORUM
M. IMBRIUM
M. SERENITATIS
P. SOMNI
M. ANGUIS
P. PUTREDINUS
M. CRISIUM
O. PROCELLARUM
M. VAPORUM
M. MARGINIS
S. AESTUUM
M. TRANQUILLITATIS
M. UNDARUM
W
S. MEDII
M. FECUNDITATIS
M. SPUMANS
M. SMYTHII
L. AUTUMNI
M. COGNITUM
M. NECTARIS
L. VERIS
M. HUMORUM
M. NUBIUM
-30°
P. EPIDEMIARUM
M. AUSTRALE
-60°
S

FAR SIDE
N

60°
30°
M. MARGINIS
M. MOSCOVIENSE
M. SMYTHII
W
M. ORIENTALE
M. AUSTRALE
M. INGENII
-30°
a
-60°
S

IC 134

Distribution of mare deposits
denotes mare; O, oceanus; S, sinus; P, palus; L, lacus.
on the lunar near side and far side (Lambert equal area projection). (a) M
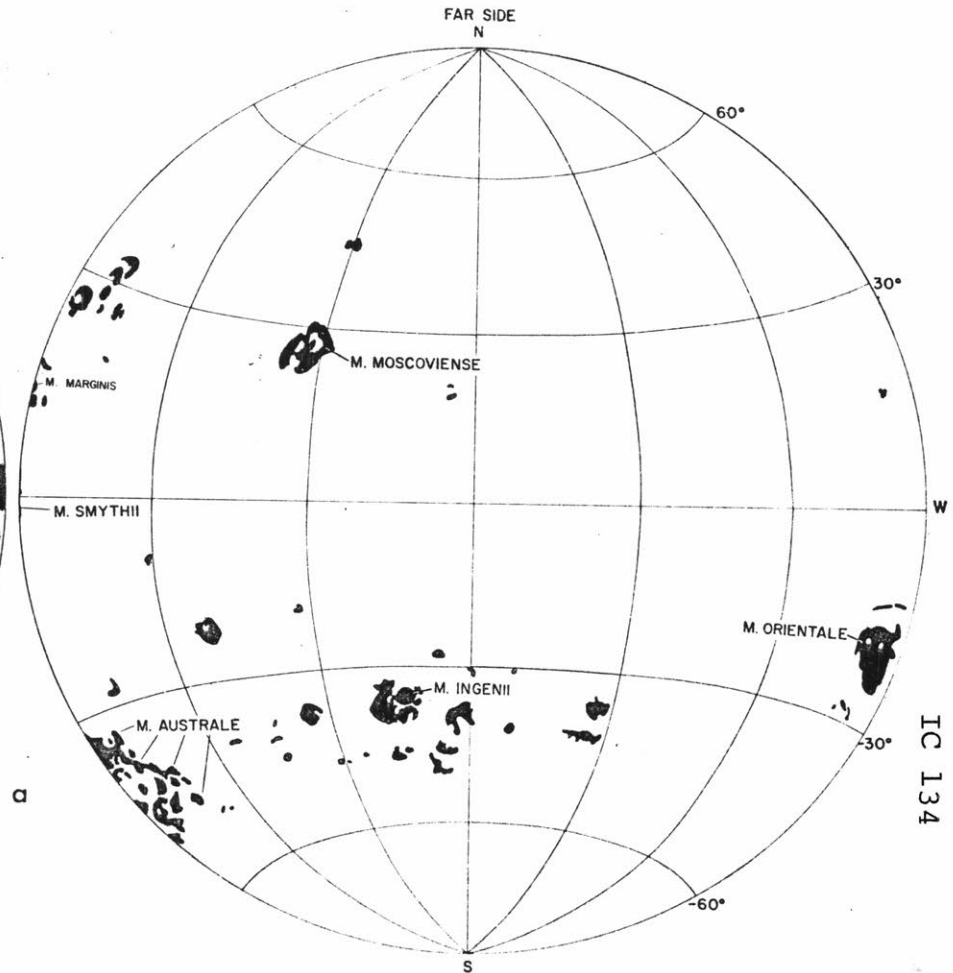
Figure IC 7. (Head, 1976)

3.5 AE. The closest recent terrestrial analogue to lunar volcanic deposits are the flood basalts and Hawaiian lavas although the origin of even these terrestrial basalts is likely to be tied to terrestrial tectonics. A summary of estimated volumes for lunar, terrestrial and Martian volcanics is provided in Table IC-6 (compiled from Head, 1975; CTV).

In major element chemistry lunar basalts are strongly enriched in FeO and in some cases TiO_2 and depleted in Al_2O_3 with respect to most terrestrial basalts (Figure 8, from Gast, 1972). SiO_2 content for lunar basalts is low with respect to terrestrial values (Table IC-2). The Hi-Ti basalts are not strictly basalts unless their SiO_2 content is recalculated for a bulk chemistry with lower amounts of TiO_2. The ranges of CaO and MgO content are roughly comparable for lunar and terrestrial basalts. Both lunar basalts and basaltic achondrites are depleted in K_2O and Na_2O with respect to terrestrial basalts (Figure IC-9, from Gast). The composition of lunar feldspars reflect this low K and Na content (Figure IC-10, from Papike et al., 1976).

The lunar basalts are in extremely reduced state and contain no water of lunar origin. Almost all iron occurs as Fe^{2+} with up to a few tenths of a percent being reduced

Table IC-6 Estimated volumes of basalt.
        (Head, 1975, CTV)

Location	Estimated volume ($\times 10^6 km^3$)
Earth: Decca, India	.7
Columbia and Snake River	.3
Siberia	.25
Parana, Brazil	.20
(Mauna Loa	.05)
Bushveld (plutonic complex)	.10
Mars: Olympus Mons	2.6
Moon: Tranquillitatis	.26
Fecunditatis	.13
Nectaris	.08
H_2, h_2 Imbrium	.04
Circular maria	5.2
Whole moon basalts	10.
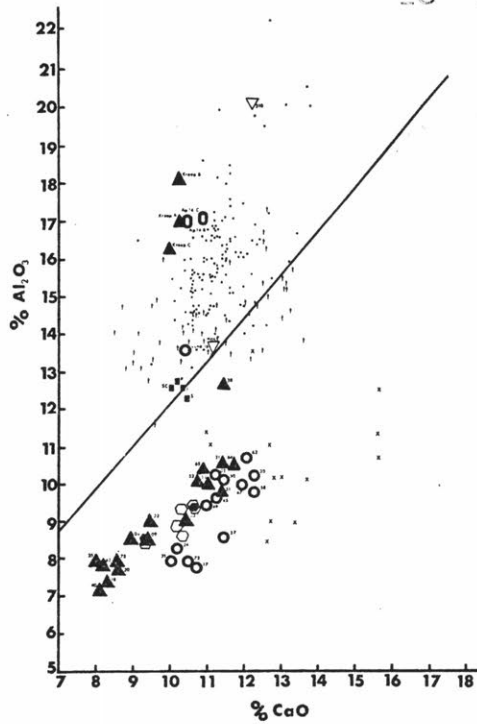
Figure IC 8. (Gast, 1972)

a

CaO and Al₂O₃ contents of lunar basalts, basaltic achondrites, and terrestrial basalts. Symbols are as follows: ○ Apollo 11 basalts, ▲ Apollo 12 basalts, △ KREEP, 0 Apollo 14 samples, ⟨⟩ Apollo 15 basalts, ▦ basaltic achondrites, · oceanic ridge basalts, † Icelandic basalts, and × post-erosional Hawaiian basalts. The solid line shows the locus of chondrites and basaltic achondrites. Both terrestrial and lunar basalts appear to divide into groups that fall on either side of this line; i.e. the Al-rich (ORB on Earth and non-mare basalt on the Moon) group with an Al/Ca ratio greater than the meteorite ratio and the Al-poor rocks with low Al/Ca ratios (nepheline norma-tive basalts on Earth and mare basalts on the Moon) lower than the meteorite ratio. Given the very plausible assumption that the Al/Ca ratio of both planets is meteoritic, this observation suggests that two distinct petrogenetic fractionation trends are involved in producing liquids with these compositions.
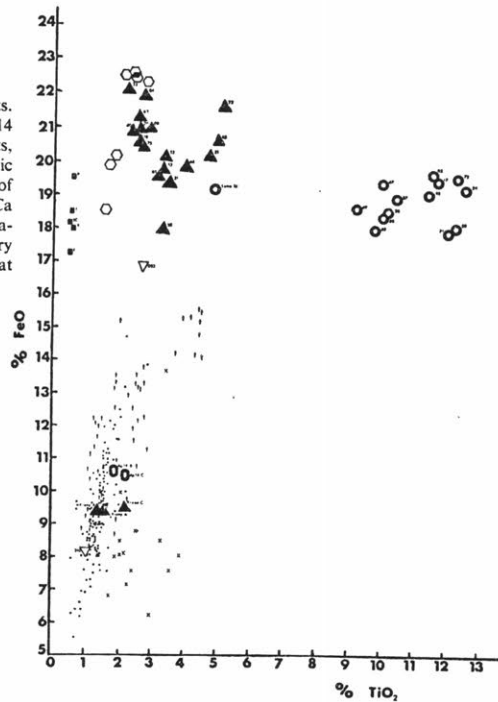
c

Total Fe (as FeO) and TiO₂ contents of lunar basalts, basaltic achondrites, and terrestrial basalts. Symbols same as Figure **a**. The extreme TiO₂ contents of Apollo 11 basalts are clearly shown here. However, other mare basalts (Luna 16) also tend to have relatively high TiO₂ contents relative to terrestrial basalts.
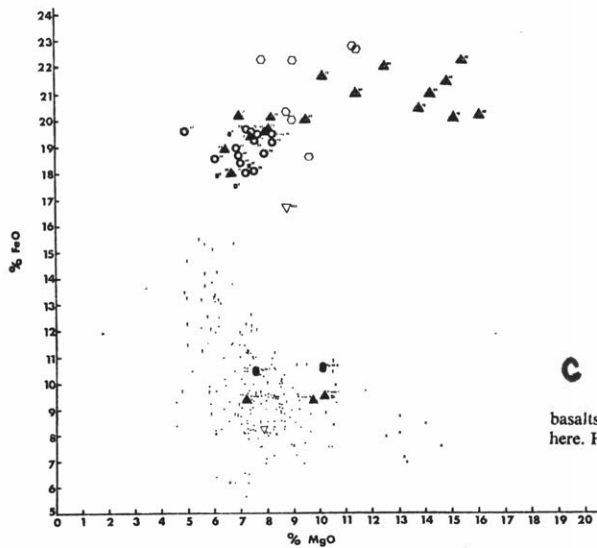
b

FeO and MgO contents of lunar basalts, basaltic achondrites, and terrestrial basalts. Symbols same as Figure **a**. The three groups of terrestrial basalts shown here were chosen to illustrate the extremes in total Fe (as FeO), FeO, Al₂O₃, and TiO₂ contents found in terrestrial basalts. A much more extensive compilation – e.g. Manson (1967) – of terrestrial basalts would still show a very marked gap between the total Fe content of lunar and terrestrial basalts. The high MgO Apollo 12 basalts are probably the result of olivine (Fa 68–72) accumulation.
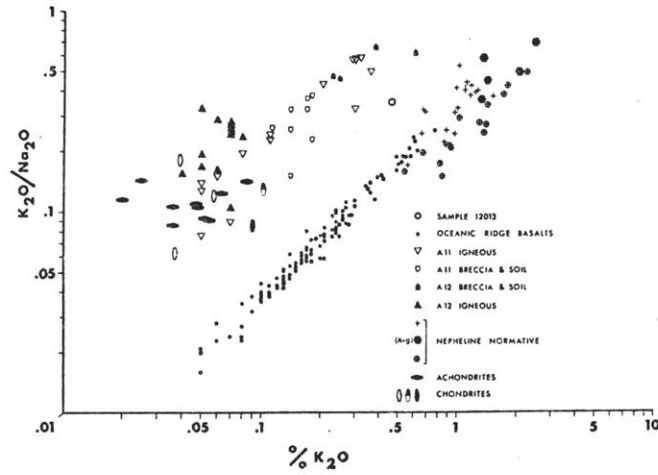
K₂O and Na₂O content of terrestrial and lunar basalts.

Figure IC 9. (Gast, 1972)
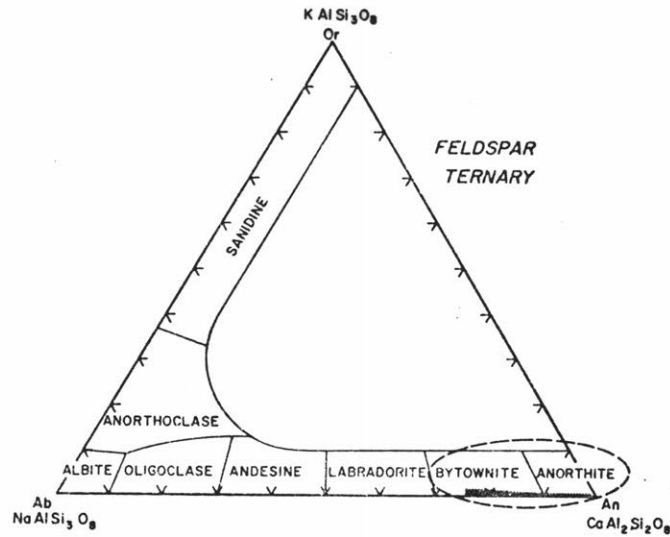
Feldspar ternary plot showing limited compositional range
of feldspars in mare basalts.

Figure IC 10.   (Papike et al., 1976)

to metalic iron. Unlike terrestrial basalts, no detectible Fe^{3+} is found in lunar basalts. The reduced state of titanium and chromium (Ti^{3+}, Cr^{2+}) are rare in terrestrial basalts but occur in significant amounts in lunar basalts (Burns et al., 1973). The oxygen fugacity value of lunar samples for a given temperature is several orders of magnitude below those for terrestrial basaltic lavas (Sato et al., 1973).

The rare earth element patterns for most terrestrial basalts are strongly enriched for the light rare earths (Figure IC-11, from Jahn and Nyquist, 1976). This pattern is found in none of the lunar basalts although the high titanium basalt REE pattern is somewhat similar to that for terrestrial oceanic tholeiites. A notable distinction of lunar mare basalts is the "europium anomaly" exhibited in their REE pattern. This relative depletion of Eu is linked to the lunar reducing conditions which allow Eu^{2+} to be stable. The geochemical behavior of Eu^{2+} is distinct from Eu^{3+}; Eu^{2+} can readily enter the Ca site in feldspar lattices. The europiun anomaly is generally interpreted as indicating the removal of feldspar from the source region of mare basalts prior to their generation (see summary in Taylor, 1975, p. 154-159).
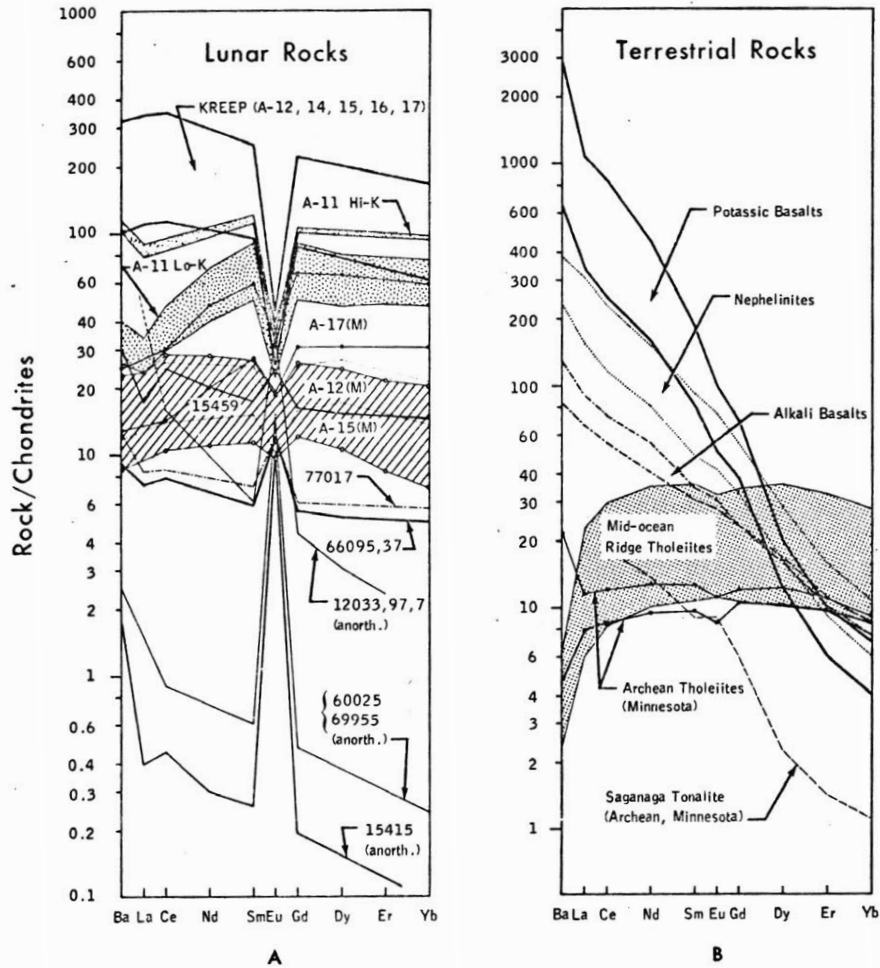
Ba and REE abundance patterns for various lunar and terrestrial rocks. The
difference in the shapes of the patterns is very striking. In the case of lunar rocks,
KREEP and mare basalts (A-11, Hi-K, Lo-K, A-17(M), A-12(M), and A-15(M))
have distinct negative Eu anomalies. In contrast, all anorthositic rocks (15459,
77017, 66095, 12033, 60025, 69955 and 15415) have positive Eu anomalies but
much lower total REE abundances. VHA basalts or troctolitic rocks (not shown)
have REE abundances intermediate of those of KREEP and anorthositic rocks. In
the terrestrial case, two Archean tholeiites from Minnesota have REE patterns
comparable with the oceanic ridge or island arc tholeiites; and an Archean tonalite
shows a strong depletion in heavy REE. Sources: Gast et al. (1970), Hubbard and
Gast (1971), Hubbard et al. (1972, 1974), Schnetzler et al. (1972), Laul and Schmitt
(1973), Philpotts et al. (1974), Rhodes and Hubbard (1973), Kay et al. (1970), Kay
and Gast (1973), Arth and Hanson (1972) and Jahn et al. (1974)

Figure IC 11.   (Jahn and Nyquist, 1976)

Comparisons of element abundances between Apollo

12 basalt 12009 (a possible primary partial melt from the

interior) and type 1 carbonaceous chondrites (primitive

solar system material) is shown in Figure IC-12, from Taylor,

1975. Taylor (1975) suggests three and perhaps four stages

of fractionation for lunar material to account for these

differences: (1) pre-accretional fractionation (loss of

volatiles and probably also siderophiles), (2) post-accretional

wide-spread early melting (see below) with fractionation

creating a zoned lunar mantle, (3) later partial melting

of this mantle leading to further element fractionation,

and (4) possible fractionation of this melt en route to the

surface and/or during surface crystallization.

Similar elemental comparisons can be made be-

tween terrestrial mantle derived basalts (e.g., oceanic

tholeiites) and Apollo 15 olivine basalt 15555. Figure IC-13

(from Taylor, 1975) illustrates the general depletion of

K and Na in lunar basalts and the enrichment of Fe and Cr.

b. Chronology

One of the most notable characteristics of lu-

nar rocks is their age. Lunar mare basalts crystallization

ages range from about 3.2 to 3.85 AE. A summary of many

of the isotopic age dating results and appropriate refer-

ences is provided by Taylor (1975) and shown in Table IC-7.
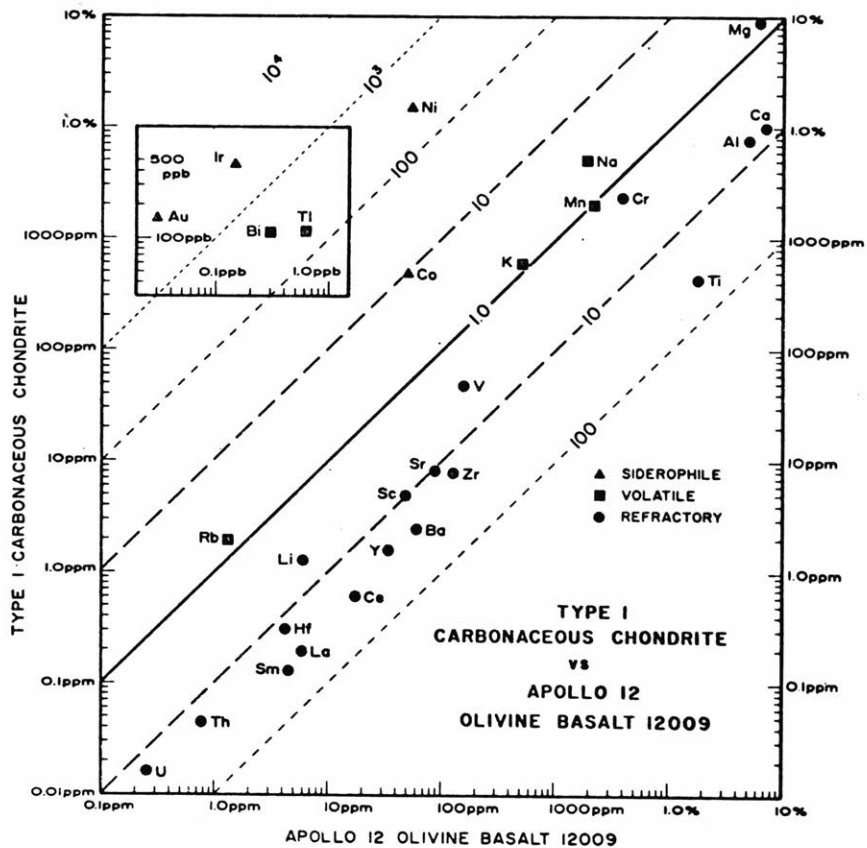
Comparison of the average composition of Type I carbonaceous chondrites (data from Mason) taken as representative of the abundances of the nonvolatile elements in the solar system nebula, with those in a primitive Apollo 12 olivine basalt 12009. This sample is one of the best examples of an unfractionated primary melt from the lunar interior. Points lying along the 45° diagonal full line indicate equality in composition. Increasing distance from the diagonal line indicates increasing disparity in composition. The dashed lines indicate limits for differences by factors of 10, 100, 10³, and 10⁴. Elements lying to the right of the equal abundance line are enriched in the lunar sample. Those lying to the left are depleted.

The volatile, siderophile and refractory elements are indicated by distinctive symbols.

Note the very wide dispersion of abundances, with some volatile and siderophile elements depleted in the lunar sample by factors of 10³–10⁴. Note the rather uniform enrichment of the refractory elements by factors of 10–20. Three stages of fractionation separate 12009 from the primitive abundances. These are (a) preaccretion separation of volatile and siderophile elements, (b) differentiation following initial lunar melting at about 4.5–4.6 aeons to form source region of maria basalts, (c) partial melting in source region at 3.2 aeons to produce 12009. This olivine basalt reached the surface as a liquid, so that its composition is not affected by a fourth stage of subsequent fractional crystallization.
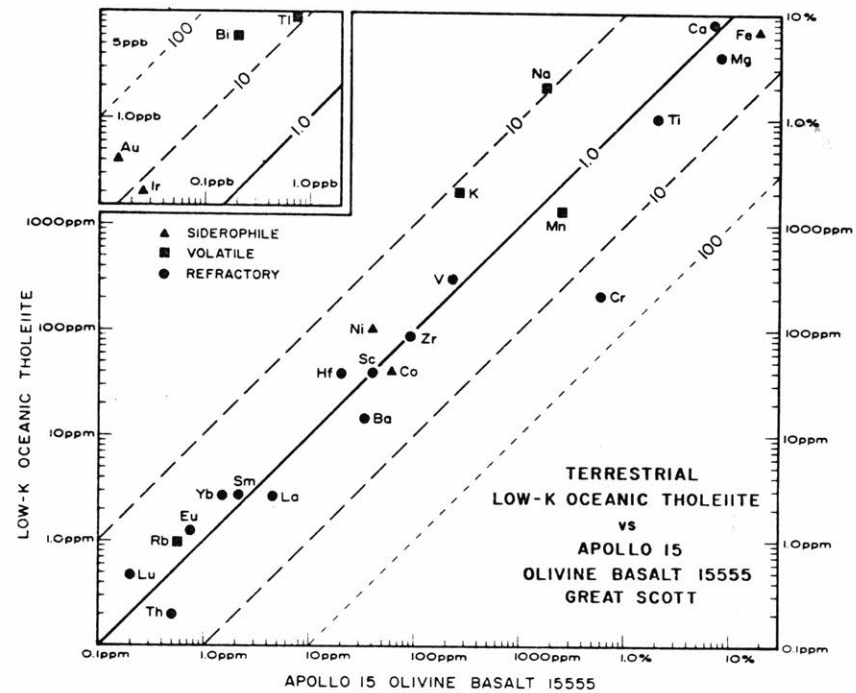
Comparison of the element abundances in low-K oceanic tholeiites (taken as representative of an important terrestrial primary magma) with that of Apollo 15 olivine basalt 15555, a typical lunar primary magma. Construction of the diagram as for Fig. 4.31.

Note that there are many similarities in composition but that a few decisive differences remain. These include the diagnostic lunar element Cr, greatly enriched in the lunar basalt, and the alkali elements Na, and K, which show their characteristic lunar depletion. The rare volatile (Bi, Tl) and siderophile (Au, Ir) elements also show a characteristic lunar depletion.

Figure IC 13. (Taylor,1975)

IC 142

Figure IC 12. (Taylor, 1975)

Ages of Maria Basalts.

	Age (aeons)	Rock type	Sample no.	Method	Reference	T BABI (p. 65) (aeons)
Apollo 14	3.96	Al-basalt	14053	Rb-Sr	101	4.60
	3.95	Al-basalt	14053	$^{40}Ar-^{39}Ar$	102	—
	3.95	Al-basalt	14321	Rb-Sr	101	4.24
Apollo 17	3.83	High Ti	75055	Rb-Sr	103	—
	3.82	High Ti	70035	Rb-Sr	104	—
	3.76	High Ti	75055	$^{40}Ar-^{39}Ar$	102	—
	3.74	High Ti	75083	$^{40}Ar-^{39}Ar$	105	—
Apollo 11	3.82	Low K	10062	$^{40}Ar-^{39}Ar$	106	—
	3.71	Low K	10044	Rb-Sr	107	4.52
	3.63	Low K	10058	Rb-Sr	107	—
Apollo 11	3.68	High K	10071	Rb-Sr	107	3.86
	3.63	High K	10057	Rb-Sr	107	3.90
	3.61	High K	10024	Rb-Sr	107	3.84
	3.59	High K	10017	Rb-Sr	107	3.80
	3.56	High K	10022	$^{40}Ar-^{39}Ar$	108	—
Luna 16	3.45	Al-basalt	B-1	$^{40}Ar-^{39}Ar$	109	—
	3.42	Al-basalt	B-1	Rb-Sr	110	—
Apollo 15	3.44	Quartz basalt	15682	Rb-Sr	111	4.06
	3.40	Quartz basalt	15085	Rb-Sr	111	—
	3.35	Quartz basalt	15117	Rb-Sr	111	—
	3.33	Quartz basalt	15076	Rb-Sr	111	—
	3.32	Olivine basalt	15555	Rb-Sr	111	—
	3.31	Olivine basalt	15555	$^{40}Ar-^{39}Ar$	112	—
	3.26	Quartz basalt	15065	Rb-Sr	111	—
Apollo 12	3.36	Olivine basalt	12002	Rb-Sr	107	4.56
	3.30	Olivine basalt	12063	Rb-Sr	107	4.33
	3.30	Olivine basalt	12040	Rb-Sr	107	4.64
	3.27	Quartz basalt	12051	$^{40}Ar-^{39}Ar$	108	—
	3.26	Quartz basalt	12051	Rb-Sr	107	4.48
	3.24	Olivine basalt	12002	$^{40}Ar-^{39}Ar$	108	—
	3.24	Quartz basalt	12065	$^{40}Ar-^{39}Ar$	108	—
	3.18	Quartz basalt	12064	Rb-Sr	107	4.98
	3.16	Quartz basalt	12065	Rb-Sr	107	4.38

Table IC 7.   (Taylor, 1975)

The oldest major group is the high-titanium basalts although some of the Apollo 14 feldspathic basaltic clasts are older. Figure IC-14 (from Papike et al., 1976) illustrates the bi-modal distribution of the basalt ages of returned samples into old high-Ti and 'young' low-Ti groups although there is also a hint of an old low-Ti group.

Internal mineral Rb-Sr isochrons used for obtaining many of the above crystallization ages (e.g., Figure IC-15, from Papanastassiou and Wasserberg, 1971) also provide an initial $^{87}Sr/^{86}Sr$ (I) value. Measured values for initial $^{87}Sr/^{86}Sr$ for lunar samples are shown in Figure IC-16 (from Jahn and Nyquist, 1976). The range of these I values indicate that the source regions of the mare basalts were heterogeneous at the time of partial melting. The lunar mantle must have developed a heterogeneous nature prior to $\sim$4.0 AE.

c.   Two stage melting hypothesis

An increasing amount of data indicates the outer 100-500 km of the moon was partially or totally molten very shortly after accretion of the planet. Most theories of mare basalt petrogenesis call for a later partial remelting of various portions of the solidified magma ocean. A few of the most compelling arguments for this popular hypothesis of early lunar evolution are outlined below.
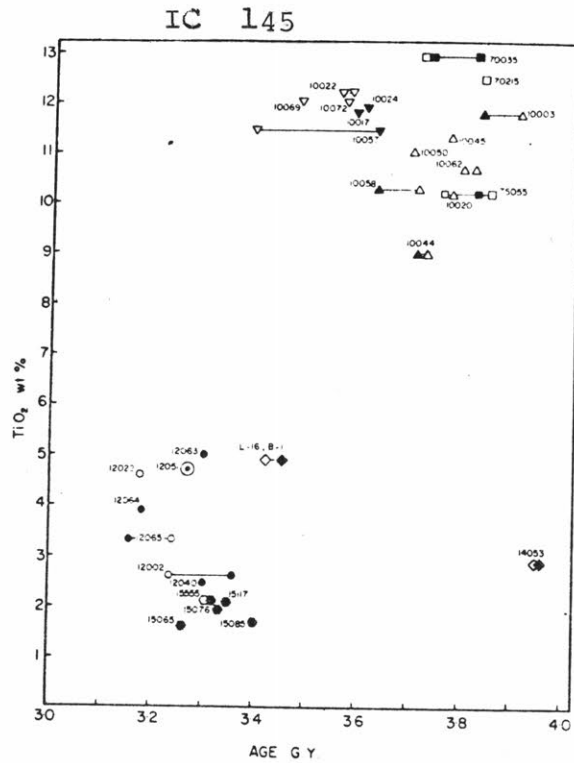
Ages of mare basalts. Open symbols indicate $^{40}Ar/^{39}Ar$, and solid symbols Rb-Sr. Triangles indicate Apollo 11 low K, and inverted triangles Apollo 11 high K.

Figure IC 14.
(Papike et al.,
1976)
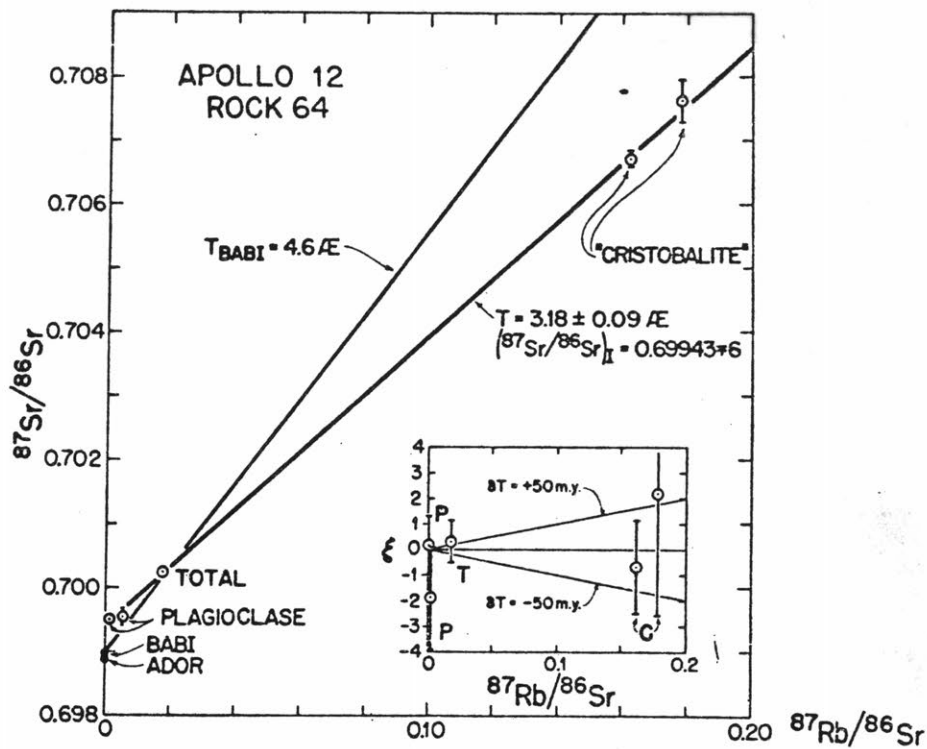
Rb-Sr evolution diagram for rock 12064. The best fit parameters as well as the reference 4.6 AE isochron and BABI composition are shown. The total range of enrichment in $(^{87}Sr/^{86}Sr)_m$ is 1.2%.

Figure IC 15.   (Papanastassiou and Wasserburg, 1971)
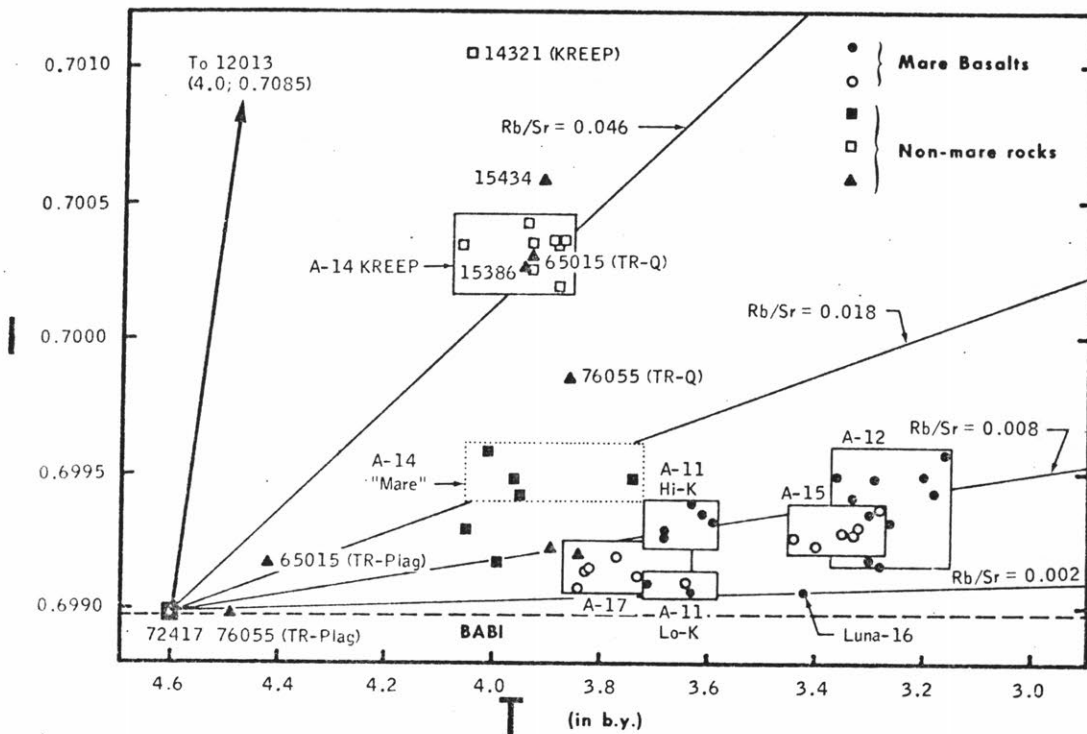
Sr isotope evolution diagram (or *I*, *T* plot) for lunar samples. The majority of the data presented here are from the works of the C.I.T. group. Other data are as reported by workers at the Australian National University, the University of Minnesota, the Johnson Space Center, the University of California at Los Angeles, and U.S. Geological Survey, Denver

Figure IC 16.   (Jahn and Nyquist, 1976)

The composition of the lunar crust was first
inferred from anorthosite fragments found in Apollo 11 soil
(Wood et al., 1970). If the major element composition of
lunar material was roughly chondritic, the original surface
would have to be melted to about 200 km depth to account
for the presence of such an observed anorthositic crust
(a floating cumulate formed by crystal fractionation).
The europium anomality observed in all lunar basalts (Figure
IC-11) further suggests the prior removal of large amounts
of plagioclase from the source region of mare basalts (e.g.,
Philpotts and Schnetzler, 1970; Taylor and Jakes, 1974).

Rb-Sr isotopic data provide further evidence
that Rb last separated from Sr in a global fractionation
event around 4.4 - 4.5 AE (Papanastassiou and Wasserburg,
1971). A model age (T_{BABI}) of when Rb and Sr were last
fractionated can be estimated from whole rock data assum-
ing an initial $^{87}Sr/^{86}Sr$ value equal to that found in ba-
saltic achondrites (Figure IC-15). Most T_{BABI} ages clus-
ter around 4.5 AE (see Table IC-7) indicating the moon,
or specifically the source regions of most basalts, behaved
approximately as a closed system with no major later frac-
tionation in Rb/Sr. The discovery of a dunite differentiate
with a crystallization age of 4.55 AE (Papanastassiou and
Wasserburg, 1975) tightens the Rb-Sr case for early lunar

differentiation.

Sm-Nd isotopic systematics for an Apollo 17 basalt (Lugmair et al., 1975) indicate a fractionation event of the parent material at 4.35 AE. Independent U-Pb chronologies for Apollo 17 basalts (Tera and Wasserburg (1974) also indicate similar ages (4.43 AE) for an early lunar differentiation, with later derivation of the basalts from a closed U/Pb system.

Solomon and Chaiken (1976) recently examined a variety of plausible thermal evolution models to account for the age of observable structural features (or lack of) on the lunar surface. There are no features indicative of large compressional or tensional stresses since the formation of the major basins and emplacement of the lunar maria. The only thermal models that can account for this lack of whole planet volume change through 4 AE requires an initial hot surface and cold interior. They argue the original "magma ocean" could not have been deeper than 300 km nor shallower than 100 km.

d.   Mare basalt source regions

The mare basalt magmas are believed to have been derived as partial melts generally from the lunar mantle which, from the previous discussion, include a 100-300 km deep fractionated zone originating from an early magma

ocean. The details of the geochemical structure of the

mantle are not entirely agreed upon although common features

include basal zones of olivine and pyroxene cumulates, crus-

tal plagioclase (late floating cumulate) and some sub-crustal

residual material that is generally enriched in incompati-

ble elements (Taylor and Jakes, 1974; Hollister, 1975; Hub-

bard and Minear, 1975; Wood, 1975; Walker et al., 1975;

Taylor, 1975; Longhi, 1977; Soloman and Longhi, 1977).

Two such models of the lunar mantle composition are shown

in Figure IC-17 (from Taylor, 1975) and Figure IC-18 (from

Hollister, 1975).

Hypotheses for the genesis of mare basalts are

circularly dependent on models of the lunar interior. Most

current models involve simple remelting of various cumulate

layers with or without assimilation of other heterogeneous

pockets or more primitive (deeper, unfractionated) material.

An unbiased critical review of competing models of mare

basalt petrogenesis has not been presented and is beyond

the scope of this description. Discussion of a variety

of these models include Walker et al. (1975), Ringwood and

Green (1975), Hubbard and Minear (1975), Drake and Consol-

magno (1976), O'Hara et al. (1975), Kesson and Ringwood

(1976), Ma et al. (1976), Ringwood and Kesson (1976), Shih

and Schonfeld (1976), and Taylor and Jakes (1974, 1977).
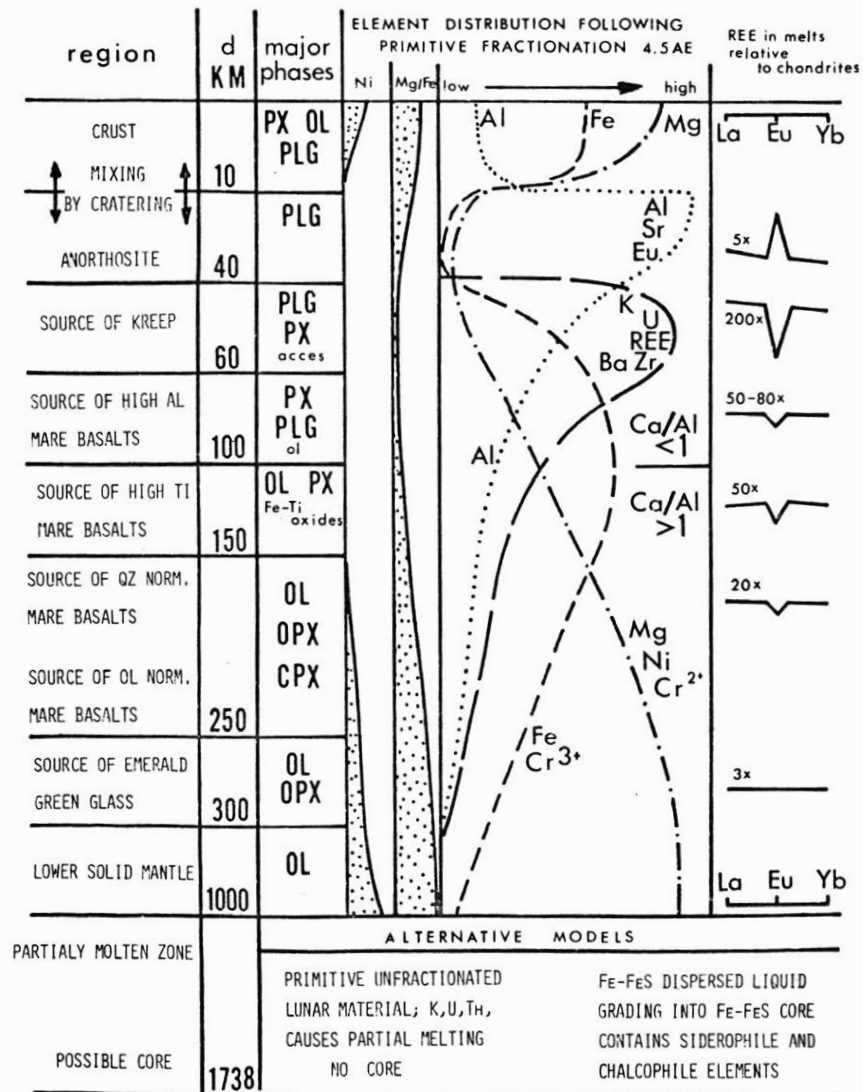
Figure IC 17. (Taylor, 1975
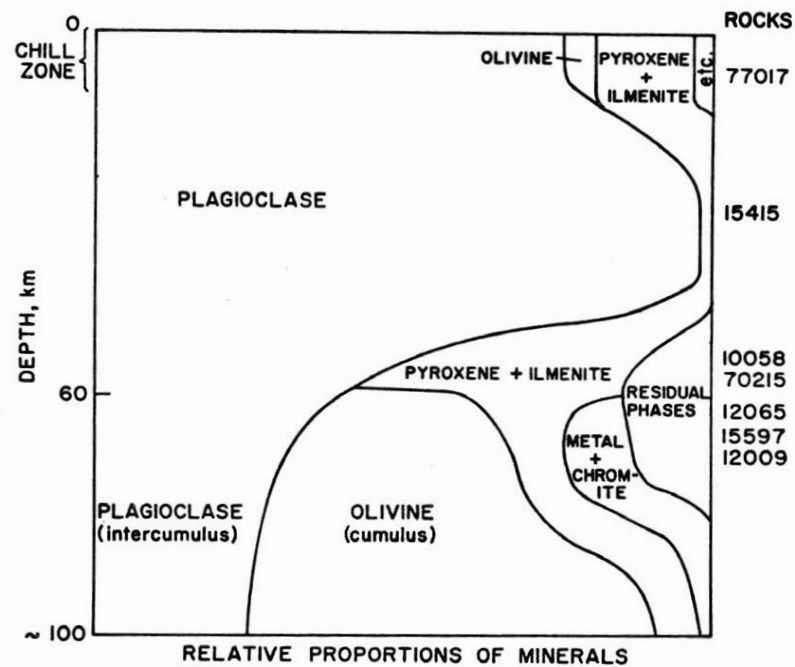
Relative proportions of minerals in shell A as a function of depth, after crystallization of shell A. The mineral proportions do not take into account the change in composition by addition of melt from below 100 km. The thickness of the chill zone is arbitrary. The source region, based on the model, for some well-characterized samples is indicated.

Figure IC 18. (Hollister, 1975)

IC 150

High pressure equilibrium experiments on lunar basalts (e.g., Hays and Walker, 1974) can be used to estimate depth of partial melting and the mineralogy of the residuum (e.g., Ringwood and Essne, 1970) assuming the sample represents the equivalent of a primary (unfractionated) liquid. There is still much discussion concerning the degree to which particular samples can be considered quenched primary melts or the products of significant fractionization prior to extrusion (O'Hara et al., 1975). The extensive literature concerning experimental studies has been recently evaluated and reviewed (Kesson and Lindsley, 1976). There is a widespread opinion that the low-Ti parental magma formed by partial melting of an olivine-pyroxene mantle at depths of 200-500 km. There is less agreement concerning the high-Ti basalts with the two prevalent views being (a) partial melting of an olivine-pyroxene-ilmenite source at $\sim$120 km, or (b) partial melting at or below 240 km of an olivine-pyroxene source that is either intrinsically enriched in Ti or contaminated by Ti enriched phases formed at different depths. Both the orange and green glass present anomalities and may represent partial melts of an olivine-pyroxene source at depths of 400 km or more. (Alternatively, these unusual glasses may be products of large degrees of partial melt.)

Although no experimental data exist for the
Luna 16 high alumina basalts, their bulk chemistry suggests
they could be derived by partial melts of the lower crust
or upper mantle ($\sim$40-100 km)(Kurat et al., 1976). The low
initial strontium ratio for Luna 16 basalts (see Figure
IC-16) suggests a distinct source region comparable in Rb/
Sr to that for the low-K high-Ti basalts.

3.   Unanswered Questions

Further detailed and extensive study of existing
lunar samples will certainly clarify some of the models
for mare basalt petrogenesis and lunar evolution in gen-
eral. Before any of these models can be generally accepted,
the following questions must be answered concerning the
relation of the lunar samples to the whole moon:

(a)   How representative are the samples of the major
geochemical units on the moon? What is the relative glo-
bal proportions of rock types identified in the samples?
What is the geochemistry of unsampled regions?

(b)   What is the temporal sequence of mare basalt types?
Are the current patterns seen in the lunar samples repre-
sentative?

Answers to these questions are essential in deter-
mining the composition and degree of heterogeniety (verti-
cal and lateral) of the lunar mantle. The temporal and

volumetric relations between global basalt types put constraints on thermal models related to basalt petrogenesis. Until further samples are obtained, remote sensing techniques are the only means by which to derive answers to the above questions. Information concerning regional and global geochemistry that can be derived from spectral reflectance measurements is discussed in the remaining sections.

II. REMOTE SENSING OF THE MOON

II.   REMOTE SENSING OF THE MOON

A.   General: Current Techniques of Remote Sensing

Definition and characterization of planetary surface

units provide the basic framework for understanding the

planet as it currently exists as well as the placing con-

straints on its past history.   A variety of techniques cur-

rently exist which provide information about a surface

from remote observations (Figure IIA-1 and Table IIA-1,

from Head et al., 1976).   All but one of these remote sens-

ing techniques involve the detection of electromagnetic

radiation; only segments of the electromagnetic spectrum,

however, have been utilized in remote observations (see

Figure IIA-1).   Many observations can only be made from

orbit due to the absorption characterisitics of the earth's

atmosphere.

Existing remote sensing techniques were examined in

detail by Head et al. (1976, 1977) and subdivided into three

types according to how the information they provide is used

for mapping the geology and geochemistry of unvisited plan-

etary surfaces: (1)   Characterizing (C in Table IIA-1)

techniques allow the classification and characterization

of chemical composition, lithology, or physical features.

(2)   Defining techniques (D) help to define the boundaries

and extent of units.   (3)   Supporting techniques (S) pro-

Figure IIA 1. Radiation ulilized by remote sensing techniques.
(Head et al., 1976, 1977)

Technique	Type	Use or potential use in mare areas
γ-ray spectroscopy	C	Provides regional variations in Th, K, Ti, Fe, Mg, concentration; low spatial resolution but general correlation with mapped units.
X-ray spectroscopy	C	Provides regional variations in Al/Si ratios. Regional variations seen between and within maria.
UV spectroscopy	S	Potential supporting technique.
Spectral Reflectance	C	Provides quantified information on composition, mineralogy, and soil maturity; e. g., TiO_2 content of mature mare soil, major mafic mineral content and composition.
Spectral Imagery	D	Reveals boundaries of units characterized by specific spectral reflectance properties. When images are quantitative, some characterizing properties can be mapped if the correct spectral bands are used.
Albedo	D, C	Used qualitatively in basic distinction of mare units from highlands. Quantitative albedo measurements are used to subdivide mare units. Within an area of similar maturity, can be used as an indication of compositional variation.
Polarimetry	S	Provides information on the surface regolith (as a combined function of complex refractive index and particle size).
Visual Observations, Photography	D, C	Used in basic definition of unit boundaries and extent (regional topography, and local topography such as flow fronts). Other observations such as surface texture and qualitative estimates of crater density are useful in unit characterization.
Infrared Radiometry	S	Measures thermal inertia $\sqrt{K\rho C}$; Surface density (blockiness) major influence but other parameters may have an effect.
Spectral Emittance	C(?)	May provide information on Si/O ratio and also mineralogy, if soil particle size is large. Little data available.
Radar (Backscatter and Imagery)	D,C,S	Radar imagery helps define extent of some units. Backscatter may also be helpful as a characterizing and supporting technique by providing information on crater density, block distributions, regolith thickness, and composition.
α-particle	S	Provides regional variations in ^{222}Ra and ^{210}Po.

Table IIA 1. Uses of remote sensing techniques.
(Head et al., 1976, 1977)

IIA 157

vide additional useful information but are not necessarily

fundamental to the unit characterization or definition.

The remote sensing techniques that will be discussed

in detail in the following sections and used for geochem-

ical exploration are spectral reflectance and multi-spectral

imaging. Both techniques utilize the spectral character

of reflected solar radiation in the visible and near infra-

red spectral region. The basic principles of the techniques

(described in Section IIC and IID) rely on well-defined

absorption characteristics of transition metal ions (Fe,

Ti, Cr, etc.) in minerals. Spectral reflectance measure-

ments refer to continuous spectra, generally measured for

a single small area with 50-300Å resolution through the

spectral range of .3 to 2.5μm. Spectral reflectance mea-

surements provide information about the mineralogy of the

surface material and are thus a characterizing technique.

Multi-spectral imaging is used to map a particular spectral

parameter (intensity ratio) in two dimensions. If the

spectral characteristics of a unit can be uniquely defined

with a few parameters, multi-spectral imagery obtained

at the characteristic wavelengths is used to map the regional

extent of the unit. Multi-spectral imagery is thus a de-

fining technique and is currently used through the spectral

range .35 to 1.0μm (being limited by the sensitivities of

two-dimensional detectors available).

II. REMOTE SENSING OF THE MOON

B. Outline of Previous Work in Spectral Reflectance

Prior to the late 1960's, most of the astronomical observations concerning the color of the moon was either photographic imagery or broad band photometry. The photometry was obtained primarily with the classical astronomical filters: U (.35μm), B (.45μm), V (.55μm). This early work showed that small color differences exist from place to place on the moon, but no geological or geochemical significance was discerned or attempted. A thorough summary of this data can be found in McCord (1968a).

In the late 1960's, two types of research were begun which have since both merged and expanded into the general field of spectral reflectance of the lunar surface. In 1968 high precision photoelectric measurements were obtained of the reflectance from .40 to .80μm of many (83) small lunar areas relative to a standard lunar area (McCord,1969a). Such measurements were later expanded to include the spectral range from .40 to 1.10μm for about 20 areas (McCord and Johnson, 1969). Concurrently, spectral reflectance measurements in the visible and near infrared were being made in the laboratory for samples of powdered rocks and minerals (White and Keester, 1966; Adams and Filice, 1967). It was recognized that the spectral differences observed remotely using a telescope were intimately related

to and dependent on the geochemistry of the material observed (Adams, 1968; Adams and McCord, 1970). Strong supporting independent evidence for this hypothesis was provided by the interpretation of transmission spectra of oriented crystals using crystal field theory (e.g., Burns and Fyfe,1967 Burns,1970a). The interpretations of transmission spectra of minerals provided sound theoretical basis for linking the spectral characteristics of rocks and minerals to their geochemistry (see Section II-C-1).

An abundant amount of research concerning spectral reflectance ensued, largely as an outcome of this intial pioneering work by McCord and Adams. For this review, the relatively recent telescopic and laboratory research results reported in the scientific literature have been divided for convenience into six catagories and are outlined below. Some papers have signficant amounts of material that fall into more than one category. Not included are a scattering of additional broad-band lunar photometry that either confirm earlier work or are not relevant to a discussion of spectral features of lunar material.

1.   Laboratory Reflectance Measurements: General

During the last decade, a large number of reflectance spectra have been obtained in the laboratory for powdered samples of rocks, minerals, and soils. The spectral region of interest here is from .30 to 2.5μm. The laboratory

measurements have been obtained generally with a high resolution $(50\overset{o}{A})$ spectrometer that measures the diffuse reflectance of a sample relative to that of a "white" standard such as smoked MgO.

About ten years of research on the spectral reflectance of lunar, meteoritic, and terrestrial samples is presented by Adams (1974, 1975). The direct relationship between laboratory reflectance measurements of returned lunar soil and telescopic measurements of the surface at the landing area was described by Adams and McCord (1970). A sequence of research reports followed as more lunar samples became available (Adams and McCord, 1971a, b, 1972, 1973). The problems of how the optical properties of lunar soils are related to those of the parent rock was discussed by Adams and McCord (1971a) and Nash and Conel (1973). A review of the spectral reflectance properties of lunar soil is in preparation (Adams and Charette, 1977).

An extensive catalogue of spectral reflectance curves for a variety of terrestrial rocks and minerals with roughly-defined geochemistry is provided by Hunt and Salisbury (1970, 1971, 1976a, b), Hunt et al., (1971a, b, 1972, 1973a, b, c, 1974), and Salisbury et al. (1975). Reflectance spectra of carefully chosen meteoritic samples have been extensively analyzed and catalogued by Gaffey (1973, 1976). The problems of deconvolving a rock spectrum to

obtain information about the mineral components is discussed by Adams (1976) and in more detail by Gaffey (1977). Variations in the spectral properties of minerals in a prepared mixture is presented by Pieters (1972, 1974) and Nash and Conel (1974).

2.   Telescopic Reflectance Measurements: General

Most of the telescopic spectral reflectance measurements have been made with some form of a photoelectric filter photometer. The wavelength range and resolution has varied, but to date most measurements have been limited in the near-infrared to the spectral sensitivity of an S-1 photomultiplier detector ($\lambda < 1.1 \mu$m) (e.g., see McCord et al., 1972a), although a few low resolution lunar spectra have been obtained to 2.5μm (McCord and Johnson, 1970).

A variety of reports have been presented containing a large number of telescopic lunar reflectance spectra (McCord et al., 1972a, b; Pieters and McCord, 1976; Pieters, 1977). The time variation of relative lunar color was examined by McCord (1969b) and found to be small with no evidence for significant luminescence (McCord, 1967). The general phase function of the moon was described by Hapke (1971) and was measured by Lane and Irving (1973). The wavelength dependence of the phase coefficient was measured also by Lane and Irving for nine filters from .35 to 1.0μm

and later by Nygard (1975) with 25 filters from .3 to 1.1μm.

The spectral types evident in spectra of about 200 small (10 to 20 km diameter) lunar areas were presented by McCord et al. (1972a). An analysis of the relationship between the spectra of these areas and the geologic units defined by the USGS mapping program was summarized by Charette et al. (1974). Spectral data for the then current and proposed Apollo landing sites were presented by McCord et al. (1972b).

3. Telescopic Spectral Images

Three distinctly different techniques have been used to obtain spectral images of the moon: (1) photography, (2) line scan, and (3) vidicon imagery. A thorough review and discussion of multispectral mapping is given by McCord (1976).

The most widely used photographic color-difference images were published by Whitaker in 1972. Higher quality pictures have since been produced, but are unpublished (Whitaker, personal communication). Barbarshov (1973) used the same photographic technique to produce a color difference image of the full moon. He calibrated and digitized the image and published a low spatial resolution map (in color) of the color difference data.

A low spatial resolution spectral map of Mare Serenitatis and Mare Tranquillitatis was produced by Soderblom (1970) from photoelectric line scans with high photoelectric precision

using three visible filters. Later a similar high-precision
low-resolution spectral map of the full moon was produced (Soder-
blom et al., 1976).

Digital vidicon spectral images have been obtained by
two independent groups, one at MIT and the other at JPL. The
latter has concentrated on intensive study of specific regions
(e.g., Johnson et al., 1975b), and have often integrated other
forms of remote sensing with the spectral data (see Section
6 below). The MIT group (McCord et al., 1976, 1977) has under-
taken a program to map the entire lunar frontside at high spatial
resolution ($\sim$2 km) with three carefully chosen spectral band-
passes. A number of spectral images from this larger program
have also been used in specific studies of lunar geology (see
Section 6 below).

4.   Laboratory Reflectance Measurements: Applied

As the number of available laboratory lunar spectra in-
creased, the information that could be derived from spectral
reflectance data of the moon became increasingly more defined.
With the return of the first samples (Adams and Jones, 1970;
Adams and McCord, 1970; Conel and Nash, 1970), the direct
link between laboratory and telescopic measurements was made.
The darkening of lunar soil with surface age was first discussed
by Adams and McCord in 1971b. Effects of dark basalt glasses
(artificial) in lunar soils was further discussed by Adams

and McCord (1971a) and by Nash and Conel (1973). The spectral

dominance of pyroxenes in reflectance spectra of lunar rocks

was described by Adams and McCord (1971a, 1972) along with

a discussion of the geochemical interpretations that can be

derived from the energy of characteristic absorption bands.

Diffuse reflectance measurements of pyroxenes were interpreted

in more detail by Adams (1974).

Using reflectance spectra of magnetic separates for num-

erous Apollo 16 soils, Adams and McCord (1973) linked the spectral

maturation of lunar soils with the accumulation of the dark

glass-rich agglutinates. The effects of maturation on a re-

flectance spectrum of lunar soil was further characterized

by Adams and Charette (1975). The related geochemical processes

involved with agglutinate formation were discussed by Charette

and Adams (1975a) and Rhodes et al. (1975).

Laboratory reflectance measurements of mature mare soil

samples were used to define the relationship between TiO_2 con-

tent and continuum slope in the blue and ultraviolet (Charette

et al., 1974). An understanding of this relationship led to

the prediction of high-titanium material in the Apollo 17

region (Pieters et al., 1973). A clarification of this tech-

nique for determining TiO_2 content from remote observations

is presented by Adams (1977). The identification of the dark

mantling material at Apollo 17 resulted from laboratory spec-

tra of the orange and black glasses obtained at Shorty crater

(Pieters et al., 1974; Adams et al., 1975). A method for determining the FeO content for lunar soils from reflectance measurements is being examined by Charette and Adams (1977).

5. Telescopic Reflectance Measurements: Applied

After the general spectral types of lunar maria and highland regions had been defined (McCord et al., 1972a), it became possible to use telescopic spectral reflectance measurements to solve specific problems of geology and geochemistry. Many regions of dark mantling material were shown to have unique spectral characteristics (Pieters et al., 1973) that were later linked to the orange and black glass beads of Apollo 17 (Pieters et al., 1974; Adams et al., 1975). From spectra for over 30 areas in Mare Humorum (Johnson et al., 1973) it was determined that two basaltic units filled the central basin, one a medium-high titanium basalt, the other a low titanium basalt. The geochemical units of this region were later more explicitly defined using more remote sensing information (see Section 6 below). The sampled and unsampled mare basalt types were defined and partially characterized from spectra of over 120 mature mare regions (Section III;Pieters and McCord, 1976). This characterization of basalt types allowed a regional description of the basalt types at the recent Luna 24 landing site in Mare Crisium

using   vidicon spectral imagery (Pieters et al., 1976).

A characterization of the spectral types for spectra of high-land and mare craters was presented by Pieters (1977).

6. Spectral Reflectance: Application with other

    forms of remote sensing

A current trend of applied research is to integrate

data from numerous remote sensing sources for one specific

region or problem.   It is recognized that the whole is of-ten greater than the sum of its parts.   Spectral reflectance

lends itself particularly well to synthesis studies that

aim at in-depth description of regional geology or geochem-istry.   In some cases, however, the results of synthesis

studies have not been significantly useful.   The approach

of the synthesis team as well as the inherent value of the

data are not uniform for all studies reported.   An evalu-ation of the various remote sensing techniques currently

in use can be found in Head et al. (1976a, b) as they apply

to unit definition and characterization.

Most remote sensing synthesis studies have been con-cerned with particular regions.   These include Mare Imbrium

(Schaber et al., 1975), Mare Serenitatis (Thompson et al.,

1974), Mare Humorum (Pieters et al., 1975), Lamont (John-son et al., 1975a), Aristarchus (Zisk et al., 1976), and

Flamsteed (Pieters et al., 1977). Saunders et al., (1977)

have converted a variety of remote sensing data to a

database that can be conveniently manipulated using com-

puter processing techniques. A few studies have been di-

rected towards understanding more completely "special"

types of lunar areas such as areas of dark mantling mater-

ial (Pieters et al., 1973; Adams et al., 1975) or areas

of suspected highland volcanism or sources of KREEP

material (Malin, 1973; Head and McCord, 1977).

II.   REMOTE SENSING OF THE MOON

C.   Principles of Spectral Reflectance

1.   Optical Properties of Minerals

In order for reflection spectroscopy to be accepted and used as a technique for remotely determining surface mineralogy, the principles of physics and chemistry that govern optical absorption in minerals must be sufficiently understood. Absorption (transmission) spectra have been obtained for a variety of terrestrial, meteoritic, and lunar rocks and minerals generally through the spectral range from 0.30 to 2.50μm (e.g., Burns et al., 1975, Bell et al., 1975). Over this spectral range there are primarily three general types of absorption features observed: (a) bands due to crystal field electronic transitions within a transition metal ion, (b) bands due to intervalence charge transfer transitions between two neighboring ions, and (c) molecular vibrational bands. Since the few vibrational bands (attributable to OH^-, CO_3^{2-} ligands as well as H_2O and CO_2 molecules) are not observed in lunar material, only the electronic absorptions will be discussed here. The strength and sharpness of absorption features in a spectrum varies somewhat as a function of temperature (Sung et al., 1977) and pressure (Mao and Bell, 1972).

a. Crystal Field Transitions of Transition Metal

Ions

The first series transition metals (Table TIIC-1;
from Burns, 1970a) constitute about 40% of the earth
(primarily iron) and play at least a comparable role
in extraterrestrial material (Mason, 1966). In rock
forming minerals, ions of these elements are char-
acterized by incompletely filled inner $3\underline{d}$ atomic or-
bitals (see Table 1). In an isolated environment,
the five $\underline{d}$ orbitals of transition metal ions are de-
generate although the spatial distribution of elec-
tron density in each orbital is distinct (Figure
II-C-1a from Burns, 1970a). When a transition me-
tal ion is incorporated into a crystal structure or
is surrounded by negatively charged ligands, the en-
ergy level of the $\underline{d}$ orbitals loose their degeneracy.
Electrons in the orbitals are repelled by the surround-
ing ligands with the resulting energy level of each
orbital being dependent on the orientation of the
electron orbital with respect to the ligands. In
crystal field theory, the anions are considered as
point charges and any covalent interaction between
anion and cation is ignored. For an ion in a regu-
lar octahedral crystal field (six-fold coordination)
the d_{z^2} and $d_{x^2-y^2}$ orbitals, which are oriented along

Electronic configurations and crystal field stabilization energies of transition metal ions in octahedral co-ordination

Number of 3d electrons	Ion	High-spin state				Low-spin state			
		Electronic configuration t_{2g}	e_g	Unpaired electrons	CFSE	Electronic configuration t_{2g}	e_g	Unpaired electrons	CFSE
0	Ca^{2+}, Sc^{3+}, Ti^{4+}			0	0			0	0
1	Ti^{3+}	↑		1	$\frac{2}{5}\Delta_o$	↑		1	$\frac{2}{5}\Delta_o$
2	Ti^{2+}, V^{3+}	↑ ↑		2	$\frac{4}{5}\Delta_o$	↑ ↑		2	$\frac{4}{5}\Delta_o$
3	V^{2+}, Cr^{3+}, Mn^{4+}	↑ ↑ ↑		3	$\frac{6}{5}\Delta_o$	↑ ↑ ↑		3	$\frac{6}{5}\Delta_o$
4	Cr^{2+}, Mn^{3+}	↑ ↑ ↑	↑	4	$\frac{3}{5}\Delta_o$	↑↓ ↑ ↑		2	$\frac{8}{5}\Delta_o$
5	Mn^{2+}, Fe^{3+}	↑ ↑ ↑	↑ ↑	5	0	↑↓ ↑↓ ↑		1	$\frac{10}{5}\Delta_o$
6	Fe^{2+}, Co^{3+}, Ni^{4+}	↑↓ ↑ ↑	↑ ↑	4	$\frac{2}{5}\Delta_o$	↑↓ ↑↓ ↑↓		0	$\frac{12}{5}\Delta_o$
7	Co^{2+}, Ni^{3+}	↑↓ ↑↓ ↑	↑ ↑	3	$\frac{4}{5}\Delta_o$	↑↓ ↑↓ ↑↓	↑	1	$\frac{9}{5}\Delta_o$
8	Ni^{2+}	↑↓ ↑↓ ↑↓	↑ ↑	2	$\frac{6}{5}\Delta_o$	↑↓ ↑↓ ↑↓	↑ ↑	2	$\frac{6}{5}\Delta_o$
9	Cu^{2+}	↑↓ ↑↓ ↑↓	↑↓ ↑	1	$\frac{3}{5}\Delta_o$	↑↓ ↑↓ ↑↓	↑↓ ↑	1	$\frac{3}{5}\Delta_o$
10	Zn^{2+}, Ga^{3+}, Ge^{4+}	↑↓ ↑↓ ↑↓	↑↓ ↑↓	0	0	↑↓ ↑↓ ↑↓	↑↓ ↑↓	0	0

Table IIC 1.   (Burns, 1970a)

IIC 171
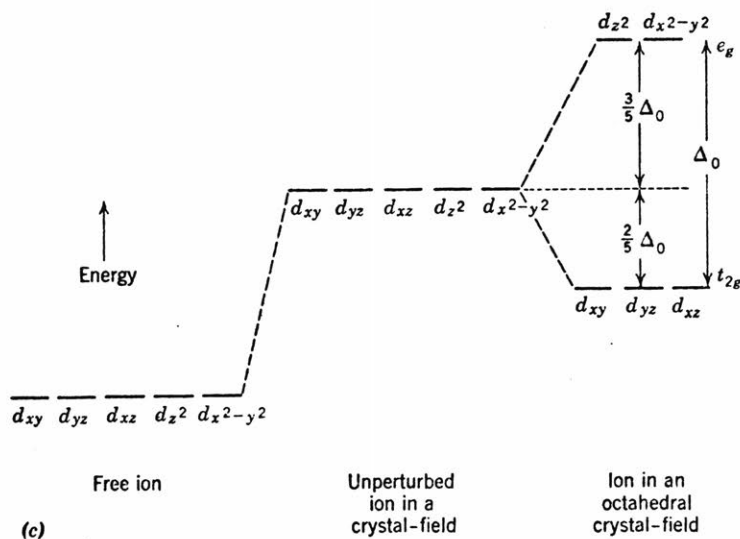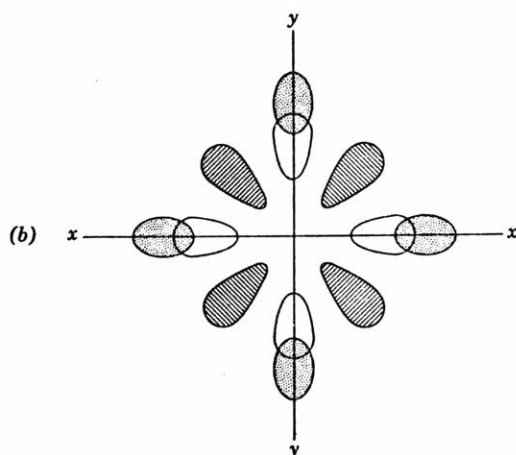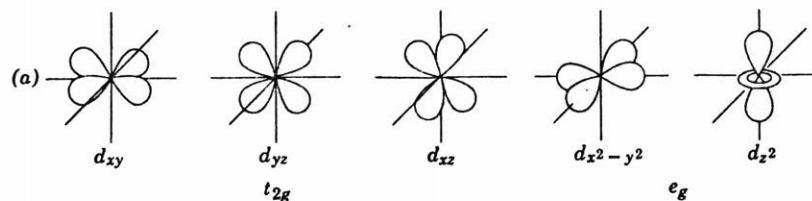
Orientations and relative energy levels of d orbitals in an octahedral crystal-field. (a) Electron distribution in d orbitals; (b) the x-y plane of a transition-metal ion in an octahedral crystal-field. The d_{xy} orbital is cross-hatched, the $d_{x^2-y^2}$ orbital is open, and the ligands are stippled. (c) d orbital energy level diagram.

Figure IIC 1.   (Burns, 1970a)

the axes of the octahedron, are of higher energy than
the d_{xy}, d_{yz}, and d_{xz} (Figure II-C lc). Distortions
of the octahedral site will cause further splitting
of the d orbital energy levels. This energy separ-
ation of the d orbitals is largely dependent on the
type and valence of transition metal ion as well as
the crystal field environment it is subjected to
(Burns and Fyfe, 1967).

Absorptions occur in the spectra of minerals
containing transition metal ions as a d orbital elec-
tron is excited to a higher energy state by an incom-
ing photon. The energy of the absorption is equiva-
lent to the difference in energy between the ground
state and excited state of the ion. Absorption fea-
tures characteristic of particular ions, in particular
crystal structures, can be interpreted and predicted
by the application of crystal field theory to describe
the relative energies of the d orbitals (Burns, 1970a).
Absorption characteristics of a material are thus
directly linked to its mineralogy.

Two types of crystal field d orbital transitions
can be considered: (1) spin allowed and (2) spin
forbidden, with the latter being about two orders
of magnitude less intense than the former. Both

types occur in the transmission spectrum of an ortho-
pyroxene shown in Figure IIC -2 (from Burns 1970a).
The two broad absorptions centered near 1 and 2 mi-
crometers are due primarily to Fe^{2+} (with six $\underline{d}$ or-
bital electrons) in the distorted M2 octahedral site
of the pyroxene. These absorptions for which both
the ground state and the excited state have the same
number of unpaired electrons are spin allowed. The
sharp weak absorptions that occur at higher energies
here are attributable to spin forbidden transitions
of Fe^{2+} (Burns and Vaughan, 1975) for which the ex-
cited state has a spin multiplicity different from
the ground state.

b. Charge Transfer Transitions

Many of the intense mineral absorptions that
occur in the visible and ultraviolet arise from elec-
tronic transitions between neighboring ions. Since
there is possible overlap between electron orbitals
of neighboring ions, the anions should not be treated
as point charges in this interaction and crystal
field theory is inappropriate to interpret the anion--
cation and cation-cation charge transfer transitions.
Recently, molecular orbital theory, which provides
a more complete description of the electric structure
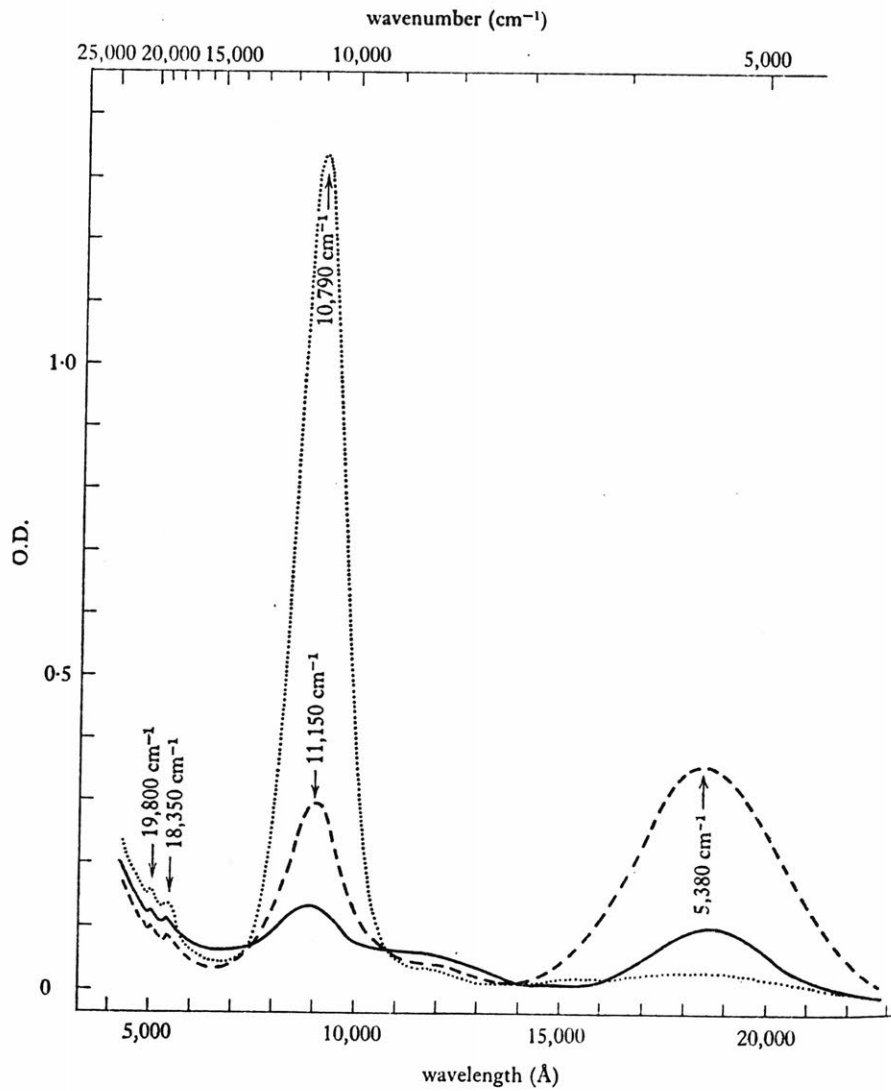
Polarized absorption spectra of orthopyroxenes. . . . α spectra; - - - β spectra; —— γ spectra.
(a) bronzite, Fs$_{14.5}$, from Bamle, Norway.

Figure IIC 2.   (Burns, 1970a)

of a compound, has been used successfully for the
calculations of the energy of many such transitions
(Tossel et al., 1974; Loeffler et al., 1974, 1975)
and has achieved good agreement with experimental
values for band centers (Burns et al., 1976).

Oxygen-to-metal charge transfers bands generally
occur well into the ultraviolet and are thousands
of times more intense than the crystal field bands
discussed above (Bell et al., 1975). The side wings
of these bands extend into the visible and often into
the near infrared causing the continuum of most sil-
icates to be curved with increasing absorption towards
the ultraviolet.

Cation-cation intervalence charge transfer ab-
sorptions occur between metal ions in adjacent coor-
dination sites sharing a common edge or face and are
directional or strongly polarization dependent. Since
both the concentration of metal ions and the degree
of orbital overlap affect the intervalence charge
transfer, such absorptions are observed with a wide
range of intensities (Burns and Vaughan, 1975). Some
of the most common homonuclear intervalence transfer
transitions are $Fe^{2+} \rightarrow Fe^{3+}$ and $Ti^{3+} \rightarrow Ti^{4+}$. A variety
of heteronuclear charge transfer processes can also

occur between the different oxidation states of iron and titanium, the most common of which is $Fe^{2+} \rightarrow Ti^{4+}$ (Burns and Vaughan, 1975).

Since a variety of charge transfer and crystal field absorptions overlap in the visible and ultraviolet, it has been difficult to empirically interpret absorption features in this part of the spectrum. Bell et al. (1975) and Huguenin (1975) have made considerable progress in band assignment for $O^{2-} \rightarrow Fe^{3+}$ in ferric oxides. Burns et al. (1976) have sorted out a number of the numerous transitions involving titanium and iron in terrestrial and lunar materials.

2. Reflectance of Minerals and Rocks

   a. Physical components of reflection.

The optical properties of minerals discussed above have been examined primarily using transmission spectroscopy of oriented individual grains where the percent transmission or absorbance is measured through the material as a function of wavelength. Reflection spectroscopy, on the other hand, is defined as the wavelength dependence of the ratio of the light reflected from a surface to that incident upon it. Most natural surfaces are rough or particulate and the reflected radiation contains both (1) a specular

and (2) a diffuse component (Figure IIC -3). The strength of each component in natural reflection is directional, i.e., dependent on the geometry of illumination and observation.

The specular component of directional reflectance from a silicate powder or soil is a first surface reflection and is described by Fresnell's equations for reflection from a dielectric. Figure IIC -4 shows the percent reflectance for a single surface reflection as a function of phase angle for a silicate with a real refraction index of 1.5. The phase angle is the angle between the source-object-detector, or the sum of the angle of incidence and the angle of reflection. The Brewster angle for such a material is near 57 degrees and the total reflected radiation is therefore 100% polarized at a phase angle of about 114 degrees. This specular component of reflection contains no measurable spectral information in the spectral range between .3 and 2.5μm. The variations of the absorption coefficient in the visible and near infrared are too small to significantly effect the refractive index.

The diffuse component of surface reflection contains radiation that has been transmitted through
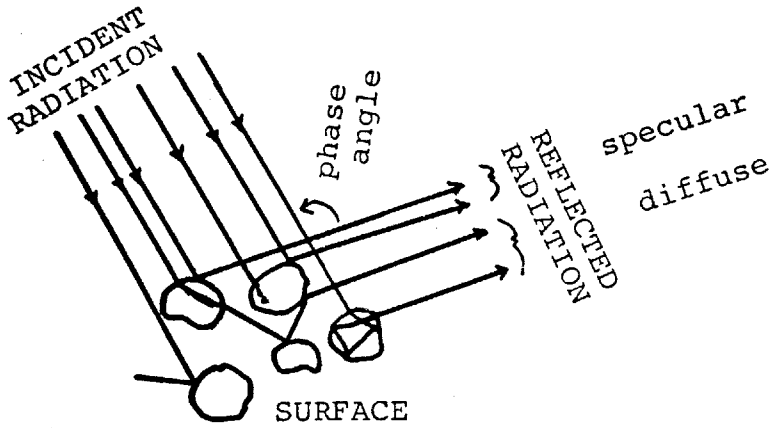
Figure IIC-3

Components of
reflected radiation

Specular Reflection and Polarization for n = 1.5
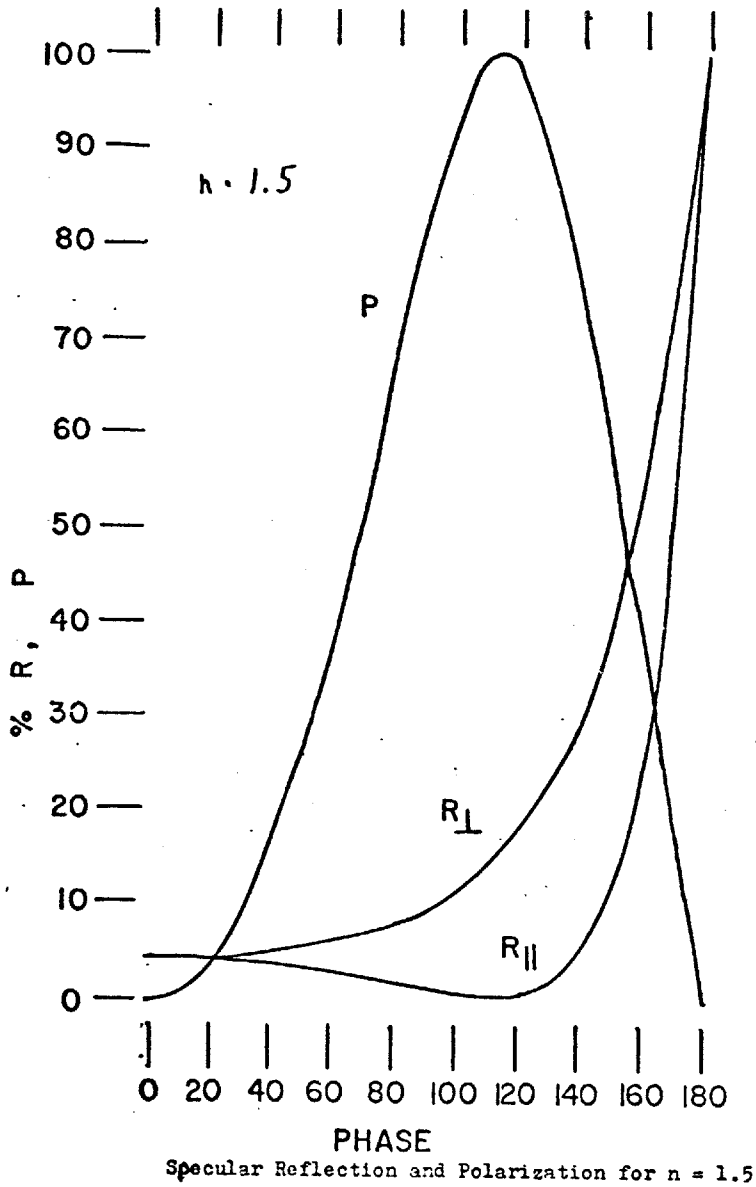
Figure IIC 4.

one or more grains and scattered randomly back into
space. This body component contains all the spectral
information of transmitted light; it is the sum of
transmission through randomly oriented crystals.
This random orientation of surface crystals, however,
causes any phase or polarization information from
birefringent materials to be scrambled and lost.
Nearly "pure" diffuse reflectance can be measured
in the laboratory by placing the sample in a white
diffusing sphere. Such an arrangment either (1)
causes diffuse light to be incident upon the sample,
or (2) allows the detector to view only the integrated
reflected radiation   Most of the
specular component of reflection is thus eliminated.

   b.   Mean optical path length (MOPL)

   For any given material the strength of absorption
features in a reflectance spectrum varies according
to both the absorption coefficient and the average
distance light is transmitted through the particles,
or the mean optical path length (MOPL). For a mix-
ture of materials, this MOPL is a complicated func-
tion of both the particle size and the general opa-
city of the components. Figure IIC -5 illustrates
the effects of particle size on the strength of an
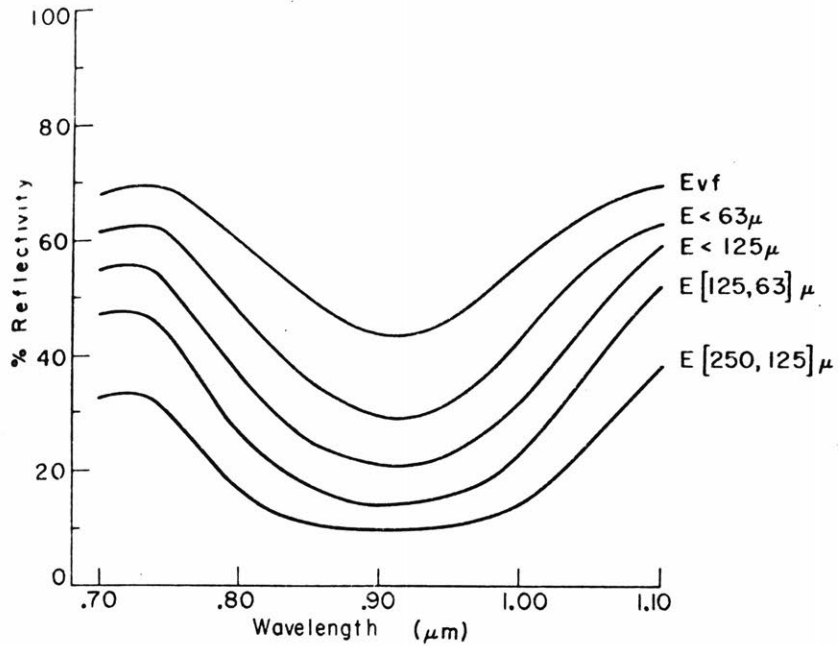
Diffuse reflection spectra of the absorption band of En_{89} for various particle sizes.

Figure IIC 5
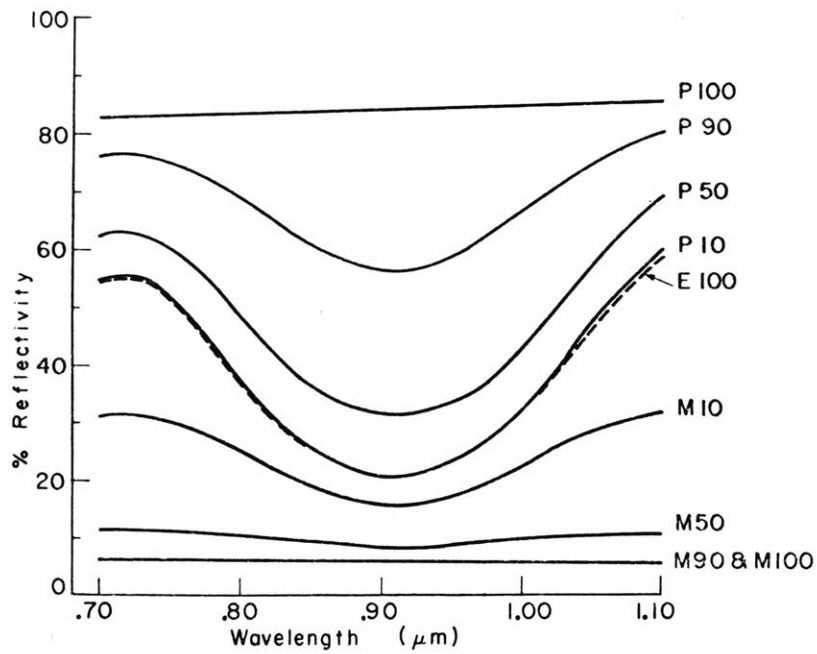
Diffuse reflection spectra of the absorption band of En_{89} for mixtures with plagioclase and magnetite. The particle size for all mixtures is $< 125\ \mu m$.

Figure IIC 6.

absorption band centered at .91μm in the spectrum
of an orthopyroxene, En_{89}. A measure of the band
depth is listed in Table TIIC. -2. As the particle
size decreases, the sample becomes brighter and the
band depth decreases due to a reduction of the MOPL
with increased scattering at particle interfaces.
For a near transparent substance, such as SiO_2 glass,
the MOPL was estimated to be between 2-4mm for par-
ticles between 500-250μm in diameter, <2mm for par-
ticles between 250-125μm, and only hundreds of micro-
meters for particles <125μm (Pieters, 1972, Appendix
A). These estimates of MOPL are upper limits; the
MOPL for semitransparent materials would be smaller.

The general opacity of a material strongly ef-
fects the MOPL of reflected radiation. Figure IIC -6
contains spectra for mineral mixtures with particle
size held constant. These mixtures contain various
amounts of (1) a material with a well-defined absorp-
tion band (the orthopyroxene of Figure IIC -5), (2)
a very absorbing but featureless material (magnetite),
and (3) a featureless transparent material (iron-free
plagioclase). The addition of transparent material
brightens the mixture and the addition of absorbing
material darkens the mixture, but in a nonlinear manner.

Table IIC 2. Band depth of samples measured

1	2	3	4
		$R_p(.91)/R_p(.73)$	
SAMPLE	PARTICLE SIZE (microns)	DIFFUSE	90° phase
E [250,125]	250 > ps > 125	.29[1]	.25
E [125, 63]	125 > ps > 63	.29	.31
E<125	less than 125	.37	.38
E<63	less than 63	.47[2]	.44
Evf	very fine	.62[2]	.56
P100	less than 125	1.01	1.04
P90	less than 125	.74	.77
P50	less than 125	.50	.53
P10	less than 125	.37	.40
E100	less than 125	.37	.38
M10	less than 125	.49	.52
M50	less than 125	.74	.75
M90	less than 125	.87	.91
M100	less than 125	.87	.92

1 saturated band

2 partially packed

The reduction of band depth (Table IIC -2), by an

addition of 10% magnetite, is equal to the reduction

effects of a 50% addition of plagioclase. The absorb-

ing material severely reduces the MOPL whereas the

transparent material simply dilutes the spectral

features.

   c.   Spectral features of minerals

   The absorption features in reflectance spectra

for a variety of mineral powders have been measured

in the laboratory (see Section IIB for a review).

Most of these features can be well understood from

crystal field theory if the geochemistry of the ma-

terial is sufficiently well defined. The uniqueness

of absorption features in well characterized minerals

has been examined by Adams (1975) and is best summa-

rized in the "λ-λ" figure of IIC - [7] (from Adams,

1975). To form this omni-mineral figure, the energy

of each absorption in a reflectance spectrum was dis-

cerned, and the short wavelength (high energy) band

position was plotted against the long wavelength (low

energy) band position. Those minerals that have more

than two absorption features occur on the plot more

than once; those minerals that have a single absorp-

tion band are plotted separately. Many of the sub-

Plot of centers of absorption bands in the diffuse reflectance spectra of several common minerals. Minerals having only one main band are plotted on the lower scale. Minerals with two or more bands in their spectra are designated by points in the main upper field. Hydroxyl and water bands at 1.4 and 1.9 μm are not used. Bands for minerals species and for glasses plot in separate fields. See text for discussion. Diop-sal = disoside-salite; bio-phlog = biotite-phlogopite; aug = augite; pige = pigeonite; opx = ortho-pyroxene; dolo = dolomite; epid = epidote; actin-hornb = actinolite-hornblende; trem-ged-kaer = tremolite-gedrite-kaersutite; amph = amphibole; enst = enstatite; chlor = chlorite; Fo = forsterite; Fa = fayalite; Ab = albite; Olig = oligoclase; And = andesine; Lab = labradorite; Byt = bytownite; An = anorthite.

Figure IIC 7.   (Adams, 1975)

tleties of a reflection spectrum are lost in such

a figure, but it illustrates the fact that most min-

erals can be characterized by their absorption fea-

tures.   The major non-opaque constituents of lunar

basalts (pyroxene, olivine, plagioclase, and glass)

are discussed below.

i.   PYROXENES.   Two major spin-allowed Fe^{2+} ab-

sorption bands occur in the diffuse reflectance spec-

trum of pyroxene (Figure IIC $-_8$).   These bands cen-

tered near 1µm and 2µm define a pyroxene trend in

Figure IIC2-5; they vary as a function of pyroxene

composition in a well-ordered manner.   Figure IIC -9

is a similar $\lambda-\lambda$ plot with only pyroxenes included.

The distinction between orthopyroxenes and clino-

pyroxenes is clear in this figure.   The trend of band

centers proceeds to the right with increasing Fe and

Ca content of the pyroxenes.   The quantification of

this compositional trend is shown in Figure IIC 1-0

(from Adams, 1975).   Several pyroxenes (e.g., clino-

pyroxenes with Cr^{3+} or Fe^{3+}) have a more complicated

spectrum with more than two bands present.   These

pyroxenes define different   but distinct regions

in Figure IIC - 7.

ii.   OLIVINE.   Several transitions occur for Fe^{2+}
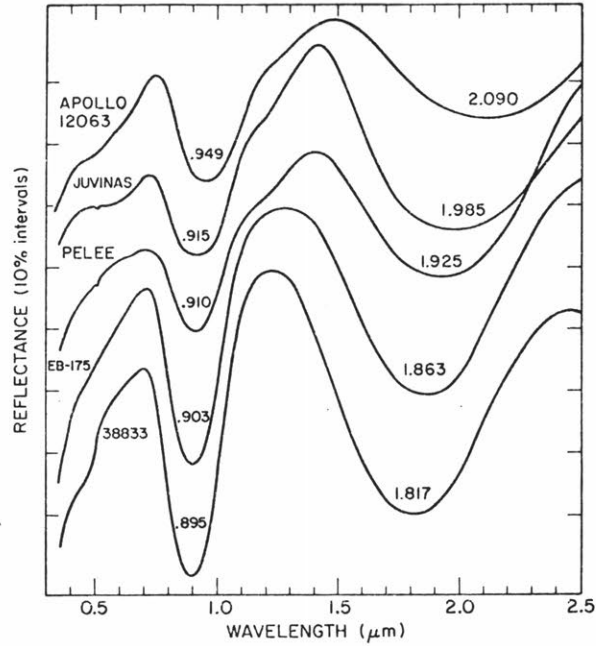
Diffuse reflectance spectra (relative to MgO) of pyroxenes. Samples 38833, EB-175, and Pelee are orthopyroxenes and increase in Fe in that order. Juvinas is a pigeonite, and Apollo 12063 is a subcalcic augite.

Note the two prominent Fe^{2+} absorption bands for all samples, and the shift of both bands to longer wave-lengths from bottom to top of the figure.

Figure IIC 8.   (Adams, 1974)
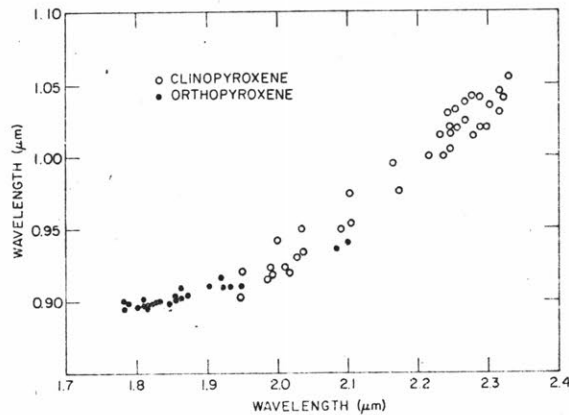
Wavelengths of centers of absorption bands near 1 μm and 2 μm in the diffuse reflectance spectra of pyroxenes. Orthopyroxene bands shift to longer wavelengths with increasing amounts of iron, whereas clinopyroxene bands shift to longer wavelengths with increasing calcium content.

Figure IIC 9.   (Adams, 1974)
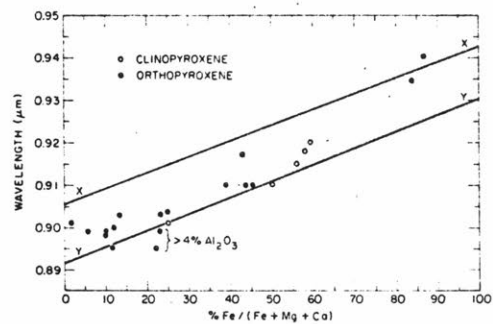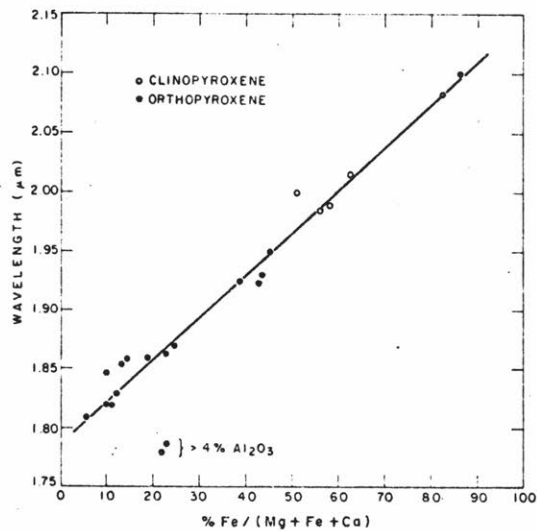
Absorption band centers of orthopyroxenes and low-calcium clinopyroxenes as a function of Fe/(Mg + Fe + Ca). Lines labeled X and Y (bottom) indicate polarized absorption bands [*Burns*, 1965].
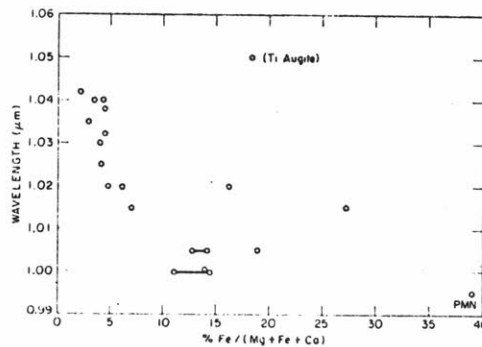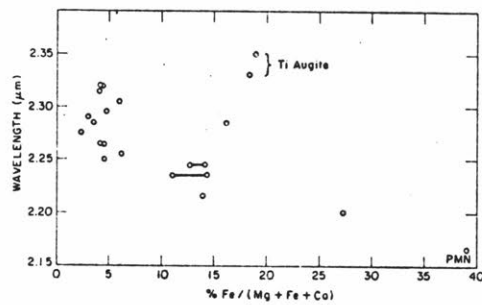
Centers of main absorption bands of calcic clinopyroxenes as a function of Fe/(Mg + Fe + Ca). Tie lines connect end members of zoned pyroxenes. PMN represents pyroxmangite.
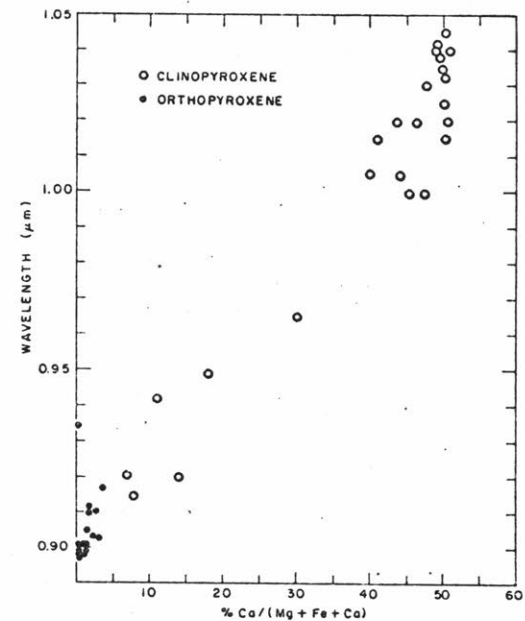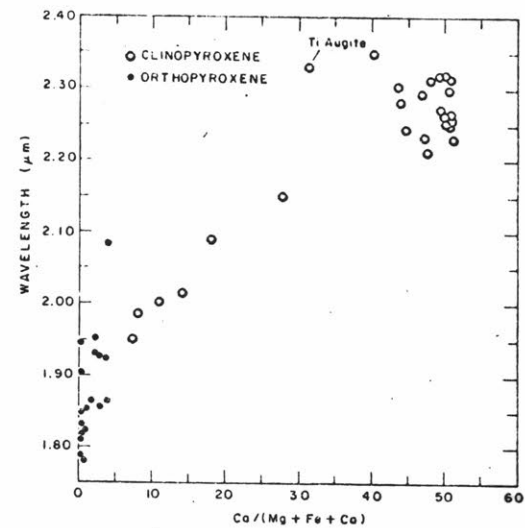
Centers of the main Fe^{2+} absorption bands of pyroxenes versus Ca/(Mg + Fe + Ca). Bands shift to longer wavelengths with increasing Ca.

Figure IIC 10.   (Adams, 1974)

in the centrosymmetric M_1 and the non-centrosymmetric M_2 sites of olivines (Burns, 1970b). In a diffuse reflectance spectrum, the combination of these transitions is a broad non-symmetric band with a minimum between 1.0 and 1.1µm (Figure IIC-11). The depth of this composite band increases with increasing iron and the center shifts to longer wavelengths. The overall extinction coefficient for olivine is much less than that for pyroxenes; pure olivine ($\sim Fo_{50}$) is relatively bright.

iii. FELDSPARS. Pure plagioclase has a feature-less spectrum (see Figure IIC-6). However, when even small amounts of Fe^{2+} and Fe^{3+} are accommodated in the Ca or Al sites, distinct absorption features are discernable. When only Fe^{2+} is present (as in the lunar case), the plagioclase feldspars show a broad crystal field absorption band with a minimum between 1.1 and 1.3µm as seen in Figure IIC-12 (from Adams and McCord, 1971a). It appears that the position of this band is controlled by the % anorthite (Adams, 1975).

iv. GLASS. Two broad absorptions generally occur near 1 and 2µm if Fe^{2+} is present in a pure (not devitri-fied) glass. These two bands are not only much broader than those that occur in pyroxenes, but they are also closer together (Figure IIC-13). The 1µm band is due to Fe^{2+}
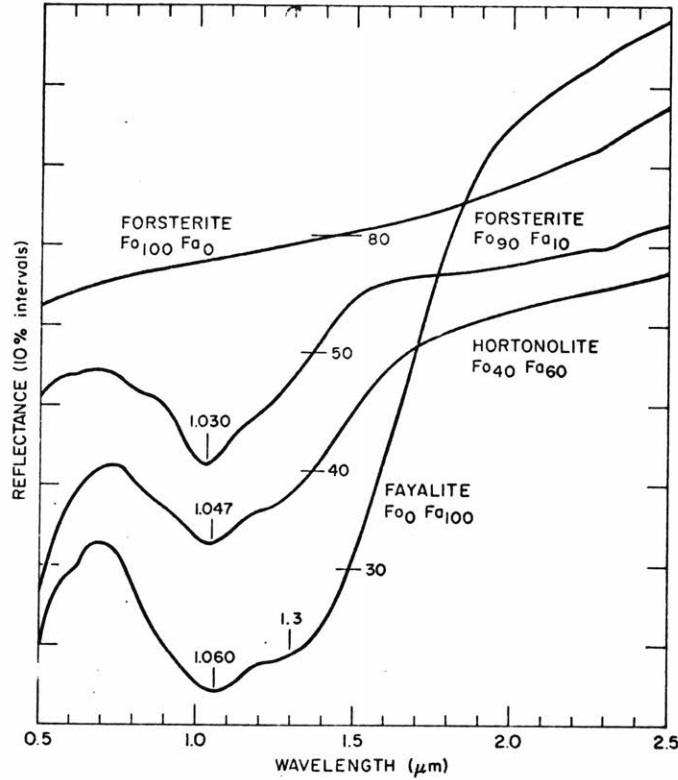
Diffuse reflectance spectra (relative to MgO) of olivine minerals. The Fe^{2+} absorption band near 1 μm increases in depth and shifts to longer wavelengths, and the 1.3 μm inflection enlarges with increasing iron content of the minerals. Horizontal lines crossing the curves that are labeled with a two-digit number indicate percent reflectance.

Figure IIC 11. (Adams, 1975)
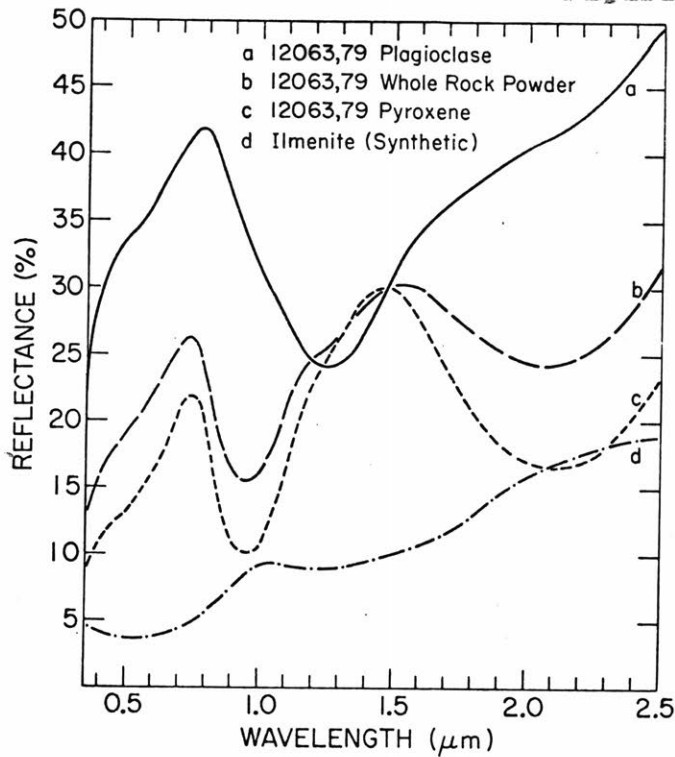
Figure IIC 12. (Adams and McCord, 1971a)

Spectral reflectivity of Apollo 12 basalt powder 12063 and plagioclase and pyroxene separates from the same rock. Ilmenite is a synthetic sample.

in octahedral sites whereas the $2\mu m$ band, when present,

is possibly due to Fe^{2+} in a tetrahedral site (Boon and

Fyfe, 1972). Transmission spectra of synthetic glass in-

dicate that the strength of the $1\mu m$ band is directly related

to the iron concentration in the glass (Bell et al., 1976).

For lunar materials, the term "glass" has often been used

to refer to the dark glass-welded aggregates abundant in

soils. These agglutinates are an inhomogeneous mess of

glass, mineral fragments, submicroscopic particles and

sometimes native iron. A broad weak band exists near $1\mu m$

in agglutinate spectra (Adams and Charette, 1977). The

strength of this band appears to be related to FeO content

of the soil but in a complicated manner dependent on the

other ill-defined components of the agglutinates (see Sec-

tion IIC-1a).

    d. Spectral components of a whole rock spectrum

        A rock is usually composed of a mixture of min-

erals and the strength of an absorption band is a function

of the composition of the absorbing mineral, the average

particle size, and also the opacity of the other components,

with the latter often being a dominant effect. The spec-

tral component from each constituent mineral of lunar rock

12063 can be seen in Figure IIC-12 (from Adams and McCord,

1971a). The whole rock spectrum is clearly dominated by
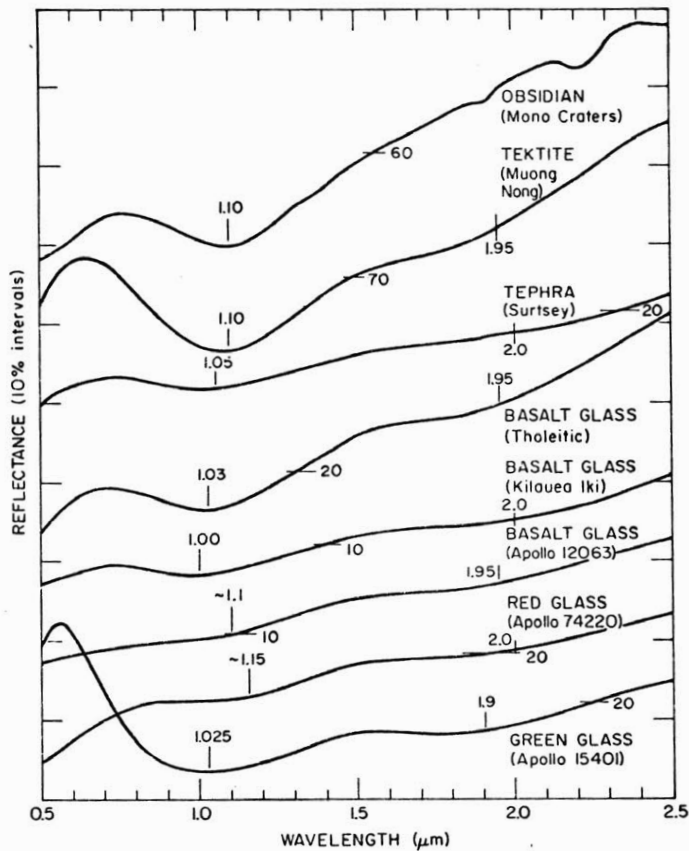
Diffuse reflectance spectra of iron-bearing glasses. The broad Fe^{2+} bands above 1 μm and below 2 μm are characteristic of glasses.

Figure IIC 13.   (Adams, 1975)

2 /28/73 #7   HARAIYA ASU   (26)
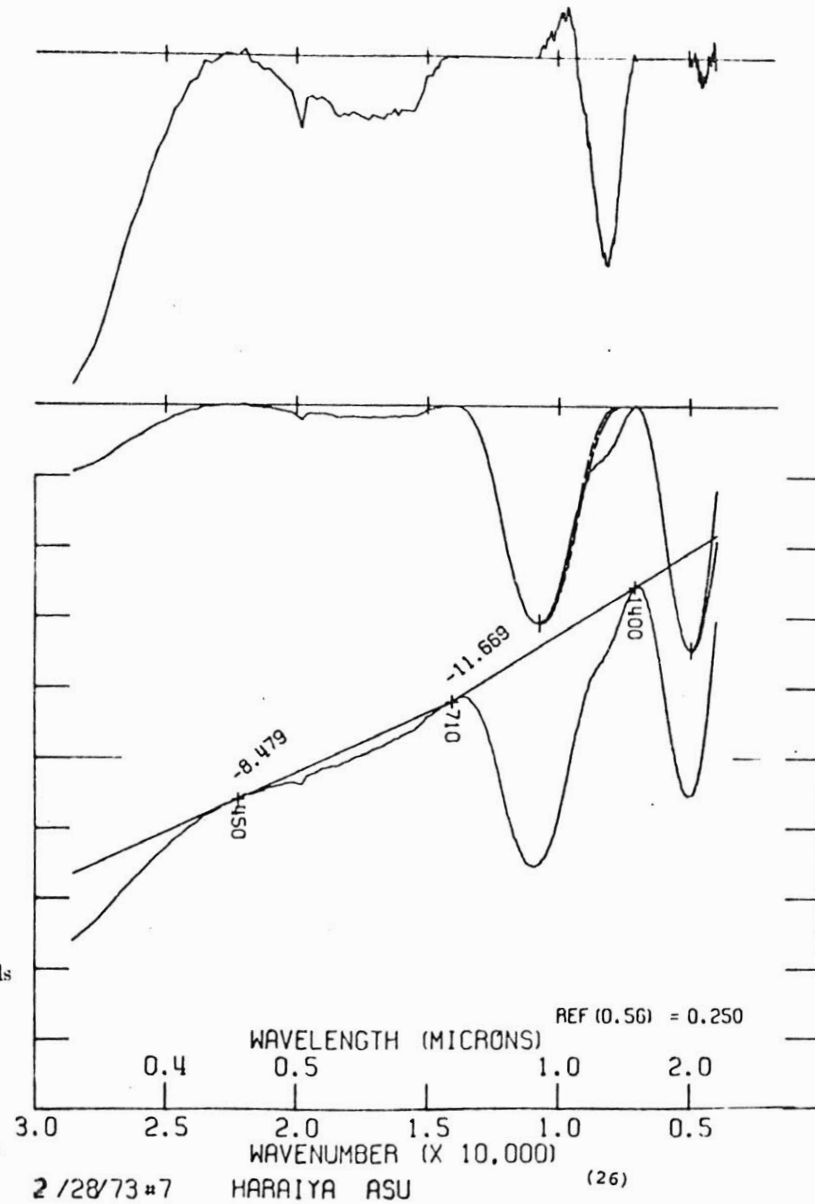
Figure IIC 14.   (Gaffey, 1975)
Deconvolution of the Haraiya meteorite spectrum.

the pyroxene component (51% modal abundance). The promi-

nent 1.25μm Fe^{2+} band of the plagioclase (27%) is seen as

a subtle but distinct inflection in the whole rock spectrum.

Ilmenite darkens the spectrum.

Subtle features can nevertheless often be deconvolved

from a spectrum using computer processing techniques (Gaf-

fey, 1975). There are two basic difficulties which must

be overcome in order for a rock or soil spectrum to be

deconvolved into the spectral components for each mineral

present. First, the general slope of the continuum must

be removed. (This means the wings of poorly-defined high

energy (UV) absorptions that always effect the slope of

the visible and near infrared spectrum must be eliminated.)

Secondly, the stronger absorption bands need to be suffi-

ciently well defined and removed so that remnant weaker

bands can be examined. Figure IIC-14 illustrates such

a deconvolution of the spectrum for the Haraiya meteorite

(from Gaffey, 1975). As described in the previous section,

the wavelength and symmetry of each absorption band is di-

rectly a function of the mineralogy of the sample; the rela-

tive strength of bands from different minerals in a whole

rock spectrum can be used to estimate the relative modal

abundances of constituent minerals (Gaffey, 1975).

II.   REMOTE SENSING OF THE MOON

 D.   Spectral Reflectance of Lunar Material

    The application of spectral reflectance measurements

to understanding the lunar surface incorporates both the

laboratory measurements of returned lunar samples and the

telescopic measurements of small lunar regions (10 to 20

km in diameter). An additional source of spectral infor-

mation comes from multi-spectral imagery which allows gen-

eral spectral differences to be mapped in two dimensions.

(Most of the spectral data relevant to the following dis-

cussion is derived from coordinated research of two groups--

one organized by McCord at MIT/Hawaii and the other by

Adams at University of Washington, Seattle.)

    1.   Soils

        As mentioned in the review of Section IIB, the

laboratory measurement of a representative soil sample from

Apollo 11 was in close agreement with the telescopic measure-

ment (.3 to 1.1μm) of the landing site (Adams and McCord,

1970). Figure IID-1 (from McCord and Adams, 1973) illus-

trates the agreement between the telescopic spectra and

the laboratory spectra of soils returned from subsequent

missions. The early studies by Adams and McCord demonstrated

(1) that the telescopic spectra of small regions were com-
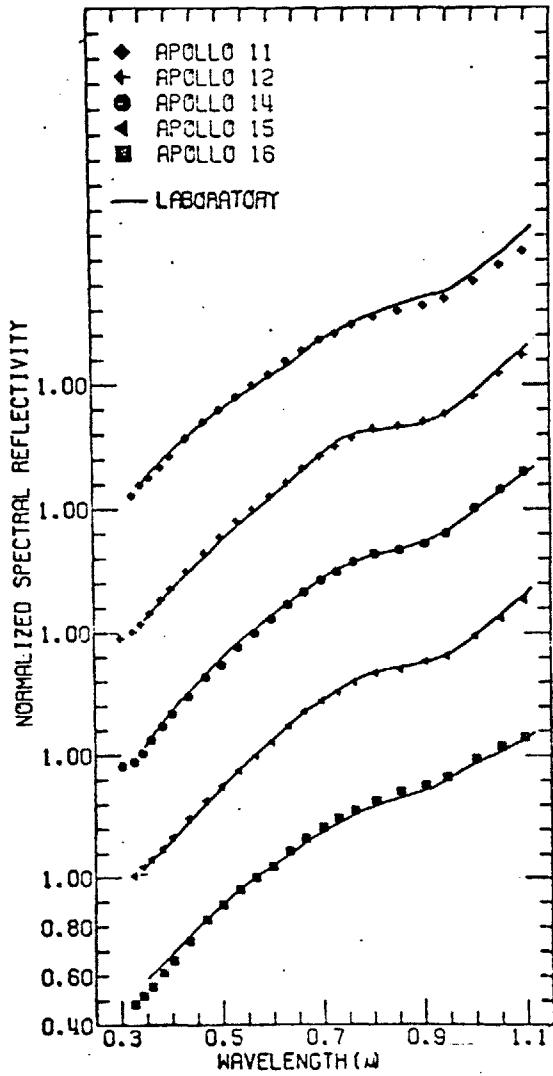
Figure IID 1.

Spectral reflectance of soil from the Apollo landing sites. Points are telescopic spectra; solid lines are laboratory measurements.
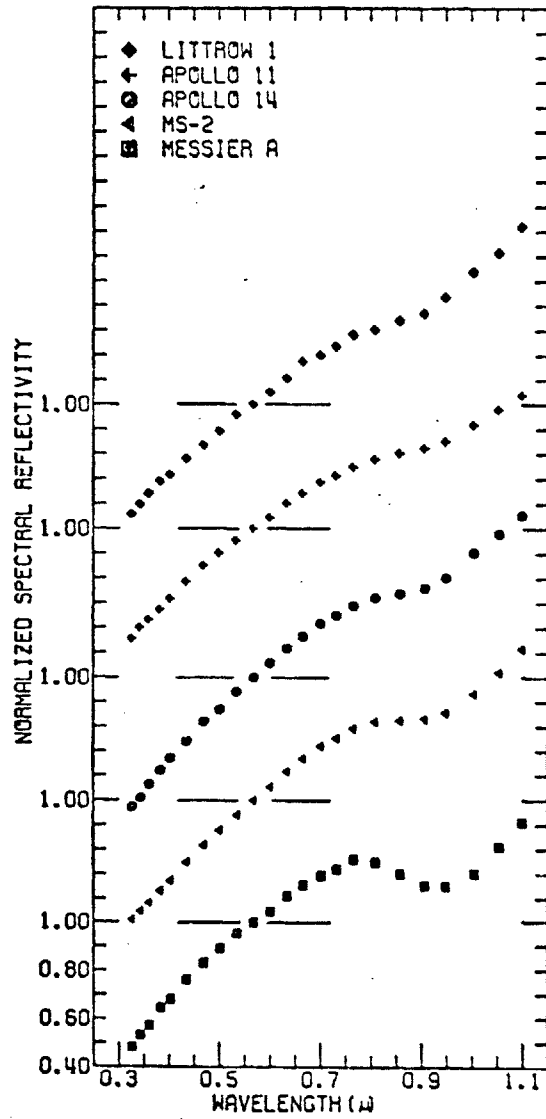
Figure IID 2.

Spectral reflectance measurements for representative lunar areas (telescopic).

parable to spectra of <u>soils</u>, rather than rock fragments
or chips, and (2) that well-chosen soils can be considered
representative of the surrounding 10 - 20 km regions measured
telescopically.

When compared to other solar system objects and
terrestrial samples, mature lunar soil has a distinct spec-
trum: a steeply sloped red continuum with a very weak ab-
sorption band near 1μm and sometimes also 2μm (Figure IID-2).
Mercury is the only object with a comparable red spectrum,
but without distinct absorption bands (McCord and Adams,
1972; Vilas and McCord, 1976; McCord and Adams, 1976; Adams
and McCord, 1977). Only through extensive study of the
lunar samples has the significance of this peculiar char-
acter of lunar soil spectra been illuminated.

Lunar soils are largely derived from the prevalent
rock type of the region (with a small amount of contamina-
tion due to lateral transport of impact material). The
main weathering mechanism is largely micrometeoroid bombard-
ment, although the processes involved in soil development
are not all defined. As the soil matures, particles are
finely crushed and broken and also welded together by im-
pact generated melts into friable aggregates called agglu-
tinates (e.g., McKay et al., 1974). The subsequent accum-
ulation of these dark agglutinitic particles dramatically

changes the <u>mineralogy</u> of the soils from that of the parent
rocks, although the bulk composition only undergoes a minor
(contamination) alteration. As a soil matures, the spec-
tral changes that occur are mostly due to the replacement
of mineral fragments with the absorbing glass-welded agglu-
tinates (Adams and McCord, 1973). The spectrum of a mature
soil is almost wholely dominated by the spectral character-
istics of the multi-component agglutinates. A discussion
of the special character of agglutinates is thus presented
here before a general discussion of soil spectra.

     a. <u>Agglutinates</u>

     Adams has used a magnetic separation technique
to separate the agglutinitic and non-agglutinitic components
of a soil (Adams and McCord, 1973). Shown in Figure IID-3
(from Adams and McCord, 1973) are spectra for   bulk soil
(B) samples 67461 and 68841,   the agglutinitic (magnetic--
M) separate, and   the non-agglutinitic (non-magnetic--N)
component. The albedo of the bulk soil is intermediate
between that of the agglutinitic and non-agglutinitic con-
centrates. Mature soils contain $\gtrsim 60\%$ agglutinates as meas-
ured by the magnetic separation technique. The chemistry
of lunar soil may be somewhat partitioned between aggluti-
nitic and non-agglutinitic components with the ferromagnesian
elements concentrated in the agglutinates (Rhodes et al.,
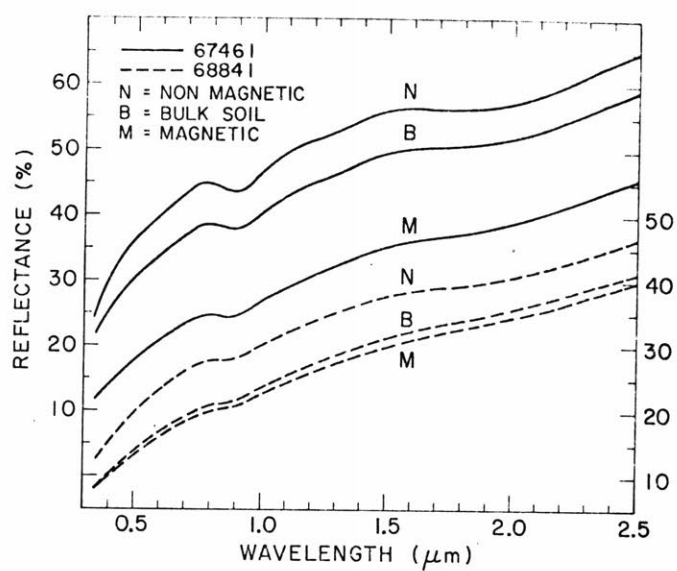
Spectral reflectance curves (relative to MgO) of Apollo 16 soil samples 67461 and 68841, and of their magnetic and non-magnetic fractions. The magnetic fraction consists of glass-welded aggregates (agglutinates) and always is darker than the parent soil.

Figure IID 3.   (Adams and McCord, 1973)

1975). Since it is these agglutinates that dominate the
spectrum of such soils, it is useful to understand the spec-
tral nature of a number of key components that have a special
character in lunar agglutinates: Fe-Ti bearing glasses,
Fe^0 (microscopic), and ilmenite and other opaque phases.
The spectral character of the mineral fragments, which
are significant components in agglutinates, but often with
subtle spectral effects, were discussed in greater detail
in Section IIC-2c.

i. Fe-Ti RICH GLASS. A relatively pure Fe-
Ti rich glass sample was separated from soil sample 10084.
The spectral reflectance properties of this glass are shown
in Figure IID-4. The color of lunar glasses is caused pri-
marily by various electronic transitions between and within
Fe^{2+}, Ti^{3+} and Ti^{4+} ions. Using transmission spectroscopy
and controlled experimental techniques, Bell et al. (1976)
have carefully documented the spectral effects of iron
and titanium concentrations in synthetic glasses as a func-
tion of oxygen fugacity. These concentration systematics
were shown to be equally valid for reflectance spectra of
glasses (Wells and Hapke, 1977). Figures IID-5a,b (from
Bell et al., 1976) illustrate the following spectral char-
acteristics for glasses produced at oxygen fugacities com-
parable to the lunar condition: (1) An iron-rich, titanium

MAG = 10.0

Figure IID 4.
Spectral reflectance
of a glass separate
from Apollo 11 soil.

REF (1.00) = 0.148

WAVELENGTH (MICRONS)
0.4   0.5   1.0   2.0

3.0   2.5   2.0   1.5   1.0   0.5
WAVENUMBER (X 10,000)
12/29/71 #7   10084,66 GLASS SEPARATE
CONTINUUM = METALLIC IRON - MOD 2

Wave number, 10³cm⁻¹

Wave number, 10³cm⁻¹
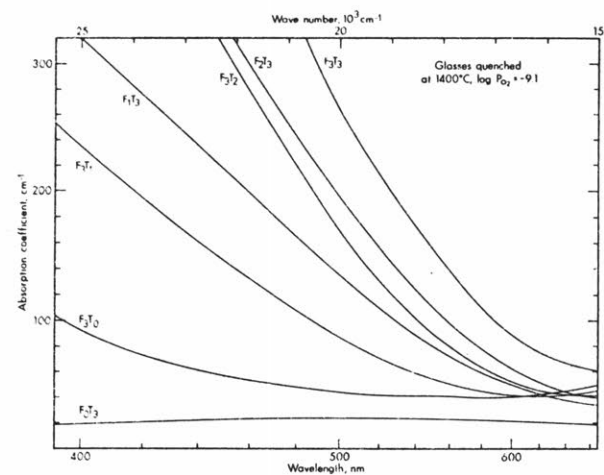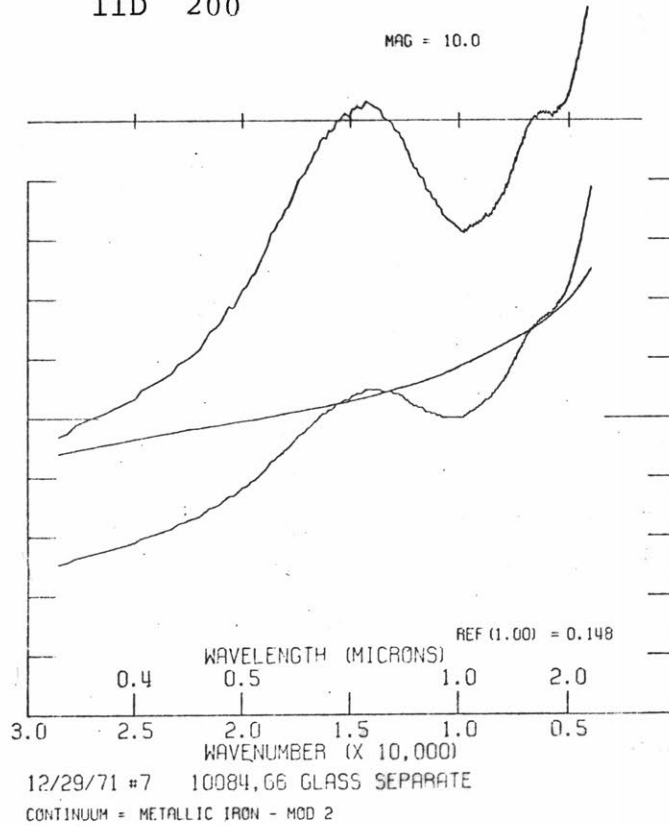
a   Spectral region 400–660 nm for the glasses whose slope at 20,000 wave numbers is plotted in Fig. 5.

Figure IID 5. (Bell et al., 1976)
Absorption of glasses containing
various amounts of iron and ti-
tanium. F_0--F_3 indicates increasing
iron; T_0-T_3 indicates increasing
titanium.
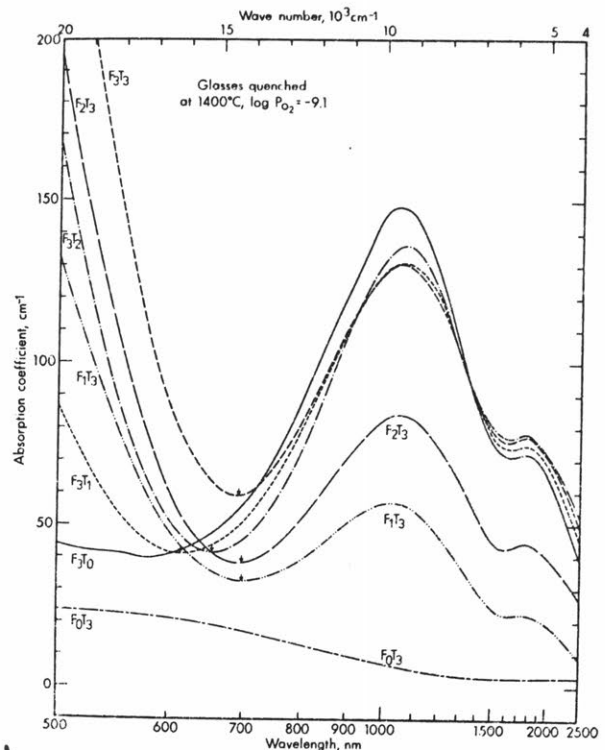
b   Continuation of the observations plotted in Fig. 6 to 2500 nm (four wave numbers).

free glass is weakly absorbing throughout the visible region
(minimum absorption between .5 and .6μm; i.e., green glass)
and contains a well-defined Fe^{2+} broad absorption band (crys-
tal field) centered around 1.0μm.   (2)   If titanium is in-
cluded in an iron-rich glass, a strong absorption occurs
toward the blue and ultraviolet (i.e., red glass), the strength
of which is related to the amount of titanium. The strength
of this absorption is also very sensitive to the effective
oxygen fugacity. The Fe^{2+} 1.0μm feature is only slightly
affected by the addition of titanium. (3) Only the concen-
tration of iron affects the strength of the broad 1.0μm
feature. (4) The concentration of both iron and titanium
affect the strength of the UV absorption (with titanium
perhaps playing a stronger role.) (5) In a Ti-rich glass
without iron, a relatively weak absorption is detected near
.5μm due primarily to Ti^{3+} (crystal field absorption) al-
though $Ti^{3+} \rightarrow Ti^{4+}$ may also occur (charge transfer absorption).
This feature is associated with a purple color of such glasses
and increases in strength with lower oxygen fugacity. These
transitions were identified by Burns et al. (1976).

Due to the strong absorption towards the
ultraviolet, iron- and titanium-bearing glasses are certain
to have a significant effect on the continuum slope of re-
flectance spectra for mature lunar soils. The very broad

1μm feature common to reflectance spectra of all mature

lunar soils is typically a result of FeO in the agglutini-

tic glass (Charette and Adams, 1977b).

ii. Fe^0. Small particles of iron metal were

observed in the first returned lunar soils (Agrell, 1970).

From magnetic and Mossbauer techniques, it was further

shown (e.g., Housley et al., 1973) that submicroscopic metal

grains are enriched in mature soils. Evidence has been

accumulating that these fine metal grains have a signifi-

cant effect on the spectrum of a lunar soil even though

they account for <1% of the bulk composition. Hapke et

al. (1975) propose that the principle darkening effect

for lunar soils is submicroscopic Fe^0 formed in impact events

and solar wind sputtering. Gaffey (1976) showed that al-

though metal iron is opaque to visible and near infrared

radiation, its spectral character in reflected radiation

is a distinctive smooth but red continuum. For meteorite

specimens, a red continuum is clearly associated with Fe^0

content in a mineral mixture. This is an observed and

well-documented effect (Gaffey, 1974, 1976) although theo-

retical descriptions of how iron particles interact with

light in a mineral mixture are complicated by the fact

that iron is a conducting material rather than a semi-transparent

dielectric. A key difference between lunar agglutinitic

metal and that found in meteorites is particle size--the
lunar particles in agglutinates are submicroscopic (~ 200Å)
whereas the meteoritic iron is easily identified with nor-
mal petrographic techniques. Mie theory calculations by
Conel (1970) show that the extinction due to scattering
and absorption of radiation by submicroscopic particles
of iron or ilmenite is much stronger in the blue and ultra-
violet than in the near infrared. The overall spectral
effects of submicroscopic metal iron inclusions, therefore,
is to preferentially absorb blue and ultraviolet radiation
(whatever the cause). With further theoretical and labor-
atory analyses, a distinction between scattering and reflec-
tion effects should be possible.

Recently Bell and Mao (1977) have been
able to obtain a transmission spectrum for a portion of
a lunar agglutinate that is rich in submicroscopic Fe^0 par-
ticles. For comparison they produced thin (10 - 100Å) coat-
ings of Fe^0 on transparent powders (silica glass). The re-
sults are shown in Figure IID-6. Their data show an increased
absorption towards the ultraviolet associated with the
metal iron. Although they could not guarantee that no ox-
idation had occurred during the laboratory analysis for
both the lunar sample and the coated grains, the similar-
ity between the two iron-bearing spectra is striking.
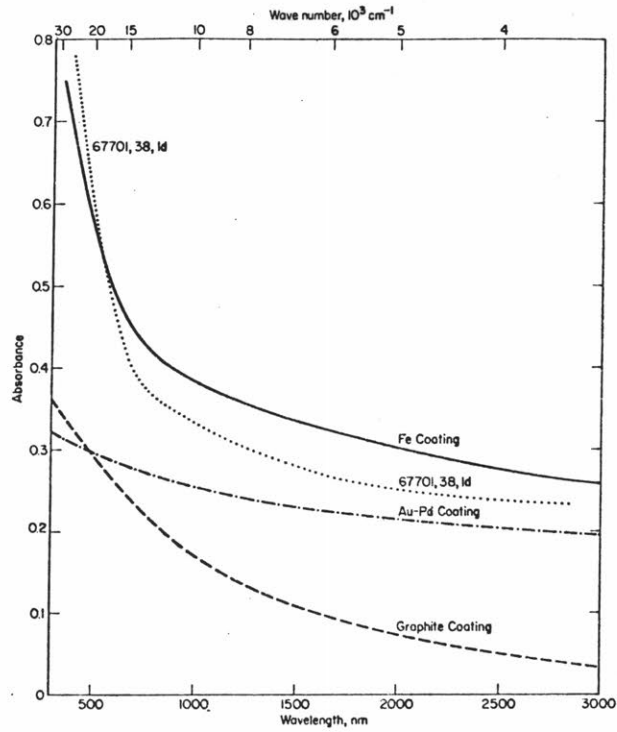
Figure IID 6.
(Bell and Mao,
1977)

Optical spectra of Fe, Au-Pd alloy, and graphite
coatings on silica glass, and the optical spectra of agglutinate
specimen 67701,38,1d.
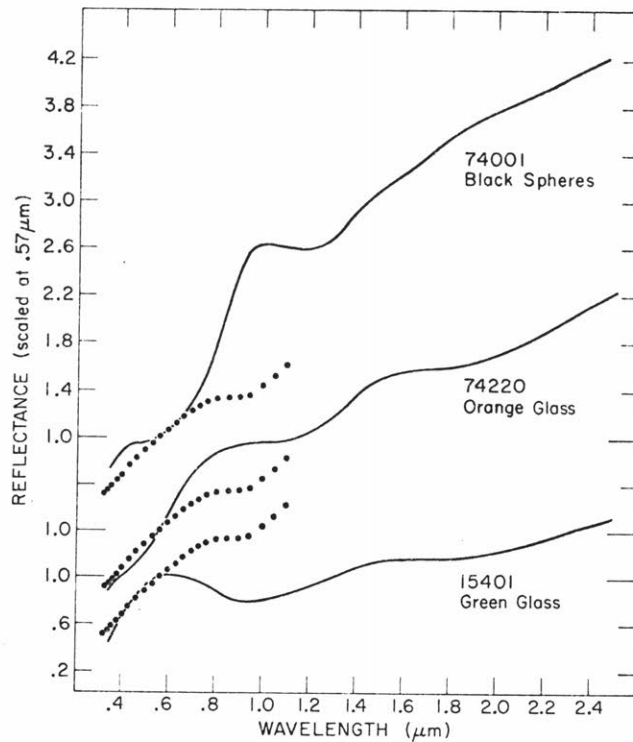
Figure IID 7.
(Adams et al.,
1975)

Spectral reflectance for the orange glass and related soils. Superimposed on each
spectrum is the spectrum for the standard lunar area MS-2 (closed circles).

A purely empirical piece of evidence for
the effects of Fe^0 on mature soil spectra results from attempts
to characterize the lunar continuum sufficiently well to
examine superimposed absorption characteristics. It was
found that a fit of Gaffey's (1977) iron metal continuum
to a lunar soil spectrum accounted remarkably well for the
red slope in the near infrared. Such a continuum was re-
moved from the spectra in Figure IID-9-16 to examine the
1μm feature in better detail. For very dark soil, it ap-
pears the continuum approximation of Fe^0 is not as good
as for bright soil.

Although the effects of submicroscopic
iron particles on a reflectance spectrum of lunar soils
are currently poorly understood, it is likely that they
are significant. Small amounts of metallic iron probably
contribute to the darkening of the soil and help account
for the distinctive red continuum of lunar soils.

iii. ILMENITE AND OPAQUES. Ilmenite is the
most abundant opaque mineral in lunar samples and accounts
for up to 25% of modal abundances for the igneous basalts.
Ilmenite is present in lunar agglutinates as remnant min-
eral fragments, some of which are very finely dispersed
throughout the glassy matrix. Although the dominant effect
of opaque ilmenite particles in a soil is to darken the

soil and lower the spectral contrast of other mineral fea-
tures (see Section IIC-2d), ilmenite is not without its
own spectral character. Two prominent absorption features
near .65 and 1.25μm were observed for the unique thin il-
menite plates in the glassy spheres of 74001 (Figure IID-1-7,
from Adams et al., 1975). The finest grain size in basal-
tic rocks do not generally allow the spectral character
of ilmenite to contribute to a rock spectrum. However,
if the particles are sufficiently small, they could inter-
act significantly with the reflected radiation. Small il-
menite particles primarily contribute to the darkness of
the agglutinitic material but for some samples may also
allow the 1.25μm ilmenite band to slightly affect the sym-
metry of the 1μm absorption in a soil spectrum.

        iv. MINERAL COMPONENTS. The spectral char-
acteristics of the other major mineral components in lunar
basalts, and hence in soil agglutinates, was discussed
in Section IIC. Briefly, these include: two strong, sym-
metric absorption bands near 1 and 2μm from pyroxenes;
a broad, nonsymmetric absorption band near 1μm from olivine;
and a weak band near 1.3μm from iron-bearing plagioclase.
Mineral spectral features are strongest in immature soils
and barely discernable (if at all) in mature soils.

b. <u>Soil spectra</u>

The mineralogy of mature lunar soils is large-
ly a combination of remnant mineral and lithic fragments
and complex, multi-component agglutinates. Table IID-1
lists various soil components, their spectral absorptions
and the approximate magnitude of effect from these absorp-
tions on a soil spectrum. In order to derive useful com-
positional information from a bulk soil spectrum, it is
necessary to isolate and identify each particular absorption.

i. STRONG ABSORPTIONS. Although albedo dif-
ferences are close to a factor of two between maria and
highland mature regions, it is remarkable that the spectral
differences between such regions ($.3 - 1.1\mu$m) are generally
less than $\sim$10% (McCord et al., 1972). There are at least
three competing strong absorptions that dominate the gen-
eral structure of a mature (agglutinate-rich) mare soil
spectrum throughout the visible and near infrared spectral
region: the Fe-Ti bearing glass, the finely dispersed
iron, and opaques (primarily ilmenite). All of these ab-
sorptions darken the soil, perferentially through the vis-
ible toward the ultraviolet. All three of these components
exist in mare soils and are thus expected to contribute
spectrally to some degree. Which (if any) plays the pri-
mary role in all lunar soil spectra is the subject of much

TABLE IID-1 Effect of various absorption features on soil
or rock spectra.

Soil or Rock Component	Absorptions	Mature Soil	Immature Soil	Rocks
		Effects on Spectra of:		
Pyroxene	.90-1.0μm	subtle	strong	dominant
	1.8-2.3μm	subtle	strong	dominant
Plagioclase	1.3μm	trace?	subtle	strong
Olivine	1.0μm	-	subtle	strong
Ilmenite	UV-IR	strong	subtle	subtle
	.6, 1.2μm	trace?	-	-
Glass (Fe-Ti bearing)	UV-IR	strong	subtle	-
Glass (Fe-rich)	1.0μm	subtle	subtle	-
Fe^0	UV-IR	strong?	subtle	-

discussion and will not be resolved here. A few observations and conclusions, however, can be made independent of this controversy.

All the strong darkening effects depend on Fe or Fe + Ti. Thus, for soils of equal maturity (same accumulation of agglutinates) the more Fe- and Ti-rich soils are darker. This point is obvious in the gross distinction between highland and maria and also seems to hold for Apollo 14 soils relative to Apollo 16. For mare soils, however, other factors are also present.

For mare soils, the strong absorption in the blue and ultraviolet approaches saturation. For example, as the iron and titanium content increase, soils do not get redder as they would if Fe-Ti spectral absorption were the only effect (Bell et al., 1976); instead they get bluer (Charette et al., 1974). This can be understood by referring to the simple diagram in Figure IID-8. Shown are three hypothetical spectra with stronger absorption in the blue (B) relative to the red (R). Whatever is responsible for the B/R color, spectrum II is affected by twice as much absorbing material as I, and spectrum III by twice as much as II. In transmitted light, the absorption strengths would follow the ratio 1:2:4. If the increased
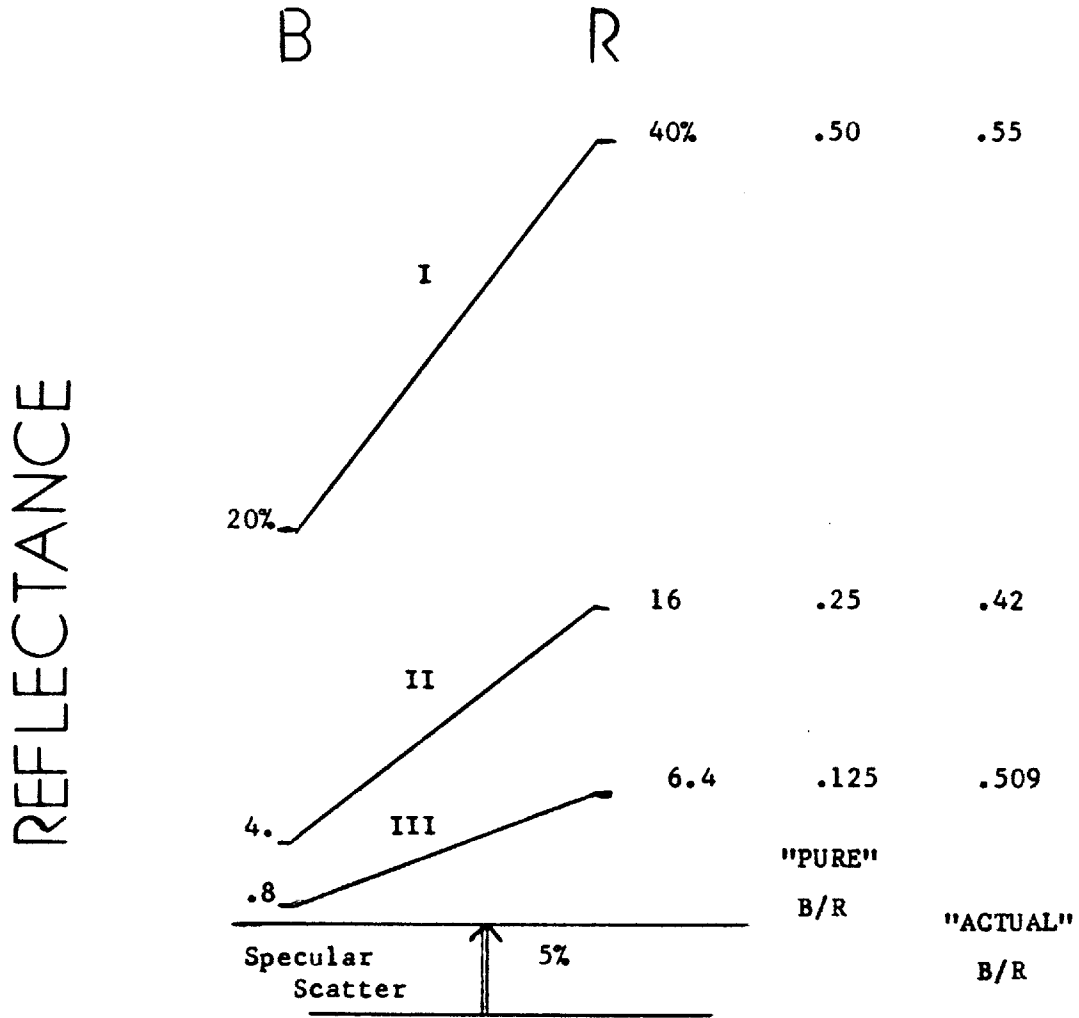
Figure IID 8.   Effects of specular scatter on spectral contrast.

absorption was the <u>only</u> factor that influenced the reflec-
tance, the color ratio B/R should be .5, .25 and .125 for
spectra I, II, and III respectively. However, even totally
opaque particles scatter a significant amount of radiation
from specular reflection without imparting any spectral
information. This specular scattered component is estimated
to be 5% here. (A lower bound of 3-1/2% can be inferred
from the far UV albedo measurements of the moon (Luke et
al., 1973) since all surface material is effectively opaque
at those wavelengths.) When the scattered component is in-
cluded in reflected radiation, the actual color ratios meas-
ured (see Figure IID-8) would show spectrum II to indeed
be redder than I (although not as much as it should be).
The dark spectrum III, however, would actually be <u>bluer</u>
than spectrum II. Thus, increasing a (red) absorption strong-
ly darkens the soil so much that spectral contrast is gra-
dually lost and the spectrum becomes flatter, or relatively
bluer. Highland soils may be bright enough to discern real
absorption differences (e.g., becoming redder with increas-
ing iron in Fe-Ti-bearing glasses). Mare soils are nearly
saturated in the blue and ultraviolet and become <u>bluer</u> with
increasing Ti-content, presumably because of Fe-Ti glass
absorption. The concept of spectral contrast for mare soils
has recently been reexamined by Adams (1977).

Thus, two general spectral parameters for mature soils that can be interpreted compositionally are albedo and continuum slope. Note that the interpretation of measured continuum slope is dependent on the overall brightness of the surface.

ii. SUBTLE ABSORPTIONS. There are a number of small subtle features superimposed on the general red continuum of lunar soils, the most prominent of which is a small absorption near 1μm in the spectra of Figure IID-1 and 2. In order to examine these in greater detail, the red continuum must be estimated and removed. A number of techniques for determining this continuum have been tried. If this step is not performed correctly, then measured band centers can be offset from actual centers and erroneous compositional interpretations can result.

One of the most promising estimates for the lunar continuum is the iron metal continuum used by Gaffey (1977). Such a continuum has been used for a variety of lunar soil samples shown in Figures IID -9-16 (plotted as a function of energy). In these figures a metal continuum has been fitted through the laboratory sample spectra at .73 and 1.5μm. The spectra have been scaled to unity at 1.0μm. The fit seems to be a reasonably good
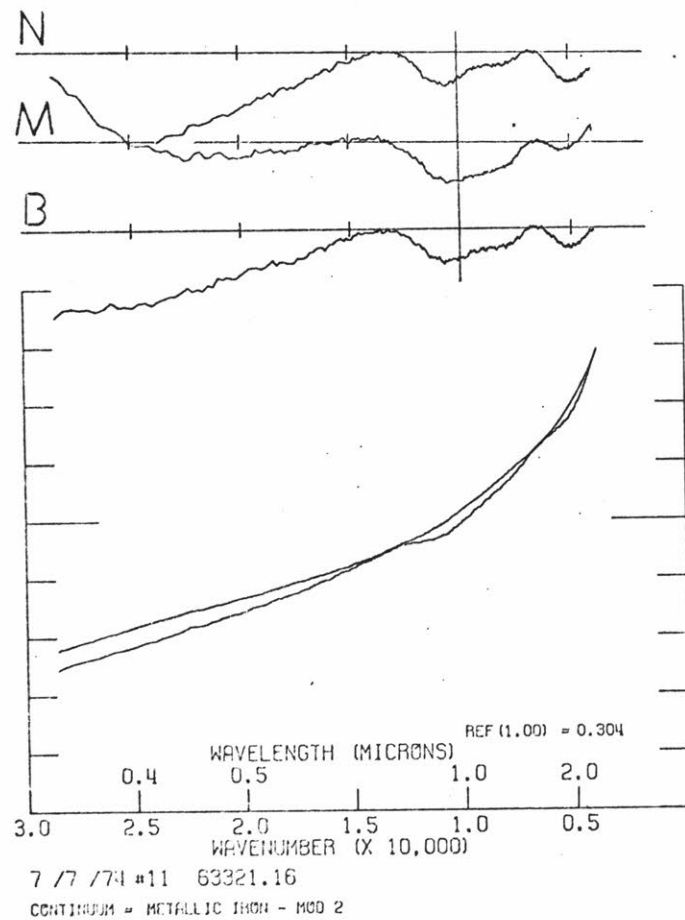
Figure IID 9. Spectral reflectance
for lunar soil 63321. An iron continuum
has been fit to the spectrum. Shown
above the spectrum are residual absorptions
after the removal of the continuum for the
bulk soil (B), magnetic separate (M), and
nonmagnetic separate (N).
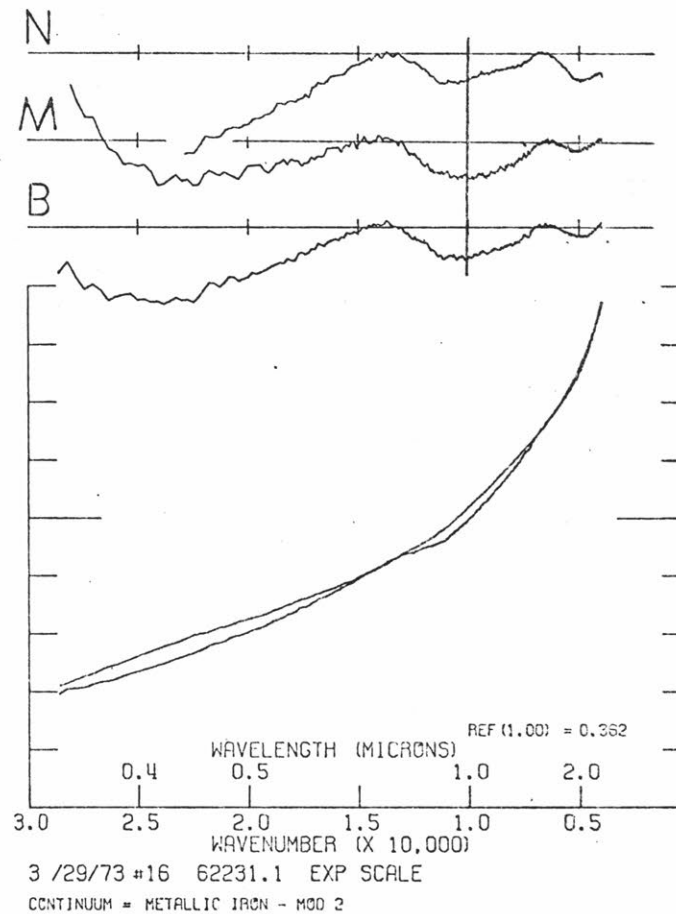
Figure IID 10. Similiar to Figure IID 9,
for lunar soil 62231.

N

M

B

REF (1.00) = 0.522

WAVELENGTH (MICRONS)

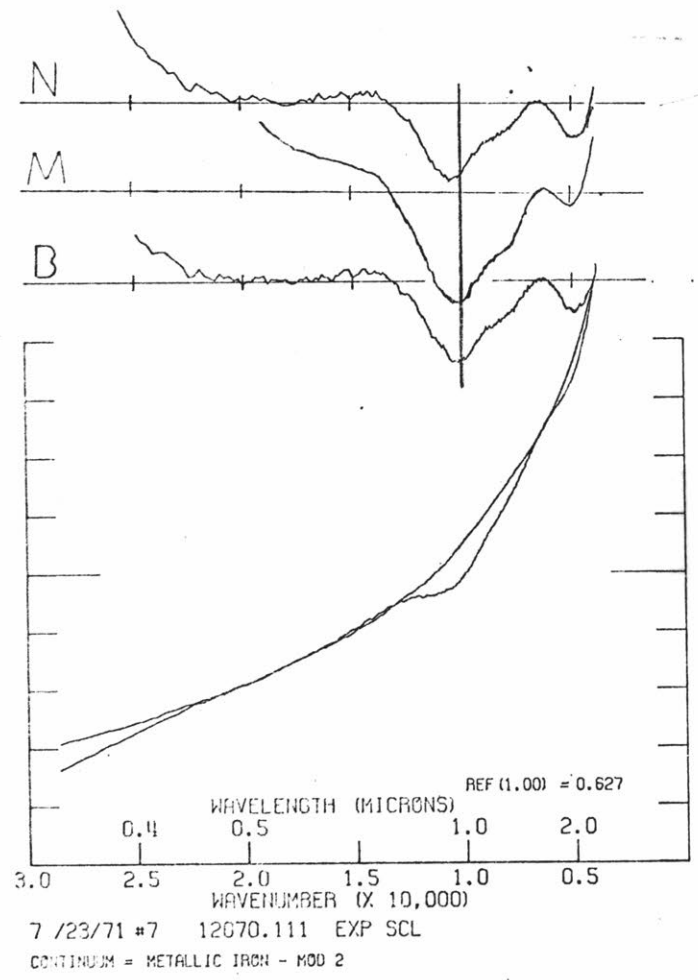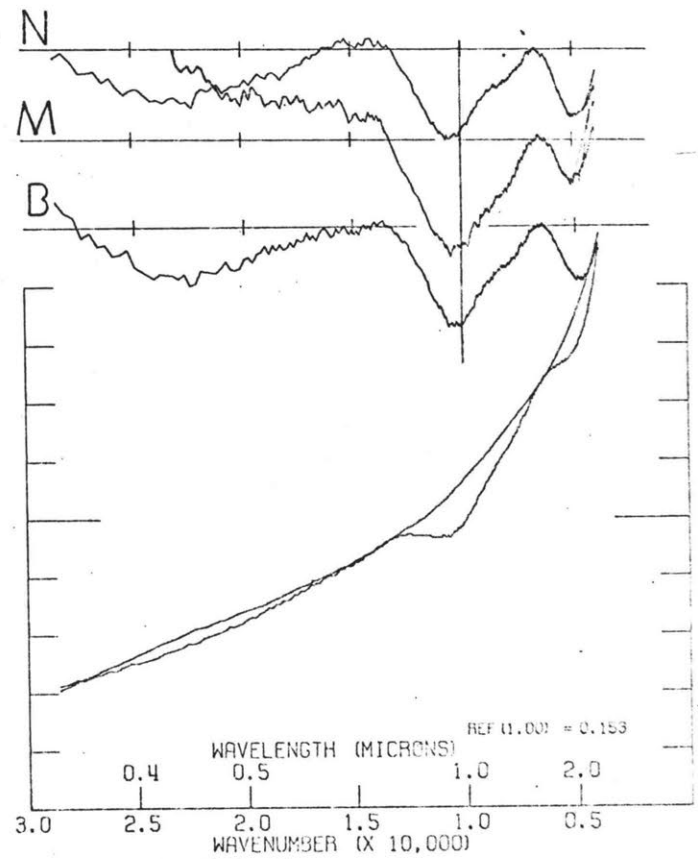0.4   0.5   1.0   2.0

3.0   2.5   2.0   1.5   1.0   0.5
WAVENUMBER (X 10,000)

7 /11/74 #5   10084.896   (EXP SCALE)

CONTINUUM = METALLIC IRON - MOD 2

Figure IID 11.
Similiar to Figure IID 9,
for lunar soil 10084.

N

M

B

REF (1.00) = 0.171

WAVELENGTH (MICRONS)

0.4   0.5   1.0   2.0

3.0   2.5   2.0   1.5   1.0   0.5
WAVENUMBER (X 10,000)

4 /2 /73 #3   75080.5   EXP SCALE

CONTINUUM = METALLIC IRON - MOD 2
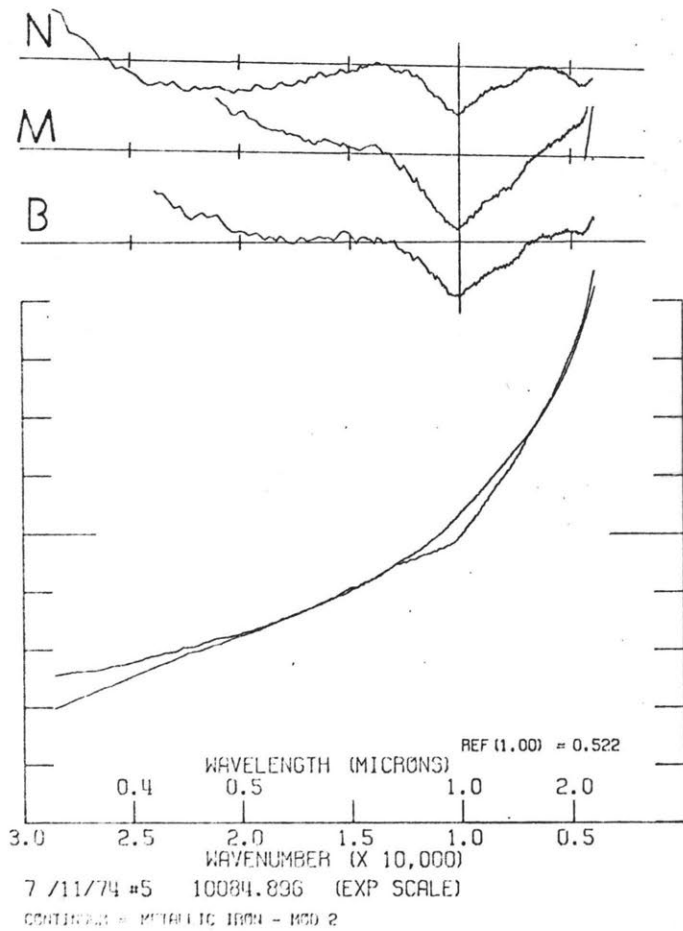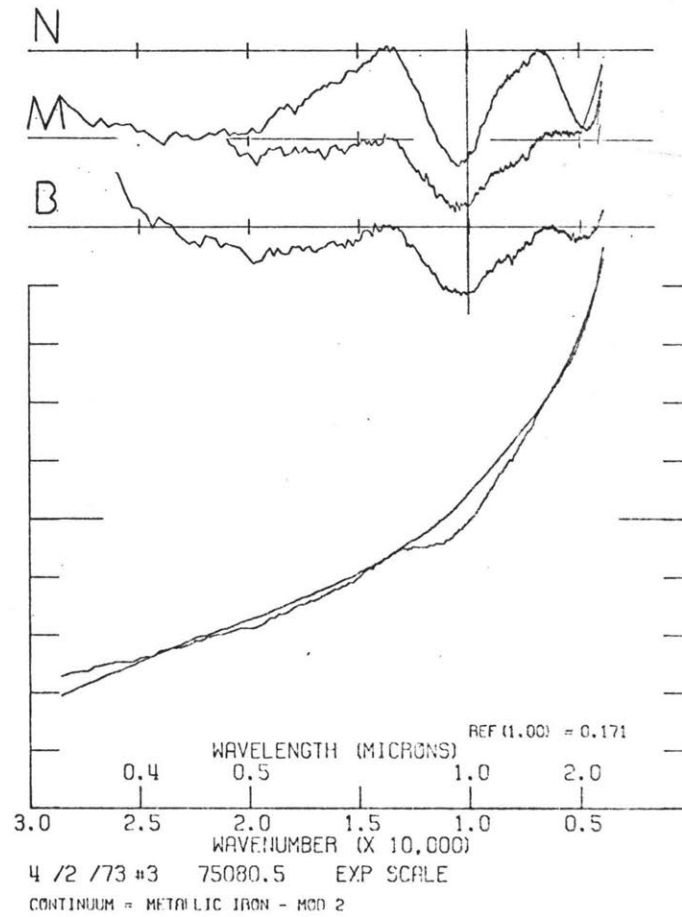
Figure IID 12.
Similiar to Figure IID 9,
for lunar soil 75080.

Figure IID 13.
Similiar to Figure IID 9,
for lunar soil 12070.

Figure IID 14.
Similiar to Figure IID 9,
for lunar soil 12042.

REF (1.00) = 0.129

WAVELENGTH (MICRONS)
0.4   0.5   1.0   2.0

3.0   2.5   2.0   1.5   1.0   0.5
WAVENUMBER (X 10,000)
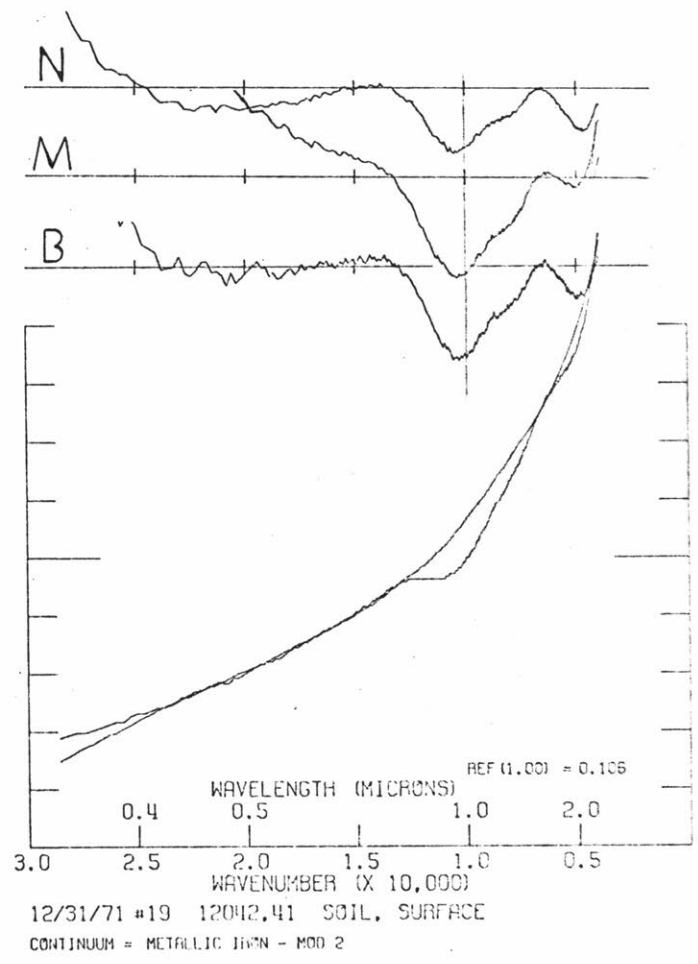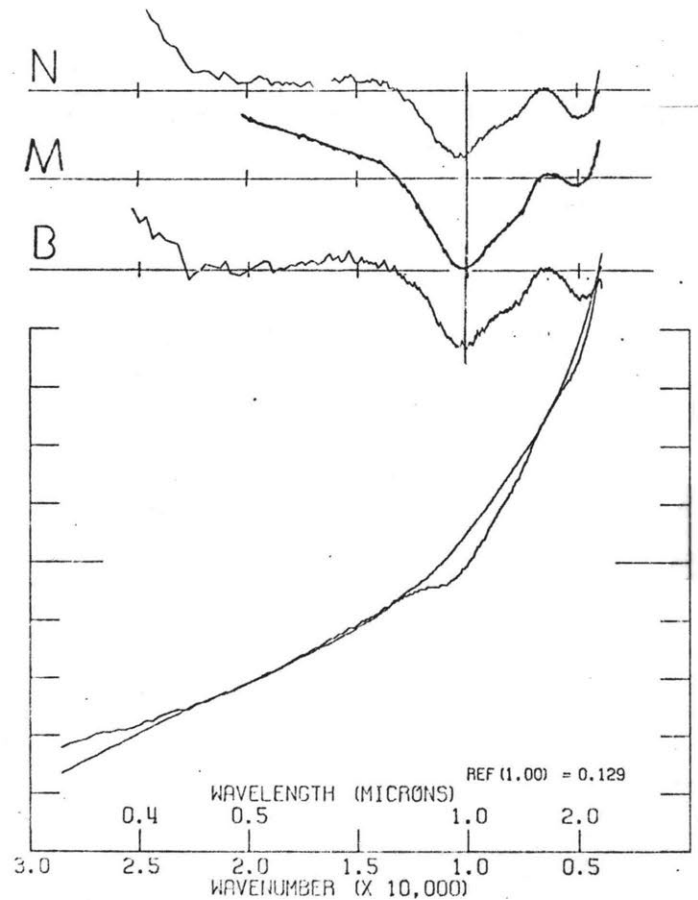
12/27/71 #21   15021.114
CONTINUUM = METALLIC IRON - MOD 2

Figure IID 15.
Similiar to figure IID 9,
for lunar soil 15021.

REF (1.00) = 0.153

WAVELENGTH (MICRONS)
0.4   0.5   1.0   2.0

3.0   2.5   2.0   1.5   1.0   0.5
WAVENUMBER (X 10,000)

1 /5 /72 #9   15471.37
CONTINUUM = METALLIC IRON - MOD 2

Figure IID 16.
Similiar to Figure IID 9,
for lunar soil 15471.

approximation above 5000Å. A ratio has been formed between

the continuum and bulk soil spectrum (B) and is displayed

in the figures above the spectrum. Similar ratio spectra

were formed for the magnetic (M) and nonmagnetic (N) soil

separates and are displayed above the bulk soil spectra.

Most of the remnant mineral fragments are concentrated in

the nonmagnetic fractions (Adams and McCord, 1973).

In most of the spectra presented in Figures

IID9-16, the following subtle features can be noted: (1)

There is a broad composite feature near 1μm with the peak

off-center to shorter wavelengths and a distinct shoulder

towards longer wavelengths.   (2) There is often a second

less intense feature near 2μm, the intensity of which var-

ies greatly. It is unclear whether the variations short-

wards of .7μm are real or simply an effect of the contin-

uum removal procedure. For the reasons outlined below the

1μm soil feature is interpreted as a composite pyroxene

and glass band and the 2μm feature is primarily the 2nd

pyroxene band (Adams and Charette, 1977).

Sample 63321 (Figure IID-9) is an immature

soil (magnetic component or agglutinate content ∿32%) and

the non-magnetic fraction (N) is dominated by mineral frag-

ments. The pair of absorptions at ∿.91 and 1.9μm can be

clearly interpreted as orthopyroxene (Adams, 1974). A

second band, almost resolvable at $\sim$1.25μm, is likely to

be due to feldspar. This interpretation is in good agree-

ment with the mineralogy of the sample and the Apollo 16

site in general. The spectral features of these two min-

erals are severely degraded in the bulk soil spectrum (B)

by a broad deep feature near 1μm most noticeable in the

magnetic separate (M).

This broad 1μm feature is tentatively

identified as the Fe^{2+} 1μm glass band. Examine the spec-

trum for mature soil 62231 (Figure IID-10) which has a

bulk composition similar to 63321 (FeO $\sim$ 4%, TiO_2 $\sim$ .35%)

but with agglutinates dominating the soil mineralogy. The

bulk sample and non-magnetic separate spectra only contain

a trace of the orthopyroxene features. The magnetic sepa-

rate spectrum is dominated by the broad 1μm feature. Since

very few mineral fragments remain in this agglutinate sam-

ple, the 1μm feature is likely due to the Fe^{2+} glass band

described in Section IID1a. (The band observed here may

be slightly offset to shorter wavelengths by a hint of rem-

nant orthopyroxene.) Even though it is

weak in this sample, the broad symmetric band at $\sim$1.0μm

contains the same spectral properties as those identified

in glass separates (Figure IID-4) and with transmission

spectroscopy of glass (Figure IID-5).

Turning to the more mafic mare soils (Figures IID1-11-16), all spectra appear to contain a combination of various proportions of pyroxene and glass features. The non-magnetic fraction of the least mature soil shown here (75081, agglutinates ~30%) shows a spectrum dominated by clinopyroxene with characteristic bands near .95 and 2.1µm (Adams, 1974). There is little evidence for any contribution of the glass band. In the magnetic separate spectrum, the .95µm band is degraded and the 2.1µm band almost eliminated as the broad glass band begins to appear.

All the other mare soils show a composite clinopyroxene and glass band at 1µm. The glass band is the strongest in the magnetic agglutinate fractions and weakest in the non-magnetic fractions. The .95 - 1.0µm clinopyroxene band seen in the non-magnetic separates shifts to slightly longer wavelengths as it is diluted by the 1µm glass band.

Note that for glass-rich mare soils of approximately equal FeO content, the depth of the 1µm band is less strong for the dark soils (Apollo 11) than for lighter soils (Apollo 12 and 15). This lower spectral contrast of the 1µm band is probably due to an effect similar to that illustrated in Figure IID-8: if significant absorption has already occurred throughout the spectrum (dark

soil), the effects of a second absorption (the glass band)
are not as strong as they would be for brighter soils.
On the other hand, since highland mature soils are gener-
ally bright, an increase in the FeO content is expected
to increase the 1μm band depth (Charette and Adams, 1977a).

In summary, subtle spectral features can
be identified in spectra of mature lunar soils: a substan-
tial iron glass band and also weaker pyroxene bands (Adams
and Charette, 1977). It is unclear whether small components
of plagioclase and ilmenite in mare soils can contribute
a detectable feature near 1.3μm. For less mature soils,
the pyroxene bands are stronger and a plagioclase band may
be identified. If these weak bands can be accurately re-
solved, the composition of the pyroxene and (perhaps) plagio-
clase can be identified. As mentioned previously, correct
identification is in part dependent on how accurately the
effects of the red continuum have been removed. Since the
strength of the 1μm glass band has been shown to vary as
a function of FeO content (Bell et al., 1976), it should
be possible to estimate the FeO content of a mature soil
from the depth of the band (Charette and Adams, 1977b).
In order to accomplish this, the 1μm pyroxene band must
also be removed from the composite 1μm band, and the lower

spectral contrast effects of dark soils would have to be calibrated to lighter soils. Even without spectral contrast calibration, differences in the depth of the 1µm feature can nevertheless be interpreted in terms of relative FeO content if one compares mature soils of similar albedo and assumes that the minor pyroxene content is similar and that the soil development processes have homogenized all soils to the same degree.

2. <u>Rocks and Craters</u>

Since most of the lunar surface is covered with
a mature soil, the emphasis of many detailed spectral re-
flectance studies of lunar material has been directed towards
understanding the properties of these soils. It is recog-
nized that the mineralogy of lunar rocks, on the other hand,
is used by petrologists to identify the major lunar basalt
types. Currently, there is a lot of activity (Adams and
associates) to obtain spectra for a sufficient number of
lunar rock powders and chips in order to identify spectral
characteristics of the various distinct rock types identi-
fied by the petrologists. Although a number of preliminary
reports have become available (e.g., Charette and Adams,
1975, 1977a) this work is still in progress. Thus, this
section will only briefly discuss some of the current lab-
oratory reflectance results, the likely output, and the
difficulties inherent in the undertaking. Telescopic spec-
tra of craters (the closest lunar surface analogue to rock
samples) are discussed in Section IV.

Shown in Figure IID-17 are reflectance spectra
(unscaled) of a variety of lunar mare rock powders and
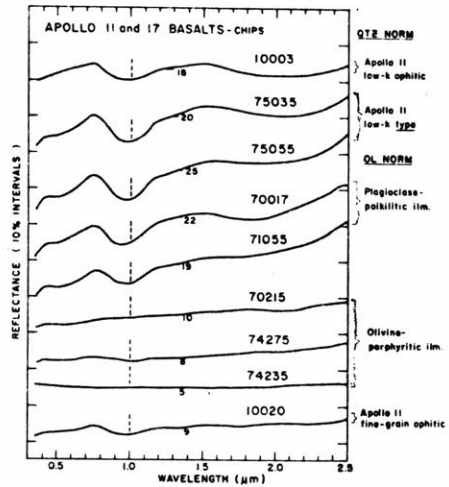chips. The spectra have been grouped by Adams and Charette

APOLLO 11 and 17 BASALTS-CHIPS

QTZ NORM

10003 — Apollo 11 low-k ophitic

75035 — Apollo 11 low-k type

OL NORM

75055 — Plagioclase-poikilitic ilm.

70017

71055

70215 — Olivine-porphyritic ilm.

74275

74235

10020 — Apollo 11 fine-grain ophitic

REFLECTANCE (10% INTERVALS)

WAVELENGTH (μm)

APOLLO 12 BASALTS-POWDERS

12009

12022

12063

12038

REFLECTANCE (10% INTERVALS)

WAVELENGTH (μm)

I. OLIVINE-PIGEONITE

A Olivine "Vitrophyre"

II. ILMENITE-BEARING

A Phyric ilmenite-bearing olivine basalt

B Aphyric ilmenite-bearing olivine basalt

III. FELDSPATHIC

A Subophitic feldspathic basalt

APOLLO 15 BASALTS-POWDERS

QTZ NORM

15065 — Porphyritic Clinopyroxene

15058

15499 — Porphyritic cpx basalt vitrophyre

OL NORM

15555 — Porphyritic Olivine

15016 — Vesicular Olivine

REFLECTANCE (10% INTERVALS)

WAVELENGTH (μm)

FIGURE a   Apollo 11 and 17 basalt (interior) chips. Basalt classifications by Warner (2) for Apollo 11 and Papike et al. (7) for Apollo 17. Dashed vertical lines are placed at 1.0 μm over each spectra. The integers below each spectra are the absolute reflectance values at the marked wavelength.
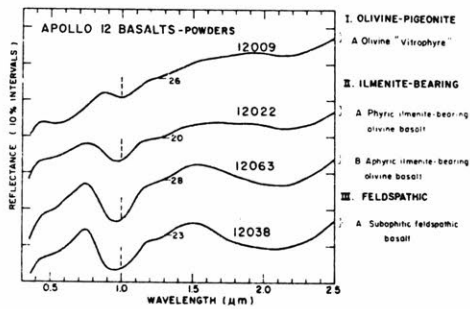
FIGURE b   Apollo 12 basalt powders. Classification by James and Wright (3).
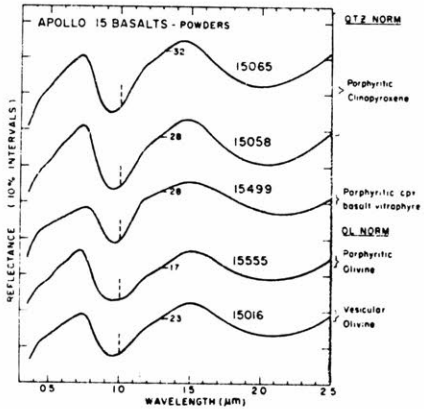
Figure IID 17.
(Charette and Adams, 1975)

FIGURE c   Apollo 15 basalt powders. Classification by Rhodes and Hubbard (4).

WAVELENGTH (MICRONS)

REF (1.00) = 0.140

WAVENUMBER (X 10,000)

12/28/71 #20   10003.00 ROCK

CONTINUUM = METALLIC IRON — MOD 2
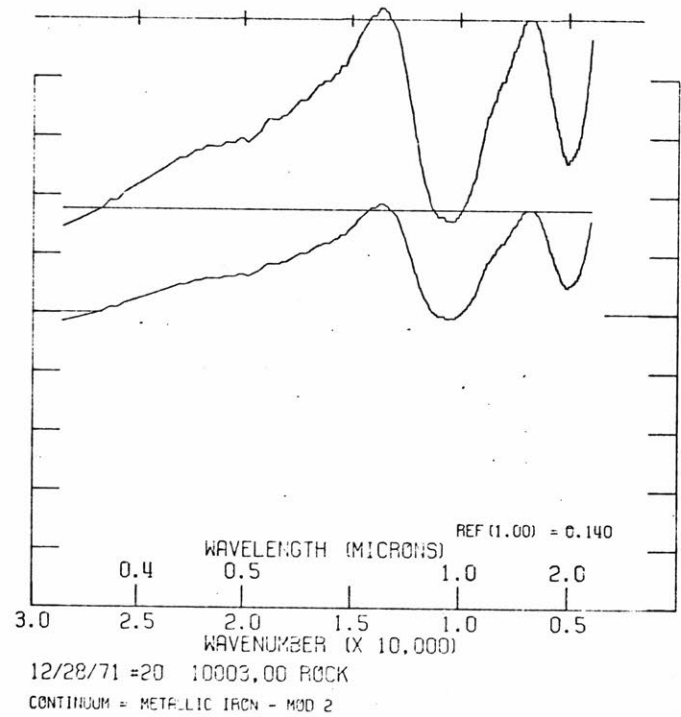
IID   223

0 12/28/71 #20 10003.00 ROCK

WAVELENGTH (MICROMETERS)
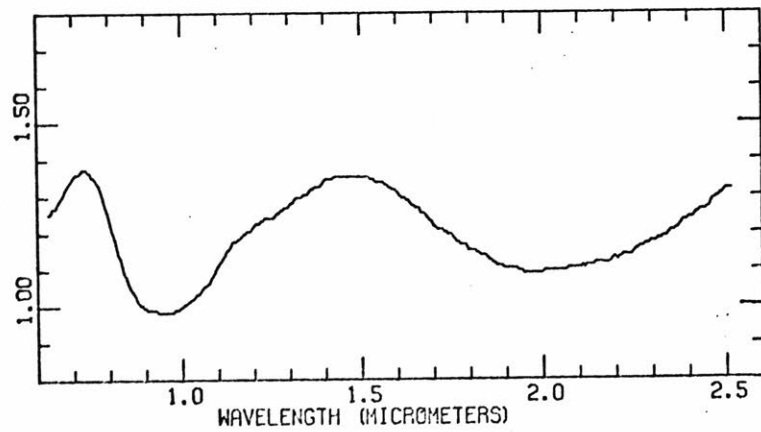
Figure IID 18.

Spectral reflectance of lunar sample 10003 (expanded verticle scale).

according to rock types identified by Warner (1971), James
and Wright (1972), Rhodes and Hubbard (1973), and Papike
et al. (1974). The albedo for each spectrum is marked for
one wavelength. Some of the principle conclusions by Charette
and Adams include: (1) Differences in basalt types can
be recognized in reflectance spectra as the presence or
absence of olivine bands, pyroxene bands at different wave-
lengths, plagioclase bands, and ilmenite bands. (2) Intra-
site differences are often more easy to distinguish than
inter-site differences since some basalt types having dif-
ferent origins may nevertheless have similar spectra (mineraology).

The spectral contrast of the spectra in Figure
IID-17 is dependent on the effective grain size--which is
smaller for powders than for chips. The grain size of the
rock and its degree of brecciation also effect this spec-
tral contrast. Fortunately, computer processing techniques
can be used to enhance the details of a spectrum. Compare
the spectra of 10003 in Figure IID-18 with the top spec-
trum in Figure IID-17a. As discussed in Section IIC2,
one should be able to deconvolve such spectra into features
due to specific mineral components such as pyroxene, plagio-
clase, olivine, ilmenite and glass. If a spectra deconvo-
lution is successful the composition of minerals such as
pyroxene can be identified. To some extent, the relative

proportions of mineral phases can also be described from
the relative strength of mineral absorption bands.

Thus, the first step in laboratory spectral reflec-
tance studies of lunar rocks and powders by Adams and as-
sociates is to identify the specific mineral spectral fea-
tures that can be associated with the major lunar rock types.
This project necessarily draws on an extensive background
of reflectance studies of minerals and rocks. A number
of related programs will likely ensue in order to have a
solid background for interpreting remotely obtained spec-
tra for fresh lunar surfaces:

(a) The individual spectral features for minerals
in mixture of minerals are quantatively identified using
computer processing techniques. This would eventually al-
low the inverse process--the creation of likely spectra
for possible mineral mixtures. This step is essential if
quantative identification of the mineralogy of unknown
assemblages is desired.

(b) It is unlikely that most lunar craters have
excavated a single rock type. It is thus necessary to deal
with the complicated spectral character of known and pos-
sible mixtures of unrelated rock types. For example, vary-
ing the proportions in a mixture of pigeonite, clinopyroxene,
olivine, and plagioclase should have small, but definable,

effects on a rock spectrum. Since the variations will be subtle as the proportion of minerals change, computer processing techniques will be required for detection and quantification of the spectral changes.

(c) The mineralogy that can be determined from reflectance spectra must be translated into terms that are meaningful to other geochemists studying lunar samples. Currently, for example, the pyroxenes in lunar mare rock types are distinguished by the compositional trends during crystallization. Spectral reflectance techniques, on the other hand, will be able to identify the composition (Ca, Fe, Mg) of the average pyroxene or perhaps the relative proportions of different pyroxenes (pigeonite, sub-calcic augite, etc.). The average pyroxene composition of a regional basalt type will be a major parameter for distinguishing mare basalt types using remote sensing techniques. The concept of "average pyroxene composition" needs to be considered as a possible meaningful geochemical parameter by lunar geochemists who are concerned with lunar basalt types on the smaller scale of the lunar samples.

3. Telescopic Spectral Measurements

Although the general lunar spectrum is distinct from spectra of all other solar system objects (except Mer-

cury) the spectral variations from place to place on the
moon are small (<10%). Much of the effort concerning tele-
scopic lunar spectral reflectance measurements has been
to identify such spectral differences and to derive inter-
pretations from the parallel lunar sample studies for ob-
served spectral characterisitics. Quantitative analysis
requires precision better than 1% which, for telescopic
observations, has only been available for about 10 years
(McCord, 1968a). Current telescopic data available with
adequate precision include spectra (.3 to 1.1µm) obtained
for small lunar areas (10-20 km diameter) with a filter
photometer (McCord, 1968a) and two-dimensional spectral
images at wavelengths between .4 and 1.0µm obtained with
a vidicon digital imaging system (McCord et al., 1975, 1976b).

It is anticipated that near-infrared spectra (.65 -
2.5µm) will soon be available for selected lunar regions
using recently developed telescopic instrumentation (McCord,
1977). Continuous infrared spectra are exceptionally dif-
ficult to obtain due to atmospheric absorptions. Prelim-
inary results (McCord, 1977) show that thermal emission
begins to become detectable beyond 2.1µm under full moon
viewing conditions. Theoretical calculations, (R. Clark,
in preparation) indicate, however, that this minor compo-
nent of lunar radiation between 2 - 2.5µm can be defined

sufficiently to be removed.

a. Relative Reflectance Spectra

Spectra for a variety of lunar regions were shown in Figures IID-1 and 2. Both the strong and subtle absorptions that affect the lunar spectrum were discussed in the previous sections. To distinguish the small differences between spectra, a technique is used by which each spectrum is divided by the spectrum of a standard area with the resulting spectrum being a relative reflectance spectrum. The standard area commonly used is MS-2 in central Mare Serenitatis (18° 40' N, 21° 21' E). The spectrum for MS-2 is second from the bottom in Figure IID-2. Note that this spectrum is not perfectly smooth and contains an easily identifiable $1\mu m$ feature. Thus, although all systematic spectral differences observed in relative reflectance spectra are significant, the position and symmetry of absorption features are not absolutely accurate but rather are relative to the features observed for MS-2. Relative reflectance spectra can be obtained from telescopic observations with minimal processing since both the atmospheric and instrumental effects usually cancel in the ratio.

When relative reflectance spectra were obtained for over 150 regions, a classification was made according to the general morphology of the region: mare, upland, mare crater, and upland crater. The spectral types evident

in spectra for these groups were discussed by McCord et

al. (1972a) and by Charette et al. (1974). A fifth group

of regions (dark mantled areas) formed an additional dis-

tinct spectral type and was discussed by Pieters et al.

(1973). Examples of relative reflectance spectra for the

four major spectral types are shown in Figure IID-19.

Spectra for the maria show a wide range of continuum slope

in the blue and ultraviolet that was correlated with TiO_2

content (see Section IID1). Mare crater spectra show a

strong absorption feature near $1\mu m$ characteristic of pyroxenes

(see Section IV). Most highland regions appear spectrally

similar (although work in progress indicates there are

a variety of subtle distinctions between highland surface

units). Highland craters can be easily distinguished from

mare craters. See Section IIB for a review of some of the

applications of these lunar spectral types.

An important aspect of this classification

for telescopic data was that similar spectral types could

be seen in laboratory data (Adams and McCord, 1972). Re-

call that relative reflectance spectra show the very small

and subtle spectral differences between two surfaces. The

fact that the same systematic small features also appear

in laboratory measurements of soils shows fairly conclusively

that the laboratory measurements are indeed comparable to
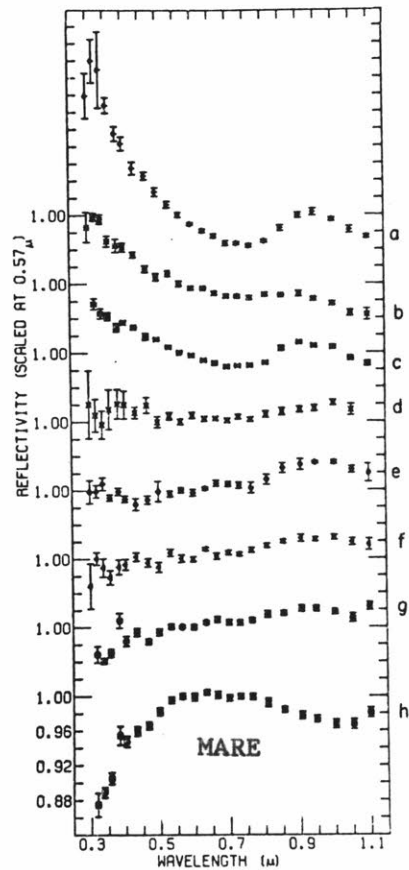
Relative spectral reflectivity for a series of background mare areas ranging from 'blue' mare (Sea of Tranquility 1) to 'red' mare (Sea of Cold 2). (a) Sea of Tranquility 1; (b) Sea of Moisture 0; (c) Luna 16 landing site; (d) Fra Mauro 15; (e) Le Monnier; (f) Sea of Moisture 51; (g) Plato C; (h) Sea of Cold 1.
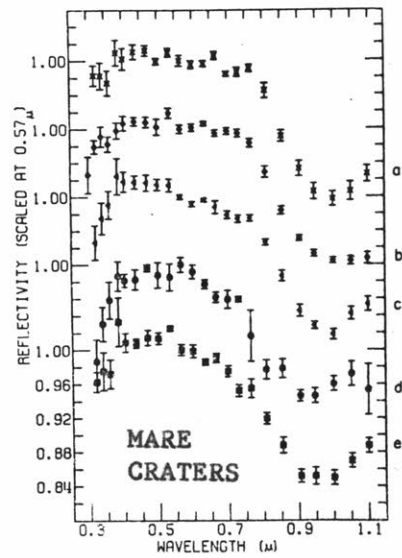
Relative spectral reflectivity for (a) Linne; (b) Sea of Moisture 45; (c) Messier A; (d) Kepler; (e) Mosting C.
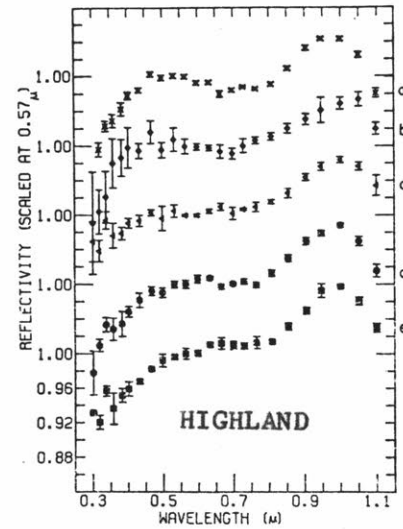
Relative spectral reflectivity for (a) Descartes 3; (b) Fra Mauro 7; (c) uplands 7; (d) Sea of Moisture 41; (e) Alphonsus 2.
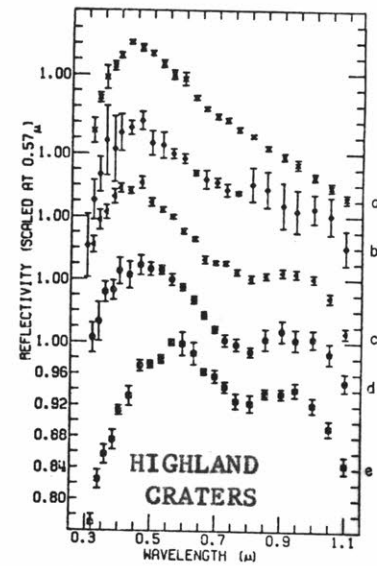
Relative spectral reflectivity for (a) Proclus; (b) Censorinus 2; (c) Descartes 2; (d) Fra Mauro 6; (e) Tycho 1. Relative reflectivity is the ratio of the reflectivity of one area to that of the standard area (in this study an area in the Sea of Serenity).

Figure IID 19. (from McCord et al., 1972)

to the telescopic measurements even though they differ by $\sim 10^6$ in area of surface measured.   Shown in Figure IID-20 are reflectance spectra for representative laboratory soils relative to MS-2 (from Adams et al., 1977).   In order to form these spectral ratios, the laboratory spectra were transformed to the same spectral bandpasses as used for the telescopic observations.   It is clear that the laboratory spectra for soils contain the same subtle features observed in the purely telescopic data of Figure IID-19.

Currently spectra for close to 400 lunar areas exist.   Relative reflectance spectra for many of these areas have been used extensively in the analysis and applications described in Sections III and IV.

b.   Spectral Imagery

The early relative reflectance studies also indicated there were certain regions of the spectrum that were critical in characterizing various surface units. The wavelengths .38, .40, .57, .77, .95 and $1.06\mu m$ were chosen for two-dimensional spectral mapping (e.g., McCord et al., 1976).   Three particuarly useful wavelengths are .40, .57, and $.95\mu m$ (Charette et al., 1974).

If an image is obtained at $.40\mu m$ for a given lunar region and a similar image at $.57\mu m$, the two images can be processed and digitally divided using computer processing techniques.   The resulting $.40/.57\mu m$ ratio image
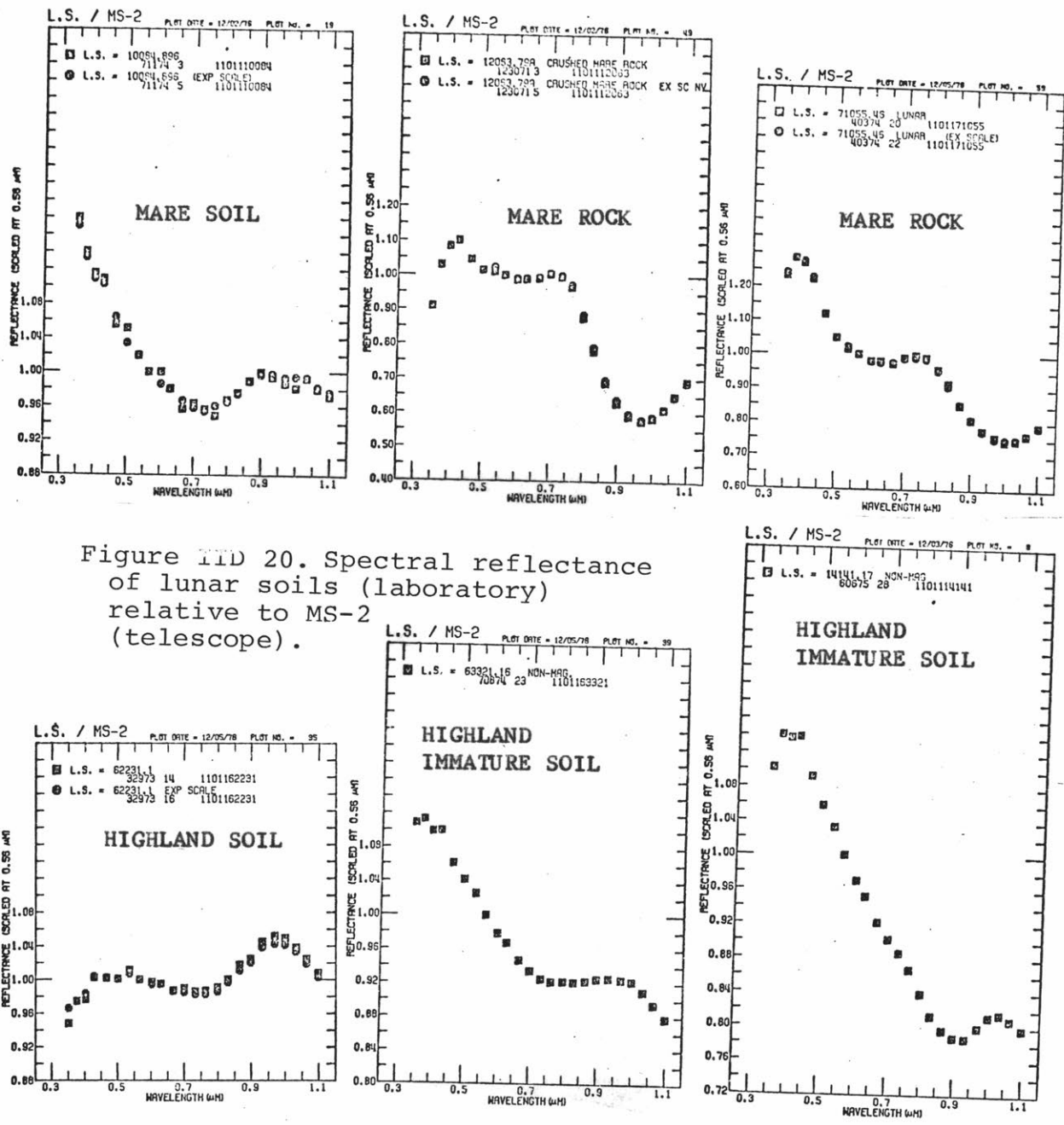
Figure IID 20. Spectral reflectance
of lunar soils (laboratory)
relative to MS-2
(telescope).

contains quantified spatial information on continuum slope
variations and can be used to "map TiO_2 content" for mare
surface (Charette et al., 1974; McCord et al., 1976; Pie-
ters and McCord, 1976). Since the spectral variations are
nevertheless very small, the ratio images must be computer
enhanced to display the data. Shown in Figure IID-21 are
mosaics of vidicon data for the Flamsteed area of the moon
(McCord et al., 1976b). Figure IID-21a is a slightly en-
hanced .57µm image and is comparable to a normal albedo
image. Figures IID21-b and c are both .40/.57µm ratio images,
each enhanced to bring out different details in the maria.
Note the distinct nature of the 'bluest' flow is only evi-
dent in the strongly processed image of Figure IID-21c.
This Flamsteed region is discussed in further detail in
Section IIIE2.

The ratio .95/.57µm ratio image is particularly
useful for identifying and examining the areal extent of
immature surfaces. This spectral parameter is mentioned
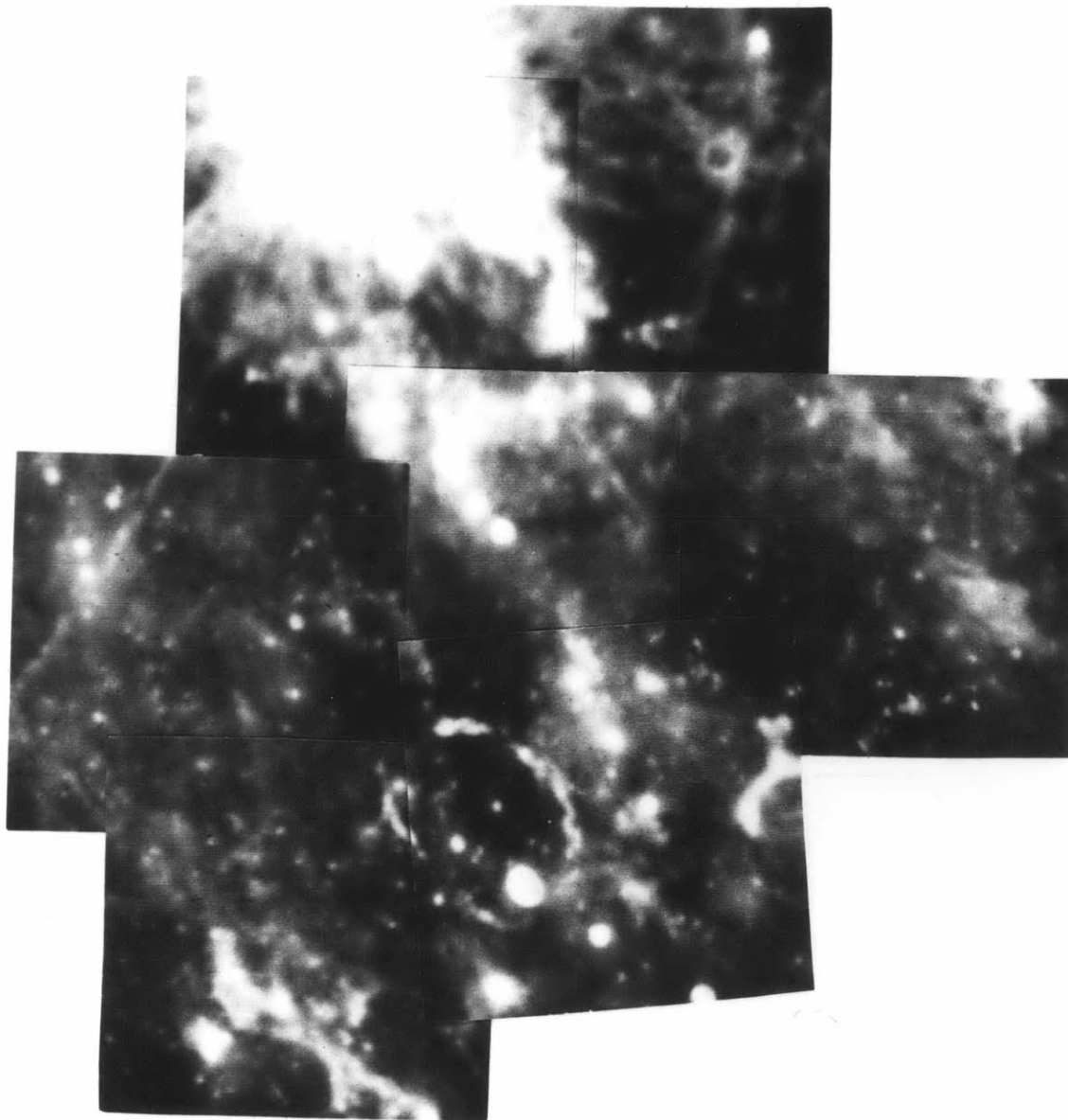in greater detail in Section IV.

234

Figure IID 21a. Vidicon image mosaic (λ = .57μm) of the Flam-
    steed region of Oceanus Procelliarum slightly contrast en-
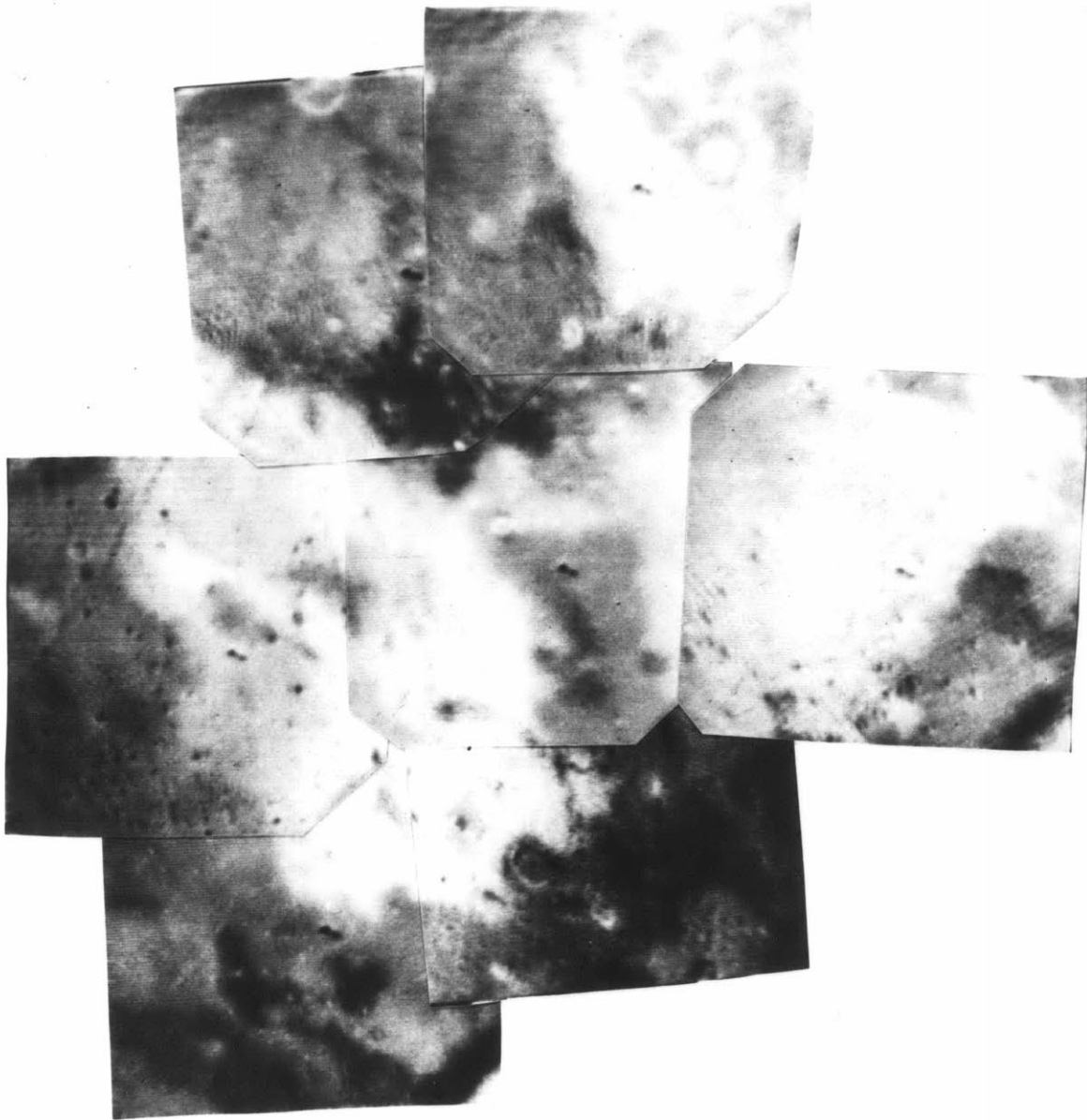   hanced to bring out details in the mare.

235

Figure IID 2lb. Vidicon spectral ratio image mosaic (.40/.57
μm) of the same region shown in Figure IID-21a. The
images have been contrast enchanced dark to light to show
a 12% color difference. Bright indicates relatively bluer
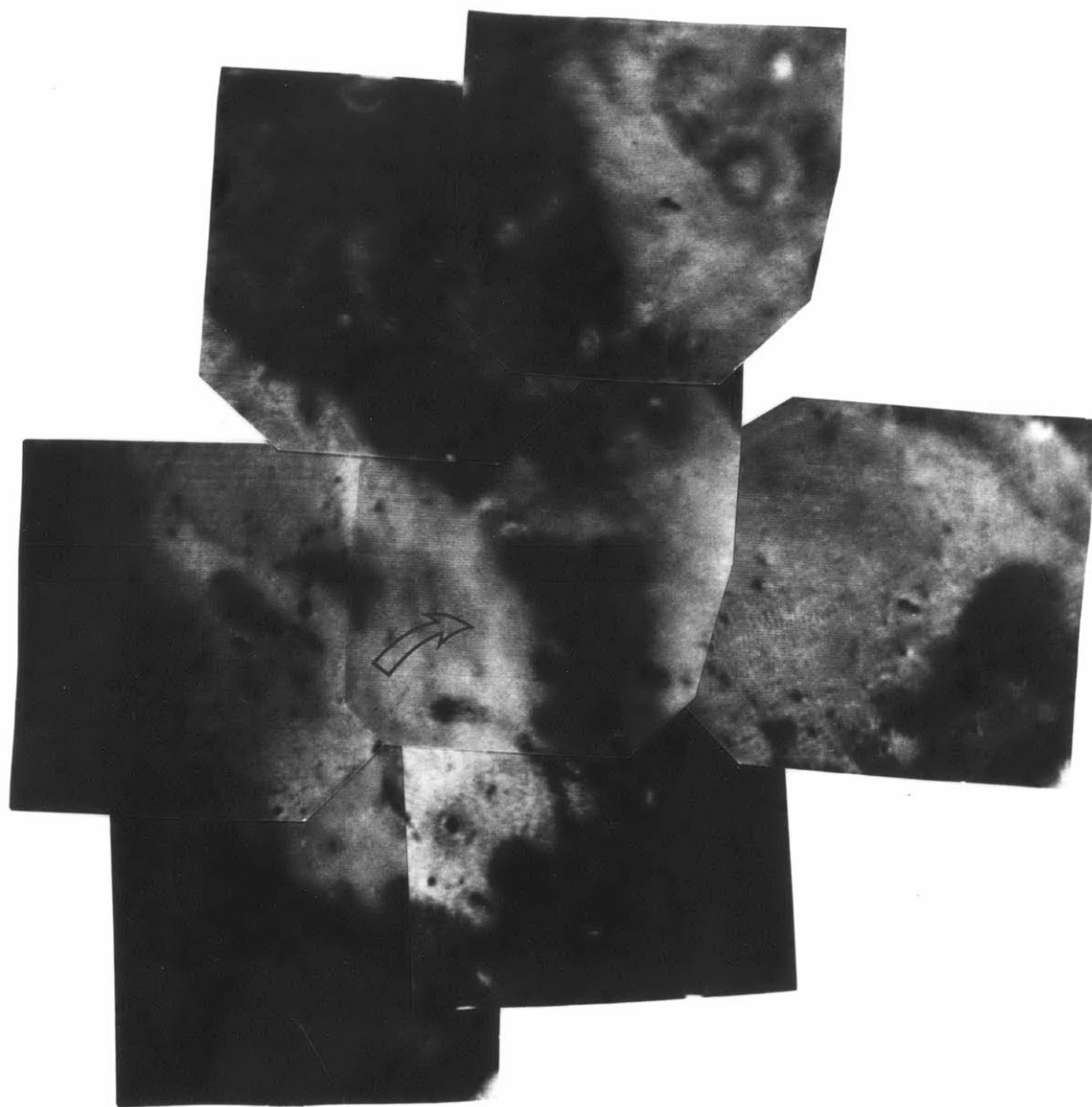(higher TiO_2 content).

Figure IID 21c. Same vidicon ratio image mosaic as Figure
    II 21b contrast enhanced further to show the bluest unit
    (indicated by arrow). This is likely to be the last
    basalt flow of the region and contains the highest con-
    tent of TiO_2.

III.   LUNAR BASALT TYPES I: SOIL SPECTRA (.3 to 1.1μm)

The material presented in Sections III and IV consti-
tute much of the scientific output of this thesis. These
sections are largely in the form of manuscripts that were
prepared as the thesis progressed. The content concerns
the classification of remotely-obtained lunar reflectance
spectra and the applications of spectral reflectance data
to the characterization and distribution of lunar mare
basalt types. The material presented in the two previous
sections provides the detailed background on the nature
of basalts and spectral reflectance techniques that cannot
be included in a (page-limited) published manuscript.

Section III includes discussion of lunar mare soil
spectra presented in three parts. The spectral character-
ization of lunar mare basalt types is presented first fol-
lowed by two applications of the spectral information:
a discussion of the Luna 24 landing area and a preliminary
report concerning a major unsampled basalt type in the
western maria.

Section IV includes a discussion of lunar crater spec-
tra for both mare and highland regions.

The major conclusions that can be drawn from the cur-
rently available spectral reflectance data are summarized
in Section V.

Characterization of lunar mare basalt types:
I. A remote sensing study using reflection spectroscopy of surface soils

CARLE PIETERS*† and THOMAS B. McCORD*†

Remote Sensing Laboratory, Department of Earth and Planetary Sciences, M.I.T.
Cambridge, Massachusetts 02139

Abstract—Telescopic reflection spectra of mature mare surfaces are used to identify and characterize major basalt types on the frontside of the moon. The spectra are classified according to (1) continuum slope and (2) near-infrared features. This study indicates that there are major lunar basalt types that are unlikely to have been sampled during the landing missions. Regions of basalt exist in the western maria with a TiO_2 content comparable to that of Apollo 11 but with infrared characteristics that indicate a distinctly different composition. Samples from two landing sites, Apollo 12 and Luna 16, may contain fragments of a nearby basalt unit compositionally different from the dominant basalt type of the landing area.

INTRODUCTION

LUNAR MARE BASALTS play an important role in understanding the evolution of the crust and mantle, although they account for less than 1% of a 60 km thick lunar crust (Head, 1975). The creation of models of lunar basalt petrogenesis (e.g., Green et al., 1975; Hubbard and Minear, 1975; O'Hara et al., 1975; Walker et al., 1975; Kesson, 1975) requires a detailed characterization of the geochemistry of the basalts as well as a description of the sequence and location of emplacement. Mare basalt samples returned from five different areas have been studied in detail and several general basalt classifications have been proposed (e.g., Taylor, 1975; Rhodes et al., 1975). Remote sensing techniques can then be used to characterize unexplored lunar areas which, of course, is most of the lunar surface. In this paper we present a classification of lunar mare basalt types derived through the analysis of telescopic reflectance spectra of mature mare surface areas.

With the exception of fresh craters and areas of high relief, it is the glassy agglutinate-rich mature soils that are observed by all geochemical remote sensing techniques. Mature mare surfaces contain in excess of 70% agglutinates (e.g., Charette and Adams, 1975). A valid classification of lunar basalt types nevertheless can be derived from reflectance spectra of mature surfaces if the following assumptions are accepted: (1) soils are derived largely from the local dominant surface basalt type, (2) the processes and effects of soil maturation are the same on all maria, and (3) during the 2.5 to 4 b.y. since emplacement, all mare surfaces

---

studied (uppermost 1 cm) have reached an equivalent maturity.

Given the above assumptions and knowing the sensitivity of spectral reflec-
tance to geochemistry (e.g., Adams 1974, 1975; McCord and Adams, 1973), it is
likely that differences in spectral reflectance observed remotely between mare
areas are due to differences in geochemistry of the dominant surface basalt type
of the region. The lunar basalt types discussed in the following sections are
derived from spectra of mature areas: no craters or highland regions are included
in this study. The classification is based on two sets of parameters. The first
concerns the slope of the reflectance spectrum in the blue and ultraviolet which is
directly related to the percent TiO_2 in the surface soil (Charette et al., 1974). The
second set of parameters concerns the near-infrared portion of the spectrum
which is strongly affected by electronic absorptions in mafic minerals and glass.

Data Description

Telescopic spectra of about 400 small (5–20 km diameter) lunar areas have
been obtained using a filter photometer covering a spectral range of .3 to 1.06 μm.
A description of the equipment and observing techniques is given in McCord et al.
1972. Over 100 of these areas are in mature mare regions and are included in the
study presented here. A few spectra obtained prior to 1970 over a comparable
spectral range were also included in this study (McCord and Johnson, 1969;
Johnson and Soderblom, 1969; McCord et al., 1969). Many of these mare areas
were chosen in order to characterize units evident in multi-spectral maps. The
location of these mare areas are indicated by over-sized symbols in the frontis-
piece map. More precise coordinates of these small areas can be obtained from
the authors on request. Not shown on the map are the more than 30 areas in Mare
Humorum discussed previously by Pieters et al. (1975).

Since the spectral reflectance differences between mature soils are small, we
have analyzed the telescopic data in the form of relative reflectance spectra. To
form a relative reflectance spectrum, $\bar{R}(\lambda)$, the spectrum of an area is divided by
the spectrum of a standard mare area, MS-2 (18.7°N, 21.5°E). The result is scaled
to unity at 0.57 μm to eliminate the effects of albedo differences. This procedure
removes most of a steeply sloped continuum (increasing reflectance towards
longer wavelengths) and allows the subtle spectral differences to be analyzed in
detail. Relative reflectance spectra are shown in Fig. 1 for many of the areas
included in this study.

Many mare areas were observed during more than one night as a check for
consistency of the measurements. Two mare areas, one in the east and one in the
west of the lunar frontside, were observed more than 20 times through four
lunations to determine if the phase of the moon during an observation affected the
relative reflectance spectrum sufficiently to cause a misclassification. The results
of these multiple observations indicated that although small phase effects on
differential color do occur (see McCord, 1969), they are fairly well defined and do
not change the general spectral character of a relative reflectance spectrum.
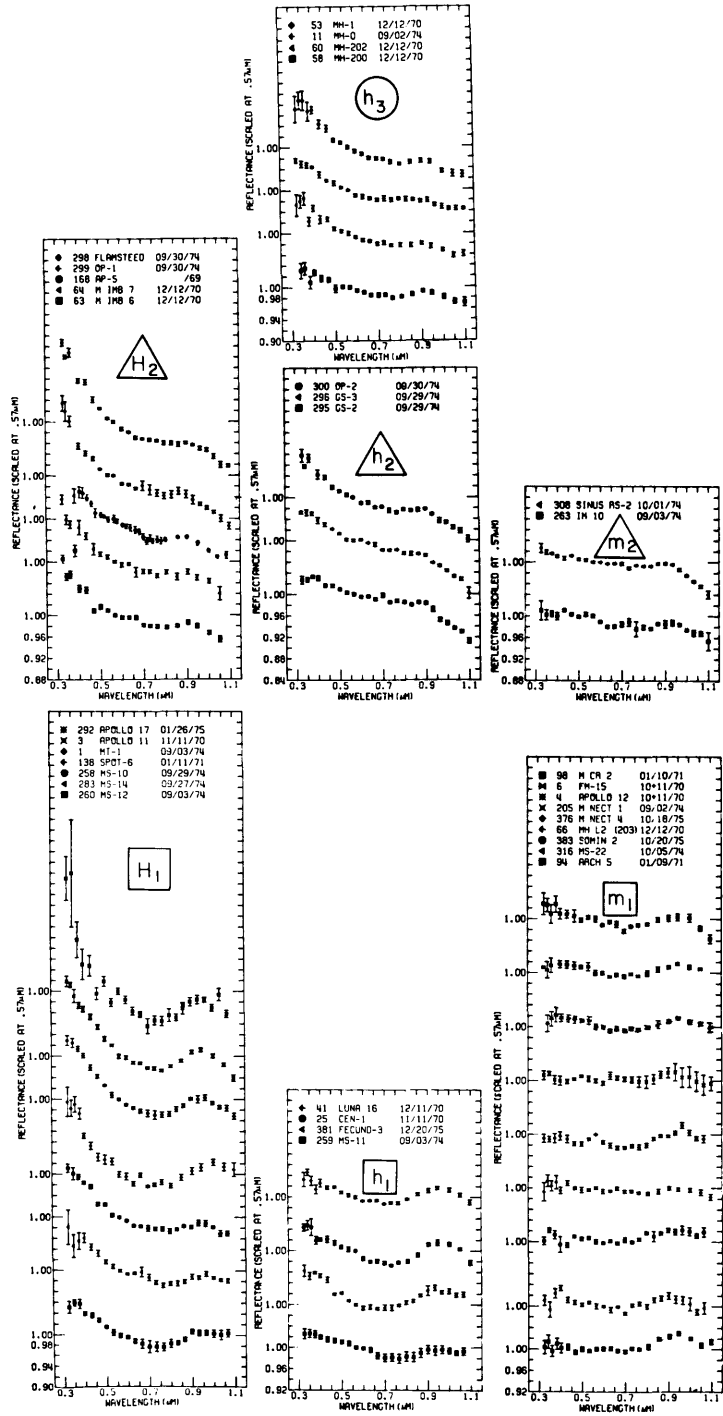
CLASSIFICATION OF REFLECTANCE SPECTRA

The major spectral types evident in most lunar reflectance spectra have been described by McCord *et al.* (1972). It was noted that in mare spectra the continuum slope in the blue below .57 μm varied considerably ($\pm$ 8–10%). In the near-infrared beyond .8 μm small variations were noted but no apparent pattern was evident. Much progress has been made during the last few years in understanding the reasons for these spectral differences and the accumulation of new telescopic spectra has allowed more refined classification of the spectra.

A. *TiO$_2$ content*

The variations in the ultraviolet of continuum slope for mare regions were suspected of being caused at least partly by charge transfer absorptions involving titanium (e.g., $Fe^{+2} \rightarrow Ti^{+4}$, $Ti^{+3} \rightarrow Ti^{+4}$). The assignment of these bands is being derived using transmission spectra, crystal field theory, and molecular orbital theory (e.g., Loeffler *et al.*, 1975; Burns *et al.*, 1976). The systematics of the absorptions in glasses have been studied as a function of titanium and iron content and oxygen fugacity (Mao and Bell, 1973; Bell and Mao, 1976). Due to the intense nature of these absorptions their effect on diffuse reflectance measurements are only partially understood. The accumulation of dark iron and titanium-rich glassy agglutinates in mature mare soils not only darkens the soils (Adams and McCord, 1973), but also severely lowers the spectral contrast observed (Adams and McCord, 1971). The latter effect causes a steeply sloped lunar reflectance spectrum to flatten (or appear "bluer").

In the laboratory, the continuum slope of returned soil spectra was studied systematically and the relation between TiO$_2$ content and continuum slope was empirically defined (Charette *et al.*, 1974). The critical dependence of this relationship on maturity was also defined in the laboratory. We have converted this TiO$_2$—continuum slope relationship to allow the percent TiO$_2$ of a soil to be determined from the slope of a telescopic relative reflectance spectrum for a mature mare area (Fig. 2). The function plotted in Fig. 2 is: $\%TiO_2 = ae^{b\bar{R}}$, where $a = 8.12 \times 10^{-7}$ and $b = 14.88$. The range of continuum slope values for a given landing site arises from observational error. These include not only measurement errors but also the small systematic variations in spectral contrast due to differences in phase angle. The range of TiO$_2$ content for a given landing site material is the range of measured values for returned soils that are approximately representative of the region (Heiken, 1974; Vinogradov, 1971). The most likely value estimated for each parameter is shown by a solid line in Fig. 2. The accuracy of the TiO$_2$ relationship to continuum slope is about 1% in TiO$_2$ content and is primarily a function of the accuracy of the telescopic data. The accuracy associated with distinguishing the TiO$_2$ content of one area relative to another is closer to $\frac{1}{2}\%$.

The reflectance spectrum continuum slope relative to MS-2 was determined for all mare regions observed telescopically and the soil TiO$_2$ content estimated

h₃

	53	MH-1	12/12/70
	11	MH-0	09/02/74
	60	MH-202	12/12/70
	58	MH-200	12/12/70

H₂

	298	FLAMSTEED	09/30/74
	299	OP-1	09/30/74
	168	AP-5	/69
	64	M IMB 7	12/12/70
	63	M IMB 6	12/12/70

h₂

	300	OP-2	09/30/74
	296	GS-3	09/29/74
	295	GS-2	09/29/74

m₂

| | 308 | SINUS RS-2 | 10/01/74 |
| | 263 | IM 10 | 09/03/74 |

H₁

	292	APOLLO 17	01/26/75
	3	APOLLO 11	11/11/70
	1	M1-1	03/03/74
	138	SPOT-6	01/11/71
	258	MS-10	09/29/74
	283	MS-14	09/27/74
	260	MS-12	09/03/74

h₁

	41	LUNA 16	12/11/70
	25	CEN-1	11/11/70
	381	FECUND-3	12/20/75
	259	MS-11	09/03/74

m₁

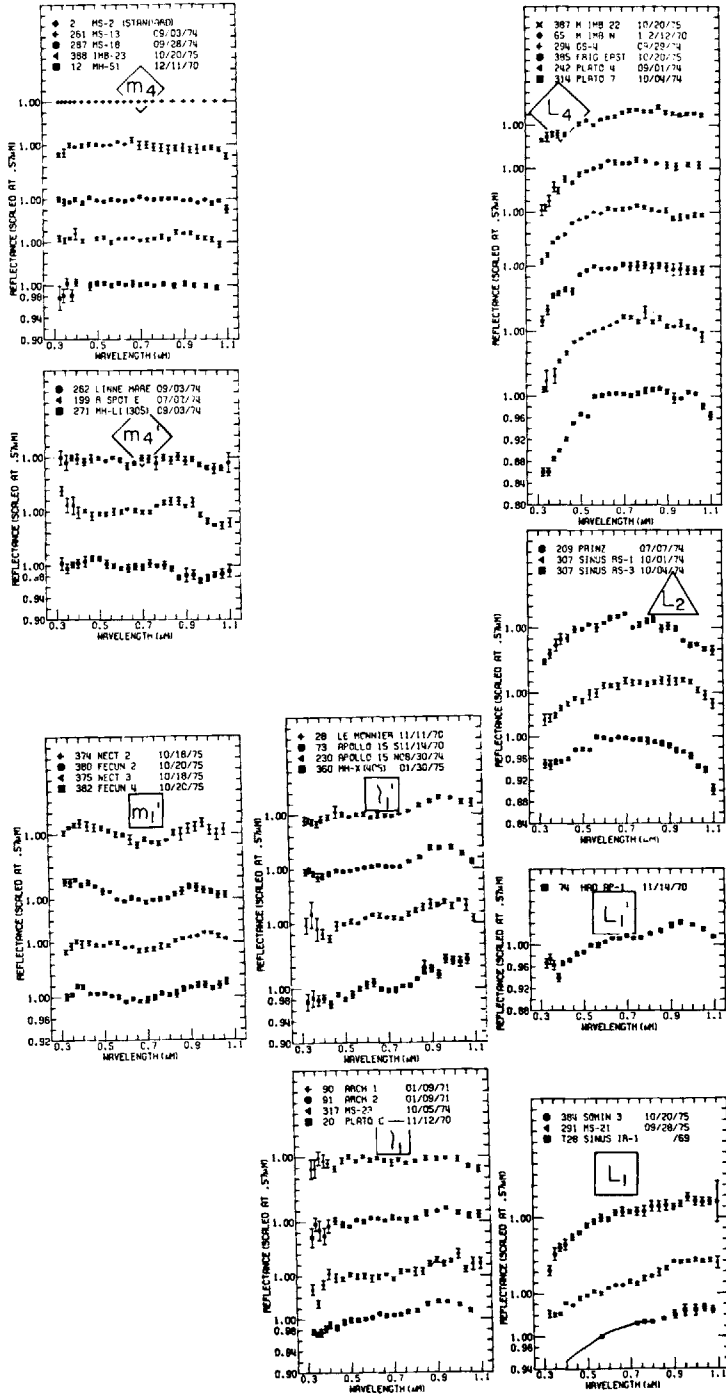| | 98 | M CR 2 | 01/10/71 |
	6	FM-15	10·11/70
	4	APOLLO 12	10·11/70
	205	M NECT 1	09/02/74
	378	M NECT 4	10·18/75
	66	MM L2 (203)	12/12/70
	383	SOMIN 2	10/20/75
	316	MS-22	10/05/74
	94	ARCH 5	01/09/71

Fig. 1. Relative reflectance spectra of mature mare regions. All spectra are relative to MS-2. The spectra have been characterized and grouped according to the parameters listed in Table 1.
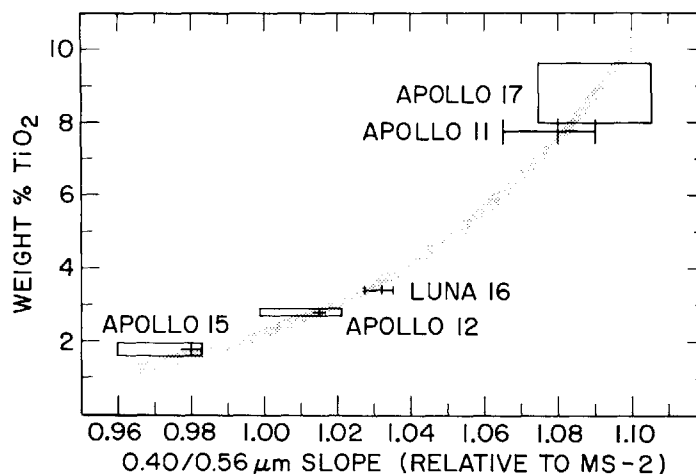
Fig. 2. Relationship between the wt.% TiO₂ in lunar soil and slope of the reflectance spectrum (after Charette *et al.*, 1974). The data for percent TiO_2 are measured values for returned soils (Heiken, 1974; Vinogradov, 1971). The data for reflectance spectrum slope between .40 and .57 m are the values derived from telescopic spectra of the landing sites.

from the relationship shown in Fig. 2. The relationship between TiO_2 content and curve slope is less precise for low-Ti soils partly because of the nature of the function in Fig. 2 and partly because other spectral effects currently under study may be important for redder soils. The areas were divided into five groups according to increasing TiO_2 content using the spectral parameters listed in Table 1a. Examples of relative reflectance spectra for many areas in each group are shown in Fig. 1. The symbols on the frontispiece map marking the areas studied are color coded according to TiO_2 content. There seems to be a continuous range of TiO_2 content for the areas observed. This is contrary to that measured for the returned samples which show a gap between high- and low-Ti basalts. This difference is probably due to limited sampling.

B. *Infrared features*

Well-defined absorption bands occur in near infrared spectra of rocks and minerals and are diagnostic of the type of mafic minerals present. These absorptions arise from d-orbital electronic transitions in transition metal ions (Fe, Ti, Cr, etc.) in a crystal environment (e.g., Burns, 1970). Iron-rich glasses also have diagnostic infrared absorption bands (Mao and Bell, 1973; Bell and Mao, 1976). Reflection spectra of lunar rocks contain characteristic near-infrared absorptions due to the various types of pyroxene and olivine present (e.g., Adams 1974, 1975).

The lunar soils, however, are a combination of mineral fragments, glass, and agglutinates. A mature soil contains in excess of 70% agglutinates, the mineralogy of which is poorly known. The agglutinates can be described as glass-welded

Table 1. Spectral parameters used for distinguishing mare basalt types.

1a	$\bar{R}_{40/.56}$	% TiO$_2$ (soil)	Class	Map color
	< .98	(< 1.5)	L-low	Red
	.98–1.00	1.5–2.0	l-med. low	Orange
	1.00–1.025	2–3	m-medium	Yellow
	1.025–1.06	3–5.5	h-med. high	Green
	> 1.05	> 5	H-high	Blue

1b	Type	Map symbol	Description of relative reflectance infrared feature
	1	□	Bump concave downward (symmetric around .95 μm)
	1'	⊡	Same as 1 plus a slope change at .35–.40 μm
	2	△	Linear decrease in reflectance beyond .90 μm
	3	○	Small bump near .90 μm with a constant or increased reflectance beyond 1.0 μm
	4	◇	Featureless (same as MS-2)
	4'	◇	Small to large dip concave upward
	U	☆	Unclassified or unclear

aggregates of mineral fragments and devitrified soil material. Finely dispersed grains of Fe° are also found in agglutinates (e.g., Agrell *et al.*, 1970). The strong absorption bands evident in spectra of fresh basalt are no longer present in the spectrum of mature soils. The weak features observed in soil spectra in the near infrared are a subdued combination of a dominant glass band (Fe^{+2}) and bands arising from the few remaining pyroxene and olivine mineral fragments (Charette and Adams, 1976; Charette *et al.*, 1976). Although differences which are known to have geochemical significance occur in the infrared spectra of mare surfaces, quantitative interpretations of these variations are difficult without further investigations. An important step toward such a refined interpretation of soil spectra is the recognition of infrared spectral features that are associated with regional basalts.

A sufficient number of mare spectra exist now to identify systematics that occur in the near-infrared spectra for many areas. A classification scheme for mare spectra was derived using the infrared spectral parameters listed in Table 1b. With additional data this classification probably could be subdivided. The location of these areas is indicated on the frontispiece map; each type is indicated with a different shape of symbol. Examples of the relative reflectance for many areas in each type is shown in Fig. 1.

DISCUSSION

This first characterization of global mare basalt surfaces according to their spectral features reveals some otherwise unobtainable geochemical information

for areas beyond the landing sites. Some interesting results immediately evident are discussed below.

A. *Western high-Ti regions*

Regions of basalt with a TiO_2 content comparable to that at Apollo 11 and 17 occur in the western portion of the moon. However, the infrared classification of the spectra indicates that the western high-Ti basalts (H_2) are compositionally distinct from those in the east (H_1): the 1 μm (Fe^{+2}) absorption is stronger for the western basalts (Fig. 3). A quantitative interpretation of this distinction is being derived through laboratory studies on lunar soils (Charette and Adams, 1976). Furthermore, the areal extent of the younger (Boyce, 1975) western high-Ti basalts seems to be much less than that of the eastern basalts. The Flamsteed Region is the type-area for these distinct western high-Ti basalts. A few of the Imbrium basalts may have the same high-TiO_2 content, but the vast majority of extensive Imbrium and Procellarum "blue" basalts related to those at Flamsteed are apparently only medium high in titanium content. Global spectral imagery, such as the frontispiece by Soderblom and Boyce (1976), graphically displays this small areal extent of the high-Ti (as opposed to moderately high-Ti) western basalts.

B. *Unsampled basalt types*

The spectra of all mare landing sites are classified as type 1 (see Fig. 1 and frontispiece map). It is thus unlikely that any significant amount of samples has been returned from basalt types 2, 3, and 4. Of these unsampled basalts, there are at least three specific types that cover a large lunar surface area and occur in several locations: (1) the Flamsteed/Imbrium high- to medium-high Ti basalts (H_2, h_2, m_2); (2) the Humorum/S. Procellarum medium-high Ti basalts (h_3) (Pieters *et al.*, 1975); and (3) the low-Ti basalts (very red) of Frigoris and Imbrium (L_4).

C. *Minor components in returned samples*

Since impact processes cause a redistribution of surface material, it may be possible that some of the minor components of returned samples are from unsampled regions. The major "contaminant" at Apollo 15 and 17 is the material from the surrounding highland. The Apollo 11 site is also slightly contaminated by highland material, but spectral images (e.g., Soderblom, 1970; Johnson *et al.*, 1975) indicate that within a radius of 100 km there are no other major mare units. However, there are distinctly different basaltic units within 100 km of the Apollo 12 and Luna 16 landing sites.

For the Apollo 12 landing area it was shown using crater degradation studies (Soderblom and Lebofsky, 1972) that there exist two neighboring units of differing age; the landing site is located in the older unit. Spectral data support this distinction and characterize the younger unit (a few kilometers from the landing
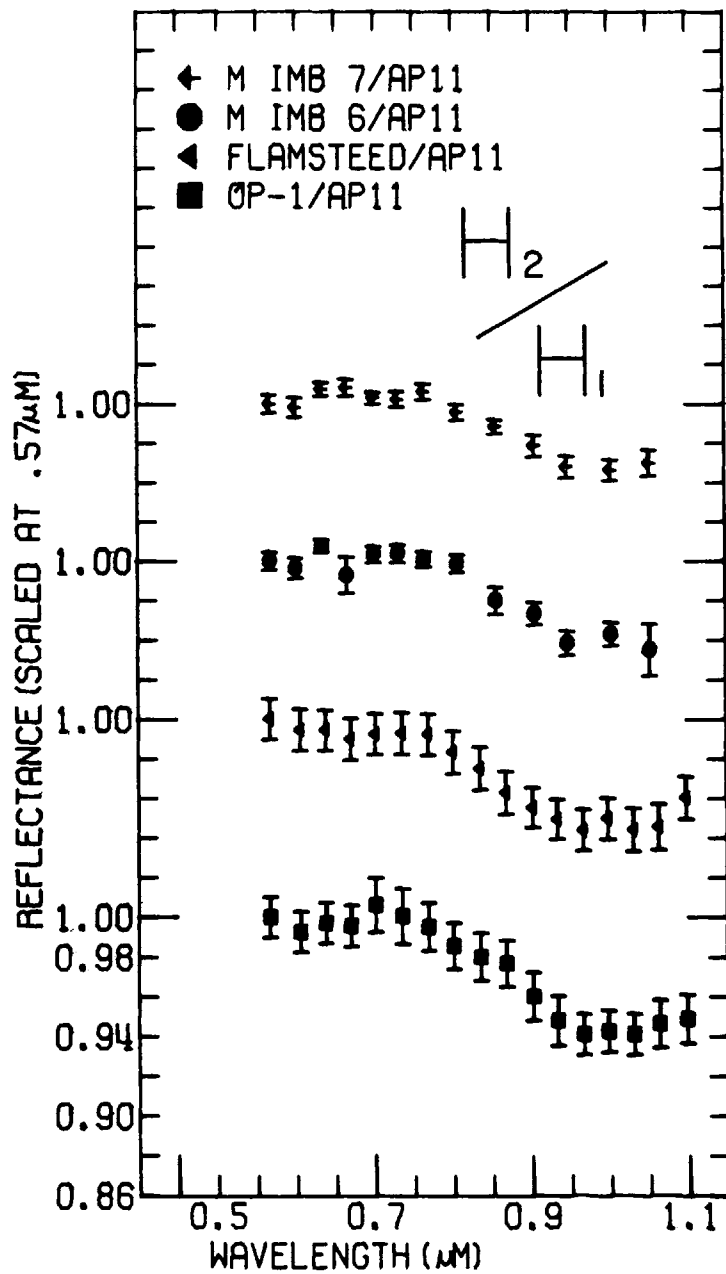
247

Characterization of lunar mare basalt types   2685

Fig. 3. Reflectance spectra of type H_2 basalts relative to Apollo 11 (H_1). Since the slope of the continuum is approximately the same for spectra of these two basalt types, their relative reflectance spectra are featureless below about .7 μm. The difference in the 1 μm absorption feature between spectra of H_2 and H_1 basalt types is clearly evident in these relative reflectance spectra.
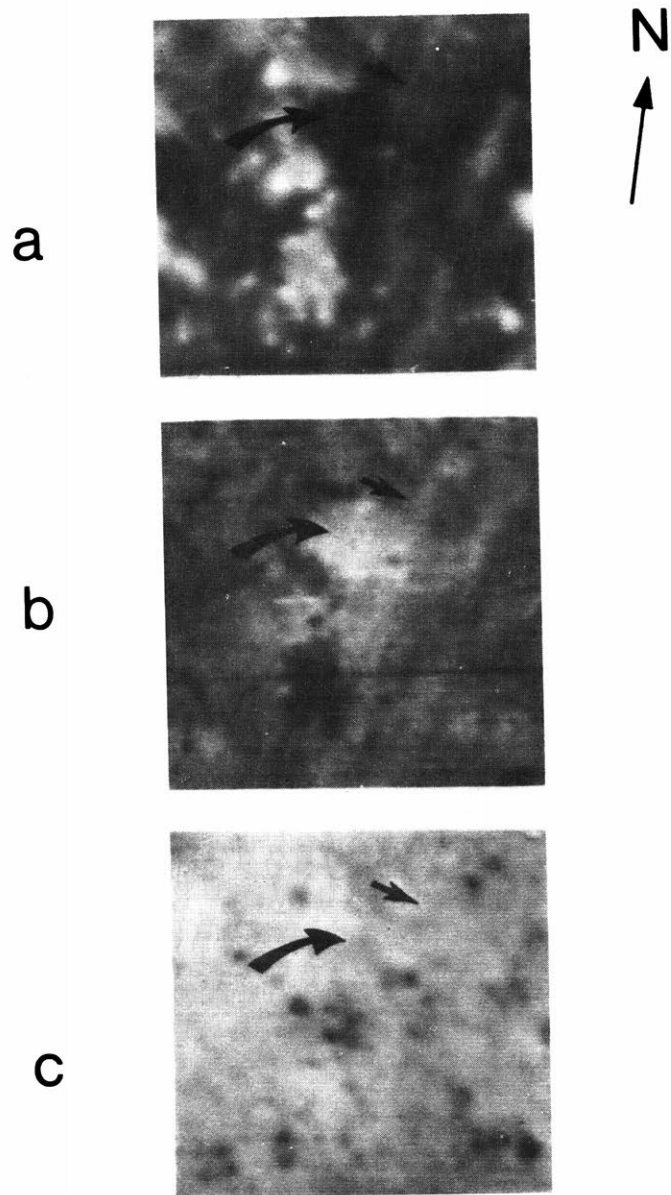
C. Pieters and T. B. McCord

Fig. 4. Vidicon spectral images of the Apollo 12 landing area. The landing site is indicated with a short arrow. Area S III B is indicated with a long arrow. Field of view is about 150 km. Images were obtained digitally for the same area through a sequence of filters with a silicon vidicon detector and processed using standard image processing techniques (McCord *et al.*, 1976). (a) Image taken through a .57 μm filter. (b) Ratio image: .40/.57 μm contrast enhanced. (c) Ratio image: .97/.57 μm contrast enhanced.

+ 167 AP 4
● 11 MHO
◀ 389 S 111 B
■ 4   APOLLO 12

REFLECTANCE (SCALED AT .57μM)

1.00

1.00

1.00

1.00

0.96

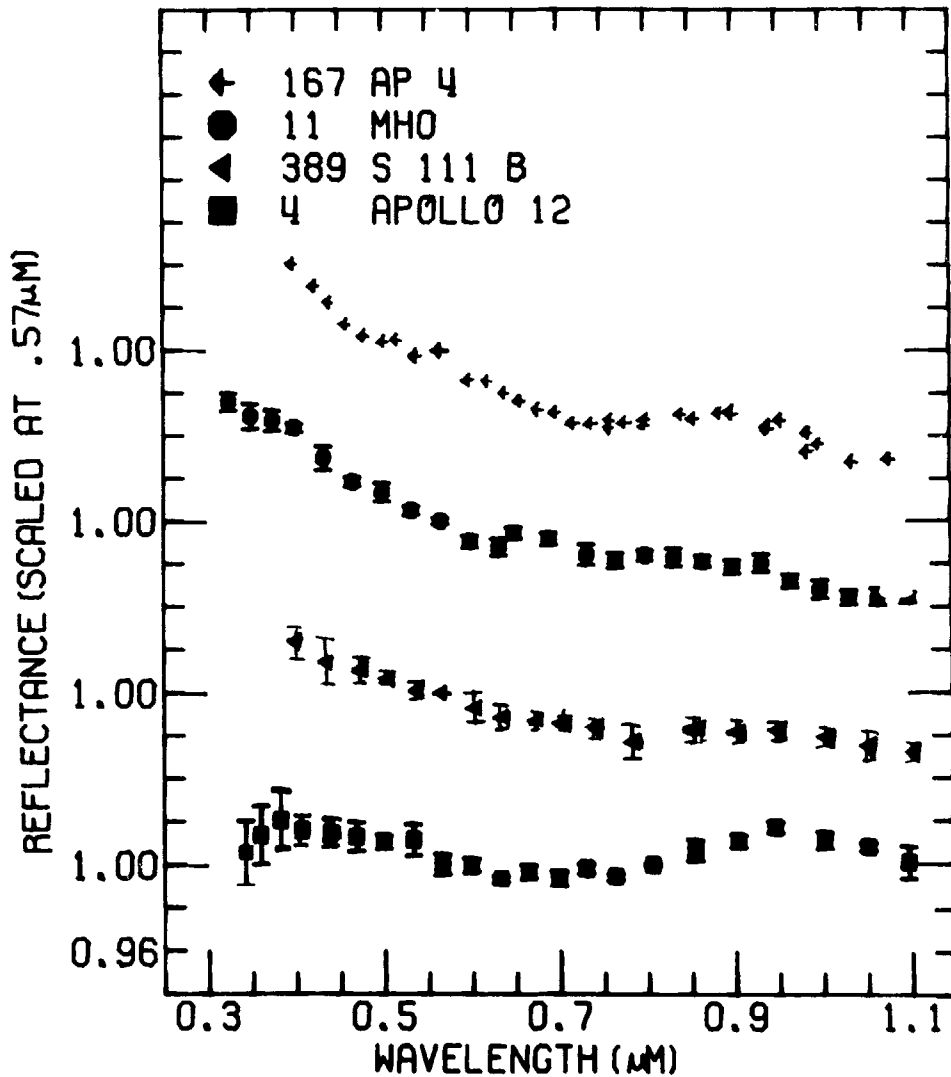0.3   0.5   0.7   0.9   1.1

WAVELENGTH (μM)

Fig. 5. Reflectance spectra relative to MS-2 for mare areas in the Apollo 12 region (Apollo 12 and S III B), in Mare Humorum (MHO), and in southern Procellarum (AP 4).

site) as a basalt with a slightly higher TiO_2 content. Figure 4 contains high resolution spectral vidicon images (McCord et al., 1976) of the Apollo 12 region; the field of view is about 150 km. The .40/.57 μm ratio image allows the mare soil TiO_2 content to be mapped. Note the small tongue of higher titanium material (brighter) a few kilometers to the east of the landing site. This corresponds closely to the unit independently mapped by Soderblom and Lebofsky (1972). Although no spectra exist for this small unit, a spectrum exists for the area marked S III B (Johnson and Soderblom, 1969) which seems to be an extension of the material

C. PIETERS and T. B. McCORD

near Apollo 12. The relative reflectance spectrum for area S III B is shown in Fig. 5 along with spectra of the Apollo 12 landing site and two examples of basalt type h_3. We have tentatively assigned the area S III B to the basalt type h_3. If future spectra confirm this classification, then some of the Apollo 12 ilmenite basalts (e.g., Rhodes *et al.*, 1975) may be derived from this nearby unit and thus may well be samples of a major "unsampled" basaltic unit.

Spectral images of Mare Fecunditatis indicate that the Luna 16 landing site is in a rather small unit (approximately 150 km in diameter) surrounded by basalts with a lower TiO_2 content. The Luna 16 unit can be seen as a bluish area on the frontispiece spectral map by Soderblom and Boyce (1976) and as a distinct area on the color difference map by Barbarshov (1973). Unpublished higher spatial resolution spectral images of the region by McCord and by Whitaker further substantiate the distinction between two basalt types in close proximity in the Luna 16 region. Although there is a difference in TiO_2 content between these two units, the spectra are both classified as type 1 (Fig. 1, Frontispiece map). The boundaries seen in the multispectral images match closely those seen in the independently derived age unit maps of Boyce (1976); Luna 16 is located in the older of the two units.

CONCLUSION

For the near future remote sensing techniques are the only means to determine the geochemistry of unsampled lunar regions. The data presented here have been used to show that a variety of basalt types exist on the frontside of the moon. Many basalt types covering a major portion of the maria have not been sampled. The spectral reflectance measurements of surface soil presented here have allowed the % TiO_2 to be discerned for the major basalt types. It may also soon be possible to estimate the FeO content from such soil spectra (Charette and Adams, 1976). Spectra of fresh mare craters will further define the geochemistry of the unsampled basalts by allowing components of the mineralogy to be identified (e.g., composition of pyroxene and olivine). It is, however, not until data from orbital geochemical experiments are available that remote sensing techniques will be fully utilized in lunar exploration.

REFERENCES

Adams J. B. (1974) Visible and near-infrared diffuse reflectance spectra of pyroxenes as applied to remote sensing of solid objects in the solar system. *J. Geophys. Res.* **79**, 4329–4335.

Adams J. B. (1975) Uniqueness of visible and near-infrared diffuse reflectance spectra of pyroxenes and other rock-forming minerals. In *Infrared and Raman Spectroscopy of Lunar and Terrestrial Minerals* (C. Karr, Jr., ed.), p. 91. Academic Press, New York.

Adams J. B. and McCord T. B. (1971) Optical properties of mineral separates, glass and anorthositic fragments from Apollo mare samples. *Proc. Lunar Sci. Conf. 2nd*, p. 2183–2195.

Adams J. B. and McCord T. B. (1973) Vitrification darkening in the lunar highlands and identification of Descartes material at the Apollo 16 site. *Proc. Lunar Sci. Conf. 4th*, p. 163–177.

Agrell S. O., Scoon J. G., Muir I. D., Long J. V. P., McConnell J. D. C., and Peckett A. (1970) Observations on the chemistry, mineralogy and petrology of some Apollo 11 lunar samples. *Proc. Apollo 11 Lunar Sci. Conf.*, p. 93–128.

Barbarshov N. P. (1973) Photometric map of the visible side of the Moon. Academy of Sciences of the Ukrainian SSR, Kiev.

Bell P. M. and Mao H. K. (1976) Oxygen fugacity in the lunar regolith: A systemic study of the relationship between composition, oxygen fugacity and optical spectra of lunar and synthetic glasses (abstract). In *Lunar Science VII*, p. 44–45. The Lunar Science Institute, Houston.

Boyce J. M. (1975) Chronology of the major flow units in the western nearside maria. In *Papers presented to the Conference on Origins of Mare Basalts and Their Implications for Lunar Evolution*, p. 11–14. The Lunar Science Institute, Houston.

Boyce J. M. (1976) Relative ages of flow units in the lunar nearside maria (abstract). In *Lunar Science VII*, p. 85–87. The Lunar Science Institute, Houston.

Burns R. G. (1970) *Mineralogical Applications of Crystal Field Theory*, p. 224. Cambridge Univ. Press, Cambridge.

Burns R. G., Loeffler B. M., Parkin K. M., Abu-Eid R. M., and Leung I. S. (1976) Visible-region spectra of the moon: Progress towards characterizing the cations in Fe–Ti bearing minerals (abstract). In *Lunar Science VII*, p. 108–110. The Lunar Science Institute, Houston.

Charette M. P. and Adams J. B. (1975) Agglutinate as indicators of lunar soil maturity: The rare gas evidence at Apollo 16. *Proc. Lunar Sci. Conf. 6th*, p. 2281–2289.

Charette M. P. and Adams J. B. (1976) Determination of the iron content of lunar soils using remote spectral reflectance measurements. Submitted to *J. Geophys. Res.*

Charette M. P., Adams J. B., Soderblom L. A., Gaffey M. J., and McCord T. B. (1976) Age-color relationships in the lunar highlands (abstract). In *Lunar Science VII*, p. 132–134. The Lunar Science Institute, Houston.

Charette M. P., McCord T. B., Pieters C., and Adams J. B. (1974) Application of remote spectral reflectance measurements to lunar geology classification and determination of titanium content of lunar soils. *J. Geophys. Res.* **79**, 1605–1613.

Green D. H., Ringwood A. E., Hibberson W. O., and Ware N. G. (1975) Experimental petrology of Apollo 17 mare basalts. *Proc. Lunar Sci. Conf. 6th*, p. 871–893.

Head J. W. (1975) Lunar mare deposits: Areas, volumes, sequence, and application for melting in source areas. In *Papers presented to the Conference on Origins of Mare Basalts and Their Implications for Lunar Evolution*, p. 66–71. The Lunar Science Institute, Houston.

Heiken G. (Compiler) (1974) *A Catalog of Lunar Soils*. NASA-JSC, U.S. Gov. Printing Office. 221 pp.

Hubbard N. J. and Minear J. W. (1975) A physical and chemical model of early lunar history. *Proc. Lunar Sci. Conf. 6th*, p. 1057–1085.

Johnson T. V. and Soderblom L. A. (1969) Relative reflectivity (0.4 μ to 1.1 μ) of the lunar landing site Apollo 7. *J. Geophys. Res.* **74**, 6046–6048.

Johnson T. V., Matson D. L., Phillips R. J., and Saunders R. S. (1975) Vidicon spectral images: A geophysical study of the Lamont feature (abstract). In *Lunar Science VI*, p. 444. The Lunar Science Institute, Houston.

Kesson S. E. (1975) Mare basalts: Melting experiments and petrogenetic interpretations. *Proc. Lunar Sci. Conf. 6th*, p. 921–944.

Loeffler B. M., Burns R. G., and Tossell R. G. (1975) Metal → metal charge transitions: Interpretation of visible-region spectra of the moon and lunar materials. *Proc. Lunar Sci. Conf. 6th*, p. 2663–2676.

Mao H. K. and Bell P. M. (1973) A study of charge-transfer and crystal-field spectra of iron and titanium in synthetic "basalt" glass as a function of PO_2. Carnegie Inst. Ann. Report Dir. Geophys. Lab. 1972–1973, p. 629–631.

McCord T. B. (1969) Time dependence of lunar differential color. *Astronom. J.* **74**, 273–278.

McCord T. B. and Johnson T. V. (1969) Relative spectral reflectivity 0.4–1 μ of selected areas of the lunar surface. *J. Geophys. Res.* **74**, 4395–4401.

McCord T. B. and Adams J. B. (1973) Progress in remote optical analysis of lunar surface composition. *The Moon* **7**, 453–474.

McCord T. B., Johnson T. V., and Kieffer H. H. (1969) Differences between proposed Apollo sites. 2. Visible and infrared reflectivity evidence. *J. Geophys. Res.* **74**, 4385–4388.

McCord T. B., Charette M., Johnson T. V., Lebofsky L. A., Pieters C., and Adams J. B. (1972) Lunar spectral types. *J. Geophys. Res.* **77**, 1349–1359.

McCord T. B., Pieters C., and Feierberg M. A. (1976) Multispectral mapping of the lunar surface using groundbased telescopes. *Icarus.* In press.

O'Hara M. J., Humphries D. J., and Waterson S. (1975) Petrogenesis of mare basalts: Implications for chemical, mineralogical, and thermal models for the moon. *Proc. Lunar Sci. Conf. 6th*, p. 1043–1055.

Pieters C., Head J. W., McCord T. B., Adams J. B., and Zisk S. (1975) Geochemical and geological units of Mare Humorum: Definition using remote sensing and lunar sample information. *Proc. Lunar Sci. Conf. 6th*, p. 2689–2710.

Rhodes J. M., Hodges F. N. and Papike J. J. (1975) Mare basalts: Major element composition and classification. In *Papers presented to the Conference on Origins of Mare Basalts and Their Implications for Lunar Evolution*, p. 135–139. The Lunar Science Institute, Houston.

Soderblom L. A. (1970) "The Distribution and Ages of Regional Lithologies in the Lunar Maria." Ph.D. dissertation, California Inst. of Tech., Pasadena.

Soderblom L. A. and Lebofsky L. A. (1972) Technique for rapid determination of relative ages of lunar areas from orbital photography. *J. Geophys. Res.* **77**, 279–296.

Soderblom L. A. and Boyce J. M. (1976) Distribution and evolution of global color differences on the moon (abstract). In *Lunar Science VII*, p. 822–824. The Lunar Science Institute, Houston.

Taylor S. R. (1975) *Lunar Science: A Post-Apollo View*, p. 372. Pergamon Press, Elmsford, New York.

Vinogradov A. P. (1971) Preliminary data on lunar ground brought to earth by automatic probe "Luna-16." *Proc. Lunar Sci. Conf. 2nd*, p. 1–16.

Walker D., Longhi J., Stolper E. M., Grove T. L., and Hays J. F. (1975) Origin of titaniferous lunar basalts. *Geochim. Cosmochim. Acta* **39**, 1219–1235.

III.
    E. Applications
        1. Luna 24

REGIONAL BASALT TYPES IN THE LUNA 24 LANDING AREA
AS DERIVED FROM REMOTE OBSERVATIONS

Carle Pieters and Thomas B. McCord*

Remote Sensing Laboratory, Department of Earth and Planetary Science,
M.I.T., 37-487, Cambridge, Mass. 01239

John B. Adams

Dept. of Geological Science, University of Washington
Seattle, Washington 98195

*Currently on leave of absence at the Institute for Astronomy,
University of Hawaii at Manoa, Honolulu, Hawaii

Abstract. The Soviet spacecraft Luna 24 landed in Mare Crisium and returned samples that are expected to be much like the low titanium basalts from Luna 16 and Apollo 12. This conclusion is based on earth-based spectral reflectance measurements and multispectral imagery of the Mare Crisium region and uses a background of laboratory measurements of the spectral properties of Lunar soils. These data are used to describe the regional context and composition of the Crisium basaltic units. The returned sample may also contain minor components of a high-titanium basalt and a very low titanium basalt as well as highland material.

A classification and characterization of surface mare basalt types has been derived from the remote observations of the spectral reflectance of mature mare soils (Pieters and McCord, 1976; Adams and Pieters, 1976). Multispectral ratio images allow the areal distribution of mare units to then be mapped (McCord et. al., 1976a). Using our experience with the spectral properties of lunar soils derived in the laboratory, we have examined both kinds of remotely obtained spectral information for the region containing the Luna 24 landing site. We describe here the basalt types most likely to have been sampled and place the samples in a regional context.

The Soviet Luna 24 spacecraft landed in Mare Crisium (12° 45' N, 62° 12' E) and returned a 2m core sample to earth (Aviation Week, Aug. 18, 1976, p. 18).

Figure 1 is a sketch map of the region showing the location of the landing site. The geology of the region has been described by Olson and Wilhelms (1974) as extensive dark plains material (basaltic). About 10 km from the landing site is a small region mapped by Olson and Wilhelms as dark mantling material primarily on the basis of its lower albedo. The land-

ing site is indicated in the vidicon image mosaics (McCord et. al., 1976b) of Figure 2 by a small arrow. A relative reflectance spectrum (.3 to 1.1μm) for the region M Cr-2, indicated with a large arrow, was included in the mare basalt classification scheme and is shown in Figure 3 (from Pieters and McCord, 1976). Useful spectra for three additional areas in Mare Crisium were obtained previously (McCord, 1968) over a more limited spectral range (.4 to .8μm).

The .40/.56μm spectral reflectance ratio has been shown to be sensitive to the TiO_2 content of mature mare soils and an estimation of the TiO_2 content for the region M Cr-2 was made (Charette et. al., 1974). This relationship between .40/ .56μm reflectance ratio and soil TiO_2 con-
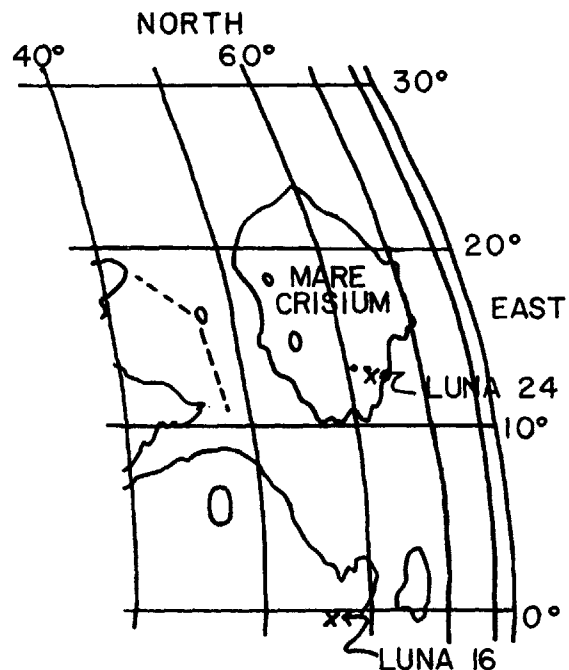

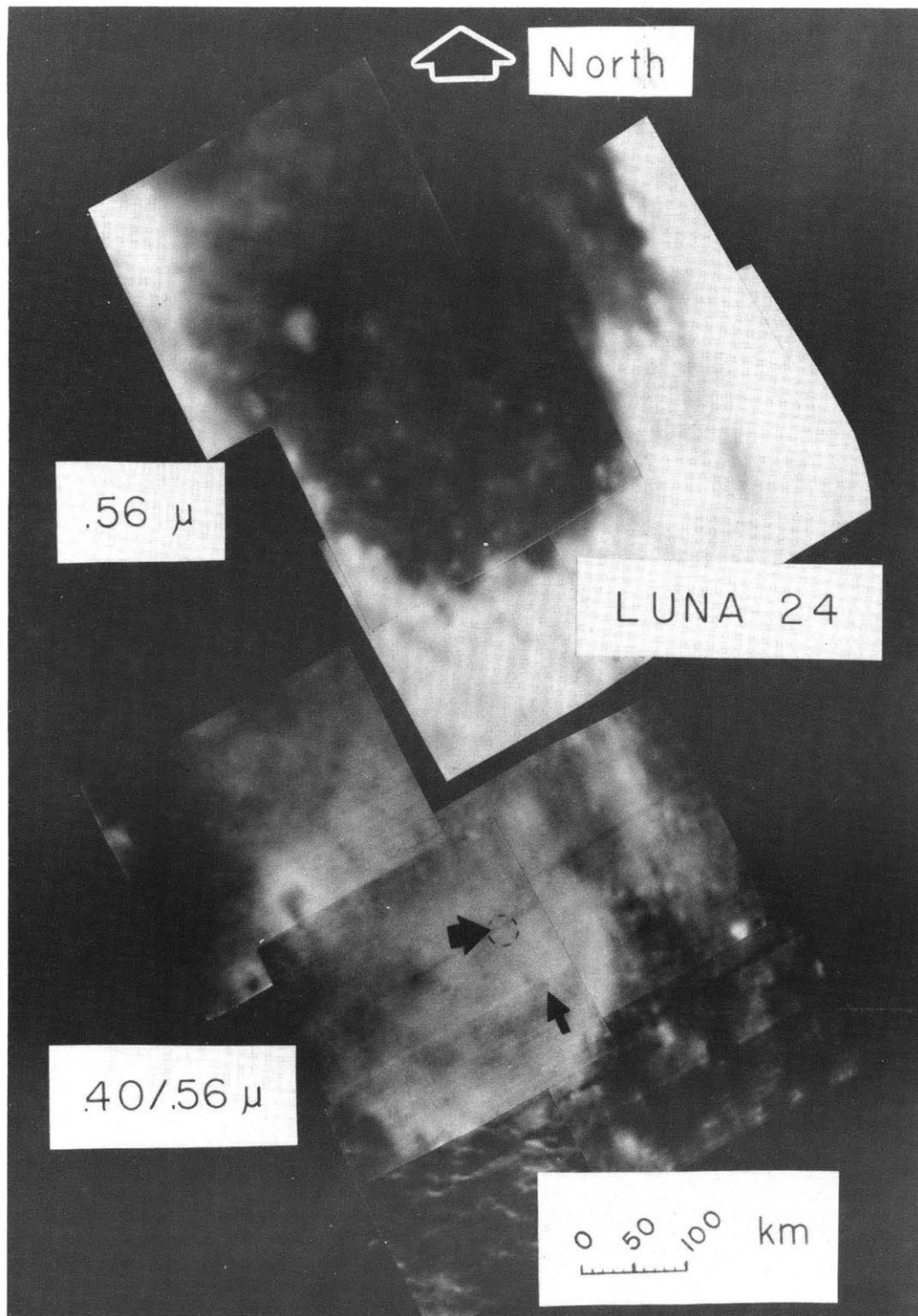Figure 1. Sketch map of the eastern limb of the moon showing the location of the Soviet Luna 24 landing site.

Figure 2. Vidicon image mosaics of southern Mare Crisium. TOP: .56μm
image slightly contrast enhanced to bring out features in the mare.
The Luna 24 landing site is indicated by a small arrow. The large
arrow indicates the region for which a spectrum was obtained (M Cr-2).
BOTTOM: .40/.56μm ratio image contrast enhanced with the grey tone
variation dark to light indicating a 12% difference in the .40/.56μm
ratio.

tent is shown in Figure 4 for mature mare soils. Figure 2-bottom is a contrast enhanced .40/.56μm ratio image mosaic of the landing site region with the grey tone variation dark to bright spanning a 12%

difference in the .40/.56μm ratio.
     From these data the following conclusions can be drawn:
     1) A major unit filling central Mare Crisium is composed of low-titanium ba-
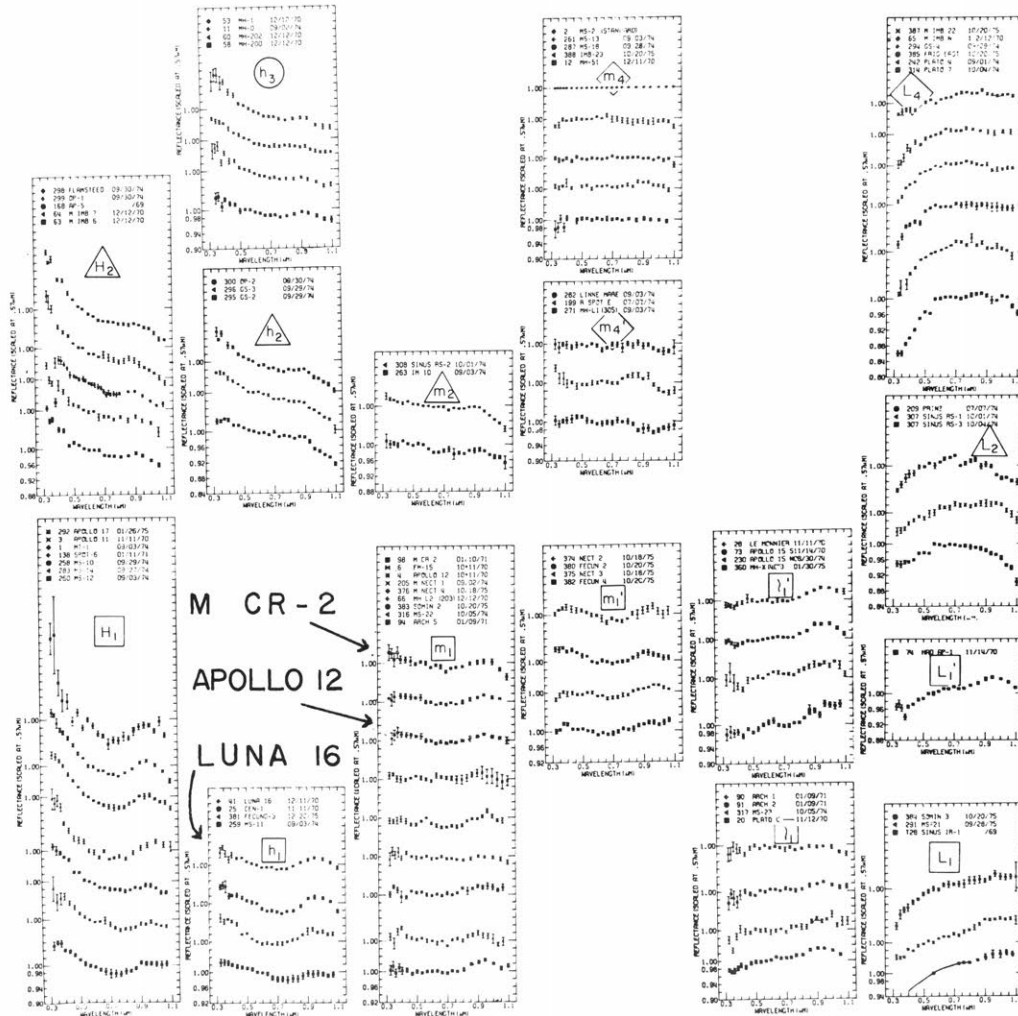
Figure 3. Relative reflectance spectra of mature mare regions. All spectra are relative to the standard area MS-2. These spectra are composed of reflectance ratios for 25 filters between .33 and 1.1μm scaled to unity at .56μm. The intervals marked along the vertical axis are .02 in reflectance ratio. The horizontal intervals are 500Å (or .05μm). The spectra have been characterized and grouped according to TiO_2 content and the nature of infrared spectral features. The spectra indicate the Mare Crisium low-titanium basalt is comparable to that at Luna 16 and to a lesser extent to that at Apollo 12.

salts much like those found by Luna 16 and to a lesser extent by Apollo 12. This conclusion is made from noting the shape of the spectrum for M Cr-2 (Figure 3) and comparing it to spectra of other basalt types observed. The vidicon ratio image mosaic (Figure 2) indicates regional continuity between the telescopic site M Cr-2 and the Luna 24 landing site.

2) The Luna 24 landing site itself is in a inhomogeneous area. The returned core could have sampled either or both of two low titanium basalt units which differ in (soil) TiO_2 content by about 2%. From the vidicon spectral ratio data of Figure 2-bottom and the TiO_2 relationship of Figure 4, the weight % TiO_2 expected for these Mare Crisium soils is 2-4%.

3) The Eratosthenian crater Picard,

200 km to the west of the Luna 24 site, has apparently excavated higher titanium material (Figure 2), assuming the ejecta soil surrounding the crater has matured to the same extent as the background mare. If the stratigraphy evident at Picard extends to the Luna 24 region, it is likely that the low-titanium surface basalt at Luna 24 is underlain by high titanium material.

4) 100 km to the north of the landing site there exists a low titanium (<1.5%) basalt unit that is distinct from that at the Luna 24 landing site. The spectral boundaries for this unit (upper left in Figure 2-bottom) do not correspond to albedo variations (Figure 2-top). From the vidicon spectral ratio data of Figure 2 and the TiO_2 relationship of Figure 4, this low-titanium basalt is shown to be
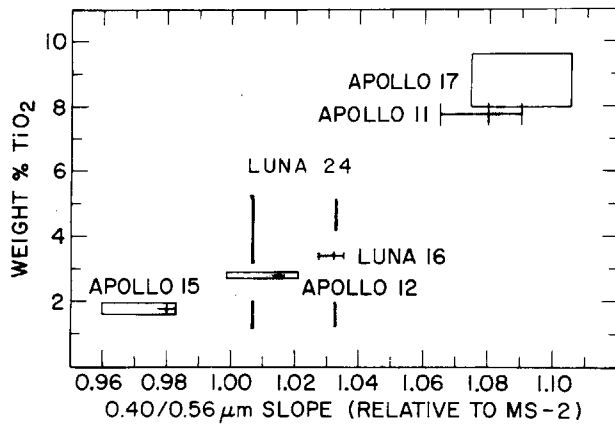
Figure 4. Relationship between the wt%
TiO$_2$ in the lunar mare soil and the
slope of the reflectance spectrum
(.40/.56μm ratio) relative to the
slope of the spectrum for the stan-
dard area MS-2 (after Charette et.
al., 1974). This relationship for
telescopic data was first substanti-
ated through laboratory reflectance
measurements of lunar samples. The
data for percent TiO$_2$ are measured
values for returned soils. The data
for reflectance spectrum slope are
the values derived from telescopic
spectra of the landing sites (from
Pieters and McCord, 1976). Reflec-
tance values for soils from
the major low-titanium basalts in
Mare Crisium near Luna 24 are de-
rived from the vidicon spectral
ratio data calibrated with the
spectrum for M Cr-2.

comparable to those at Apollo 15 in TiO$_2$
content. Since no spectra exist for this
unit, however, further geochemical dis-
tinction cannot be made.
    Thus, the basalt types returned by Luna
24 are likely to be the familiar low-
titanium basalts of Luna 16 and Apollo
12. The returned sample may also include
some components of a high titanium basalt,
a very low titanium basalt, and highland
material. Although the spectral data pre-
sented here cannot confirm the existence
of mantling material in the region, such
material would be expected to be evidenced
by a component of glass droplets (Heiken
et. al., 1974; Adams et. al., 1974). The
degree to which these additional compo-
nents are included in the core is depen-
dent on the local cratering history and
the continuity of underlying stratigraphy.

The return of Luna 24 will certainly in-
crease our knowledge of the known lunar
basalt types, but there still remain majo
and extensive unsampled mare units.

                    References

Adams, J. B., C. Pieters, and T. B. Mc-
    Cord, Orange glass: Evidence for re-
    gional deposits of pyroclastic origin
    on the moon, Proc. of the Fifth Lunar
    Conf., 1, 171-186, 1974.
Adams, J.B., and C. Pieters, 1976 (in
    preparation).
Charette, M. P., T. B. McCord, C. Pieters
    and J. B. Adams, Application of Remote
    Spectral Reflectance Measurements to
    Lunar Geology Classification and Deter
    mination of Titanium Content of Lunar
    Soils, J. Geophys. Res., 79(11), 1605-
    1613, 1974.
Heiken, G. H., D. S. McKay, R. W. Brown,
    Lunar deposits of possible pyroclastic
    origin, Geochim. Cosmochim. Acta, 38,
    1703-1718, 1974.
McCord, T. B., Color differences on the
    lunar surface, Ph.D. thesis, Califor-
    nia Institute of Technology, Pasadena,
    Calif., 1968.
McCord, T. B., C. Pieters, and M. A.
    Feierberg, Multispectral Mapping of
    the Lunar Surface Using Ground-Based
    Telescopes, Icarus, 29, 1-34, 1976.
McCord, T. B., M. A. Feierberg, M. Grabow,
    More multispectral maps of the lunar
    surface using groundbased telescopes,
    1976 (in preparation).
Olson, A. B., and D. E. Wilhelms, Geologi(
    map of the Mare Undarum quadrangle of
    the moon, USGS Map 1-837.
Pieters, C., and T.B. McCord, Character-
    ization of Lunar Mare Basalt Types:
    I. A Remote Sensing Study Using Re-
    flection Spectroscopy of Surface Soils,
    Proc. of the Seventh Lunar Conf., 1976
    (in press).

UPDATE: Luna 24 information

During the 8th Lunar Science Conference, the following information concerning Luna 24 was presented:

(1) Crater degradation age determinations by J. Boyce (UsGS, Flagstaff) indicated two major age units in the Mare Crisium area. The surface basalt in the region of the Luna 24 landing site is estimated to be of an age comparable to Apollo 15 basalts. Older basalts are exposed in an ill-defined region to the west of the landing site and also in an area to the northeast. These older basalts are expected to be slightly younger than Apollo 11 basalts. A small northeast section of Mare Crisium (far from the landing site) appears to be the youngest unit.

(2) Butler et al. (JSC) described the geological setting of the Luna 24 region as derived from orbital photographs. Of particular interest is the 6.5 km crater Farenheit ($\sim$16 km from the landing site). This crater penetrates to 1200m with 5 diffuse bands being identified in the crater wall. The Luna 24 region also contains abundant secondary craters associated with a ray pattern of the distant (1200 km away) crater Giordano Bruno.

(3) Preliminary descriptions of the returned core sample made by Barsukov et al. (USSR) as best interpreted include:

a. The core drilled to a nominal depth of 225 cm. However, the upper ∿60 cm were not recovered in the returned sample.

b. Most of the sample consists of various layers of immature regolith with a high content of coarse grained rock fragments.

c. Chemical analysis of some of the fragments classified them as very low titanium (∿1%) mare basalts. Their aluminum content is high and KREEP component low.

These new data allow the following possible interpretations of the Luna 24 spectral information (Pieters et al., 1976):

I. The Luna 24 core sampled only the surface unit seen by remote sensing techniques. If the very low titanium basalts are representative of this surface unit, then the calibration of % TiO_2 as derived from continuum slope is <u>inaccurate</u> for very low titanium basalts. Due to the nature of the calibration curve, such an inaccuracy would not be greatly surprising for unsampled low Ti basalts. (This has been pointed out in all papers discussing the nature of this calibration.)

II. The Luna 24 core is composed largely of a (subsurface) unit distinct from the general surface unit in southeast Mare Crisium. Supporting this interpretation

is the relationship between the age units of Boyce and the spectral units of Pieters et al. and the fact that the core seems to be largely a sample of relatively fresh ejecta. The Boyce 'old' age unit is roughly spatially comparable to the very low titanium basalt to the north-east defined by the spectral images. Furthermore, the spectrally mottled region extending to the west of the landing site is again comparable to the 'old' unit defined in that area. These combined data indicate the sequence of mare fill for Mare Crisium may have been: (a) early high-Ti basalt (excavated by Picard) followed by or con-temporaneous with (b) a very low titanium basalt (Boyce's 'old' unit; spectrally red) and a later (c) medium low-Ti basalt (2-4% TiO_2) emplaced about 3.3 b.y. ago. This medium low-Ti surface unit is perhaps thin especially to the west of the landing site. The freshness of the sam-pled material indicates it could easily be largely ejecta excavated (by Farenheit?) from a proposed very low-Ti sub-surface unit (b).

The basic problem in understanding the spectral information is determining what the Luna 24 core actually sampled. Analysis of the core material itself should dis-tinguish which of the above possibilities are more likely correct:

If the dominant basalt type throughout the core is the very low-Ti basalt and it is found to be comparable in age to Apollo 15 basalts ($\sim$3.3 b.y.), then one would conclude this very low-Ti basalt is likely to be the surface unit and interpretation I is probable. The spectral calibration of low-Ti basalts would have to be reevaluated. A significant component, however, of unrelated basalt types of higher TiO_2 in the core would weaken this interpretation.

On the other hand, if the very low-Ti basalts are found to be relatively old, interpretation II would be more probable; the sample would be interpreted largely as ejecta from a subsurface unit. Some component of younger medium low-Ti material would be expected somewhere in the core.

Potentially, the Luna 24 core could contain one of the richest assortments of mare basalt types returned to date.

2. <u>Synthesis study of the Flamsteed region of Oceanum</u>

    <u>Procellarum</u>

Full moon spectral imagery (e.g., Barbarshov, 1973) indicates that only a small portion of the western 'blue' basalts are comparable in continuum slope to those of the east (e.g., Apollo 11). This is confirmed by the filter photometry measurements (Pieters and McCord, 1976) that further show the western high-Ti basalts to be distinct and compositionally different from those sampled at Apollo 11 and Apollo 17. A synthesis study was undertaken to better understand the regional geology and define the geochemistry for a case area of western high-Ti basalts--the Flamsteed area of Oceanus Procellarum. Representative spectra for this region were included in the previous basalt classification study (H_2, h_2, h_3). Vidicon spectral images (shown in Figure IID-21) were used to map the extent of these units. The preliminary results from this study were presented at the 8th Lunar Science Conference. New data are presented here to update the following published abstract. A more extensive discussion of the Flamsteed region will be prepared for publication during summer, 1977.
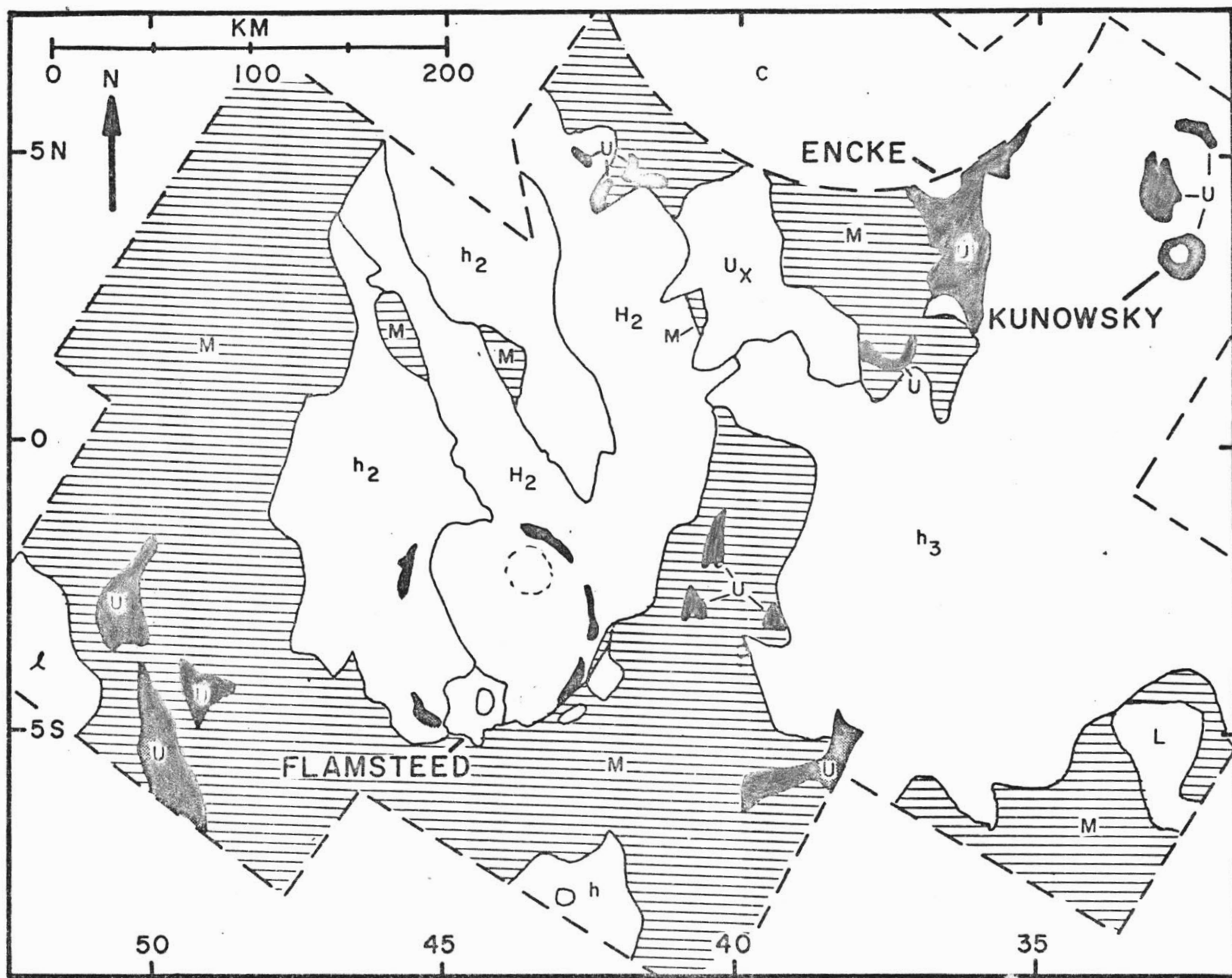
GEOLOGY AND GEOCHEMISTRY OF THE FLAMSTEED REGION OF OCEANUS PROCEL-
LARUM: A PRELIMINARY REPORT BASED ON REMOTE SENSING AND LUNAR SAMPLE INFORMA-
TION.   C. Pieters[1], J. B. Adams[2], R. Bryan[3], J. W. Head[3], T. B. McCord[1,4],
S. Zisk[5]. [1]Dept. of Earth and Planetary Sci.; M.I.T., Camb., Ma. 02139; [2]Dept
Geol. Sci., Univ. Wash., Seattle; [3]Dept. Geol. Sci., Brown Univ., Prov., R.I.
02912; [4]Univ. Hawaii at Manoa, Honolulu, 96821; [5]NEROC Haystack Observ., West-
ford, Ma. 01886.

The Flamsteed region of Oceanus Procellarum displays a number of mare and
highland geologic units which are important in the geologic framework and vol-
canic history of the western maria. Fig. 1 shows the distribution of major
units in the Flamsteed region and was derived using remote sensing techniques
and lunar sample information. The principal techniques (1) used in defining
unit boundaries included a) vidicon spectral ratio images, b) earth-based
photographs (albedo), c) orbital photography. Other techniques essential for
unit characterization and interpretation include a) reflectance spectra (0.3-
1.1 μm), b) radar backscatter maps, c) radar topography, d) spectra and compo-
sitional analysis of returned samples from the Apollo sites. Relative ages
were obtained by superposition relationships and crater degradation techniques
(2).

On the basis of unit characteristics, distribution, and superposition re-
lationships, the following history is outlined: A cratered uplands existed in
the region prior to mare emplacement and consisted of normal feldspathic high-
land crust (U) and local development of a spectrally red unit similar to other
"red spots" (U_x) (3,4,5). Earliest exposed mare material is a series of low-
Ti basalts (L,l,m) which flooded the upland topography. Mare ridges developed
on these units and the crater Flamsteed formed prior to the emplacement of
later basalts. The last major phase of volcanism was characterized by moder-
ately high-Ti basalts (H_2, h_2, h_3) spreading as relatively thin flows over
preexisting maria. Flow emplacement is generally controlled by preexisting
local and regional topography including mare ridges developed on earlier maria.
The geochemical characterization of these units is based primarily on
spectral reflectance measurements (.33-1.06 μm) of small (~10 km) regions
within the units and similar laboratory reflectance measurements (.35-2.5 μm)
of returned lunar soil samples. The spectrally defined basaltic units are
characterized with respect to other basalt types for the frontside of the
moon (6). Although a number of units can be distinguished from each other
with this data, characterization of the mineralogy is incomplete until spectra
to 2.5 μm can be obtained for fresh craters within each unit.

References   (1) Head, J.W. et al. (1976) Lunar Science VII, p. 357.
(2) Boyce, J. (1976) Proc. Lunar Sci. Conf.VII,p. 2719-2728.   (3) Malin, M.
(1974) Earth, Planet. Sci. Lett. 21, p. 331-341.   (4) Pieters, C. et al.
(1975) Proc. Lunar Sci. Conf.VI, p. 2689-2710.   (5) Wood, C.A. and J.W. Head
(1975) Origins of Mare Basalts, LSI, p. 189.   (6) Pieters, C. and T.B. McCord
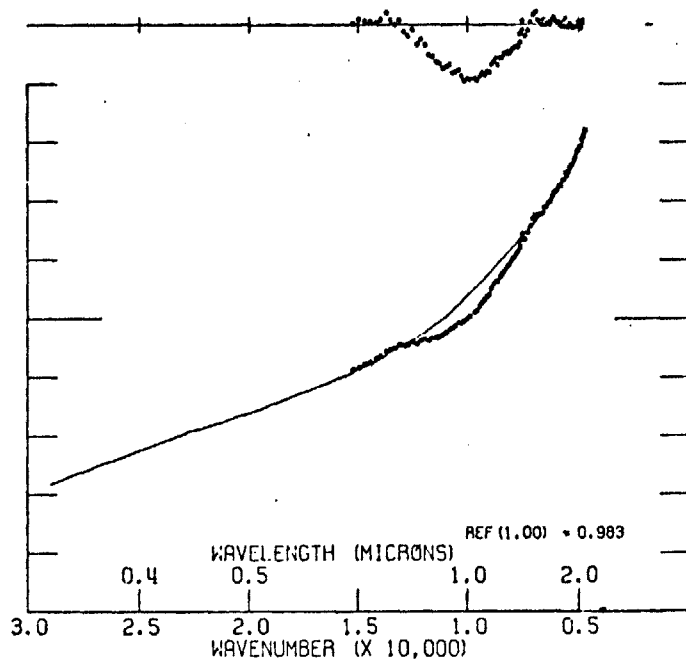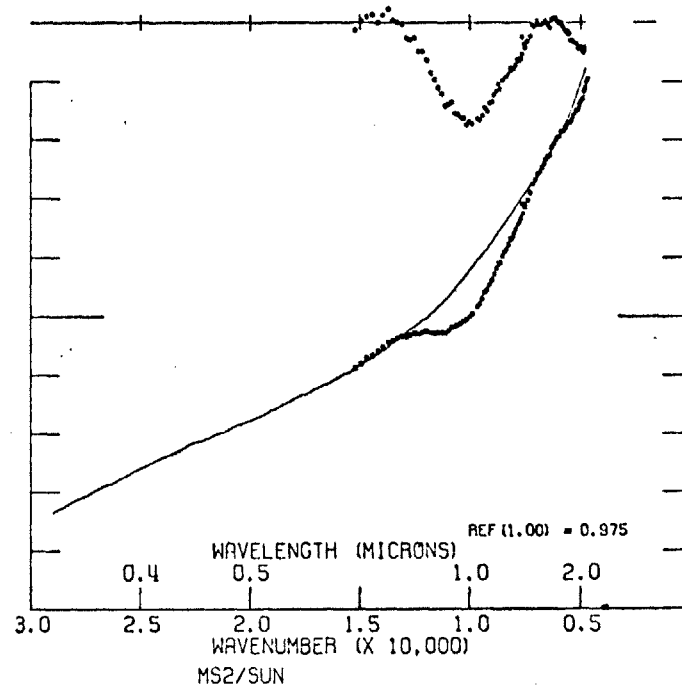(1976) Proc. Lunar Sci. Conf. VII, p. 2677-2690

SYMBOL	DESCRIPTION	INTERPRETATION
C	High albedo; high frequency of rays and satellitic craters surrounding Kepler.	Kepler ejecta; underlying material significantly affected by cratering event.
Mare		
H_2	Low albedo; type area NE interior of Flamsteed P indicated with dashed circle; continuum slope (.40/.56 μm) relatively blue; 1 μm absorption feature (Fe^{+2}) stronger and broader than Tranquillity soils. Several associated sinuous rilles.	Titaniferous basalt. A young basalt with a soil composition that ranges from 5-8.5% TiO_2; probably different from older eastern high-Ti basalts in mineralogy; more glass-rich than basalts of Mare Humorum (h_3); related to Imbrium high-Ti basalts. Unsampled.
h_2	Spectrally much like H_2 but with continuum slope slightly (1-2%) less blue.	Titaniferous basalt. A young medium-high-Ti basalt with soil TiO_2 3-5%; related to H_2 in minerology. Unsampled.
h_3	Continuum slope equally blue as h_2 but distinct from H_2 and h_2 in infrared spectral character; 1 μm feature (Fe^{+2}) strong but less broad.	Titaniferous basalt. A young medium-high Ti basalt with soil TiO_2 3-5%; related to medium-high-Ti basalts of NE Mare Humorum (4). Unsampled.
m	Continuum slope comparable to Apollo 12; most extensive unit of the region (no spectra exist to allow further investigation).	Low-Ti basalt. Soil composition 2-3% TiO_2; older than H_2, h_2, and h_3 basalts. Unclassified.
l	Continuum slope slightly red (comparable to Apollo 15 landing site); not an extensive surface unit in this region.	Low-Ti basalt. Soil composition 1.5-2% TiO_2. Unclassified.
L_4	High albedo; Relatively red continuum slope; 1 μm feature stronger than for other low-Ti units of the region. Extensive development of mare ridges.	Low-Ti basalts. Soil composition possibly less than 1.5% TiO_2. Unsampled.
Upland U	Moderately high albedo; continuum slope relatively red. Topographically higher than mare.	Crater remnants and associated uplands. Mostly feldspathic islands surrounded by mare material.
U_x	Moderately high albedo; upland plains and crater remnants; strong UV absorption causing very red continuum slope; regionally high.	Undesignated highlands. Suspected of being related to other uniquely red highland regions, some of which may be of volcanic origin.

UPDATE: Characterization of the 1µm spectral dif-
ferences between the eastern and western
high-Ti basalts

Good quality infrared spectra (.65 to 2.15µm) were

obtained by McCord (1977) for representative lunar regions.

Shown in Figure IIIE-1 (McCord, unpublished) are spectra

for mature soil regions: Apollo 11 (H_1 basalt), Flamsteed

(the case area for H_2 basalts), OP-4 (h_3 basalt to the

east of Flamsteed), MH-O (case area for h_3 basalt in Mare

Humorum), and the standard MS-2 (m_4 basalt) in Mare Sereni-

tatis. These spectra have been further processed in order

to examine the nature of the 1µm absorption. An iron con-

tinuum was fitted to the data (Figure IIIE-2) and removed

using the techniques of Gaffey (1977) described in Section

IID-1b for laboratory samples. The residual absorption

features for the five regions are shown in Figure IIIE-3.

The background discussion of Section IID-1 can be used

to describe the observed spectral features. The follow-

ing spectral characteristics should be noted: (1) the

lack of a second pyroxene feature at 2µm for Apollo 11

and Flamsteed, (2) the relative strength of the 1µm fea-

ture for Flamsteed relative to Apollo 11, and (3) the longer

wavelength position of the 1µm minimum for Apollo 11 and

Flamsteed with respect to MH-O and MS-2. The relative

Figure IIIE 1.Recent telescopic spectra for lunar
mare soils, .65 to 2.1μm. (McCord, 1977)

REF (1.00) = 0.983

WAVELENGTH (MICRONS)

0.4   0.5   1.0   2.0

3.0   2.5   2.0   1.5   1.0   0.5

WAVENUMBER (X 10,000)

AP 11/SUN

CONTINUUM = METALLIC IRON - MOD 2

REF (1.00) = 0.975

WAVELENGTH (MICRONS)

0.4   0.5   1.0   2.0

3.0   2.5   2.0   1.5   1.0   0.5

WAVENUMBER (X 10,000)

MS2/SUN

CONTINUUM = METALLIC IRON - MOD 2

Figure IIIE 2.   An iron continuum is fit to the telescopic spectra.
The residual absorption features in the telescopic
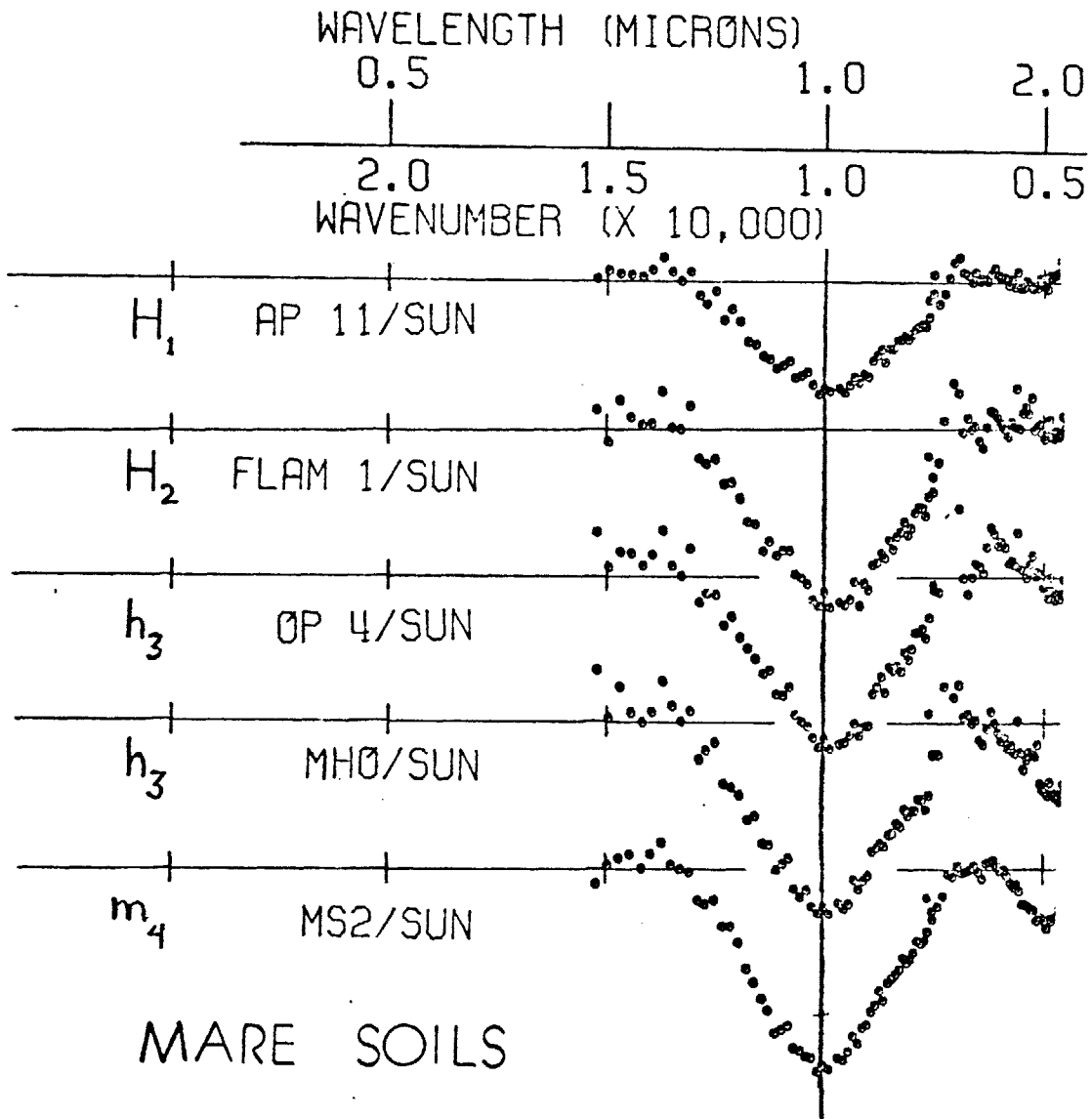spectra are shown above the spectra.

Figure IIIE 3. Residual absorption features for the spectra of figure 1 after an iron continuum has been removed.

strength of the glass and pyroxene bands derived from these spectra for the various basalt types are summarized in Table TIIIE-1. The strength of the continuum absorption in this table is derived from the visible spectra.

The spectral distinction between Apollo 11 (H_1) basalts and Flamsteed (H_2) basalts concerns the strength of the glass (Fe^{2+}) band; Flamsteed spectrum has a stronger band than Apollo 11. The spectral distinction between the two western high-Ti basalts, represented by Flamsteed (H_2) and MH-O (h_3), is a stronger pyroxene feature in the spectrum for h_3 basalts than for H_2 basalts.

Table TIIIE-1.

Absorption Strengths in basalt type spectra

H_2 (Flamsteed)	h_3 (Humorum)	H_1 (Apollo 11)	m_4 (MS-2)	Soil Absorption
Strong	Strong	Weak	Strong	Glass Band
Weak	Strong	Weak	Strong	Pyroxene Band
Strong	Strong	Strong	Weak	Continuum Absorption

IV. LUNAR BASALT TYPES II: SPECTRA OF CRATERS
(.3 to 1.1μm)

CHARACTERIZATION OF LUNAR MARE BASALT TYPES-II:

SPECTRAL CLASSIFICATION OF FRESH MARE CRATERS

Carle Pieters

Remote Sensing Laboratory
Dept. of Earth and Planetary Sciences
MIT 37-487
Cambridge, Mass. 02139

Abstract

Telescopic reflectance spectra (.3 - 1.1μm) of fresh craters are presented and classified according to the spectral features observed. These spectra are the closest lunar surface analogue to laboratory spectra obtained for lunar rock powders. Mineral absorption features can be identified in these crater spectra and interpreted using returned lunar samples. Classification of lunar telescopic spectra indicates that most (>80%) of the lunar surface is composed of a finite number of discrete and describable geochemical units. Spectra of craters to 2.5μm are required for specific mineralogical determinations from remote observation.

In a previous paper, telescopic spectra of mature

agglutinate-rich mare surfaces were used to develop a clas-

sification of mare basalt types (Pieters and McCord, 1976).

It was assumed that as regional basalt surfaces weathered

to soil they maintained geochemical identity, although most

original mineralogical character was lost. Lunar mare re-

gions were characterized in the previous study by soil TiO_2

content as derived from continuum slope and by near-infrared

spectral features. The data indicate that a variety of

specific basalt types exists on the frontside of the moon,

the majority of which have not been sampled in any of the

Apollo or Luna landing mssions.

Spectra of rock powders contain diagnostic absorption

features that can be used to define the mineral constituents

present (Adams, 1974, 1975; McCord et al., 1976a). Due to

the special character of agglutinate-dominated lunar soils,

however, it has been difficult to identify the mineralogy

of the original basalts using spectral reflectance techniques.

The spectral properties of lunar soils are now better under-

stood and changes in optical properties that occur during

soil maturation have been described (Adams and McCord, 1973;

Adams and Charette, 1975). The objective of the current

spectral reflectance study is to further define and char-

acterize the optical properties of fresh, relatively crys-

talline lunar surfaces. It is apparent that the best

regional analogue on the lunar surface to crystalline rock powders studied in the laboratory are fresh craters (Adams and McCord, 1972). Additional telescopic spectra of fresh craters have been obtained from .3 to 1.1μm. It is anticipated that spectra to 2.5μm for a few craters will be available in the near future (McCord, 1977). Lunar sample studies are being undertaken in parallel with telescopic observations to define the characterisitic spectral features of petrographically defined rock types (Charette and Adams, 1975, 1977). The ultimate objective of such a combined program is to identify from absorption features the major mineral phases (e.g., pyroxene, olivine, plagioclase, ilmenite), their composition when possible, and their relative proportions for a variety of regional basalt types previously described (Pieters and McCord, 1976).

Presented here is the first step of the observational program: a classification and analysis of the currently available spectra (.3 to 1.1μm) for fresh lunar craters. The data are used to further confirm that the majority of the lunar surface is made up of a finite number of rock types; some are distinct while others may be gradational. Although higher spatial resolution and greater spectral coverage are required to identify specific mineralogies, these data show that mineral absorption features do exist

in fresh crater spectra with systematic variations that
can be directly interpreted in terms of mineral composition.

A. Observations and Data Description

Telescopic spectra of about 400 small (5-25 km diameter)
lunar areas have been obtained using a filter photometer
covering the spectral range from .3 to 1.1μm. Based on
their location and general morphology, most regions can
be easily classified as mare, upland, mare crater or upland
crater. The general spectral types of such a classifica-
tion was discussed by McCord et al. (1972) and Charette
et al. (1974). Over 60 fresh crater regions have now been
observed telescopically during one or more lunations. Due
to observational difficulties (see below), data for ∿10
regions were unacceptable and not included in this analy-
sis. A minor amount of useful data was obtained with a
vidicon spectrometer/polarimeter (.6 - 1.0μm). The loca-
tion of the craters used in this study are indicated by
oversized symbols in Figure 1.

There are a variety of observational limitations that
make reliable spectra of fresh craters difficult to obtain.
Most spectrometers measure radiation sequentially as a
function of wavelength. The photometer used to obtain the
data discussed here requires 2 minutes to cycle through
25 filters. During this time, two unavoidable situations

allow the object to 'wobble' in the optical path up to about
2 second of arc (about 4 km on the lunar surface): nor-
mal atmospheric turbulance and imperfect lunar tracking
of the telescope. This spatial uncertainty during two min-
utes generally does not affect data for mature soil regions
since the albedo of the region is homogeneous on a scale
larger than the observed area. For fresh bright craters,
however, the albedo variations are large over small areas
and the integrated radiation measured by the spectrometer
can vary significantly during the total measurement of the
spectrum. These observational difficulties are enhanced
for small ($\lesssim 8$ km) fresh craters. Analysis of spectra for
small craters is further burdened by the problem of opti-
cal mixing that occurs with low (10 km) spatial resolution--
part of the radiation detected is from the crater and part
is from the surrounding (darker) material. For the data
presented here, observations have generally been repeated
3-5 times. A precision better than 1% is generally required
for classification.

Two additional factors influence the interpretation
of crater spectra. Craters excavate material that may
not be homogeneous with depth. Thin surface units may be
vertically mixed by the cratering event. Also, the spec-
tral characteristics of fresh material are known to degrade

rapidly with the development of agglutinate-rich soil

(Adams and McCord, 1973). Precisely what the time scale

is for such weathering effects to be significant is unknown,

but expected to be on the order of a few hundred million

years. For large craters with sufficiently steep walls,

a mature soil is not allowed to accumulate and a spectrum

of relatively fresh material can be obtained on the rim,

even though the ejecta itself may have reached equilibrium

maturity. Most fresh crater spectra presented here seem

to have features of comparable magnitude implying matur-

ation differences are minimal.

Telescopic spectra for a variety of soils and craters

are presented in Figure 2. Note the prominent absorption

near $1\mu m$; for soils this feature is largely due to Fe^{2+} in

agglutinitic glasses (Charette and Adams, 1977), whereas

for craters this feature is due to Fe^{2+} in mineral fragments

(e.g., see Adams, 1975). The wavelength of the

absorption in crystalline lunar material is determined by

the average pyroxene composition (Adams, 1974). The sym-

metry of the lunar absorption is dependent on absorptions

due to other mineral components such as olivine and plagio-

clase. Weaker absorption features can often be discerned

in laboratory spectra in this spectral range (e.g., continuum

inflections in the blue and broad absorptions at .4 - .6

in Ti-rich pyroxenes and ilmenite). In Figure 2, the

details of the specific mineral absorption features contri-
bute small but extremely signficant variations to a general
red lunar spectrum.

B.   Classification

In order to distinguish the small variations in absorp-
tion features and develop a classification of possible rock
types, the spectra for lunar craters have been divided by
the spectrum of a standard area in Mare Serenitatis (MS2:
18°40'N, 21°25'E).   This procedure does not preserve the
absolute wavelength position of absorption features but
it does allow small spectral variations to be detected and
classified.   The relative positions of features between
areas is maintained.

The craters included in this study were first generally
classified as mare or upland craters according to the type
of terrain in which they occur.   A few exceptions were
made to this original grouping and will be discussed along
with the more detailed classification of crater spectral
types.   Since it is possible that mare craters may have
penetrated into crustal material, a classification of the
spectra for highland craters needs to be made before mare
crater spectra can be distinguished.

Relative reflectance spectra for highland crater spec-
tral types are included in Figure 3.   From the available

data, three general spectral types were distinguished according to the following characteristics: UI) The continuum is relatively blue between .5 - .7μm with an inflection towards the ultraviolet that occurs between .4 and .5μm; the .9μm absorption feature varies in strength and perhaps wavelength position resulting in a inflection between .7 and .95μm. This group was further subdivided (UIa--UIe) according to the sharpness and wavelength position of the ultraviolet inflection and according to the infrared characteristics. UII) There exists a very prominent and strong absorption band at .9μm with strong relative absorption towards the ultraviolet. UIII) The .9μm feature is weak to non-existent although there is strong relative absorption shortwards of .45μm.

Relative reflectance spectra for two major mare crater spectral types are shown in Figure 4. These two spectral types of mare craters are distinguished by: MI) The existence of two absorption bands, a strong one centered near 1μm and a weaker one near .5μm; MII) The existence of one strong band near 1μm. Each of these two types of mare craters can be further subdivided according to the wavelength position of the 1μm feature and possibly the strength of ultraviolet absorption. A third group (MIII) of mare cra-

ters have identical spectral characteristics as those iden-
tified as highland crater type UIII. These MIII spectra
are shown in the lower right of Figure 3.

A few crater spectra do not fit easily into these mare
and highland groups:

(a) The center and rim of Kepler has been observed
frequently (Figure 5A). The first whole crater spec-
trum (1-09-71), although noisy, seemed comparable to
most mare craters and Kepler was originally classified
as a mare crater (McCord et al., 1972). Since then,
additional spectra of varying quality have been obtained
which together indicate that Kepler is a fairly unique
spectral type. There exists a relative minimum in the
spectrum near .9μm and a plateau between 1.0 and 1.1μm.
A region within the ejecta from Kepler, however, con-
tained the same spectral character is group UId and
was thus classified as highland material.

(b) Three regions (Lalande, Reiner γ, and Dawes rim)
may be mixtures of a variety of mare and highland ma-
terial. Their spectra (Figure 5b) are more similar
to each other than to other craters, however, implying
perhaps related mineralogy.

(c) Hesodius B (and perhaps Dawes ejecta) is an old

crater (Eratosthenian) in a blue (high-Ti) mare. Its

spectral characteristics (Figure 5c) are consistent

with the interpretation that the surface is an inter-

mediate stage during degradiation of high-Ti basalt

to soil with maturity.

C. Discussion

Relative reflectance spectra are especially useful

for understanding spectral differences seen in two-dimen-

tional imagery. With the exception of MIII and UIII cra-

ters, the pyroxene band near .95μm is stronger in crater

spectra than in mature soils. A .95/.57μm ratio image (cf.,

McCord et al., 1976b) is thus frequently used as a data

source to easily identify immature regions and to estimate

their areal extent. Spectral ratio images at other wave-

lengths, however, do not provide sufficient information

for classification of craters. As can be seen in Figures

3-5, there is great variety in the strength of spectral

features and the wavelength   of spectral inflections.

No simple combination of spectral ratio images can distin-

guish the spectral types discerned in the crater spectra

presented here.

It has been shown previously that the general spectral

characteristics of fresh craters are essentially the same

as those for rock powders measured in the laboratory (Adams

and McCord, 1972). The strength of the features in labor-

atory measurements, however, are about 4 times as strong

as those observed telescopically. The data presented here,

together with a recently compiled atlas of similar labor-

atory data (Adams et al., 1977), reestablishes this link

between rock powders and fresh craters and will be discussed

in further detail in later publications. The laboratory

samples with spectral characteristics that are most compar-

able to those for fresh craters, both in nature and in

strength, are the non-agglutinate separates from immature

soils. Either the surface material at all craters observed

in this study has matured to some degree, causing the min-

eral spectral features to become somewhat degraded, or the

cratering event itself has created a surface material that

is not purely crystalline.

Some spectral characteristics that distinguish the sub-

groups of craters presented here appear to be gradiational

in nature. Spectral types may be related to each other

as a function of the maturity of the surface as suggested

by McCord et al. (1972) and Adams and McCord (1973). Al-

ternatively, the gradiations could be due to a mixing of

different rock types. The data presented in Figures 3-5

indicate that distinct rock types do exist and suggest
that many of the spectral variations are not simple a
matter of surface maturity.

A few cases where spectral evidence indicates a large
mare crater has excavated crustal material have already
been documented (McCord et al., 1972): Aristarchus and
Copernicus. (The soil of Copernicus ejecta, however, has
already developed to a fairly mature agglutinate-rich state.)
Additionally, from the data presented here, one group of
smaller mare craters (MIII) have apparently excavated high-
land material of the same type as that found in UIII cra-
ters. MIII craters occur near the edge of the mare on
what appears to be thinly flooded basin shelves in Mare
Humorum and Serenitatis.

A few spatial systematics can be tentatively identi-
fied in these data. All of the regions in highland group UId
and III are on basin rims. The Apollo 16 region (Descartes)
contains all of the craters identified as group UIe and
a few from UIc. Spectra of very immature lunar soils from
Luna 20 and Apollo 16 contain these same spectral charac-
teristics (Adams et al., 1977). From the data available,

the craters Aristarchus (UIa) and Mosting A (UII) are sin-
gularities in the remote observations although almost iden-
tical spectral characteristics can be identified in a few
lunar highland samples (Adams and McCord, 1972, Adams et
al., 1977). Identification of lunar samples with spectral
characteristics comparable to the craters in group UIb
and III has not been made.

The two primary absorption features observed in mare
craters have clear compositional implications. The strong
absorption features at 1μm is primarily due to clinopyroxenes
in the surface material (Adams and McCord, 1972). The
wavelength position of this band is a function of the Fe
and Ca content of the average pyroxene (Adams, 1974). If
the wavelength position of both this band and the accom-
panying one near 2μm can be measured, then the pryoxenes
composition can be determined. The feature in mare crater
MI spectra near .5μm is commonly observed in titanium-rich
rocks and is due to either titanium-rich pyroxenes or il-
menite.

The occurrence of type MI and MII craters is generally
associated with the TiO_2 content of the surface unit (as
derived from soil spectra): type MI craters occur in re-
gions that are titanium rich and type MII occur in regions

that are low titanium. Halo crater (MIb) occurs in the Copernicus ejecta blanket and is likely to have excavated high titanium basalt.

It is unfortunate that no spectra for craters within the major unsampled basalt types of the western moon (Pieters and McCord, 1976) were available for this study. A primary reason for this lack of data is the difficulty of locating a crater within the current telescopic resolution ($\sim$10 km) that is likely to have excavated only the most recent surface unit. For example, the western high-Ti flows near Flamsteed are thin and many craters seem to have excavated an earlier low-Ti unit (Pieters et al., 1977, in preparation).

D.   Conclusions.

(1)   These additional data strengthen and expand the conclusion of Adams and McCord (1973) that the spectral features evident in spectra of fresh crater are stronger than those for mature soils (Figure 2) and are due to the more crystalline nature of the surface material.

(2)   The systematic variations observed in the spectral features of these fresh craters are directly associated with variations in the mineralogy of the surface material and can be understood largely in terms of returned lunar samples. To utilize this information in a quantitative

manner, spectra to 2.5μm are required in order to examine the details of mineral absorption features.

(3)   This spectral classification of fresh craters together with the previous classification of mature mare surfaces, an unfinished classification of highland surfaces, and the orbital geochemistry data indicate that most (>80%) of the lunar surface is composed of a finite number of discrete and describable geochemical units. Even though 1/2 to 2/3 of these units are unsampled, there is some hope of understanding their general mineralogy and geochemistry in the future using remote sensing techniques.

Acknowledgements

References

Adams, J.B. (1974) Visible and Near Infrared Diffuse Reflectance Spectra of Pyroxenes as applied to Remote Sensing of Solid Objects in the Solar System. J. Geophys. Res., 79, 4329-4336.

Adams, J.B. (1975) Interpretation of Visible and Near-Infrared Diffuse Reflectance Spectra of Pyroxenes and Other Rock-Forming Minerals. Infrared and Raman Spectroscopy of Lunar and Terrestrial Minerals, Academic Press, Inc., New York, 91-116.

Adams, J.B. and Charette, M.P. (1975) Effects of Maturation on the Reflectance of the Lunar Regolith: Apollo 16 - A Case Study. The Moon, 13, 293-299.

Adams, J.B. and McCord, T.B. (1972) Electronic Spectra of Pyroxenes and Interpretation of Telescopic Spectral Reflectivity Curves of the Moon. Proc. Lunar Sci. Conf. 3rd, p. 3021-3034.

Adams, J.B. and McCord, T.B. (1973) Vitrification darkening in the lunar highlands and identification of Descartes material at the Apollo 16 sites. Proc. Lunar Sci. Conf. 4th, p. 163-177.

Adams, J.B., Pieters, C., Gaffey, M., and Catalano, C. (1977) Reflectance spectra of lunar soil samples relative to MS-2: Cumulative atlas, Dept. of Geol. Sci., Univ. of Wash., Seattle, unpublished.

Charette, M.P. and Adams, J.B. (1975) Mare basalts: Char-

  acterization of compositional parameters by spectral

  reflectance. In Origin of Mare Basalts, p. 25-28, The Lunar

  Science Institute, Houston.

Charette, M.P. and Adams, J.B. (1977) Spectral reflectance

  of lunar highland rocks, in Lunar Science VIII, p.

  172-174. The Lunar Science Institute, Houston.

Charette, M.P. and Adams, J.B. (1977b) A method for remote

  determination of the FeO content of lunar soils using

  spectral reflectance measurements, to be submitted to

  J. Geophys. Res.

Charette, M.P., McCord, T.B., Pieters, C., and Adams, J.B.

  (1974) Application of Remote Spectral Reflectance Mea-

  surements to Lunar Geology Classification and Determin-

  ation of Titanium Content of Lunar Soils. J. of Geophys.

  Res., 79, 1605-1613.

McCord, T.B. (1977) Telescopic Lunar Spectra (.6 - 2.5μm),

  in preparation.

McCord, T.B., Charette, M.P., Johnson, T.V., Lebofsky, L.A.

  and Pieters, C. (1972) Lunar Spectral Types. J. Geophys.

  Res., 77, 1349-1359.

McCord, T.B., Adams, J.B., and Huguenin, R.L. (1976a) Re-

  flection Spectroscopy: A Technique for Remotely Sensing

Surface Mineralogy and Composition. To appear in a
NASA-SP on Orbital Science.

McCord, T.B., Pieters, C., and Feierberg, M.A. (1976) Multispectral Mapping of the Lunar Surface Using Ground-Based Telescopes. Icarus, 29, 1-34.

Pieters, C. and McCord,T.B. (1976) Characterization of Lunar Mare Basalt Types: I. A Remote Sensing Study Using Reflection Spectroscopy of Surface Soils. Proc. Lunar Sci. Conf. 7th, p. 2677-2690.

Figure Captions

1. Classification of lunar bright craters based on spec-
    tral reflectance measurements. The shape of the over-
    sized symbols indicates the spectral groups discussed
    in the text. The number associated with each symbol
    is for identification of the spectra in Figure 2-5.

2. Telescopic reflectance spectra for representative lunar
    soils and craters.

3. Reflectance spectra relative to MS-2 for highland cra-
    ter material. Three major groups are distinguished.
    Group I can be further subdivided (a-e) according to
    the wavelength position of distinct spectral inflections.
    Groups UIII and MIII are spectrally equivalent although
    craters of the former are in the highlands and of
    the latter are on the edge of a mare.

4. Reflectance spectra relative to MS-2 for mare craters.
    Group I has two absorption features, one near .5μm
    and one near 1.0μm. Group II only has one major fea-
    ture near 1.0μm. Each group can be further subdivided
    according to the wavelength position of the 1.0μm feature.

5. Reflectance spectra relative to MS-2 for special crater
    groups. Kepler center and rim appear to have unique
    spectral characteristics. LaLande, Reiner Gamma, and
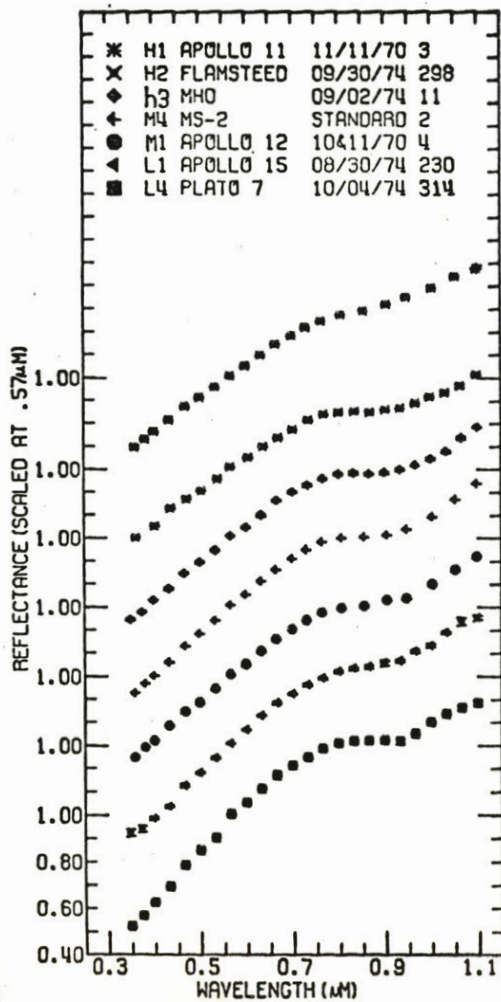
IV 293

Dawes are likely to be mixtures of material although they have roughly similar spectra. Spectra for Dawes ejecta and Hesiodus B appear to show significant maturation effects.
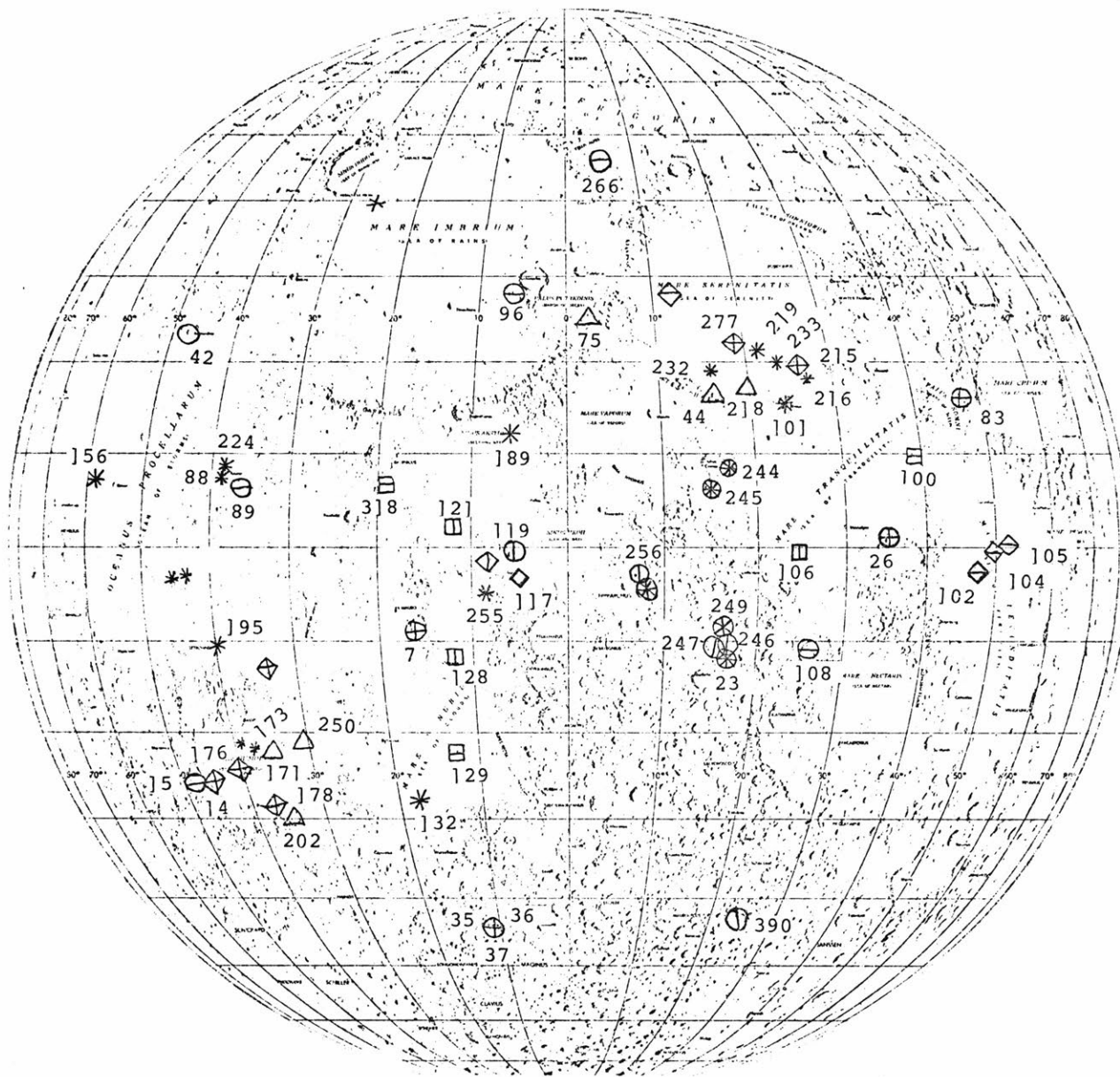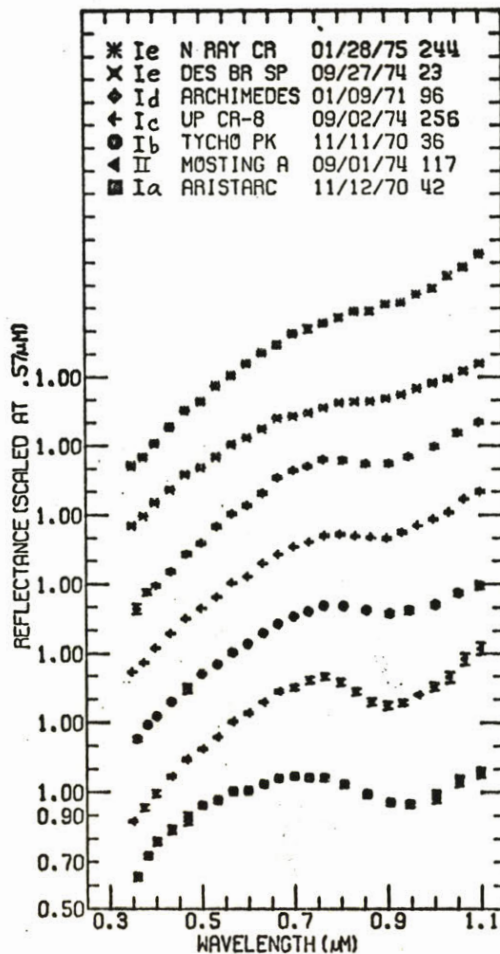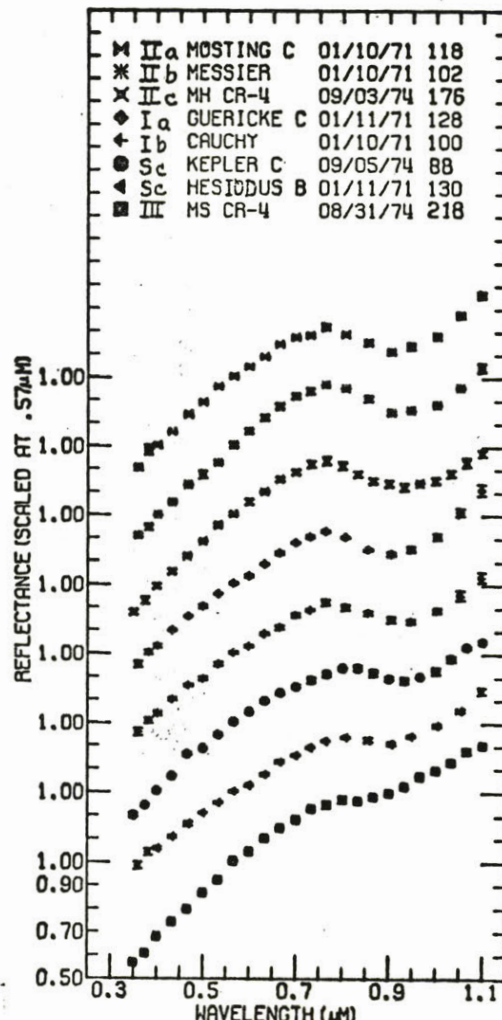
Figure 1.

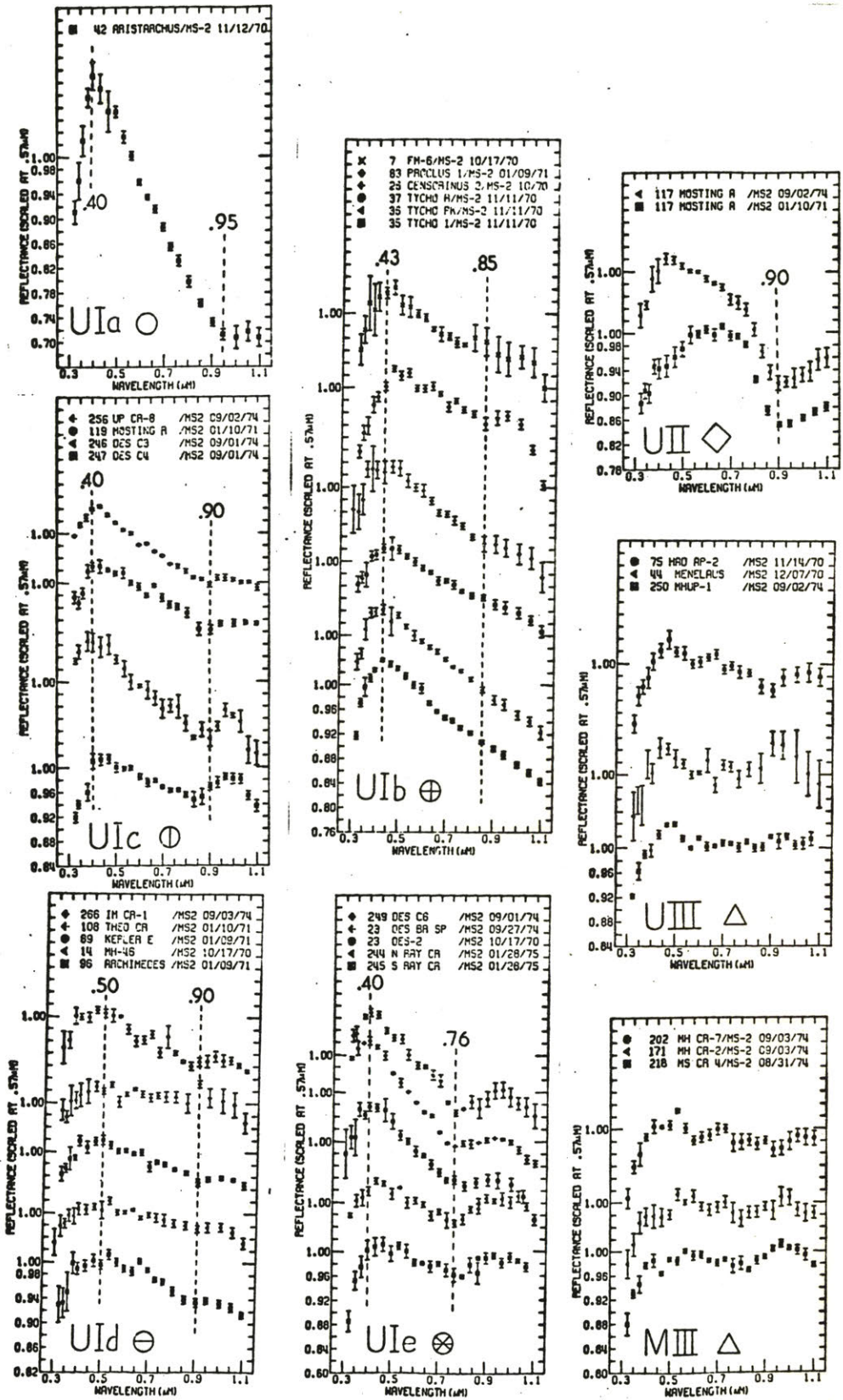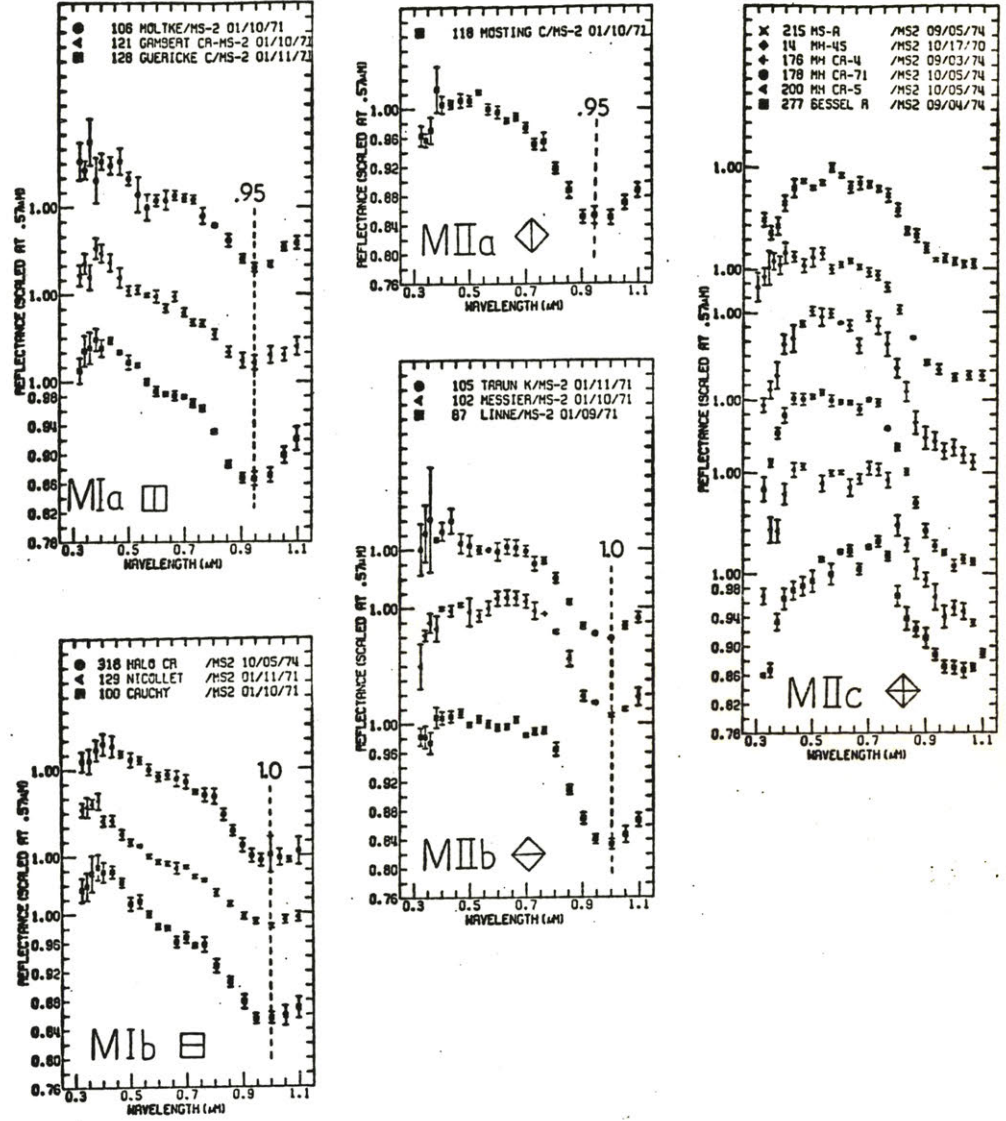MARE SOILS   UPLAND CRATERS   MARE CRATERS

Figure 2.

Figure 3.

Figure 4.
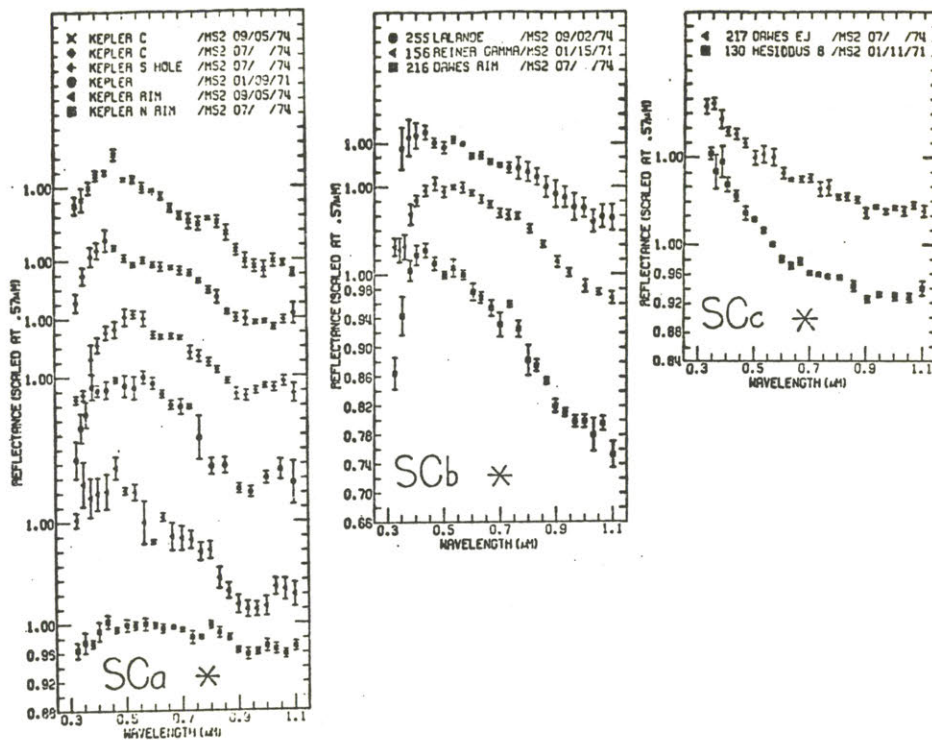
Figure 5.

V. SUMMARY AND SYNTHESIS

V. SUMMARY AND SYNTHESIS

Samples of basalts from two planets, the earth and the moon, have been studied in detail by petrologists and geochemists in order to understand the geochemistry of the interiors as well as the processes that have been part of planetary evolution. Basalts from these two planets are similar in the general sense that they have crystalized from mafic igneous melts derived by partial melting of the planet's interior. However, it is also apparent there are some fundamental differences in chemistry, age, mode of emplacement, tectonic environment, and by implication, character of the mantles. The Apollo program opened a new era of exploration; the return of the lunar samples allowed the first direct comparison of the earth with another known solar system object and deepened the understanding of our own planetary environment.

The basic nature of the samples from the moon will continue to be studied in terrestrial laboratories to further understand the evolution of the planet. However, until more comprehensive samples are obtained of yet unsampled units, it will be the role of remote sensing specialists to place limits on what can be extrapolated globally from the selective samples in hand returned by Apollo and Luna missions. Near future exploration of the lunar

surface will have to be performed using remote sensing techniques. Spectral reflectance measurements in particular have been used to derive information of surface mineralogy and geochemistry.

V.   SUMMARY AND SYNTHESIS

A.   Conclusions

Spectral reflectance data (spectra and imagery) dis-
cussed in the preceding sections allow the following gen-
eral conclusions to be made concerning mare basalt types
on the frontside of the moon.

1.   Regional basalt types exist. There are regions
up to hundreds or perhaps thousands of square kilometers
in extent of essentially uniform surface composition.
There are also groups of smaller flows that are widely
separated but nevertheless apparently identical in character.
The homogeneity of some surface units is evident in var-
ious spectral ratio images for extensive regions. The
spectral character of a few of these units have been studied
in detail, providing information to allow their regional
extent to be mapped (e.g., Mare Tranquillitatis, Central
Serenitatis, NE Humorum, West Imbrium;   see   Section
IIB). One implication of the observed regional homogeneity
is that if surface fractionation processes act to signi-
ficantly change the surface composition (or spectral char-
acter of a unit) then such processes must do so uniformly
over extensive areas.

2.   Basalt types have been characterized (from soil
spectra) in terms of certain useful geochemical character-
istics (e.g., TiO_2 content) and mineralogical features

(glass and pyroxene components).

3. About 15 spectrally <u>distinct surface units can be identified for mare soils</u>. These represent at least 6 fundamental (extensive) basalt types or related series.

(a) Apollo 12, 15 (m_1, l_1) low titanium basalts found in most nearside regions. SAMPLED.

(b) Apollo 17, 11, Luna 16 (H_1, h_1) high to medium high titanium basalts found on the eastern moon. Weak pyroxene band, weak glass (Fe^{2+}) band. SAMPLED.

(c) Flamsteed, Imbrium (H_2, h_2, m_2) high to medium titanium basalts found <u>only</u> on the western moon. Weak pyroxene band, strong glass (Fe^{2+}) band. UNSAMPLED. These basalts include the western "blue" basalts with TiO_2 content likely to be distinctly high, comparable to that at Apollo 11, but with different mafic mineralogy or composition.

(d) Mare Humorum (h_3) medium high titanium basalts found only in the western maria. Strong pyroxene band, strong glass (Fe^{2+}) band. UNSAMPLED.

(e) Serenitatis (m_4) low titanium basalts. Strong pyroxene band, strong glass (Fe^{2+}) band. UNSAMPLED.

(f) East Imbrium, Frigoris (L_2, L_4) (very) low titanium basalts. UNSAMPLED.

4. Although not all regions have been spectrally ana-
lyzed, it is clear that <u>the lunar samples represent only
a few of the major basalt types on the lunar surface</u>.
It appears that about 2/3 of the lunar maria are not repre-
sented in the lunar sample collection returned by U.S.
Apollo and Soviet Luna missions.

5. <u>All mare surfaces contain lateral variations of
compositionally heterogeneous basalts</u>. Although a few
regions contain vast areas of apparently homogeneous ba-
salt (conclusion 1) many mare regions are heterogeneous
on the lateral scale of 2-50 kilometers. This heterogeneity
is apparent in any detailed study of high resolution spec-
tral images. An example of this lateral heterogenity oc-
curs at the Apollo 12 landing area. Remote sensing stu-
dies show   two compositionally distinct units within
a few kilometers. Recent examination of the Apollo 12
ilmenite basalts indicates they are unrelated to the rest
of the Apollo 12 low-Ti basalts and may indeed represent
this second unit. These two basalt types were roughly
contemporaneous.

6. <u>Mare fill (even in the mascon basins) may also
be stratigraphically heterogeneous</u>. The only spectrally
documented case is Mare Crisium for which the likely se-
quence of mare fill, oldest to youngest, was: a high-Ti

basalt, a (very) low-Ti basalt, and a (medium) low-Ti ba-
salt. Photogeologic evidence and multispectral imagery
strongly suggests Mare Serenitatis may have had a somewhat
similar sequence of fill (high-Ti followed by low-Ti).
The western maria seem to be far more complex.

7. <u>Some basalt types are spectrally gradational sug-
gesting minor variation in geochemistry; three regional
series can be identified.</u> Two clear series are evident
in the western maria: (a) Flamsteed-Imbrium high to medium
high-Ti basalts (H_2, h_2, m_2), and (b) Mare Humorum medium
high-Ti basalts (h_3 varying in TiO_2 by about 3%). It is
suggested that the basalts for each series are derived
from the same source region with minor variation in P,
T, chemistry or degree of partial melting. The observed
variations could also be due to near surface fractionation.
The Flamsteed flows (see Figure IID-21) appear to be in-
dividually homogeneous and distinct, whereas the variations
in the Humorum basalts are regionally diffuse. Spectral
data also indicates there may exist a sequence of basalt
types in the eastern maria that range in composition from
Apollo 11 (H_1) to Luna 16 (h_1).

8. Although most mare surfaces are now composed of
mature soil, more crystalline material is excavated by
fresh craters. Spectra of fresh craters are comparable

to those obtained for laboratory samples of very immature soils and allow the mineralogy of an ejecta unit to be examined. The variations in spectral features for fresh craters are known to be directly related to specific mineral absorption features of minerals. Thus, if spectra to 2.5μm are obtained for fresh craters, components of the mineralogy of the excavated unit can be discerned.

V. SUMMARY AND SYNTHESIS

B. Inferences

The spectral information (both spectra and imagery) integrated with other global data (e.g., Ap 15, 16 orbital geochemistry, relative age units derived from crater degradation studies, thermal and geochemical models of the moon, etc.) support the following inferences.

1. The bi-modal relationship observed in both age and TiO$_2$ content of mare basalt samples is likely to be simply a matter of limited sampling. The spectral data suggest a continuum of TiO$_2$ content for mare basalts. When spectral data for TiO$_2$ are combined with crater degradation age units of Boyce (1976), a more complicated relationship emerges (e.g., Soderbloom and Boyce, 1976). From the data currently available, an update of the TiO$_2$ and age relationship of Papike et al. (1976) is estimated and is shown in Figure V-1.

2. It is unlikely that the lunar mantle is zoned in any simple global sense and that the sequence of observed basalts is simply the result of partial melting of progressively deeper regions. Thermal models show that the upper limit of a zone of partial melt in the lunar mantle becomes deeper with time. Any thermal and geochemical model for the source region of mare basalts must also account for
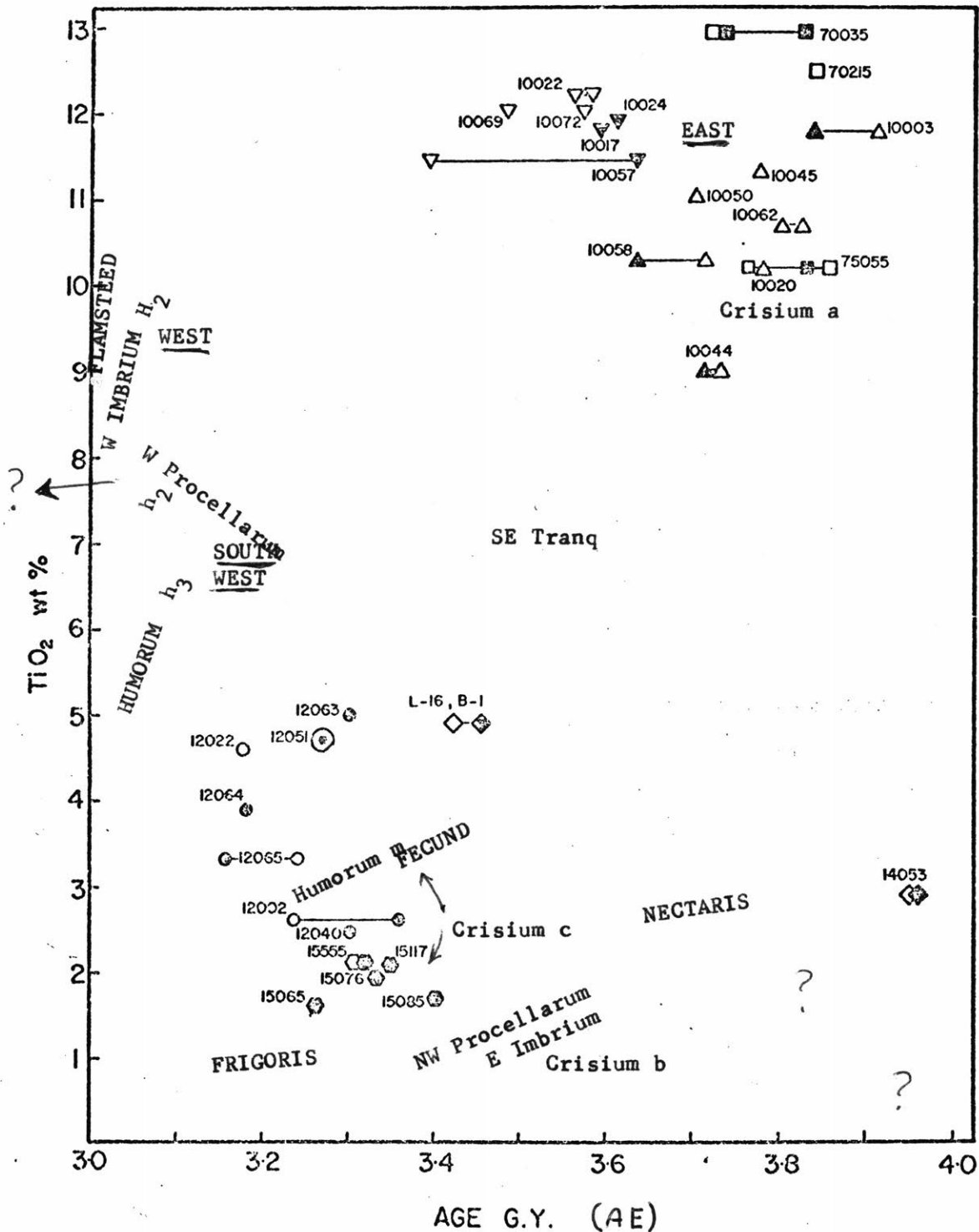
Figure V l.   Estimates of TiO$_2$ content (from continuum
slope) and age (from Boyce, 1976) for various sampled
and unsampled mare basalts.   (The TiO$_2$ content estimates
are very rough since the data are claibrated for soils.)
Lunar sample information was compiled by Papike et al.,
(1976).   Many basalt types appear to occur simultaneously.
The pattern, if there is any, suggests the earliest basalts
were either very high-Ti or very low-Ti.   Around 3.3 AE
large amounts of medium low-Ti basalts were produced.   There
appears to be an increase of TiO$_2$ with the latest basalts.

the frequently observed heterogeneity of nearly contempor-
aneous basaltic units both locally and globally. For ex-
ample, if the same source region depth was tapped for the
two Apollo 12 types of basalt, then the lunar mantle must
contain significant lateral heterogeneities. An alterna-
tive model is that different depths are tapped within
the zone of partial melting during any particular lunar
era.

    3. <u>The lunar nearside maria can be roughly divided
into two and perhaps three regions which seem to have evolved
independently in terms of both time and geochemistry</u>:
activity in the eastern maria apparently ended first; in
the western maria last; and in the southwestern maria (Hu-
morum, Nubium) perhaps sometime between the two. Orbital
geochemistry indicates a concentration of heat producing
elements in the surface rocks of the western regions, per-
haps implying a more vigorous radioactive heat source
at depth.

V. SUMMARY AND SYNTHESIS

C. Recommendations

A few specific and general recommendations for the
lunar science community (and NASA) are perhaps justified
from these results and inferences.

1. Since many major lunar basalt units have not been
sampled directly, the continued search for other distinct
basalt types as minor fragmental components of the returned
samples could significantly increase the information from the
samples. The recent discovery of VLT basalts in the Apollo
17 core shows that this is a fruitful endeavor. It is
likely that correlated studies between sample and remote
sensing geochemists can identify the type area of such
minor components.

2. Caution should be exercised in extrapolating lunar
sample information to global geochemistry. The sequence
of mare basalt extrusion is locally and globally geochem-
ically variable and complex. This is not to say regional
patterns cannot be identified and characterized, but it
is important to recognize that only a limited amount of
geochemical information is available in the samples.

3. Integrated studies between lunar sample geochemists
and remote sensing specialists should be encouraged. Two
specific topics need to be addressed:

(a) "Ground Truth" must be rigorously defined. The
largest scale observable in the laboratory is measured
in centimeters. The smallest scale currently observable
with remote sensing techniques is measured in kilometers.
The rock types identified in the samples need to be related
to regional units observed remotely. Furthermore, the
two types of data need to be expressed in the same terms.
For example, spectroscopic techniques can determine the
<u>average pyroxene</u> composition for a regional rock type (which
varies from one rock type to another). "Average pyroxene
composition", however, is somewhat a foreign concept to
petrographers.

(b) An accurate model of soil genesis needs to be
developed that quantitatively links the mineralogy and
geochemistry of the regional rock type (s) to that for
a mature soil. Most of the lunar surface has developed
a regolith and mature soil, and it is such a <u>soil</u> that is
observed using remote sensing techniques. On the other
hand, most useful laboratory geochemistry is based on crys-
talline or <u>rock</u> samples.

4. <u>An effective program of lunar surface exploration
can and should be undertaken to map the global geochemistry
of the moon</u>. The rational for such a program is twofold:

(a) The scientific understanding of the moon that resulted from the Apollo program has matured to the extent that global data will permit a maximum scientific yield from the huge investment in Apollo. The U.S. scientific expertise that has enthusiastically carried this exploration program will be dispersed if lunar exploration is terminated half-way through the sequence.

(b) If the moon is to be utilized in the future as a scientific and economic resource, the global chemistry must first be mapped and explored. With present technology, such an assessment of lunar materials and resources is relatively easy and can be done at low cost.

A limited amount of further geochemical information can and should be obtained using earth-based telescopes and recently developed spectroscopic instruments. The obvious and perhaps ultimate application of spectral reflectance techniques for remotely determining lunar geochemistry would be done from lunar orbit: continuous high resolution (1/2 km) spectroscopy (.3 - 2.5μm) of surfaces and craters with detailed two-dimensional spectral mapping at selected useful wavelengths.

The spectral reflectance study of lunar basalts presented here has shown that there are significant numbers of unexplored regions and unsolved problems that cannot

be understood simply by a more extensive study of the lunar
samples. A rigorous program of lunar exploration is cer-
tain to uncover many unexpected and extremely useful facts
about the moon. If the moon is to be utilized as a long-
range asset, rather than simply an object of interesting
beauty, detailed exploration and mapping is an essential
endeavor.

REFERENCES

RESUME

PUBLICATION LIST

References

Abu-Eid, R.M. and Burns, R.G. (1976) The effect of pressure
    on the degree of covalency of the cation-oxygen bond
    in minerals. Am. Mineral., 61, 391-397.

Adams, J.B. (1967) Lunar surface composition and particle
    size: Implications from laboratory and lunar spectral
    reflectance data. J. Geophys. Res., 72, 5717-5720.

Adams, J.B. (1968) Lunar and Martian surfaces: Petrologic
    significance of absorption bands in the near-infrared.
    Science, 159, 1453-1455.

Adams, J.B. (1974) Visible and near-infrared diffuse reflec-
    tance spectra of pyroxenes as applied to remote sensing
    of solid objects in the solar system. J. Geophys. Res.,
    79, 4829-4836.

Adams, J.B. (1975) Interpretation of visible and near-infrared
    diffuse reflectance spectra of pyroxenes and other rock-
    forming minerals. In Infrared and Raman Spectroscopy
    of Lunar and Terrestrial Materials (C. Karr, Jr., Ed.)
    Academic Press, New York, pp. 91-116.

Adams, J.B. (1977) Titanium in lunar soils: Determination
    by remote spectral reflectance measurements. To be sub-
    mitted to Geophys. Res. Let.

Adams, J.B. and Charette, M.P. (1975) Effects of maturation
    on the reflectance of the lunar regolith: Apollo 16 -
    a case study. The Moon, 13, 293-299.

Adams, J.B. and Charette, M.P. (1977) Spectral reflectance
    properties of lunar soils. To be submitted to Reviews
    of Geophys.

Adams, J.B. and Filice, A.L. (1967) Spectral Reflectance
    0.4 to 2.0 microns of silicate rock powders. J. Geophys.
    Res., 72, 5705-5715.

Adams, J.B. and Jones, R.L. (1970) Spectral reflectivity
    of lunar samples. Science, 167, 737.

Adams, J.B. and McCord, T.B. (1969) Mars: Interpretation
    of spectral reflectivity of light and dark regions.
    J. Geophys. Res., 74, 4851-4856.

Adams, J.B. and McCord, T.B. (1970) Remote sensing of lunar
    surface mineralogy: Implications from visible and near-
    infrared reflectivity of Apollo 11 samples. Proc. Apollo
    Lunar Conf., 3, 1937-1945.

Adams, J.B. and McCord, T.B. (1971a) Optical properties
    of mineral separates, glass, and anorthositic fragments
    from Apollo mare samples. Proc. Lunar Sci. Conf. 2nd,
    2183-2195.

Adams, M.B. and McCord, T.B. (1971b) Alteration of lunar
    optical properties: Age and composition effects. Science,
    171, 567-571.

Adams, J.B. and McCord, T.B. (1972) Electronic spectra of
    pyroxenes and interpretation of telescopic spectral re-
    flectivity curves of the moon. Proc. Lunar Sci. Conf.
    3rd, 3021-3034.

Adams, J.B. and McCord, T.B. (1973) Vitrification darkening
    in the lunar highlands and identification of Descartes
    material at the Apollo 16 site. Proc. Lunar Sci. Conf.
    4th, 163-177.

Adams, J.B. and McCord, T.B. (1976) Mercury: Evidence for
    an anorthositic crust from reflectance spectra (abstract).
    Conf. on comparisons of Mercury and the Moon, p.1. The
    Lunar Science Institute, Houston.

Adams, J.B. and McCord, T.B. (1977) Mercury: Evidence
    for a feldsparthic crust from spectral reflectance mea-
    surements. To be submitted to J. Geophys. Res.

Adams, J.B., Bell, P.M., Conel, J.E., Mao, H.K., McCord,
    T.B., and Nash, D.B. (1973) Visible and near-infra-red
    transmission and reflectance measurements of the Luna
    20 soil. Geochimica et Cosmochimica Acta, 37, 731-743.

Adams, J.B., Pieters, C., and McCord, T.B. (1974) Orange
    glass: Evidence for regional deposits of pyroclastic
    origin on the moon. Proc. Lunar Sci. Conf. 5th, 171-
    186.

Adams, J.B., Pieters, C., Gaffey, M., and Catalano, C. (1977)
    Reflectance spectra of lunar soil samples relative to
    MS-2: Cumulative atlas, Dept. of Geol. Sci., Univ. of
    Wash., Seattle, unpublished.

Agrell, S.O., Scoon, J.H., Muir, I.D., Long, J.V.P., McConnell,
    J.D.C., and Peckett, A. (1970) Observations on the chem-
    istry, mineralogy and petrology of some Apollo 11 lunar
    samples. Proc. Apollo 11 Lunar Sci. Conf., 93-128.

Anders, E., Ganapathy, R., Krahenbuhl, A., and Morgan (1973)
    Meteoritic material on the moon. The Moon, 8, 3-24.

Ayuso, R.A., Bence, A.E., and Taylor, S.R. (1976) Upper
    Jurassic Tholeiitic Basalts from DSDP Leg 11. J. Geophys.
    Res., 81, 4305.

Baird, A.K., Toulmin III, P., Clark, B.C., Rose, Jr., H.J.,
    Keil, K., Christian, R.P., and Gooding, J.L. (1976) Min-
    eralogic and Petrologic Implications of Viking geochem-
    ical results from Mars: Interim Report. Science, 194,
    1288-1291.

Baker, P.E. (1968) Comparative volcanology and petrology
    of the Atlantic Island-arcs. Bull. Volc., 32, 189-206.

Baker, I. (1969) Petrology of the volcanic rocks of Saint
    Helena Island, South Atlantic. Bull. Geol.Soc. Am.,
    80, 1283-1310.

Barbarshov, N.P. (1973) Light map of the visible side of
    the moon. Academy of Sciences of the Ukrainian SSR,
    Kiev.

Barshay, S.S. and Lewis, J.S. (1976) Chemistry of primitive
    solar material. Ann. Rev. of Astronomy and Astrophys.,
    14, 81-91.

Barsukov, V.L. and Florensky, C.P. (1977) The lunar soil
from Mare Crisium: Preliminary data (abstract). In
Lunar Science VIII, p. 61-63. The Lunar Science Institute,
Houston.

Barsukov, V.L., Ivanov, A.V., Nazarov, M.A., Rode, O.D.,
Stakeev, Yu.I., Tarasov, L.L., Tobelko, K.I., and Flo-
rensky, C.P. (1977) Preliminary description of the re-
golith core from Mare Crisium (abstract). In Lunar Science
VIII, p. 67-69. The Lunar Science Institute, Houston.

Bell, P.M., Mao, H.K., and Weeks, R.A. (1976) Optical spec-
tra and electron paramagnetic resonance of lunar and
synthetic glasses: A study of the effects of controlled
atmosphere, composition, and temperature. Proc. Lunar
Sci. Conf. 7th, 2543-2559.

Bell, P.M. and Mao, H.K. (1977) Optical spectra of thin
metallic coatings with application to the spectra of
lunar soil samples (abstract). In Lunar Science VIII,
p. 88-90. The Lunar Science Institute, Houston.

Bell, P.M., Mao, H.K., and Rossman, G.R. (1975) Absorption
spectroscopy of ionic and molecular units in crystals
and glass. In Infrared and Raman Spectroscopy of Lunar
and Terrestrial Materials (C. Karr, Jr., Ed.) Academic
Press, New York, pp. 1-38.

Blasius, K.R. and Cutts, J.A. (1976) Shield volcanism and
lithospheric structure beneath the Tharsis plateau, Mars.
Proc. Lunar Sci. Conf. 7th, 3561-3573.

Boon, J.A. and Fyfe, W.S. (1972) The coordination number
of ferrous ions in silicate glasses. Chem. Geol., 10,
287.

Bowen, N.L. (1928) The Evolution of the Igneous Rocks, Do-
ver Publications, Inc., New York, 332 pp.

Boyce, J.M. (1976) Age of flow units in the lunar nearside
maria based on Lunar Obriter IV photgraphs. <u>Proc. Lunar
Sci. Conf. 7th</u>, 2717-2728.

Briggs, P.L. (1976) Solar wind heating of asteroids. Masters
Thesis. MIT, Cambridge, Mass. 63pp.

Bryan, W.B., Thompson, G., Frey, F.A., and Dickey, J.S. (1976)
Inferred geologic settings and differentiation in basalts
from the deep-sea drilling project. <u>J. Geophys. Res.</u>, <u>81</u>,
4285.

Burke, K., Dewey, J.F., and Kidd, W.S.F. (1976) Dominance of
horizontal movements, arc and microcontinental collisions
during the later permobile regime. In <u>The Early History of
the Earth</u> (B.F. Windley, Ed.) John Wiley & Sons, Ltd. pp.
113-129.

Burns, R.G. (1970a) <u>Mineralogical Applications of Crystal Field
Theory</u>, Cambridge Univ. Press, London, 224 pp.

Burns, R.F. (1970b) Crystal field spectra and evidence of
cation ordering in olivine minerals. <u>Am. Mineral.</u>, <u>55</u>,
1608-1632.

Burns, R.G. and Fyfe, W.S. (1967) Crystal-field theory and the
geochemistry of transition elements. In <u>Researches in Geo-
chemistry</u> (P.H. Abelson, Ed.) John Wiley & Sons, Ltd.,
New York, pp. 259-285.

Burns, R.G. and Vaughan, D.J. (1975) Polarized electronic
spectra. In <u>Infrared and Raman Spectroscopy of Lunar and
Terrestrial Materials</u> (C. Karr, Jr., Ed.) Academic Press,
New York, p. 39-72.

Burns, R.B., Vaughan, D.G., Abu-Eid, R.M., Witner, M., and
Morawski, A. (1973) Spectral evidence for Cr^{3+}, Ti^{3+}, and
Fe^{2+} rather than Cr^{2+} and Fe^{3+} in lunar ferromagnesian
silicates. <u>Proc. Lunar Sci. Conf. 4th</u>, 983-994.

Burns, R.G., Parkin, K.M., Loeffler, B.M., Leung, I.S., and
Abu-Eid, R.M. (1976) Further characterization of spectral
features attributable to titanium on the moon. <u>Proc. Lunar
Sci. Conf. 7th</u>, 2651-2578

Cameron, A.G.W. (1973) Abundances of the elements in the solar system. Space Sci. Rev., 15, 121-146.

Carmichael, I.S.E. (1964) The petrology of Thingmuli, a tertiary volcano in Eastern Iceland. J. Petrol., 5, 435-460.

Carmichael, I.S.E., Turner, F.J., and Verhoogen, J. (1974) Igenous Petrology. McGraw Hill Book Co., 739 pp.

Carr, M.H. (1973) Volcanism on Mars. J. Geophys. Res., 78, 4049-4062.

Chapman, C.R., Morrison, D., and Zellner, B. (1975) Surface properties of asteroids: A synthesis of polarimetry, radiometry, and spectrophotometry. Icarus, 25, 104-130.

Charette, M.P. and Adams, J.B. (1975a) Agglutinates as indicators of lunar soil maturity: The rare gas evidence at Apollo 16. Proc. Lunar Sci. Conf. 6th, 2281-2289.

Charette, M.P. and Adams, J.B. (1975b) Mare basalts: Characterization of compositional parameters by spectral reflectance. In Origin of Mare Basalts, p. 25-28. The Lunar Science Institute, Houston.

Charette, M.P. and Adams, J.B. (1977a) Spectral reflectance of lunar highland rocks (abstract). In Lunar Science VIII, p. 172-175. The Lunar Science Institute, Houston.

Charette, M.P. and Adams, J.B. (1977b) A method for remote determination of the FeO content of lunar soils using spectral reflectance measurements. To be submitted to J. Geophys. Res.

Charette, M.P. McCord, T.B., Pieters, C., and Adams, J.B. (1974) Application of remote spectral reflectance measurements to lunar geology classification and determination of titanium content of lunar soils. J. Geophys. Res., 79, 1605-1613.

Chayes, F. (1975) Statistical petrology. _Carnegie Inst. Ann. Report Dir. Geophys. Lab. 1974-1975_, 542-550.

Clayton, R.N., Onuma, N., and Mayeda, T.K. (1976) A classification of meteorites based on oxygen isotopes. _Earth Plan. Sci. Lett._, _30_, 10-18.

Conel, J.E. (1970) Coloring of synthetic and natural lunar glass by titanium and iron. _Jet Prop. Lab. Space Prog. Sum._, _3_, 26-31.

Conel, J.E. and Nash, D.B. (1970) Spectral reflectance and albedo of Apollo 11 samples: Effects of irradiation and vitrification and comparisons with telescopic observations. _Geochim. Cosmochim. Acta_, Suppl. 1, 2013.

Dalrymple, G.B., Silver, E.A., and Jackson, E.D. (1973) Origin of the Hawaiian Islands. _Amer. Sci._, _61_, 294-308.

DePaolo, D.J. and Wasserburg, G.J. (1976) Inferences about magma sources and mantle structure from variations of $^{143}Nd/^{144}Nd$. _Geophys. Res. Lett._, _3_, 743.

Dollfus, A. (1961) Visual and photographic studies of planets at the Pic du Midi. In _Planets and Satellites_ (G. P. Kuiper and B.M. Middlehurst, Eds.) Univ. of Chicago Press, Chicago. p. 534-572.

Dollfus, A. and Auriere, M. (1974) Optical polarimetry of planet Mercury. _Icarus_, _23_, 465-482.

Drake, M.J. and Consolmagno, G.J. (1976) Critical review of models for the evolution of high-Ti mare basalts. _Proc. Lunar Sci. Conf. 7th_, 1633-1657.

Duke, M.B. and Silver, L.T. (1967) Petrology of eucrites, howardites and mesosiderites. _Geochim. Cosmochim. Acta_, _31_, 1637-1665.

Eichelberger, J.C. (1974) Magma contamination within the volcanic pile: Origin of andesite and dacite. _Geology_, 29-33.

Engel, A.E.J., Engel, C.G., and Havens, R.G. (1965) Chemical characteristics of oceanic basalts and the upper mantle. Geol. Soc. Am. Bull., 76, 719-734.

Faure, G. and Powell, J.L. (1972) Strontium Isotope Geology, Springer Verlay, New York. 188 pp.

Florensky, C.P., Basilevsky, A.T., Burba, G.A., Nikolaeva, O.V., Pronin, A.A., Volkov, V.P. and Ronca, L.B. (1977) First panoramas of the Venusian surface (abstract). In Lunar Science VIII, p. 302-304. The Lunar Science Institute, Houston.

Frey, F.A., Bryan, W.B., and Thompson, G. (1974) Atlantic Ocean floor: Geochemistry and petrology of basalts from legs 2 and 3 of the Deep-Sea Drilling Project. J. Geophys. Res., 79, 5507-5527.

Gaffey, M.J. (1973) A systematic study of the spectral reflectivity characteristics of the meteorite classes with applications to the interpretation of asteroid spectra for mineralogical and petrological information. Ph.D. dissertation, M.I.T., Cambridge, Mass. 355 pp.

Gaffey, M.J. (1975) Qualification of spectral reflectance characteristics for mineralogical and petrological information. Paper and abstract presented at Annual Meeting of AAS/DPS, Columbia, Maryland, 17-21 February, 1975.

Gaffey, M.J. (1976) Spectral reflectance characteristics of the meteorite classes. J. Geophys. Res., 81, 905-920.

Gaffey, M.J. (1977) Deconvolution of laboratory reflectance spectra of whole rock powders into spectral components for each constituent mineral. In preparation.

Gaffey, M.J. and McCord, T.B. (1976) Asteroid surface materials from reflectance spectroscopy: A review. Proc. of IAU Col. #39, Lyons, France.

Gast, P.W. (1967) Trace element fractionation and the origin
of tholeiitic and alkaline magma types. Geochim. Cosmochim.
Acta, 32, 1057-1086.

Gast, P.W. (1972) The chemical composition and structure of the
Moon. The Moon, 5, 121-148.

Glikson, A.Y. (1976) Earliest Precambrian ultramafic-mafic vol-
canic rocks: Ancient oceanic crust of relic terrestrial
maria? Geology, 201-205.

Goldstein, R.M., Green, R.R., and Rumsey, H.C. (1976) Venus
radar images. J. Geophys. Res., 81, 4807-4817.

Green, D.H. (1971) Composition of basaltic magmas as indicators
of conditions of origin: application to oceanic volcanism.
Phil. Trans. Roy. Soc. Lond., 268, 707-725.

Green, D.H. (1972) Archean greenstone belts may include terres-
trial equivalents of lunar maria? Earth Plan. Sci. Lett.,
15, 263-270.

Green, D.H. (1975) Genesis of Archean peridotitic magmas and
constraints on Archean geothermal gradients and tectonics.
Geology, 3, 15-18.

Green, D.H. and Ringwood, A.E. (1967) The genesis of basaltic
magmas. Contrib. Mineral. Petrol., 15, 103-190.

Green, D.H., Nicholls, I.A., Viljoen, J., and Viljoen, R.
(1975a) Experimental demonstration of the existence of per-
idotitic liquids in earliest Archean magmatism. Geology,
3, 11-14.

Green, D.H., Ringwood, A.E., Hibberson, W.O., and Ware, N.G.
(1975b) Experimental petrology of Apollo 17 mare basalts.
Proc. Lunar Sci. Conf. 6th, 871-893.

Hapke, B. (1971) Optical properties of the lunar surface. In
Physics and Astronomy of the Moon (Z. Kopal, Ed.) Academic
Press, New York, pp. 155-211.

Hapke, B., Cassidy, W., and Wells, E. (1975) Effects of vapor
deposition procession on the optical, chemical and magnetic
properties of the lunar regolith. The Moon, 13, 339-353.

Hart, S.R. (1971) K, Rb, Cs, Sr, and Ba contents and Sr
    isotope ratios of ocean floor basalts. Phil. Trans.
    Roy. Soc. Lond., 268, 573.

Hart, S.R., Brooks, C., Krogh, T.E., Davis, G.L., and Na-
    va, D. (1970) Ancient and modern volcanic rocks: A trace
    element model. Earth Plan. Sci. Lett., 10, 17-28.

Hays, J.F. and Walker, D. (1974) Lunar igenous rocks and
    the nature of the lunar interior. Proc. Sov.-Am. Conf.
    on Cosmochem. of Moon & Planets. The Lunar Science In-
    stitute, Houston.

Head, J.W. (1975) Lunar mare deposits: Areas, volumes,
    sequence, and implication for melting in source areas.
    In Origin of Mare Basalts, p. 66-69. The Lunar Science
    Institute, Houston.

Head, J.W. (1976) Lunar volcanism in space and time. Rev.
    Geophys. Space Phys., 14, 265-300.

Head, J.W. and McCord, T.B. (1977) Evidence for extrusive
    highland volcanics of Imbrium age: The Gruithuisen domes.
    In preparation.

Head, J.W., Pieters, C., McCord, T.B., Adams, J.B., and
    Zisk, S. (1976) Definition and detailed characterization
    of lunar surface units using remote observations (ab-
    stract). In Lunar Science VII, p. 357-359. The Lunar
    Science Institute, Houston.

Head, J.W., Pieters, C., McCord, T., Adams, J., and Zisk,
    S. (1977) Definition and detailed characterization of
    lunar surface units using remote observations. Submitted
    to Icarus.

Hekinian, R. and Thompson, G. (1976) Comparative geochem-
    istry of volcanics from rift valleys, transform faults
    and aseismic ridges. Contrib. Mineral. Petrol., 57,
    145-162.

Hollister, L.S. (1975) Evolution of the moon between 4.6 and 3.3 AE. Proc. Lunar Sci. Conf. 6th, 1159-1178.

Hollister, L.S., Trzcienski, Jr., W.E., Hargraves, R.B., and Kulick, C.G. (1971) Petrogenetic significance of pyroxenes in two Apollo 12 samples. Proc. Lunar Sci. Conf. 2nd, 529-557.

Housley, R.M., Grant, R.W., and Paton, N.E. (1973) Origin and characteristics of excess Fe metal in lunar glass welded aggregates. Proc. Lunar Sci. Conf. 4th, 2737-2749.

Hubbard, N.J. and Minear, J.W. (1975) A physical and chemical model of early lunar history. Proc. Lunar Sci. Conf. 6th, 1057-1085.

Hubbard, N.J., Rhodes, J.M., and Gast, P.W. (1973) Chemistry of lunar basalts with very high alumina contents. Science, 181, 339-342.

Huguenin, R.L. (1973a) Photostimulated oxidation of magnetite. 1. Kinetics and alteration phase identification. J. Geophys. Res., 78, 8481-8494.

Huguenin, R.L. (1973b) Photostimulated oxidation of magnetite. 2. Mechanism. J. Geophs. Res., 78, 8495-8506.

Huguenin, R.L. (1974) The formation of geothite and hydrated clay minerals on Mars. J. Geophys. Res., 79, 3895-3905.

Huguenin, R.L. (1975) Crystal field and charge transfer band assignments in iron (III) oxides and oxyhydroxides: Application to Mars. Paper and abstract presented at annual meeting of AAS/DPS, Columbia, Maryland, 17-21 February, 1975.

Huneke, J.C., Podosek, F.A., and Wasserberg, G.J. (1972) Gas retention and cosmic ray exposure ages of a basalt fragment from Mare Fecunditatis. Earth Planet. Sci. Letts., 13, 375-383.

Hunt, G.R. and Salisbury, J.W. (1970) Visible and near-infrared spectra of minerals and rocks: I. Silicate Minerals. Mod. Geol., 1, 283-300.

Hunt, G.R. and Salisbury, J.W. (1971) Visible and near-infrared spectra of minerals and rocks: II. Carbonates. Mod. Geol., 2, 23-30.

Hunt, G.R. and Salisbury, J.W. (1976a) Visible and near infrared spectra of minerals and rocks: XI. Sedimentary rocks. Mod. Geol., 5, 211-217.

Hunt, G.W. and Salisbury, J.W. (1976b) Visible and near infrared spectra of minerals and rocks: XII. Metamorphic rocks. Mod. Geol. 5, 219-228.

Hunt, G.R., Salisbury, J.W., and Lenhoff, C.J. (1971a) Visible and near-infrared spectra of minerals and rocks: III. Oxides and hydroxides. Mod. Geol., 2, 195-205.

Hunt, G.R., Salisbury, J.W., and Lenhoff, C.J. (1971b) Visible and near-infrared spectra of minerals and rocks: IV. Sulphides and sulphates. Mod. Geol., 3, 1-14.

Hunt, G.W., Salisbury, J.W., and Lenhoff, C.J. (1972) Visible and near-infrared spectra of minerals and rocks: V. Halides, phosphates, arsenates, vanadates and borates. Mod. Geol., 3, 121-132.

Hunt, G.R., Salisbury, J.W., and Lenhoff, C.J. (1973a) Visible and near infrared spectra of minerals and rocks: VI. Additional silicates. Mod. Geol., 4, 85-106.

Hunt, G.R., Salisbury, J.W., and Lenhoff, C.J. (1973b) Visible and near-infrared spectra of minerals and rocks: VII. Acidic igneous rocks. Mod. Geol., 4, 217-224.

Hunt, G.R., Salisbury, J.W., and Lenhoff, C.J. (1973c) Visible and near-infrared spectra of minerals and rocks. VIII. Intermediate igneous rocks. Mod. Geol., 4, 237-244.

Hunt, G.R., Salisbury, J.W. and Lenhoff, C.J. (1974) Visible and near infrared spectra of minerals and rocks: IX. Basic and ultrabasic igneous rocks. Mod. Geol., 5, 15-22.

Hurley, M., Batement, C., Fairbairn, W., and Pinson, Jr., H. (1965) Investigation of initial Sr^{87}/Sr^{86} ratios in the Sierra Nevada plutonic province. Geol. Soc. of Am. Bull., 76, 165-174.

Irving, A.J. (1975) Chemical, mineralogical and textural systematics of non-mare melt rocks: Implications for lunar impact and volcanic processes. Proc. Lunar Sci. Conf. 6th, 363-394.

Jahn, B. and Nyquist, L.E. (1976) Crustal evolution in the early Earth-Moon system: Constraints from Rb-Sr studies. In The Early History of the Earth (B.F. Windley, Ed.) John Wiley & Sons, Ltd.

James, O.B. and Wright, T.L. (1972) Apollo 11 and 12 mare basalts and gabbros: Classification, composition variations, and possible petrogenetic relations. Geol. Soc. of Am. Bull., 83, 2357-2382.

Johnson, D.H., McGetchin, T.R., and Toksöz, M.N. (1974) The thermal state and internal structure of Mars. J. Geophys. Res., 79, 3959-3971.

Johnson, T.V. and Soderblom, L.A. (1969) Relative reflectivity (0.4µ to 1.1µ) of the lunar landing site Apollo 7. J. Gephys. Res., 74, 6046-6048.

Johnson, T.V., Pieters, C., and McCord, T.B. (1972) Mare Humorum: An integrated study of spectral reflectivity. Icarus, 19, 224-229.

Johnson, T.V., Matson, D.L., Phillips, R.J., and Saunders, R.S. (1975a) Vidicon spectral images: A geophysical study of the Lamont feature (abstract). In Lunar Science VI, p. 444. The Lunar Science Institute, Houston.

Johnson, T.V., Matson, D.L., Phillips, R.J., and Saunders, R.S. (1975b) Vidicon spectral imaging: Color enhancement and digital maps. Proc. Lunar Sci. Conf. 6th, 2677-2688.

Kaula, W.M and Yoder, C.F. (1976) Lunar orbit evolution and tidal heating of the moon (abstract). In Lunar Science VII, p. 440-442. The Lunar Science Institute, Houston.

Kay, R., Hubbard, N.J., and Gast, P.W. (1970) Chemical characteristics and origin of oceanic ridge volcanic rocks. J. Geophys. Res., 75, 1585.

Kennedy, W.Q. (1933) Trends of differentiation in basaltic magmas. Am. J. Sci., 25, 239-256.

Kesson, S.E. (1975) Mare basalts: Melting experiments and petrogenetic interpretations. Proc. Lunar Sci. Conf. 6th, 921-944.

Kesson, S.E. and Lindsley, D.H. (1976) Mare basalt petro-genesis--A review of experimental studies. Rev. Geophys. and Space Physics, 14, 361-373.

Kesson, S.E. and Ringwood, A.E. (1976) Mare basalt petro-genesis in a dynamic moon. Earth Planet. Sci. Lett., 30, 155-163.

Kuno, H. (1967) Volcanological and petrological evidences regarding the nature of the upper mantle. In The Earth's Mantle (T.F. Gashul, Ed.) Academic Press, New York. pp. 89-110.

Kurat, G., Kracher, A., Keil, K., Warner, R. and Prinz, M. (1976) Composition and origin of Luna 16 aluminous mare basalts. Proc. Lunar Sci. Conf. 7th, 1301-1321.

Lane, A.P. and Irvine, W.M. (1973) Monochromatic phase curves and albedos for the lunar disk. Astron. J., 78, 267-277.

Larson, R.L. and Chase, C.G. (1972) Late mesozoic evolution of the western Pacific Ocean. Geol. Soc. Am. Bull., 83, 3627-3644.

Lee, T., Papanastassiou, D.A., and Wasserburg, G.J. (1976) Demonstration of ^{26}Mg excess in Allende and evidence for ^{26}Al. Geophys. Res. Lett., 3, 109-112.

Lewis, J.S. (1974a) The temperature gradient in the solar nebula. Science, 186, 440-443.

Lewis, J.S. (1974b) The chemistry of the solar system. Sci. Am., March, 1974, 283-292.

Lipman, P.W. (1977) Hawaiian volcanoes and the Taos Plateau. Seminars presented to Q21 at Los Alamos Sci. Lab, 2/11/77.

Loeffler, B.M., Burns, R.G., Tossell, J.A., Vaughan, D.J., and Johnson, K.H. (1974) Charge transfer in lunar mater-ials: interpretation of ultraviolet visible spectral properties of the moon. Proc. Lunar Sci. Conf. 5th, 3007-3016.

Loeffler, B.M., Burns, R.G., and Tossell, J.A. (1975) Metal →metal charge transfer transitions: Interpretation of visible-region spectra of the moon and lunar materials. Proc. Lunar Sci. Conf. 6th, 2663-2676.

Longhi, J. (1977) Magma oceanography: 2. Chemical Evolution (abstract). In Lunar Science VIII, p. 592-594. The Lunar Science Institute, Houston.

Lugmair, G.W. (1975) Sm-Nd systematics of some Apollo 17 basalts. In Origin of Mare Basalts, p. 107-110. The Lunar Science Institute, Houston.

Ma, M.-S., Murali, A.V., and Schmitt, R.A. (1976) Chemical constraints for mare basalt genesis. Proc. Lunar Sci. Conf. 7th, 1673-1695.

MacDonald, G.A. (1968) Composition and origin of Hawaiian lavas. Geol. Soc. of Amer. Memoir 116, 477-522.

MacDonald, G.W. and Abbott, A.T. (1970) Volcanoes in the sea: The geology of Hawaii. University of Hawaii Press, Honolulu.

Malin, M.C. (1973) Lunar red spots: Possible pre-mare materials. Earth Plan. Sci. Letts., 21, 331-341.

Mao, H.K. and Bell, P.M. (1972) Electrical conductivity and the red shift of absorption in olivine and spinel at high pressures. Science, 176, 403-406.

Mason, B. (1966) Principles of Geochemistry, John Wiley & Sons, Ltd., 329 pp.

Matson, D.L., Fanale, F.P., Johnson, T.V., and Veeder, G.J. (1976) Asteroids and comparative planetology. Proc. Lunar Sci. Conf. 7th, 3603-3627.

Mazzullo, L.J. and Bence, A.E. (1976) Abyssal tholeiites
   from DSDP leg 34: The Nazea Plate. J. Geophys. Res.,
   81, 4327.

McBirney, A.R. and Williams, H. (1969) Geology and petro-
   logy of the Galapagos Islands. Geol. Soc. Amer. Mem.
   118.

McCord, T.B. (1967) Observational study of lunar visible
   emission. J. Geophys. Res., 72, 2087-2097.

McCord, T.B. (1968a) Color differences on the lunar surface.
   Ph.D. Dissertation. Calif. Inst. of Tech., Pasadena,
   Calif., 181 pp.

McCord, T.B. (1968b) A double beam astronomical photometer.
   Applied Optics, 7, 475-478.

McCord, T.B. (1969a) Color differences on the lunar surface.
   J. Geophys. Res., 74, 3131-3142.

McCord, T.B. (1969b) Time dependence of lunar differential
   color. Astron. J., 74, 273-278.

McCord, T.B. (1976) Multispectral mapping of solar-system
   objects. IEEE Trans. of Geosci. Elec., GE-14, 135-140.

McCord, T.B. (1977) In preparation.

McCord, T.B. and Adams, J.B. (1972) Mercury: Interpreta-
   tion of optical observation. Icarus, 17, 585-588.

McCord, T.B. and Adams, J.B. (1973) Progress in remote op-
   tical analysis of lunar surface composition. The Moon,
   7, 453-474.

McCord, T.B. and Adams, J.B. (1974) The use of groundbased
   telescopes in determining the composition of the surface
   of solar system objects. Proc. Sov.-Amer. Conf. on Cosmo-
   chem. of the Moon and Planets. The Lunar Science In-
   stitute,Houston.

McCord, T.B. and Chapman, C.R. (1975a) Asteroids: Spectral reflectance and color characteristics. Astrophys. J., 195, 553-562.

McCord, T.B. and Chapman, C.R. (1975b) Asteroids: Spectral reflectance and color characteristics. II. Astrophys. J., 781-790.

McCord, T.B. and Gaffey, M.J. (1974) Asteroids: Surface composition from reflection spectroscopy. Science, 186, 352-355

McCord, T.B. and Johnson, T.V. (1969) Relative spectral reflectivity 0.4 - 1μ of selected areas of the lunar surface. J. Geophys. Res., 74, 4395-4401.

McCord, T.B. and Johnson, T.V. (1970) Lunar spectral reflectivity (0.30 to 2.50 microns) and implications for remote mineralogical analysis. Science, 169, 855-858.

McCord, T.B., Johnson, T.V., and Kieffer, H.H. (1969) Differences between proposed Apollo sites. 2. Visible and infrared reflectivity evidence. J. Geophys. Res., 74, 4385-4388.

McCord, T.B., Adams, J.B., and Johnson, T.V. (1970) Asteroid Vesta: Spectral reflectivity and compositional implications. Science, 168, 1445-1447.

McCord, T.B., Charette, M.P., Johnson, T.V., Lebofsky, L. A., Pieters, C., and Adams, J.B. (1972a) Lunar spectral types. J. Geophys. Res., 77, 1349-1359.

McCord, T.B., Charette, M.P., Johnson, T.V., Lebofsky, L. A., and Pieters, C. (1972b) Spectrophotometry (0.3 to 1.1μ) of visited and proposed Apollo lunar landing sites. The Moon, 5, 52-89.

McCord, T.B., Bosel, J.P., and Frankston, M.J. (1975) Performance of the MIT silicon vidicon imaging system at the telescope. In Image Processing Techniques in Astronomy (de Jager/Nieuwenhuijzen, Eds.) D. Reidel Publishing Co., Dordrecht. pp. 91-96.

McCord, T.B., Adams, J.B., and Huguenin, R.L. (1976a) Reflection spectroscopy: A technique for remotely sensing surface mineralogy and composition. To appear in NASA-SP on Orbital Science.

McCord, T.B., Pieters, C., and Feierberg, M.A. (1976b) Multispectral mapping of the lunar surface using ground-based telescopes. Icarus, 29, 1-34.

McCord, T.B., Feierberg, M.A., and Grabow, M. (1977) More multispectral maps of the lunar surface using groundbased telescopes. In preparation.

McDougall, I. (1976) Geochemistry and origin of basalt of the Columbia River Group, Oregon and Washington. Geol. Soc. Am. Bull., 87, 777-792.

McGee, P.A., Warner, J.L., and Simonds, C.H. (1977) Introduction to the Apollo collections: Part 1 lunar igneous rocks. NASA Johnson Space Center, Houston.

McGetchin, T.R. (1975) Solid earth geosciences research activities as LASL, July 1-December 21, 1974. Prog. Report, LA-5956, Los Alamos Scientific Lab., U.S. Energy Research and Development Admin. 93 pp.

McGetchin, T.R. and Smyth, J.R. (1977) Some mineralogical and petrogenetic implications of the Martian mantle density. In preparation.

McKay, D.S., Fruland, R.M., and Heiken, G.H. (1974) Grain size and the evolution of lunar soils. Proc. Lunar Sci. Conf. 5th, 887-906.

Miyashiro, A., Shido, F., and Ewing, M. (1970) Crystallization
and differentiation in abyssal tholeiites and gabbros from
mid-oceanic ridges. Earth Plan. Sci. Lett., 7, 361-365.

Mizutani, H., Matsui, T., and Takeuchi, H. (1972) Accretion of
the moon. The Moon, 4, 476-489.

Moorbath, S. and Bell, J.D. (1965) Strontium isotope abundance
studies and rubidium-strontium age determinations on ter-
tiary igneous rocks from the Isle of Skye, Northwest Scot-
land. J. Petrol., 6, 37-66.

Moorbath, S. and Welke, H. (1968) Lead isotope studies on igne-
ous rocks from the Isle of Skye, Northwest Scotland. Earth
Plan. Sci. Lett., 5, 217-230.

Moore, R.B., Wolfe, E.W., and Ulrich, G.E. (1976) Volcanic
rocks of the eastern and northern parts of the San Francisco
volcanic field, Arizona. J. Res. U.S. Geol. Sur., 4, 549-
560.

Murray, B.C., Belton, M.J.S., Danielson, G.E., Davies, M.E.,
Gault, D.E., Hapke, B., O'Leary, B., Strom, R.G., Suomi, V.,
and Trask, N. (1974) Mercury's surface: Preliminary des-
cription and interpretation from Mariner 10 pictures. Sci-
ence, 185, 169-179.

Murray, B.C., Strom, R.G., Trask, N.J., and Gault, D.E. (1975)
Surface history of Mercury: implications for terrestrial
planets. J. Geophys. Res., 80, 2508-2514.

Mysen, B.O. and Boettcher, A.L. (1974a) Melting of a hydrous
mantle: I. Phase relations of natural peridotite at high
pressures and temperatures with controlled activities of
water, carbon dioxide, and hydrogen. J. Petrol., 16, 520-
548.

Mysen, B.O. and Boettcher, A.L. (1974b) Melting of a hydrous
mantle: II. Geochemistry of crystals and liquids formed by
anatexis of mantle peridotite at high pressures and high
temperatures as a function of controlled activities of water,
hydrogen, and carbon dioxide. J. Petrol., 16, 549-593.

Mysen, B.O. and Holloway, J.R. (1977) Experimental determination of rare earth fractionation patterns in partial melts from peridotite in the upper mantle. Earth Plan. Sci. Lett., 34, 231-237.

Nash, D.B. and Conel, J.E. (1973) Vitrification darkening of rock powders: Implications for optical properties of the lunar surface. The Moon, 8, 346-364.

Nash, D.B. and Conel, J.E. (1974) Spectral reflectance systematics for mixtures of powdered hyperstheren, laboradorite, and ilmenite. J. Geophys. Res., 79, 1615-1621.

Nockolds, S.R. (1954) Average chemical compositions of some igneous rocks. Bull. Geol. Soc. Amer., 65, 1007-1032.

Nygard, S. (1974) Alpha Lyrae/Sun flux ratios for use in standard star calibrations: Results from three techniques. Masters thesis. MIT, Cambridge, Mass. 172 pp.

Nyquist, L.E., Bansal, B.M., Wooden, J.L., and Wiesmann, H. (1977) Sr-isotopic constraints on the petrogenesis of Apollo 12 ilmenite basalts (abstract). In Lunar Science VIII, p. 735-757. The Lunar Science Institute, Houston.

O'Hara, M.J. (1965) Primary magmas and the origin of basalts. Scottish J. Geol., 1, 19-40.

O'Hara, M.J., Humphries, D.J., and Waterston, S. (1974) Petrogenesis of mare basalts: Implications for chemical, mineralogical, and thermal models for the Moon. Proc. Lunar Sci. Conf. 6th, 1043-1055.

Papanastassiou, D.A. and Wasserburg, G.J. (1969) Initial strontium isotopic abundances and the resolution of small time differences in the formation of planetary objects. Earth Plan. Sci. Lett., 5, 361-376.

Papanastassiou, D.A. and Wasserburg, G.J. (1971) Lunar chronology and evolution from Rb-Sr studies of Apollo 11 and 12 samples. Earth Plan. Sci. Lett., 11, 37-62.

Papanastassiou, D.A. and Wasserburg, G.J. (1972) Rb-Sr age of a Luna 16 basalt and the model age of lunar soils. Earth Plan. Sci. Lett., 13, 368-374.

Papanastassiou, D.A. and Wasserburg, G.J. (1975) Rb-Sr study of a lunar dunite and evidence for early lunar differentiates. Proc. Lunar Sci. Conf. 6th, 1467-1489.

Papike, J.J., Bence, A.E., and Lindsley, D.H. (1974) Mare basalts from the Taurus-Littrow region of the moon. Proc. Lunar Sci. Conf. 5th, 471-504.

Papike, J.J., Hodges, F.N., and Bence, A.E. (1976) Mare basalts: Crystal chemistry, mineralogy, and petrology. Rev. Geophys. and Space Phys., 14, 475-540.

Philpotts, J.A. and Schnetzler, C.C. (1970) Apollo 11 lunar samples: K, Rb, Sr, Ba and rare earth concentrations in some rocks, and separated phases. Proc. Apollo 11 Lunar Sci. Conf., 1471-1486.

Pieters, C. (1972) Wavelength dependence on the polarization of light reflected from a particulate surface in the spectral region of a transition metal absorption band. Masters thesis. MIT, Cambridge, Mass. 72 pp.

Pieters, C. (1974) Polarization in a mineral absorption band. In Planets, Stars and Nebulae Studied with Photopolarimetry (T. Gehrels, Ed.) Univ. of Arizona Press, Tucson, pp. 405-418.

Pieters, C. (1977) Characterization of lunar mare basalt types-II: Spectral classification of fresh mare craters. Submitted to Proc. Lunar Sci. Conf. 8th.

Pieters, C. and McCord, T.B. (1975) Classification and distribution of lunar mare basalt types. In Origin of Mare Basalts. The Lunar Science Institute, Houston. p. 125-129.

Pieters, C. and McCord, T.B. (1976) Characterization of
    lunar mare basalt types: I. A remote sensing study us-
    ing reflection spectroscopy of surface soils. Proc.
    Lunar Sci. Conf. 7th, 2677-2690.

Pieters, C., McCord, T.B., Zisk, S., and Adams, J.B. (1973)
    Lunar black spots and nature of the Apollo 17 landing
    area. J. Geophys. Res., 78, 5867-5875.

Pieters, C., McCord, T.B., Charette, M.P., and Adams, J.
    B. (1974) Lunar surface: Identification of the dark
    mantling material in the Apollo 17 soil samples. Science,
    183, 1191-1194.

Pieters, C., Head, J.W., McCord, T.B., Adams, J.B., and
    Zisk, S. (1975) Geochemical and geological units of Mare
    Humorum: Definition using remote sensing and lunar
    sample information. Proc. Lunar Sci. Conf. 6th, 2689-
    2710.

Pieters, C., McCord, T.B., Adams, J.B. (1976) Regional ba-
    salt types in the Luna 24 landing area as derived from
    remote observation. Geophys. Res. Lett., 3, 697-700.

Pieters, C., Adams, J.B., Bryan, R., Head, J.W., McCord,
    T.B., and Zisk, S. (1977) Geology and geochemistry of
    the Flamsteed region of Oceanus Procellarum: A prelim-
    inary report (abstract). In Lunar Science VIII, pp.
    773-775. The Lunar Science Institute, Houston.

Price, P.B., Hutcheon, I.D., Braddy, D., and MacDougall,
    D. (1975) Track studies bearing on solar-system regoliths.
    Proc. Lunar Sci. Conf. 6th, 3449-3469.

Reeves, H. and Audouze, J. (1969) Heat generation in me-
    teorites during the early stage of the solar system.
    Earth Plan. Sci. Lett., 4, 135.

Rhodes, J.M. and Hubbard, N.J. (1973) Chemistry, classifi-
    cation and petrogenesis of Apollo 15 mare basalts. Proc.
    Lunar Sci. Conf. 4th, 1121-1148.

Rhodes, J.M., Adams, J.B., Blanchard, D.P., Charette, M.P.,
    Rodgers, K.V., Jacobs, J.W., Brannon, J.C., and Haskin,
    L.A. (1975) Chemistry of agglutinate fractions in lunar
    soils. Proc. Lunar Sci. Conf. 6th, 2291-2307.

Rhodes, J.M., Blanchard, D.P., Brannon, J.C., Rodgers, K.V.,
    and Dungan, M.A. (1977) Chemistry, classification and
    petrogenesis of Apollo 12 mare basalts (abstract). In
    Lunar Science VIII. The Lunar Science Institute, Houston.

Ridley, W.I. (1970) The petrology of Las Canadas volcanoes,
    Tenerife, Canary Islands. Contrib. Mineral. Petrol.,
    26, 124-160.

Ridley, W.I. (1975) On high-alumina mare basalts. Proc.
    Lunar Sci. Conf. 6th, 131-145.

Ringwood, A.E. and Essene, E. (1970) Petrogenesis of Apollo
    11 basalts, internal constitution and origin of the
    moon. Proc. Apollo 11 Lunar Sci. Conf. p. 769-799.

Ringwood, A.E. and Green, D.H. (1975) Mare basalt petrogen-
    esis (abstract). In Lunar Science VI, p. 677-679. The
    Lunar Science Institute, Houston.

Ringwood, A.E. and Kesson, S.E. (1976) A dynamic model for
    mare basalt petrogenesis. Proc. Lunar Sci. Conf. 7th,
    1697-1722.

Sagan, C. (1975) The solar system. Scientific Amer., 233, 23-31.

Salisbury, J.W., Hunt, G.R., and Lenhoff, C.J. (1975) Visible and near-infrared spectra: X. Stony meteorites. Mod. Geol., 5, 115-126.

Sato, M., Hickling, N.L. and McLane, J.E. (1973) Oxygen fugacity values of Apollo 12, 14, and 15 lunar samples and reduced state of lunar magmas. Proc. Lunar Sci. Conf. 4th, 1061-1079.

Saunders, R.S., Thompson, T.W., and Mosher, J.A. (1977) Characteristics of lunar marea: earth-based data (abstract). In Lunar Science VIII, p. 829-831. The Lunar Science Institute, Houston.

Schaber, G.G., Thompson, T.W., and Zisk, S. (1975) Lava flows in Mare Imbrium: An evaluation of anomalously low earth-based radar reflectivity. The Moon, 13, 395-423.

Schramm, D.N., Tera, F., and Wasserberg, G.J. (1970) The isotopic abundances of ^{26}Mg and limits on ^{26}Al in the early solar system. Earth Plan. Sci. Lett., 10, 44-59.

Shih, C. and Schonfeld, E. (1976) Mare basalt genesis: A cumulate-remelting model. Proc. Lunar Sci. Conf. 7th, 1757-1792.

Siems, B.A., Bush, J.H., and Crosby III, J.W. (1974) TiO_2 and geophysical logging criteria for Yakima Basalt correlation, Columbia Plateau. Geol. Soc. Amer. Bull., 85, 1061-1068.

Soderblom, L.A. (1970) The distribution and ages of regional lighologies in the lunar marea. Ph.D. Dissertation. Calif. Inst. of Tech., Pasadena, Calif.

Soderblom, L.A. and Boyce, J.M. (1976) Distribution and evolution of global color provinces on the moon (abstract). In Lunar Science VII, p. 822-824. The Lunar Science Institute, Houston.

Soderblom, L.A. and Lebofsky, L.A. (1972) Technique for rapid determination of relative ages of lunar areas from orbital photography. J. Geophys. Res., 77, 279-296.

Soderblom, L.A., Condit, C.D., West, R.A., Herman, B.M., and Kreidler, T.J. (1974) Martian planetwide crater distributions: Implications for geologic history and surface processes. Icarus, 22, 239-263.

Solomon, S.C. (1976) Some aspects of core formation in Mercury. Icarus, 28, 509-521.

Solomon, S.C. and Chaiken, J. (1976) Thermal expansion and thermal stress in the moon and terrestrial planets: Clues to early thermal history. Proc. Lunar Sci. Conf. 7th, 3229-3243.

Solomon, S.C. and Longhi, J. (1977) Magma oceanography: 1. Thermal evolution (abstract). In Lunar Science VIII, p. 884-886. The Lunar Science Institute, Houston.

Sonnett, C., Colburn, K., Schwarz, K., and Keil, K. (1969) The melting of asteroidal-sized bodies by unipolar dynamo induction from a primordial T-Tauri Sun. Astrophys. and Space Sci., 7, 446.

Swanson, D.A. (1972) Magma supply rate at Kilauea volcano 1952-1971. Science, 175, 169-170.

Sung, C.M., Singer, Parkin, K.M., Loeffler, B.M., and Burns, R.G. (1977) Temperature dependencies of crystal field transition energies and their effect on the mineralogical mapping of the lunar surface (abstract). In Lunar Science VIII, p. 919-921. The Lunar Science Institute, Houston.

Tatsumoto, M.C., Hedge, C.E., and Engle, A.E. (1965) Potassium, Rubidium, Strontium, Thorium, Uranium, and the ratio of Strontium-87 to Strontium-86 in oceanic tholeiitic basalt. Science, 150, 886-888.

Taylor, S.R. (1975) Lunar Science: A Post-Apollo View, Pergamon Press, 372 pp.

Taylor, S.R. and Jakes, P. (1974) The geochemical evolution of the moon. Proc. Lunar Sci. Conf. 5th, 1287-1305.

Tera, F. and Wasserberg, G.J. (1974) U-Th-Pb systematics on lunar rocks and inferences about lunar evolution and the age of the moon. Proc. Lunar Sci. Conf. 5th, 1571-1599.

Thompson, T.W., Shorthill, R.W., Whitaker, E.A., and Zisk, S.H. (1974) Mare Serenitatis: A preliminary definition of surface units by remote observations. The Moon, 9, 89-96.

Tilley, C.E. (1950) Some aspects of magmatic evolution. O.J. Geol. Soc. Lond., 106, 37-61.

Toksöz, M.N. (1972) The convective earth. Tech. Rev., 75, 1-7.

Toksöz, M.N. and Solomon, S.C. (1973) Thermal history and evolution of the moon. The Moon, 7, 251-278.

Tossell, J.A., Vaughan, D.J., and Johnson, K.H. (1974) The electronic structure of rutile, wustite, and hematite from molecular orbital calculations. Amer. Mineral., 59, 319-334.

Toulmin III, P., Clark, B.C., Baird, A.K., Keil, K., and Rose, Jr., H.J. (1976) Preliminary results from the Viking X-ray fluorescence experiment: The first sample from Cryse Planilia, Mars. Science, 194, 81-83.

Turner, G., Cadogan, P.H., and Yonge, C.J. (1973) Argon seleno-
    chronology. Proc. Lunar Sci. Conf. 4th, 1889-1914.

Vaniman, D.T. and Papike, J.J. (1977) The Apollo 17 drill core:
    Chemistry and stratigraphy of monomineralic fragments and
    the discovery of a new very low ti (VLT) mare basalt (ab-
    stract). In Lunar Science VIII, p. 954. The Lunar Science
    Institute, Houston.

Verhoogen, J., Turner, F.J., Weiss, L.E., and Wahrhaftig, C.
    (1970) The Earth, Holt, Rinehart & Winston, Inc., 748 pp.

Vilas, F. and McCord, T.B. (1976) Mercury: Spectral reflec-
    tance measurements (0.33 - 1.06 m) 1974/75. Icarus, 28,
    593-599.

Vinogradov, A.P. (1961) The origin of the material of the
    earth's crust. Geochemistry, 1-32.

Vinogradov, A.P. (1971) Preliminary data on lunar ground
    brought to Earth by automatic probe "Luna-16". Proc. Lunar
    Sci. Conf. 2nd, 1-16.

Walker, D., Grove, T.L., Longhi, J., Stolper, E.M., and Hays,
    J.F. (1973) Origin of lunar feldspathic rocks. Earth Plan.
    Sci. Lett., 20, 325-336.

Walker, D., Longhi, J., Stolper, E.M., Grove, T.L., and Hays,
    J.F. (1975) Origin of titaniferous lunar basalts. Geochim.
    Cosmochim. Acta, 39, 1219-1235.

Walker, D., Longhi, J., and Hays, J.F. (1976) Differentiation
    of a very thick magma body and implications for the source
    regions of mare basalts. Proc. Lunar Sci. Conf. 6th, 1103-
    1120.

Warner, J.L. (1971) Lunar crystaline rocks: Petrology and ge-
    ology. Proc. Lunar Sci. Conf. 2nd, 469-480.

Wasson, J.T. (1974) Meteorites, Classification and Properties, Springer-Verlag, New York.

Waters, A.C. (1961) Stratigraphic and lithologic variations in the Columbia River Basalt. Am. J. Sci., 259, 583-611.

Wells, E. and Hapke, B. (1977) Lunar Soil: Iron and titanium bands in the glass fraction. Science, 195, 977-979.

Whitaker, E.A. (1972) Lunar color boundaries and their relationship to topographic features: A preliminary survey. The Moon, 4, 348-355.

White, W.B. and Keester, K.L.(1966) Optical absorption spectra of iron in the rock-forming silicates. Amer. Mineral., 51, 774-791.

Windley, B.F. (Editor) (1976a) The Early History of the Earth, John Wiley & Sons, Inc., New York. 619 pp.

Windley, B.F. (1976b) New Tectonic models for the evolution of Archaean continents and oceans. In The Early History of the Earth (B.F. Windley, Ed.) John Wiley & Sons, Inc. p. 105-111.

Wones, D.R. and Shaw, H.R. (1975) Tidal dissipation: A possible heat source for mare basalt magmas (abstract). In Lunar Science VI, p. 878-880. The Lunar Science Institute, Houston.

Wood, J.A. (1975) Lunar petrogenesis in a well-stirred magma ocean. Proc. Lunar Sci. Conf. 6th, 1087-1102.

Wood, J.A., Dickey, J.S., Marvin, U.B., and Powell, B.J. (1970) Lunar anorthosites and a geophysical model for the moon. Geochim. Cosmochim. Acta, Suppl.1, 965-988.

Wright, T.L. and Fiske, R.S. (1971) Origin of the differentiated and hybrid lavas of Kilauea Volcano, Hawaii. J. Petrol., 12, 1-65.

Yoder, H.S., Jr. (1976) Generation of Basaltic Magma, National Academy of Sciences, Washington, D.C. 265 pp.

Yoder, H.S. and Tilley, C.E. (1962) Origin of basaltic magmas: An experimental study of natural and synthetic rock systems. J. Petrol., 3, 342-532.

Zisk, S.H., Hodges, C.A., Moore, H.J., Shorthill, R.W., Thompson, T.W., Whitaker, E.A., and Wilhelms, D.E. (1976) The Aristarchus-Harbinger region of the moon: Surface geology and history from recent remote sensing observations. Submitted to Icarus.

RESUME

Carle Pieters

Home:
520 Beacon 4D
Boston, Mass. 02115
(617) 262-0266

Business: (till June 1977)
MIT 37-487
Department of Earth and Planetary
     Sciences
Massachusetts Institute of Technology
Cambridge, Massachusetts 02139
(617) 253-5809 or 1708

March 1977

Education:

B.A. Math-Education	- Antioch College	1966
B.S. Planetary Science	- Mass. Inst. of Tech.	1971
M.S. Planetary Science	- Mass. Inst. of Tech.	1972
Ph.D. Planetary Geochemistry	- Mass. Inst. of Tech.	1977

Professional Experience:

Summer 1966:   Educational program development, ESI, Watertown, Mass.

September 1966 - June 1967: H.S. Math teacher, Somerville, Mass.

August 1967 - December 1969: Science Teacher (Peace Corps), Sarawak, Malasia

January 1970 - August 1971: Undergraduate Research Assistant, M.I.T. Planetary Astronomy Laboratory, Department of Earth and Planetary Sciences

September 1971 - August 1972: Graduate Fellow (Sloan Fellowship) Department of Earth and Planetary Sciences, M.I.T.

September 1972 - September 1975: DSR staff scientist, Planetary Astronomy Laboratory, Department of Earth and Planetary Sciences, M.I.T.

<u>Professional Experience:</u> (Continued)

September 1975 - June 1977: Graduate Research Assistant, M.I.T.
            Remote Sensing Laboratory, Department of Earth
            and Planetary Sciences, M.I.T.

<u>Personal Data:</u>

Citizenship: U.S.A.

<u>Professional Interests:</u>

General   Remote Sensing: Spectral Reflectance
                Planetary Astronomy
                Planetary Geology

Current Research: Characterization and distribution of lunar
            mare basalt types using remote sensing techniques

                Synthesis of spectral reflectance data with
                other planetary science information to solve
                problems of surface geology and geochemistry

                Terrestrial geological applications of remote
                sensing information

                Stellar calibration (for planetary reflectance)

                Spectral polarimetry of planetary surfaces

                Orbital geochemical experiments

CARLE PIETERS PUBLICATIONS
MIT REMOTE SENSING LABORATORY

1. McCord, T.B., M. Charette, T.V. Johnson, L.A. Lebofsky, C. Pieters, J.B. Adams. "Lunar Spectral Types." Journal of Geophysical Research, 77, 1349-1359, (1972).

2. McCord, T.B., M. Charette, T.B. Johnson, L.A. Lebofsky, C. Pieters, "Spectrophotometry (0.3 to 1.1 microns) of Visited and Proposed Lunar Landing Sites." The Moon, 5, 52-89, (1972).

3. Johnson, T.B., C. Pieters and T.B. McCord. "Mare Humorum: An Integrated Study of Spectral Reflectivity." Icarus, 19, 224-229, (1973).

4. Pieters, C., T.B. McCord, S.H. Zisk, and J.B. Adams. "Lunar Black Spots and the Nature of the Apollo 17 Landing Area," Journal of Geophysical Research, 78, 5867-5875, (1973).

5. Chapman, C.R., T.B. McCord, C. Pieters, "Spectrophotometric Study of the Composition of (1685) Toro." Astronomical Journal, 78, 502-505, (1973).

6. Pieters, Carle, "Polarization in a Mineral Absorption Band." Planets, Stars and Nebulae, (T. Gehrels, ed.), 405-418, (1974).

7. Pieters, C., T.B. McCord, M. Charette, J.B. Adams, "Lunar Surface: Identification of the Mantling Material in the Apollo 17 Soil Samples." Science, 183, 1191-1194, (1974).

8. Charette, M.P., T.B. McCord, C. Pieters, J.B. Adams, "Application of Remote Spectral Reflectance Measurements to Lunar Geology Classification and Determination of Titanium Content of Lunar Soils." Journal of Geophysical Research, 79, 1605-1613, (1974).

9. Pieters, C., T.B. McCord, J.B. Adams, "Evidence for Regional Occurrence of Orange Glass and Related Soils." Abstract, Lunar Science V, LSI, 605-607, (1974).

10. Adams, J.B., C. Pieters, and T.B. McCord, "Orange Glass: Evidence for Regional Deposits of Pyroclastic Origin on the Moon." Proceedings of the Fifth Lunar Science Conference, 1, 171-187, (1974).

11. Pieters, C., T.B. McCord, "Classification and Distribution of Lunar Mare Basalt Types." Origins of Mare Basalts, LSI, 125-129, (1975).

12. Pieters, C., J. Head, T.B. McCord, J.B. Adams, S. Zisk, "Geological and Geochemical Units of Mare Humorum: Further Definition Using Remote Sensing and Lunar Sample Information." Proceedings of the Sixth Lunar Science Conference, 2689-2710, (1975).

13. McCord, T.B., R. Huguenin, D. Mink, C. Pieters, "Spectral Reflectance of Martian Areas During the 1973 Opposition: Photoelectric Filter Photometry 0.33-1.10μm." Icarus, in press (1976).

14. Head, J., C. Pieters, T.B. McCord, J.B. Adams, S. Zisk, "Definition and Detailed Characterization of Lunar Surface Units Using Remote Observations," Icarus submitted (1976).

15. McCord, T.B., C. Pieters, M.A. Feierberg, "Color Mapping of the Lunar Surface." Icarus, 29, 1-34, (1976).

16. Pieters, C., M. Gaffey, C. Chapman, T.B. McCord, "Spectrophotometry of 433 Eros (0.33-1.0μm) and Compositional Implications." Icarus, 28, 105-115, (1976).

17. Pieters, C., "Lunar Basalt Types: Further Definition From Remote Sensing." Abstract, Lunar Science VII, LSI, 697-699, (1976).

18. Head, J.W., C. Pieters, T.B. McCord, J.B. Adams, S. Zisk, "Definition and Detailed Characterization of Lunar Surface Units Using Remote Observation." Abstract, Lunar Science VII, LSI, 357-359, (1976).

19. Pieters, C. P. Owensby, M. Gaffey, T.B. McCord, and S. Nygard, "Spectral Photometry of Bright Stars (.3 to 1.1μm) for Use as Planetary Standards," In preparation.

20. McFadden, Lucy, T.B. McCord, Carle Pieters, "Vesta: The First Pyroxene Band from New Spectroscopic Measurements," Icarus, in press (1976).

21. Pieters, C., T.B. McCord, "Characterization of Lunar Mare Basalt Types: A Remote Sensing Study Using Reflection Spectroscopy," Proceedings of the Seventh Lunar Science Conference, 2677-2690 (1976).

22. Pieters, C., T.B. McCord, and J.B. Adams, "Regional Basalt Types in the Luna 24 Landing Area as Derived from Remote Observation." Geophy. Res. Letters, October, 1976, 3, 697-700.

23. Pieters, C., Adams, J.G., R. Byran, J.W. Head, T.B. McCord, S. Zisk, "Geology & Geochemistry of the Flamstead Region of Oceanus Procellaran: A preliminary report based on remote sensing and lunar samples information," Lunar Science VIII, LSI, 1977, 773-775.

24. Pieters, C. "Polarization in a mineral absorption band II: Observations:" (Abstract) Annual AAS/DPS meeting, 19-22 January, 1977, Honolulu.

25. Pieters, C. "Characterization of Lunar Mare Basalt Types-II: Spectral classification of Fresh Mare Craters." Submitted to Proc. Lunar Sci. Conf. 8th, 1977.